

**Study on Micro-Bubble Two-Phase Flow
in a Converging-Diverging Nozzle**

March 2019

KHINE TUN NAUNG

Study on Micro-Bubble Two-Phase Flow
in a Converging-Diverging Nozzle

Graduate School of Systems and Information Engineering
University of Tsukuba

March 2019

KHINE TUN NAUNG

Abstract

A supersonic nozzle is an engineering equipment to convert enthalpy of a fluid into its kinetic energy. A supersonic nozzle for gas-liquid two-phase flow is used to accelerate the fluid flow as a two-phase ejector in a refrigeration cycle and in a Liquid Metal MHD power plant. The supersonic nozzle consists of converging and diverging sections. In the converging section, the gas-liquid two-phase flow accelerates and the velocity of the fluid reaches the sound speed at the throat. Subsequently, the supersonic flow appears in the diverging section.

Generally, the gas moves faster than the liquid in the nozzle, which is the cause of the velocity slip. Due to the velocity slip, the liquid is not accelerated enough and the conversion efficiency of the nozzle becomes low. On the other hand, one of the characteristics of the micro-bubble two-phase flow is small velocity slip. In this study, the micro-bubble two-phase flow was applied for the converging-diverging nozzle in order to reduce the velocity slip and increase the nozzle efficiency. The nozzle flow with the micro-bubbles was generated and studied for its flow characteristics.

The experimental apparatus is a blow-down type and the main parts are upper tank, lower tank and test section. The flow was observed by a high-speed video camera and examined whether it was the supersonic flow or the subsonic flow by the pressure distribution along the nozzle. The aim of this study is to investigate the flow field of the two-phase flow converging-diverging nozzle by using micro-bubbles to generate supersonic flow condition. The modified pressurized dissolution methods are also studied to generate more micro-bubbles for reducing the velocity slip. The effect of the amount of the CO₂ dissolved gas on the two-phase flow and the acceleration of bubble generation on two-phase nozzle flow were examined.

The experiment was performed with a visual blowdown experimental apparatus.

In the experiment a micro-bubble generator was attempted. The nitrogen gas (N_2) and water were used as working fluids for the experiments. The micro-bubbles were generated by the vortex breakdown in micro-bubble generator. The two-phase flow with the micro-bubbles expanded at the throat and became a supersonic flow in the diverging part. The detail bubble behavior in the nozzle was measured by image processing and other flow characteristics were revealed by pressure measurement. At the throat of the nozzle, the velocity slip ratio of micro-bubbles was smaller than that of millimeter-size bubbles.

Moreover, the pressurized dissolution method was also used to generate micro-bubble in the experiment. In the experiment, the working gas was carbon dioxide (CO_2) which solubility is higher in water than the other gas. The pressurized dissolution method is one of micro-bubble generation methods, by reducing the pressure of water after water had been saturated with gas under a high pressure. In the first attempt, the pressurized dissolution method using a converging-diverging nozzle was applied to generate a supersonic flow but it didn't succeed. Because of the homogeneous micro-bubble was not obtained at the throat. Therefore, supersonic flow was not observed in the diverging nozzle.

Therefore, the pressurized dissolution method was modified by use of four types of orifice plates before the nozzle. The shape of hole of the orifice plate was varied as 1 hole, 7 holes, 19 holes and the mesh. The idea of this modified method was the pressure of the liquid was reduced at the orifice, and the micro-bubble was generated at the converging section of the nozzle. If the flow is gas-liquid two-phase flow at the throat, the sound velocity is very low and the flow will become supersonic easily after the throat.

In the modification of pressurized dissolution method with orifice plates, both

supersonic flow and subsonic flow were formed in the experiment. Even in subsonic flow by the modified pressurized dissolution method, it was more potential for the supersonic flow compared to the original pressurized dissolution method. In the experiment, the amount of CO₂ gas was changed at the dissolution process. Even if the CO₂ dissolved gas rate increased, the equivalent bubble diameter was almost constant. Inversely the number of bubbles increased with the CO₂ dissolved gas rate. Therefore, when the amount of CO₂ increased, the void fraction in a cross section increased because the number of bubbles increased. As increasing the CO₂ dissolved rate, the void fraction increased and the bubble velocity increased at the throat. On the other hand, the liquid velocity was almost constant when dissolved gas rate was changed. Therefore, the slip velocity between the bubble and the liquid increased and pressure loss also increased. Moreover, the amount of bubble is different by changing the hole type of orifice plate such as different holes diameter and respective cross section area for each plate. In case of the orifice plate of 7 holes, liquid phase velocity is smaller than those in the others. In case of the orifice of 1 hole and 7 holes with decreasing lower tank pressure, it could be reached the sound speed at the throat and less velocity slip ratio. The flow in these experiments were expected to be supersonic flow.

The experiments in the modification of pressurized dissolution method with orifice plates could generate supersonic flow. However, it was not homogeneous supersonic flow. In order to produce homogeneous micro-bubble two-phase flow, the pressurized dissolution method was also modified by connecting two nozzles. The connecting two nozzles was used in order to generate a two-phase flow before the main nozzle for modified pressurized dissolution method because only a single-phase flow appeared at the throat in the case of a single nozzle. As increasing the CO₂ dissolved gas rate and decreasing the lower tank pressure, the bubble generation increased, and the

void fraction also increased but the liquid velocity decreased at the throat. In the experiment of the lower tank pressure $P_L=21$ kPa ($P_D=180$ kPa) and CO₂ dissolved gas rate 50%, there was observed as the liquid velocity at the throat reached the sound speed and less velocity slip ratio. Therefore, there was a proper condition to obtain the supersonic flow. In this study, we found out that the proper condition for supersonic flow was low pressure at the throat of the nozzle and the middle amount of the dissolved gas. Based on the results supersonic two-phase flows were observed in the study. The supersonic flow was generated in high void fraction cases, because of low sound speed. However, the flow was subsonic under too high void fraction cases. Because much amount of bubbles prevented the flow due to the large pressure loss.

Nomenclature

Roman

(capital letter)

A	cross-sectional area at the diverging section of the nozzle [m ²]
A_{th}	cross-sectional area of the throat [m ²]
A_U	cross-sectional area of the upper tank [m ²]
C_I	constant [-]
C_t	capacity of the tank [m ³]
C	Chisholm parameter [-]
D	diameter of the throat [m]
P_0	initial pressure [kPa]
P	pressure in the nozzle [kPa]
P_{th}	pressure at the throat [kPa]
P_D	pressure difference between upper tank and lower tank [kPa]
P_L	lower tank pressure [kPa]
P_U	upper tank pressure [kPa]
ΔP_G	pressure loss of gas [kPa/m]
ΔP_L	pressure loss of liquid [kPa/m]
ΔP_{TP}	pressure loss of two-phase flow [kPa/m]
Qu	flow rate [m ³ /s]
R	gas constant [JK ⁻¹ mol ⁻¹]
Re	Reynolds number [-]
S	velocity slip ratio [-]
S_i	cross section area of the bubbles [μm^2]

T	temperature [K]
V_L	volume of water [m ³]
V_G	volume of gas [m ³]
X	Lockhart-Martinelli parameter [-]
$X_1^{\prime}, X_2^{\prime}$	lateral edges [m]
$Y_1^{\prime}, Y_2^{\prime}$	longitudinal edges [m]

(small letter)

a	sound speed [m/s]
a_{ad}	adiabatic sound speed [m/s]
a_{iso}	isothermal sound speed [m/s]
c	constant [-]
d	equivalent diameter of micro-bubble [μm]
g	gravitational force [m/s ²]
k	inclined distance in the diverging section of the nozzle [m]
l_1, l_2	bubble movement distance [m]
m	mass of bubble [kg]
n	number of moles [mol]
p	pressure [kPa]
r_0	radius of the throat [m]
t	time [s]
u	liquid velocity along the nozzle [m/s]
u_B	bubble velocity [m/s]
u_{Bi}	single bubble velocity [m/s]
u_G	flow rate of nitrogen gas [L/min]

u_U	change of water level in the upper tank [m/s]
u_{th}	liquid velocity at the throat [m/s]
x	distance along the nozzle [m]

Greek

α	void fraction at the throat [-]
α_0	instantaneous void fraction by volume [-]
α_n	instantaneous void fraction by area ratio [-]
γ	specific heat ratio [-]
ν_L	kinematic viscosity of liquid [m ² /s]
ρ_0	instantaneous density [kg/m ³]
ρ_{G0}	instantaneous density of gas [kg/m ³]
ρ_G	density of gas [kg/m ³]
ρ_L	density of liquid [kg/m ³]
λ	friction factor [-]
Φ_L	two-phase flow friction loss multiplication factor [-]

Contents

Abstract.....	i
Nomenclature.....	v
Contents.....	1
Chapter 1	5
Introduction	5
1.1. Research background	5
1.2. Objective and thesis overview	8
Chapter 2	14
Measurement and Calculation Methods	14
2.1. Experimental setup.....	14
2.2. Nozzle design.....	15
2.3. Acquisition of flow image.....	15
2.4. Measurement of the pressure	16
2.5. Measurement of the flow rate and liquid velocity at the throat	17
2.6. Measurement of bubble velocity at the throat.....	18
2.7. Measurement of bubble size	18
2.8. Measurement of void fraction	19
2.9. Bernoulli equation in homogeneous two-phase flow model.....	22
2.10. Theoretical estimation for subsonic and supersonic two-phase flow.....	25
2.11. Calculation of CO ₂ dissolved gas rate and void fraction at the throat	30
2.12. Sound speed in homogeneous two-phase flow	31
2.13. Calculation of velocity slip ratio	31
2.14. Fractional pressure loss	32
Chapter 3	45
Micro-Bubble Generator and Millimeter-Bubble Generator.....	45
3.1. Experimental procedure	45
3.1.1. Experiment with micro-bubble generator.....	45
3.1.2. Experiment with millimeter-bubble generator	46
3.2. Experimental condition	47
3.3. Flow visualization	47
3.4. Pressure profile along the nozzle	49
3.5. The comparison of the flow rate, liquid velocity and bubble velocity at the throat.....	50

3.6. Measurement of bubble size distribution	52
3.7. Void Fraction at the throat	52
3.8. Velocity distribution along the nozzle	53
3.9. The comparison of pressure distribution between the experimental and theoretical estimation of subsonic and supersonic flow	54
3.10. The comparison of liquid velocity and sound speed at the throat.....	55
3.11. Velocity slip ratio	55
3.12. The comparison of pressure loss and void-fraction at the throat	55
3.13. Concluding remarks	56
Chapter 4	71
Pressurized Dissolution Method and Single-Phase Flow	71
4.1. Experimental procedure	71
4.2. Experimental condition	72
4.3. Flow visualization	72
4.4. Pressure profiles along the nozzle.....	73
4.5. The comparison of the flow rate and liquid velocity at the throat	73
4.6. Velocity distribution along the nozzle.....	74
4.7. The comparison of pressure distribution between the experimental and theoretical estimation of subsonic and supersonic flow.....	74
4.8. Concluding remarks	75
Chapter 5	83
Modification of Pressurized Dissolution Method with Orifice Plates.....	83
5.1. Experimental procedure	83
5.2. Experimental condition	84
5.3. Flow visualization	85
5.4. Pressure profiles along the nozzle.....	86
5.5. The comparison of the flow rate, liquid velocity and bubble velocity at the throat.....	87
5.6. Measurement of bubble size distribution	88
5.7. Void fraction at the throat.....	90
5.8. Velocity distribution along the nozzle.....	90
5.9. The comparison of pressure distribution between the experimental and theoretical estimation of subsonic and supersonic flow.....	91
5.10. The comparison of liquid velocity and sound speed at the throat.....	92

5.11. Velocity slip ratio	92
5.12. The comparison of pressure loss and void fraction at the throat	93
5.13. Concluding remarks	93
Chapter 6	119
Modification of Pressurized Dissolution Method with Connecting Two Nozzles	119
6.1. Experimental procedure	119
6.2. Experimental condition	119
6.3. Flow visualization	120
6.4. Pressure profiles along the nozzle.....	120
6.5. The comparison of the flow rate, liquid velocity and bubble velocity at the throat.....	121
6.6. Measurement of bubble size distribution	122
6.7. Void fraction at the throat.....	123
6.8. Velocity distribution along the nozzle.....	124
6.9. The comparison of pressure distribution between the experimental and theoretical estimation of subsonic and supersonic flow.....	125
6.10. The comparison of liquid velocity and sound speed at the throat.....	126
6.11. Velocity slip ratio	126
6.12. The comparison of pressure loss and void fraction at the throat	127
6.13. Concluding remarks	127
Chapter 7	149
The Comparison of Flow Conditions	149
7.1. Supersonic flow with increasing void fraction	150
7.2. Supersonic flow with decreasing throat pressure.....	150
7.3. Subsonic flow with increasing pressure loss at the throat of the nozzle.....	151
7.4. Subsonic flow with increasing pressure loss at the exit of the nozzle	151
7.5. Concluding remarks	152
Chapter 8	158
Conclusion.....	158
Acknowledgments	162
References	163
Publications	168
APPENDIX A.....	171
APPENDIX B.....	210

APPENDIX C.....217

Chapter 1

Introduction

1.1. Research background

A nozzle is a useful engineering device and used in various systems: turbines, jet propulsion, rockets and ejectors, etc. The thermal energy of high-pressure compressible fluid at the inlet of a nozzle is converted to its kinetic energy at the outlet. Generally it needs compressibility for fluid to work in a thermodynamic cycle. Therefore, incompressible fluid such liquid is not proper as the working fluid in the thermodynamic cycle. On the other hand, the thermal energy density of the liquid is high and it is preferable characteristic as the thermal working fluid. Gas-liquid two-phase flow is a mixture of the liquid and the gas, and has both characteristics of compressibility and high thermal energy density. Therefore, when gas-liquid two-phase flow is used as working fluid, a compact energy conversion system using the nozzle can be constructed.

The nozzle flow in the liquid-metal MHD power generation system with solar-assisted (Kaushik, 1995) as shown in Fig. 1.1 is one of such gas-liquid two-phase flow nozzles. The gas-liquid two-phase supersonic nozzle was used to accelerate the liquid metal in the liquid-metal MHD power plant (Branover, 1983). One of the application of this research is the gas-liquid two-phase nozzle in the liquid-metal MHD power plant. Generally, the sound speed of the gas-liquid two-phase flow is lower than that of the liquid single-phase flow. Therefore, the gas-liquid two-phase flow is choked at low speed in comparison to the liquid flow. The working fluid used in the MHD power plant, however, should be compressible because the MHD power plant uses the thermodynamic cycle. Therefore, the working flow at nozzle in the liquid-metal MHD power plant is the gas-liquid two-phase flow and the gas-liquid two-phase flow nozzle

is investigated in this study.

Two-phase flow is a kind of multiphase flow that occurs in a system containing gas and liquid. The efficiency of the two-phase flow converging-diverging nozzle with carbon dioxide increases with the diverging angle was discovered by Morimune (2009).

The two-phase flow sometimes encountered choking which is undesirable factors for industries and plants. In the converging-diverging nozzle, shown in Fig. 1.2, when the flow accelerates from subsonic to supersonic, it will reach the sound speed at the throat. If the pressure decreases from the throat, the velocity will increase. Therefore, the flow becomes supersonic. In contrast, if the pressure increases from the throat, the velocity will decrease, and the flow becomes subsonic. In the two-phase flow, when the void fraction is middle, the sound speed will be lower. The relationship of sound speed of homogeneous two-phase flow and void fraction is shown in Fig. 1.3. The presence of gas or vapor bubbles in a liquid dramatically reduces the sound speed in the liquid (Mallock, 1910; Karplus, 1958, 1961; Barclay et al., 1969; Mc William and Duggins, 1969). In particular, the sound speed is much lower in a liquid-gas mixture than in either the gas or the liquid components. For example, the sound speed of liquid (single-phase flow) is about 1440 m/s to 1480 m/s and the sound speed of gas under the atmospheric pressure is about 340 m/s, but in an air-water mixture falls to about 20 m/s (Mc William and Duggins, 1969; Kieffer, 1977). Therefore, the sound speed of the two-phase flow is very low compared to the both sound speed. In this study, the void fraction is lower than 0.2. So, it is easy to obtain the supersonic flow. Supersonic nozzle is used for increasing liquid velocity than expansion of bubbles.

When the gas-liquid two-phase flow passes through the converging-diverging nozzle, there is a problem with important impacts of velocity slip on internal flow of the engineering application (Toma, 1986). Generally, the gas moves faster than the liquid in

the nozzle, which is called as velocity slip. Due to the velocity slip, the liquid is not accelerated enough, and the conversion efficiency of the nozzle became low. On the other hand, recently, micro-bubble has been studied much (Ohnari, 2002). The micro-bubbles may be defined as the bubbles with diameters of the order of less than several tens microns, since these sizes of bubbles exhibit in fact somehow different behaviors from those observed with ordinary sized bubbles in their chemical and physical aspects (Serizawa, 2003). One of the characteristics of micro-bubbles is low velocity slip. Therefore, the micro-bubble was examined as the gas phase in the supersonic two-phase flow nozzle, where the low velocity slip and the high void fraction were expected. In this research, we were finding out lower fluctuation flow than larger bubble size.

There are several ways to generate micro-bubbles, but in the study, the method using vortex breakdown and the pressurized dissolution method were used. The method using vortex breakdown can also be used for gases with low solubility and has the advantage of being able to create bubbles under the atmospheric pressure. Therefore, stable micro-bubbles two-phase flow can be obtained, which is suitable to study the flow characteristics of micro-bubble two-phase flow. On the other hand, the pressurized dissolution method is a method of micro-bubble generation by reducing the pressure on the saturated gas in the water (Maeda, 2010), so it was used to simulate boiling two-phase flow. The boiling two-phase flow appears in the thermodynamic cycle and also can be seen in the nozzle flow. In the study, instead of heating the fluid, the pressure was reduced to generate a two-phase flow. The pressurized dissolution method is based on the Henry's law. In pressurized dissolution method; two phases are used as CO₂ and water. CO₂ is chosen for two phase flow because of higher solubility than the other gas. CO₂ dissolved gas rate has 0.88 cm³ in the atmospheric pressure at 20°C.

Therefore, it can thoroughly mix with water and form saturated liquid. When the pressure decrease from this saturated liquid, the micro-bubble will be appeared as represented in Fig. 1.4. This is an idea to use the pressurized dissolution method and generate two phase flow.

The experimental apparatus is a blow-down type and the main parts are upper tank, lower tank and test section. The flow was observed by a high speed video camera. It was examined whether it was the supersonic flow or the subsonic flow by the pressure distribution along the nozzle. Image processing measurement method was used to measure the diameter of micro-bubble. The bubbles are as a dark portion because the back light system is used. The back light is scattered at the gas-liquid interface of a bubble and does not reach the high-speed camera (Itamoto, 2011). For a small bubble, the curvature of the interface is large. Hence, the bubble in the image is captured by high-speed camera was recorded as the dark part in the personal computer. However, it is difficult to measure the accuracy of the micro-bubble diameter smaller than 10 μm (Hosokawa, 2009). Micro-bubble is an extremely small particle about 10 μm to 40 μm diameter.

1.2. Objective and thesis overview

A brief review of the literature reveals that fundamental understanding of the characteristics of micro-bubble in supersonic two-phase flow nozzle has been well established. A lot of study investigates on the micro-bubble two-phase flow and the interest for their application also increases on various engineering field (Hanafizadeh, 2010; Jamalabadi, 2018). Instead of boiling two-phase flow, it was generated by decreasing pressure.

In this study, two micro-bubble generation methods were attempted:

micro-bubble generator using a vortex breakdown and pressurized dissolution method. The micro-bubble generator is an equipment to make micro-bubbles by using vortex breakdown. The flow characteristics of the micro-bubble generator was compared with the millimeter-bubble generator. As a reference, single-phase flow was also studied.

In the present study, supersonic flow was also investigated by using the pressurize dissolution method. The supersonic flow in the nozzle, however, could not be obtained by the pressurized dissolution method because the micro-bubbles could not be produced well at the throat. It was only single-phase flow.

Therefore, pressurized dissolution method was modified by using four types of orifice in order to obtain the micro-bubbles at the throat. The plate was mounted at the upstream of the nozzle to reduce once the diameter of the flow channel. The pressure of the water flow was reduced at the orifice, and the micro-bubble was generated at the converging section of the nozzle. If the flow is gas-liquid two-phase flow at the throat, the sound velocity is very low and the flow becomes supersonic easily after the throat (Nakamura, 2014). In addition, the effect of the amount of the dissolving gas on the two-phase nozzle flow was investigated.

The pressurized dissolution method was also modified by connecting two nozzles to produce micro-bubbles as much as possible and that can form the supersonic flow. The amount of CO₂ also changed to know its effect on the production of micro-bubbles and how it effects on the flow. It is proposed to obtain the supersonic flow in the nozzle with the generation of many micro-bubbles. Micro-bubbles were generated well in this study. However, there is limitation for producing micro-bubbles to be supersonic flow.

The objective of this study is to investigate flow field of the two-phase flow converging-diverging nozzle by using micro-bubbles to generate supersonic flow

condition. The effect of the amount of the micro-bubbles on the two-phase flow and the acceleration of bubble generation on two-phase nozzle flow were examined. The influence factors on the two-phase flow such as micro-bubble size distribution, flow velocity and pressure distribution are also measured in this study. The two-phase flow with the micro-bubbles became a supersonic flow and the flow was very stable comparing with the millimeter-size bubble. In modification of pressurized dissolution method, both supersonic flow and subsonic flow were formed in my experiment. Even in subsonic flow of modified pressurized dissolution method, it was more potential for the supersonic flow compared to the original pressurized dissolution method. Therefore, the author also hopes that the findings of this study would be utilized elsewhere in related fields.

The body of this thesis is structured in this way. It begins with the current Chapter 1, introducing the background and objective of this study as well as furnishing its readers with the fundamental knowledge about two-phase flow of converging-diverging nozzle. Experimental apparatus and procedure are described in Chapter 2. Consequently, measurement and calculation methods are explained. Description of the experimental conditions and results for the micro-bubble generator and millimeter-bubble generator are made in Chapter 3. In Chapter 4, the author examines how the pressurized dissolution method and single-phase flow effect in the converging-diverging nozzle. In pressurized dissolution method, there was no observed micro-bubble at the throat and not generated supersonic flow. Therefore, pressurized dissolution method was modified with orifice plates and connecting two nozzles as Chapter 5 and Chapter 6 respectively. Chapter 5 reveals the modification of pressurized dissolution method with four types of orifice plates. Chapter 6 clarifies the modification of pressurized dissolution method with connecting two nozzles. In Chapter 7 the flow

conditions were compare such as supersonic flow and subsonic flow. Eventually, Chapter 8 summarizes the whole dissertation.

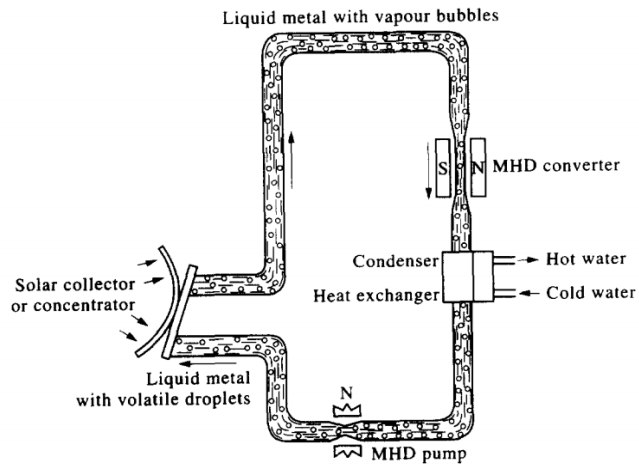


Figure 1.1. Liquid Metal MHD power generation system with solar-assisted (Kaushik, 1995).

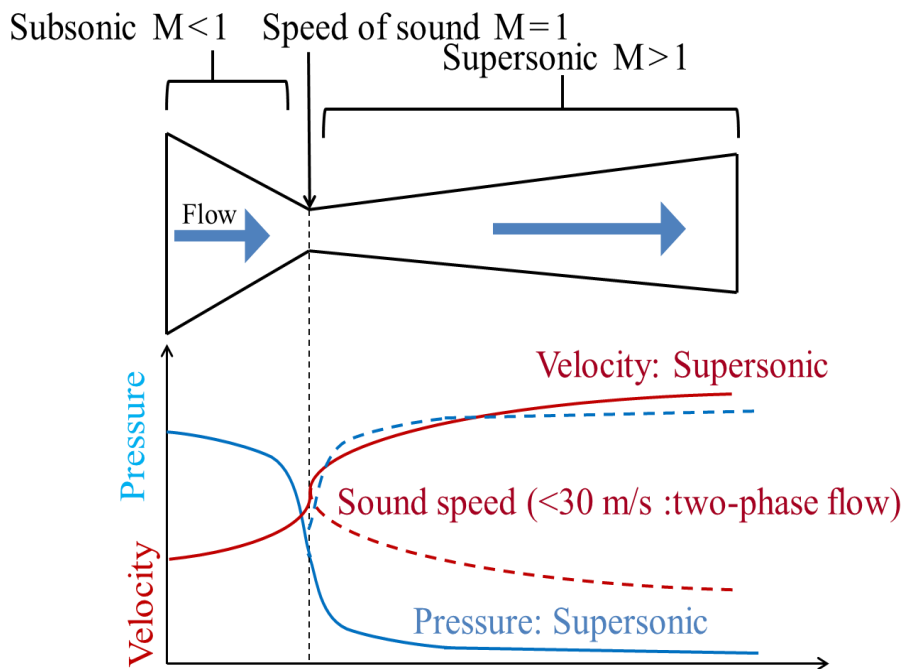


Figure 1.2. General feature in converging-diverging nozzle.

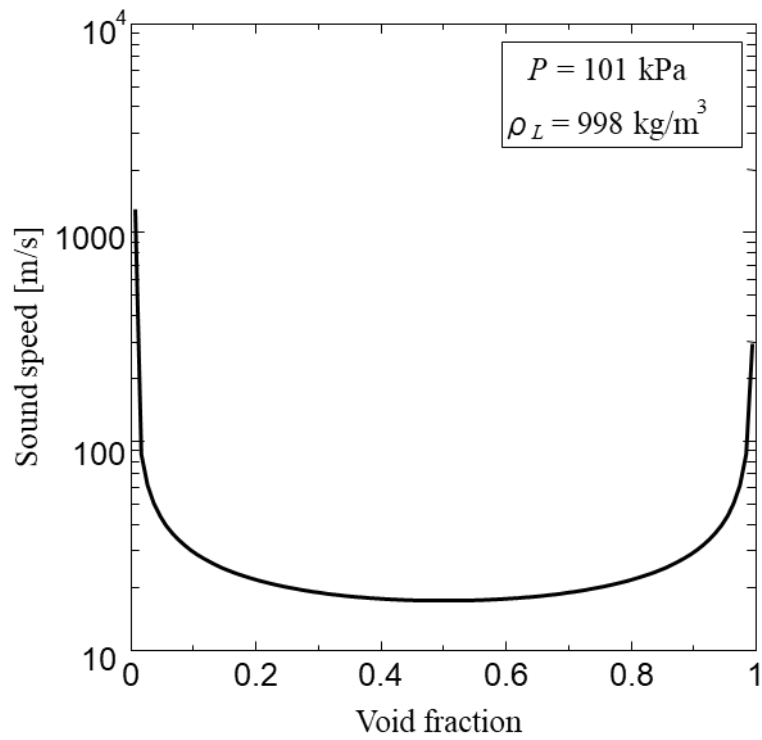


Figure 1.3. Sound speed of homogeneous two-phase flow.

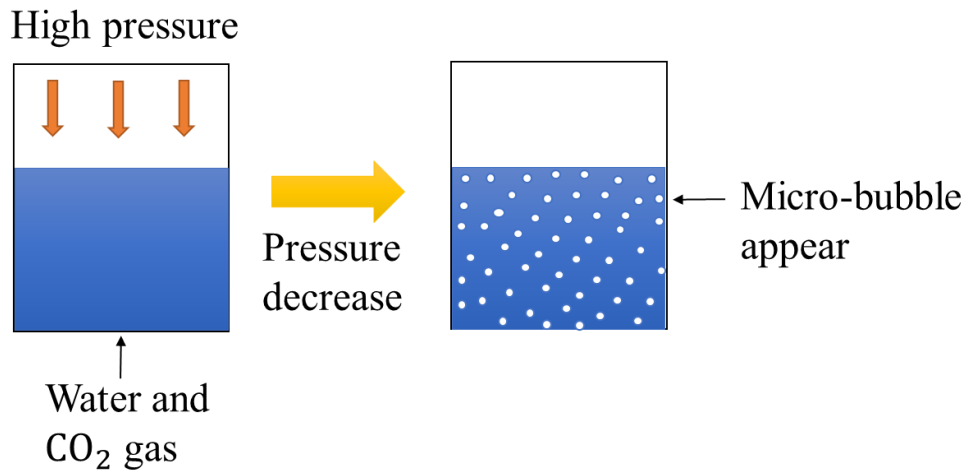


Figure 1.4. Pressurize dissolution method.

Chapter 2

Measurement and Calculation Methods

2.1. Experimental setup

The experiment of two-phase flow with micro-bubble in a converging-diverging nozzle was done in the research. The experiment was carried out for two-phase flow in a blow-down apparatus by using different tank pressures. An image and schematic of the blow-down type experimental apparatus are shown in Fig. 2.1. Figure 2.2 shows photo of the experimental apparatus. It consists mainly of an upper tank, a lower tank, a test section, pumps, a pressure gauge, an amplifier, a data logger and a personal computer. Two tanks are cylindrical shape with 1000 mm of height and 331 mm in inner diameter. The wall of the upper tank is made by transparent acrylic to be visible the flow in the tank. The covers of tanks and lower tank are made with PVC. The test section or a two-phase flow nozzle is connected with the upper and lower tank, and the pressure is taken by the pressure transducer. Then the pressure signal passes through the amplifier and data logger, and the data is received by the personal computer. Nitrogen and carbon dioxide gases are used for working gas. Carbon dioxide is used in the pressurized dissolution method and nitrogen is used in both micro-bubble generator and modified pressurized dissolution method experiments. Moreover, the two-phase flow nozzle plays a very important role in converting the thermal energy to the kinetic energy of two-phase.

In the experimental condition, the temperature of the water was kept at room temperature. The inlet temperature was approximately equal to the outlet temperature. When the valve is opened between the nozzle and the downstream water tank, the blow-down test is started to observe the flow field in the nozzle.

There are a lot of bubble generation methods with different ways and different

purposes. This research uses the micro-bubble generator to generate micro-bubble, a millimeter-bubble generator to produce millimeter-bubble and a pressurize dissolution method to generate also micro-bubble.

2.2. Nozzle design

Two-phase flow nozzle is the main part of the experiment described in Fig. 2.3. It is also called blow-down device. The walls are made of the transparent acrylic resin which is a kind of thermosetting plastic and it has light transmitting properties. The efficiency of the converging-diverging nozzle increases according to the length of the diverging section and divergent angle (Nakagawa and Morimune, 2009). The overall length of the two-phase flow nozzle is 125 mm, the throat and outlet length are 100 mm and the diameter of inlet, outlet and throat are 40 mm, 20 mm and 10 mm respectively as shown in Fig. 2.3. The pressure was measured by pressure transducer for the seven locations of pressure measuring taps with the distance of 12.5 mm, 25 mm, 37.5 mm, 57.5 mm, 77.5 mm and 117.5 mm from the inlet of the nozzle geometry respectively. The photo of converging-diverging two-phase flow nozzle is shown in Fig. 2.4. Nozzle I has 7 pressure measuring taps is represented in Fig. 2.4 (a). Nozzle II is described in Fig. 2.4 (b) without pressure measuring taps. The shape of the nozzle II is the same as nozzle I.

2.3. Acquisition of flow image

This method is used to capture the flow pattern of the experiment shown in Figure 2.5. The flow condition of the nozzle is captured with high-speed camera (REDLAKE Motion Pro HS-3). To capture the exact and sharp picture, the camera is put at one side of the nozzle and red LED is put at the other side of the nozzle. 500

images are aligned to capture per second in this experiment. The bubbles are as a dark portion because the back light system is used. The back light is scattered at the gas-liquid interface of a bubble and does not reach the high-speed camera (Itamoto, 2011). For a small bubble, the curvature of the interface is large. Hence, the bubble in the image is captured by high-speed camera was recorded as the dark part.

2.4. Measurement of the pressure

The pressure was measure at the upper tank, lower tank and the nozzle. The data was saved in the personal computer throughout the amplifier and the data logger. The pressure of pressure taps along the nozzle is measured by a semiconductor pressure transducer PMS-5M-2 500 K (determined gauge pressure range -100 kPa ~ 500 kPa) which connected to DC amplifier. All of the sensors are connected with the data logger NR-600 and the computer as shown in Fig. 2.6. In additional, the signals of the semiconductor pressure transducer and pressure gauges record at the time interval of 500 μ s within 60 seconds. Figure 2.7 shows an example of pressure measurement. Figure 2.7 is a pressure measurement result of the upper tank, the lower tank and the pressure tap No. 3 at the experimental condition No.4 shown in Table 3.1. The pressure at the pressure tap changes rapidly for a few seconds when the valve downstream of the nozzle (Fig. 2.1) is opened. After that the flow becomes quasi-steady and the pressure becomes constant. In the quasi-steady state condition, the variation of discharges and pressures with time is gradual and over short time intervals the flow appears to be steady. The pressure in the upper tank and the lower tank were change however the quasi-steady flow was generated in the downstream at the throat.

2.5. Measurement of the flow rate and liquid velocity at the throat

The upper tank is 1000 mm high and the height scale of 1 cm increments was set on the side wall of the upper tank for measuring the water level is shown in Fig. 2.8. The water level capacity 0.05 m³ in the upper tank was recorded by a digital camera in order to obtain the flow rate. Figure 2.9 shows an example of the measurement result of the water level under the experimental condition No.15 as described in Table 5.1. The water level changed almost linearly with time in the period of 5 s to 15 s and the flow rate can be obtained from the inclination of the water level to time in the period. The amount of the fluid flow passes through the upper tank per unit time is measured as the fluid flow rate and is shown in the Eq. (2.1). The flow rate was measured by the time of the changing of the water level in the upper tank. The water level was taken by a video image. The flow rate Q_u of the water flowing through the nozzle was calculated based on the time change of the water level in the upper tank. Furthermore, the averaged liquid velocity u_{th} on the cross-sectional at the throat of the nozzle was calculated by using Eq. (2.2).

$$Q_u = \frac{\Delta C_t}{\Delta t} \quad (2.1)$$

Where Q_u is the flow rate, ΔC_t is the average water capacity of the upper tank and Δt is the time average.

$$u_{th} = \frac{Q_u}{(1 - \alpha)A_{th}} \quad (2.2)$$

Here, A_{th} is the cross-sectional area at the throat and α is the void fraction at the throat.

2.6. Measurement of bubble velocity at the throat

The bubble velocity was obtained by using digital image correlation method. A single bubble velocity u_{Bi} , Eq. (2.3) was calculated by using three successive flow images at the throat shown in Fig. 2.10. l_1 and l_2 were the movement distance of single bubble. The bubble velocity u_B was obtained as the average 50 bubbles in each experimental condition by using Eq. (2.4).

$$u_{Bi} = \frac{l_1 + l_2}{0.0001 \times 2} \quad (2.3)$$

$$u_B = \frac{\sum_{n=1}^{50} u_{Bi}^n}{50} \quad (2.4)$$

2.7. Measurement of bubble size

The micro-bubble diameter could be measured in micro-bubble generator process when the micro-bubbles were generated under the atmosphere. The water including the micro-bubbles was taken after the micro-bubbles were generated fully in the upper tank. The diameter of the micro-bubbles was measured by using the microscope (KEYENCE, VHX-900). The photo of micro-bubble by the microscope is shown in Fig. 2.11.

The diameter of micro-bubble at the throat was measured from the images, captured by a high speed digital camera. The lateral edges X_1' , X_2' and longitudinal edges Y_1' , Y_2' of air bubbles were measured at the throat for the forty continuous images. The throat has an inner diameter of 10 mm. X and Y coordinates were set at the left side of the throat as (21, 52) and right side as (81, 52) respectively. An example of the bubble diameter measurement is described in Fig. 2.12. From the measurement results, the bubble diameter distribution and the aspect ratio of the equivalent bubble diameter

under each experimental condition were calculated. The bubble passing through the throat is almost ellipsoidal micro-bubble, assume as sphere and the volume V_G of the bubble is expressed by the Eq. (2.5). Equivalent bubble diameter is the diameter when bubble volume is regarded as sphere of the same volume in one bubble illustrated in Fig. 2.13.

$$V_G = \frac{4}{3} \pi \left(\frac{X'_2 - X'_1}{2} \right)^2 \left(\frac{Y'_2 - Y'_1}{2} \right) \left(\frac{0.01}{81 - 21} \right)^3 \quad (2.5)$$

Therefore, the equivalent bubble diameter d was calculated by the Eq. (2.6).

$$d = \frac{6}{\pi} V_G^{\frac{1}{3}} \quad (2.6)$$

2.8. Measurement of void fraction

There are different ways of calculation method of void fraction. For the micro-bubble generator processes, the void fraction could be measured only when the bubbles were generated at the atmospheric pressure. The volume ratio of the gas phase, that is, the ratio of the volume occupied by the bubbles within the unit volume is called the void fraction. For micro-bubble generator process, the water including the bubbles was taken 400 ml to 500 ml by a measuring cup after the micro-bubbles were generated fully. Measurement of void fraction for the micro-bubble generator process is shown in Fig. 2.14. The mass, the volume and the temperature of the water with the micro-bubbles were measured and instantaneous void fraction α_0 was calculated by using Eq. (2.7). The average void fraction was obtained by the average of instantaneous void fractions all of the micro-bubble generator experimental process. It is expected that

the void fraction become large at the throat because the bubbles are expanded by decreasing of the pressure. Therefore, the void fraction at the throat α under the assumption of the adiabatic change of the gas phase is calculated by using Eq. (2.8). The void fraction at the throat α under the assumption of the isothermal change of the gas phase is calculated by using Eq. (2.9).

$$\alpha_0 = \frac{V_L - \frac{m}{\rho_L}}{V_L} \quad (2.7)$$

$$\alpha = \frac{\alpha_0 \left(\frac{P_0}{P_{th}}\right)^{\frac{1}{\gamma}}}{(1 - \alpha_0) + \alpha_0 \left(\frac{P_0}{P_{th}}\right)^{\frac{1}{\gamma}}} \quad (2.8)$$

$$\alpha = \frac{\alpha_0 \frac{P_0}{P_{th}}}{1 + \alpha_0 \left(\frac{P_0}{P_{th}} - 1\right)} \quad (2.9)$$

Where α_0 is the instantaneous void fraction, α is void fraction at the throat, P_0 is initial pressure and P_{th} is pressure at the throat.

In the void fraction measurement of the two-phase fluid of millimeter-bubbles, the initial void fraction was calculated from the change in the water level (shown in Fig. 2.10) and the nitrogen gas flow rate after starting of the experiment. For the change in the water level, the method described in section 2.5, was taken and the flow rate of nitrogen gas was measured with the flow meter (KEYENCE FD-A 10) (see Fig.3.6). Under the experimental conditions using millimeter-bubble generator, the upper tank was set at the atmospheric pressure and the value of the flow rate was used which was indicated at the flowmeter. The moment when Millimeter-bubbles occurred in the water, it was assumed that there was no slip with the liquid phase. The initial void fraction was

calculated from the Eq. (2.10) with the rate of change in water level in the upper tank as u_U , the cross-sectional area of the upper tank as A_U , and the flow rate of nitrogen gas as u_G . The nitrogen gas flow rate was adjusted as to be approximately equal to the initial void fraction of micro-bubbles. The nitrogen gas flow rate in this experiment is 0.50 L/min (under atmospheric pressure). The void fraction was calculated by the average of the six times in each experimental condition of the millimeter-bubble generator process.

$$\alpha_0 = \frac{u_G}{60000A_U u_U} \quad (2.10)$$

For the pressurized dissolution method, the instantaneous void fraction at the throat was measured by using an image taken by the high-speed camera. X and Y coordinates were set at the left side of the throat as (21, 52) and right side as (81, 52) respectively. The throat has an inner diameter of 10 mm, therefore one pixel was 0.154 mm. The cross section of the bubble at the throat was assumed as a circle as shown in Fig. 2.12. The X coordinates of the bubbles at the throat were measured as $X1$ and $X2$. The cross section area of the bubbles S_i were calculated by using Eq. (2.11). Figure 2.12 shows an example of measurement for one captured image.

$$S_i = \pi \left(\frac{x_2 - x_1}{2} \right)^2 \left(\frac{0.01}{81 - 21} \right)^2 \quad (2.11)$$

In case of Fig. 2.15, the instantaneous void fraction was obtained as an area ratio of the bubbles' cross section to the cross section at the throat as shown by Eq. (2.12).

$$\alpha_n = \frac{\sum_i S_i}{A} \quad (2.12)$$

In here, α_n is the instantaneous void fraction and A is the cross-sectional area of the throat. The averaged void fraction at throat was calculated by using the instantaneous void fractions of successive 40 images as Eq. (2.13).

$$\alpha = \frac{\sum_{n=1}^{40} \alpha_n}{40} \quad (2.13)$$

2.9. Bernoulli equation in homogeneous two-phase flow model

For the homogeneous two-phase flow model, the density can be expressed as Eq. (2.14).

$$\rho = \alpha\rho_G + (1 - \alpha)\rho_L \cong (1 - \alpha)\rho_L \quad (2.14)$$

The momentum equation Eq. (2.15) is obtained by differentiate with x -direction the Eq. (2.14).

$$(1 - \alpha)\rho_L u \frac{\partial u}{\partial x} = -\frac{\partial p}{\partial x} - (1 - \alpha)\rho_L g \quad (2.15)$$

$$u \frac{\partial u}{\partial x} + \frac{1}{(1 - \alpha)\rho_L} \frac{\partial p}{\partial x} + g = 0 \quad (2.16)$$

Moreover, continuity equations for gas and liquid phase are;

$$\frac{\partial}{\partial t} \alpha \rho_G + \frac{\partial}{\partial x} \alpha \rho_G u = 0 \quad (2.17)$$

$$\frac{\partial}{\partial t} (1 - \alpha) \rho_L + \frac{\partial}{\partial x} (1 - \alpha) \rho_L u = 0 \quad (2.18)$$

Assuming as steady flow;

$$\frac{\partial}{\partial x} \alpha \rho_G u = 0 \quad (2.19)$$

$$\frac{\partial}{\partial x} (1 - \alpha) \rho_L u = 0 \quad (2.20)$$

Integrate of each phase;

$$\alpha \rho_G u = \text{const} \quad (2.21)$$

$$(1 - \alpha) \rho_L u = \text{const} \quad (2.22)$$

Equation (2.21) divided by Eq. (2.22);

$$\frac{\alpha \rho_G}{(1 - \alpha) \rho_L} = C_1 \quad (2.23)$$

$$\alpha = \frac{C_1 \rho_L}{\rho_G + C_1 \rho_L} \quad (2.24)$$

Equation (2.23) and Eq. (2.24) are frictionless and C_1 is constant. Then, Eq. (2.16) is integrated with x and Eq. (2.25) is obtained.

$$\frac{1}{2}u^2 + \int \frac{\alpha}{(1-\alpha)\rho_L} dp + gx = const \quad (2.25)$$

The flow changes isothermally and the left second term of the Eq. (2.25) is solved as follow;

$$\int \frac{1}{(1-\alpha)\rho_L} dp = \int \left(\frac{1}{\rho_L} + \frac{C_1}{\rho_G} \right) dp = \int \left(\frac{1}{\rho_L} + \frac{1}{p} \cdot \frac{C_1 \rho_0}{\rho_{G0}} \right) dp = \frac{p}{\rho_L} + \frac{C_1 \rho_0}{\rho_{G0}} \ln p \quad (2.26)$$

Equation (2.26) is substitute in Eq. (2.25);

$$\frac{1}{2}u^2 + \frac{p}{\rho_L} + \frac{C_1 \rho_0}{\rho_{G0}} \ln p + gx = const \quad (2.27)$$

From Eq. (2.23),

$$C_1 = \frac{\alpha \rho_G}{(1-\alpha)\rho_L} = \frac{\rho_{G0} \alpha_0}{(1-\alpha_0)\rho_L} \quad (2.28)$$

Bernoulli equation in homogeneous two-phase flow of Eq. (2.29) is obtained by substitution of Eq. (2.27) in Eq. (2.28).

$$\frac{1}{2}u^2 + \frac{p}{\rho_L} + \frac{\alpha_0}{(1-\alpha_0)\rho_L} p_0 \ln p + gx = const \quad (2.29)$$

The liquid velocity along the nozzle was calculated by using Bernoulli equation (混相流体の力学, 1989).

2.10. Theoretical estimation for subsonic and supersonic two-phase flow

A gas-liquid two-phase flow in which a large number of bubbles are dispersed in a liquid, called a bubble flow. Normally void fraction of the gas is very smaller than void fraction of the liquid. Therefore, in this section the void fraction is neglected. From the Eq. (2.19), the steady state one-dimensional flow can be written as;

$$\rho_G duA = const \quad (2.30)$$

From the Eq. (2.20);

$$\rho_L(1 - \alpha)uA = const \quad (2.31)$$

From the Eq. (2.16), momentum equation for two-phase flow with neglecting the gravity force is;

$$\rho_L(1 - \alpha)u \frac{\partial u}{\partial x} = -\frac{\partial P}{\partial x} \quad (2.32)$$

Assume the constant temperature;

$$\frac{P}{\rho_G} = const \quad (2.33)$$

From the Eq. (2.33);

$$\frac{1}{P} \frac{\partial P}{\partial x} - \frac{1}{\rho_G} \frac{\partial \rho_G}{\partial x} = 0 \quad (2.34)$$

From the Eq. (2.30);

$$\frac{1}{\rho_G} \frac{\partial \rho_G}{\partial x} + \frac{1}{\alpha} \frac{\partial \alpha}{\partial x} + \frac{1}{u} \frac{\partial u}{\partial x} + \frac{1}{A} \frac{\partial A}{\partial x} = 0 \quad (2.35)$$

From the Eq. (2.31);

$$-\frac{1}{1-\alpha} \frac{\partial \alpha}{\partial x} + \frac{1}{u} \frac{\partial u}{\partial x} + \frac{1}{A} \frac{\partial A}{\partial x} = 0 \quad (2.36)$$

From the Eq. (2.34) to Eq. (2.36);

$$-\frac{1}{P} \frac{\partial P}{\partial x} = -\frac{1}{\rho_G} \frac{\partial \rho_G}{\partial x} \quad (2.37)$$

$$= \frac{1}{\rho_G} \frac{\partial \rho_G}{\partial x} + \frac{1}{\alpha} \frac{\partial \alpha}{\partial x} + \frac{1}{u} \frac{\partial u}{\partial x} + \frac{1}{A} \frac{\partial A}{\partial x} \quad (2.38)$$

$$= \frac{1}{1-\alpha} \left(\frac{1}{u} \frac{\partial u}{\partial x} + \frac{1}{A} \frac{\partial A}{\partial x} \right) + \frac{1}{u} \frac{\partial u}{\partial x} + \frac{1}{A} \frac{\partial A}{\partial x} \quad (2.39)$$

$$= \frac{1}{\alpha} \left(\frac{1}{u} \frac{\partial u}{\partial x} + \frac{1}{A} \frac{\partial A}{\partial x} \right) \quad (2.40)$$

Substituting the Eq. (2.40) into the Eq. (2.32);

$$\rho_L(1-\alpha)u \frac{\partial u}{\partial x} = \frac{P}{\alpha} \left(\frac{1}{u} \frac{\partial u}{\partial x} + \frac{1}{A} \frac{\partial A}{\partial x} \right) \quad (2.41)$$

$$\frac{\rho_L \alpha (1 - \alpha)}{P} u \frac{\partial u}{\partial x} = \frac{1}{u} \frac{\partial u}{\partial x} + \frac{1}{A} \frac{\partial A}{\partial x} \quad (2.42)$$

$$\left[\frac{\rho_L \alpha (1 - \alpha)}{P} u^2 - 1 \right] \frac{1}{u} \frac{\partial u}{\partial x} = \frac{1}{A} \frac{\partial A}{\partial x} \quad (2.43)$$

$$\text{Then,} \quad a_{iso}^2 = \frac{P}{\rho_L \alpha (1 - \alpha)} \quad (2.44)$$

When the isothermal sound speed of Eq. (2.44) substitutes in to the Eq. (2.43), we obtain the Eq. (2.45) (混相流体の力学, 1989);

$$\left(1 - \frac{u^2}{a_{iso}^2} \right) \frac{1}{u} \frac{du}{dx} = - \frac{1}{A} \frac{dA}{dx} \quad (2.45)$$

Where a_{iso}^2 is the isothermal sound speed. Consider the case where the flow velocity reaches the sound speed at the throat and the flow becomes supersonic downstream of the throat. To simplify the calculation, it is assumed that the sound speed does not change downstream of the throat. Eq. (2.45) shows that the flow velocity increases downstream of the throat and it is the behavior of the compressive fluid. In the study the radius of the diverging section of the nozzle can be expressed as $r = r_0 + kx$. Therefore, cross-sectional area of the diverging section of the nozzle is;

$$A = \pi r^2 = \pi (r_0 + kx)^2 \quad (2.46)$$

$$\frac{dA}{dx} = 2\pi (r_0 + kx)k \quad (2.47)$$

The right side of the Eq. (2.45) becomes;

$$\frac{1}{A} \frac{dA}{dx} = \frac{2\pi(r_0 + kx)k}{\pi(r_0 + kx)^2} = \frac{2k}{r_0 + kx} \quad (2.48)$$

Therefore,

$$\left(1 - \frac{u^2}{u_{th}^2}\right) \frac{1}{u} \frac{du}{dx} = -\frac{2k}{r_0 + kx} \quad (2.49)$$

$$\ln u - \frac{1}{2} \frac{u^2}{u_{th}^2} = -2 \ln(r_0 + kx) + c \quad (2.50)$$

$$\ln u(r_0 + kx)^2 = \frac{1}{2} \frac{u^2}{u_{th}^2} + c \quad (2.51)$$

$$u(r_0 + kx)^2 = A e^{\frac{1}{2} \frac{u^2}{u_{th}^2}} \quad (2.52)$$

If $x=0$ and $u=u_{th}$, the Eq. (2.52) will become;

$$u_{th} r_0^2 = A e^{\frac{1}{2}} \quad , \quad A = u_{th} r_0^2 e^{-\frac{1}{2}} \quad (2.53)$$

$$u(r_0 + kx)^2 = u_{th} r_0^2 e^{\frac{1}{2} \left(\frac{u^2}{u_{th}^2} - 1\right)} \quad (2.54)$$

$$u(r_0 + kx)^2 = u_{th} r_0^2 \left\{ 1 + \frac{1}{2} \left(\frac{u^2}{u_{th}^2} - 1\right) + \frac{1}{4} \left(\frac{u^2}{u_{th}^2} - 1\right)^2 + \dots \right\} \quad (2.55)$$

$$u(r_0 + kx)^2 \cong u_{th} r_0^2 \left(\frac{1}{2} + \frac{1}{2} \frac{u^2}{u_{th}^2} \right) \quad (2.56)$$

$$u(r_0 + kx)^2 = \frac{u_{th} r_0^2}{2} + \frac{r_0^2}{2u_{th}} u^2 \quad (2.57)$$

Equation (2.57) becomes;

$$\frac{r_0^2}{2a} u^2 - u(r_0 + kx)^2 + \frac{u_{th} r_0^2}{2} = 0 \quad (2.58)$$

$$u = \left(\frac{r_0 + kx}{r_0}\right)^2 u_{th} \pm \sqrt{\left(\frac{r_0 + kx}{r_0}\right)^4 u_{th}^2 - u_{th}^2} \quad (2.59)$$

The velocity ratio for the supersonic two-phase flow is;

$$\frac{u}{u_{th}} = \left(\frac{r_0 + kx}{r_0}\right)^2 \pm \sqrt{\left(\frac{r_0 + kx}{r_0}\right)^4 - 1} \quad (2.60)$$

Consider the case where the flow velocity does not reach the sound speed at the throat and the flow is subsonic downstream of the throat. To simplify the calculations, assuming incompressible fluids;

$$Q = uA = const = u_{th} A_{th} \quad (2.61)$$

$$A = \pi(r_0 + kx)^2, \quad A_{th} = \pi r_0^2 \quad (2.62)$$

The velocity ratio for subsonic flow is;

$$\frac{u}{u_{th}} = \frac{A_{th}}{A} = \frac{r_0^2}{(r_0 + kx)^2} \quad (2.63)$$

The pressure equation for supersonic and subsonic two-phase flow is;

$$\frac{\rho_L}{2} u^2 + P + \frac{\alpha_0}{1 - \alpha_0} P_{th} \ln P = const \quad (2.64)$$

Where α_0 is very small. Therefore, Eq. (2.64) is written as;

$$P = P_{th} + \frac{1}{2}\rho_L u_{th}^2 - \frac{1}{2}\rho_L u^2 \quad (2.65)$$

$$P = P_{th} + \frac{1}{2}\rho_L u_{th}^2 \left[1 - \left(\frac{u}{u_{th}} \right)^2 \right] \quad (2.66)$$

Theoretical estimation for subsonic and supersonic two-phase flow is calculated by using Eq. (2.66) and compare with the experimental result pressure. However, u/u_{th} for supersonic velocity ratio is calculated by using Eq. (2.60) and u/u_{th} for subsonic velocity ratio is calculated by using Eq. (2.63).

2.11. Calculation of CO₂ dissolved gas rate and void fraction at the throat

Carbon dioxide gas can dissolve well in water. CO₂ dissolved gas rate is 0.88 cm³ under the atmosphere pressure at 20°C. CO₂ dissolved gas rate at the throat could be calculated by using that relationship. The more CO₂ rate was increase, the more dissolved gas rate was observed at the throat. The volume of gas at the throat was obtained from the Eq. (2.67).

$$\frac{P_{th} V_G}{T} = nR \quad (2.67)$$

Where, nR is constant and can be obtained by the CO₂ dissolved rate under the atmosphere at 20°C, T is the room temperature and P_{th} is the pressure at the throat. The void fraction at the throat is the ratio of the volume of the gas by the total volume of the liquid and gas and it was calculated by using Eq. (2.68).

$$\alpha = \frac{V_G}{V_L + V_G} \quad (2.68)$$

The calculation void fraction was used for comparison with the experimental void fraction. From the results, the calculation void fraction was larger than the experimental void fraction. To get the calculation void fraction result it was needed to take time. However, the experiments were done within 60 seconds. Therefore, the experimental void fraction was smaller than the calculation void fraction.

2.12. Sound speed in homogeneous two-phase flow

The adiabatic sound speed and the isothermal sound speed of a homogeneous two-phase flow were calculated by Eq. (2.69) and (2.70), respectively. Here, γ is specific heat ratio. In the study, the void fraction is estimated to be lower than 0.5 because of the micro-bubble two-phase flow. In the range of the void fraction, the sound speed decreases as the void fraction increases. Therefore, the orifice is expected to help for the flow to reach its sound speed at the throat because the micro-bubbles are generated by the pressurized dissolution method.

$$a_{ad} = \sqrt{\frac{\gamma P_{th}}{\alpha(1-\alpha)\rho_L}} \quad (2.69)$$

$$a_{iso} = \sqrt{\frac{P_{th}}{\alpha(1-\alpha)\rho_L}} \quad (2.70)$$

2.13. Calculation of velocity slip ratio

Velocity slip ratio in the gas–liquid two-phase flow, is defined as the ratio of the velocity of the gas phase to the velocity of the liquid phase. In the homogeneous

model of two-phase flow, the velocity slip ratio is assumed to be unity (no slip). It is however experimentally observed that the velocity of the gas and liquid phases can be significantly different, depending on the flow pattern. The velocity slip ratio S of the two-phase flow was calculated by using Eq. (2.71).

$$S = \frac{u_B}{u_{th}} \quad (2.71)$$

Where u_B is bubble velocity and u_{th} is liquid velocity.

2.14. Fractional pressure loss

The method of Lockhart and Martinelli is the original method that predicted the two-phase frictional pressure loss based on two-phase multiplier of the gas and liquid (Lockhart, 1949). To calculate the pressure loss of the nozzle. Firstly, the Reynolds number is should be calculated by using Eq. (2.72). Assume that homogeneous flow in the study.

$$Re = \frac{uD}{\nu_L} \quad (2.72)$$

Gas and liquid phase fractional pressure drop are obtained with Eq. (2.73) and Eq. (2.74).

$$\Delta P_G = -\frac{dp}{dz} = \lambda \frac{1}{D} \frac{1}{2} \rho_G u^2 \quad (2.73)$$

$$\Delta P_L = -\frac{dp}{dz} = \lambda \frac{1}{D} \frac{1}{2} \rho_L u^2 \quad (2.74)$$

Lockhart-Martinelli parameter is defined as;

$$X^2 = \frac{\Delta p_L}{\Delta p_G} \quad (2.75)$$

Chisholm parameter turbulence-turbulence flow is $C=21$ and two-phase flow friction loss multiplication factor is;

$$\phi_L^2 = 1 + \frac{C}{X} + \frac{1}{X^2} \quad (2.76)$$

Pressure loss for two-phase flow is;

$$\Delta P_{TP} = \phi_L^2 \Delta P_L \quad (2.77)$$

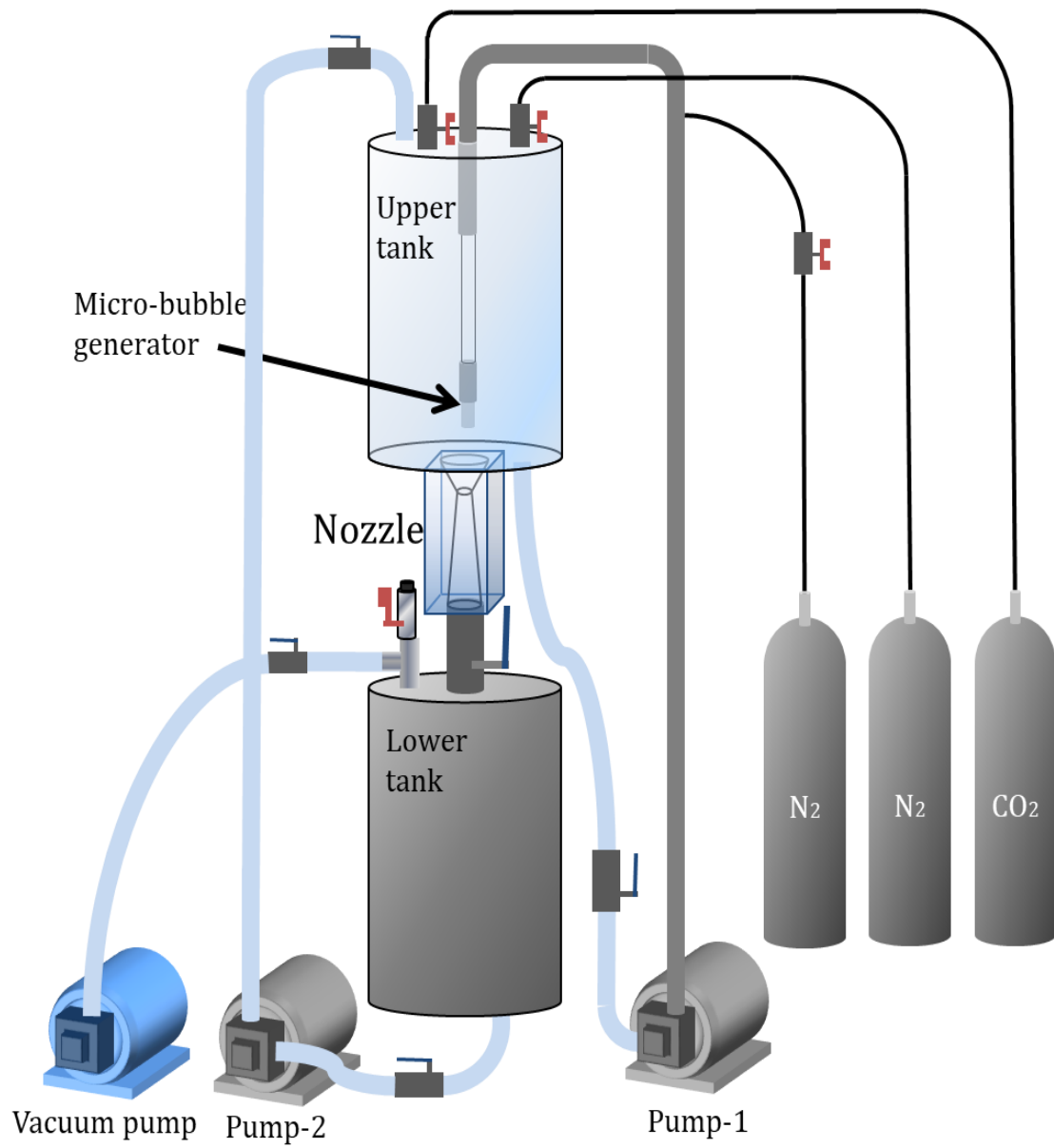


Figure 2.1. Experimental apparatus.



Figure 2.2. Photo of experimental apparatus.

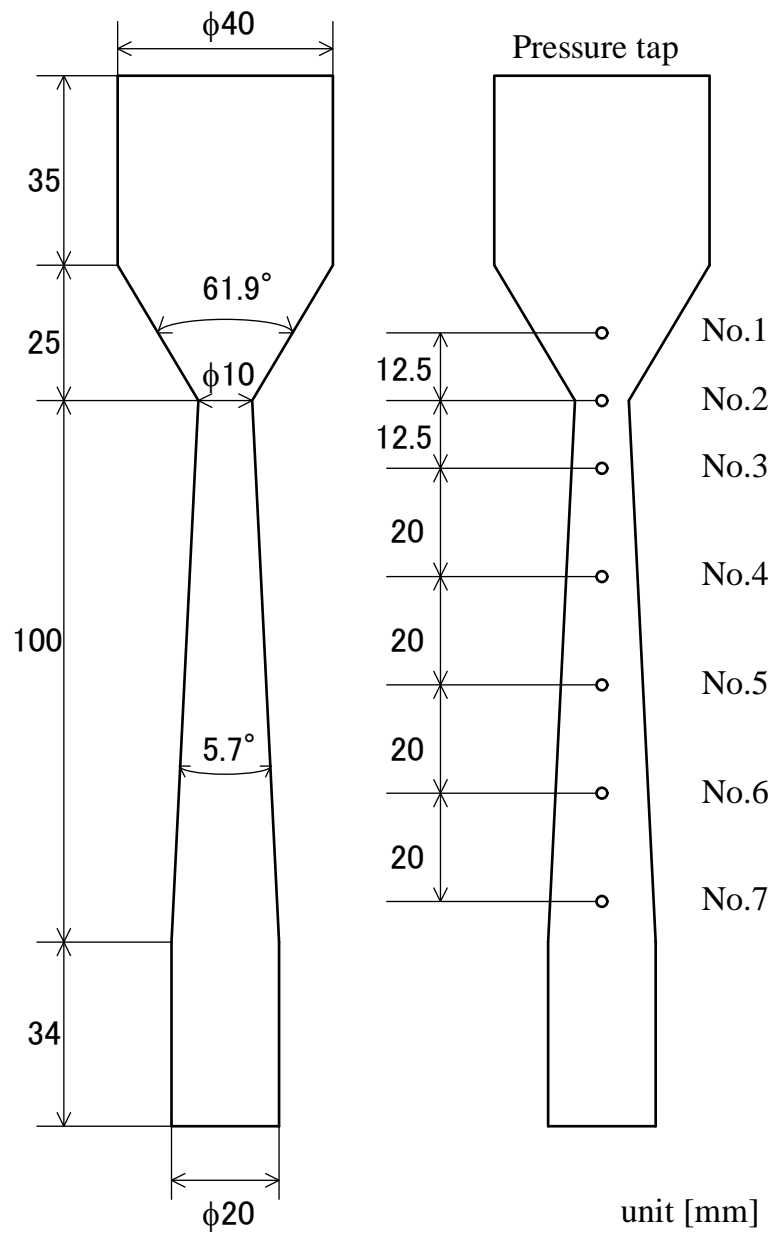
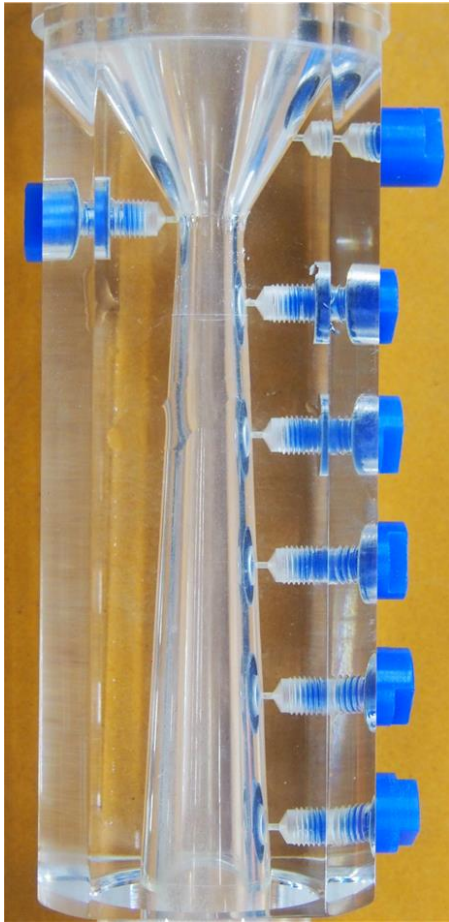


Figure 2.3. Converging-diverging nozzle.



(a) Nozzle I (with pressure taps)



(b) Nozzle II (without pressure taps)

Figure 2.4. Photo of the two-phase flow nozzles.

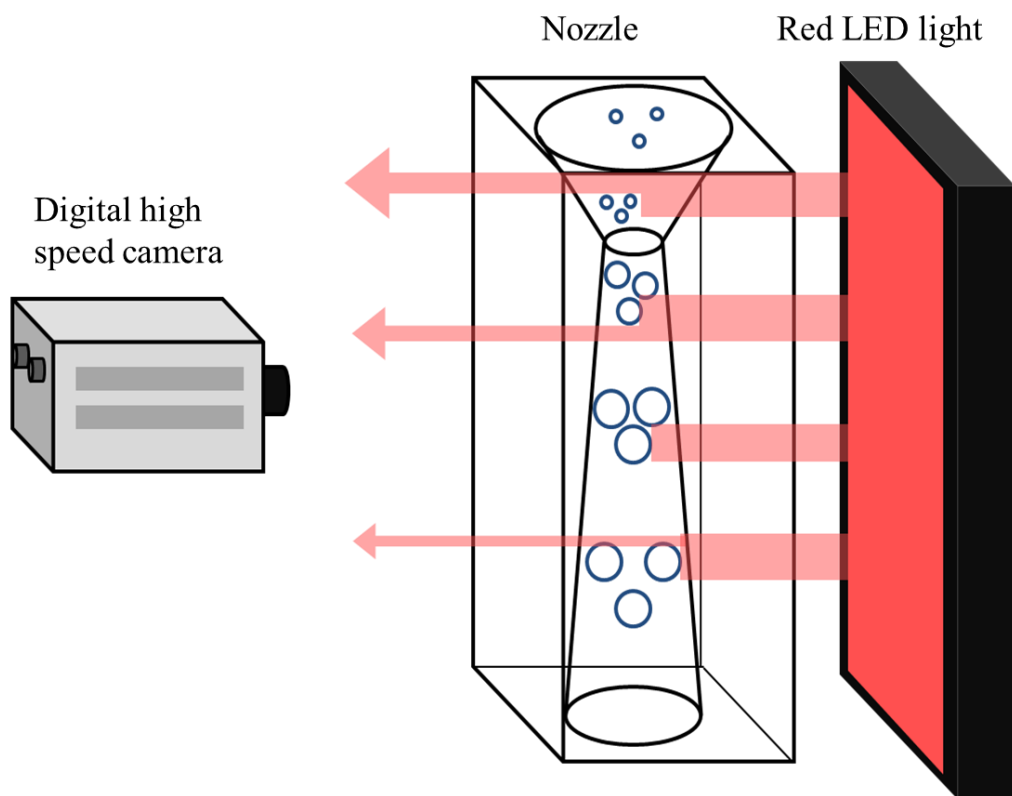


Figure 2.5. Method of taking photo for the flow.

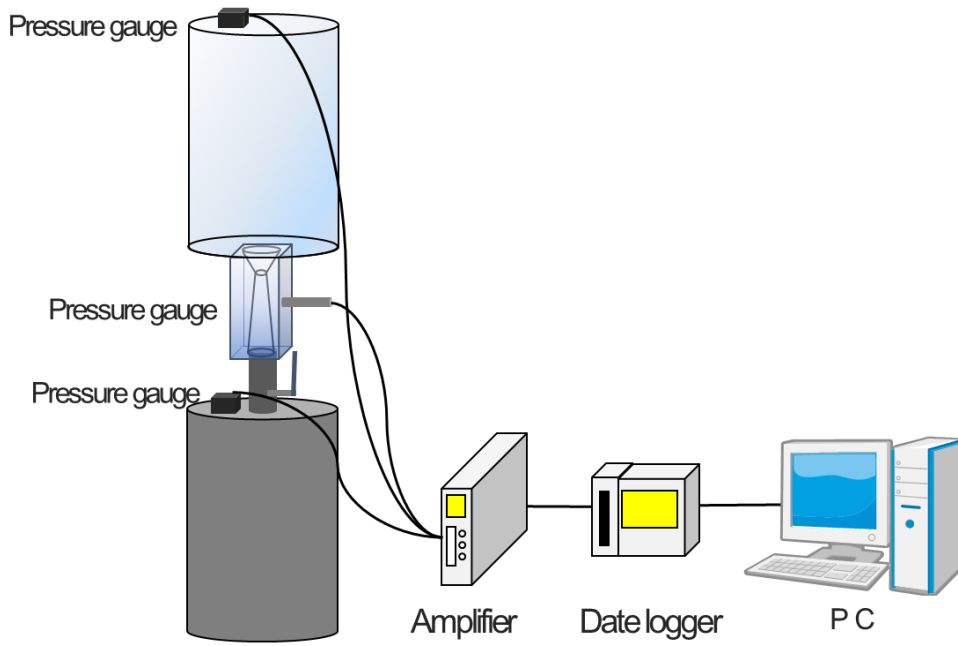


Figure 2.6. Measurement of the pressure.

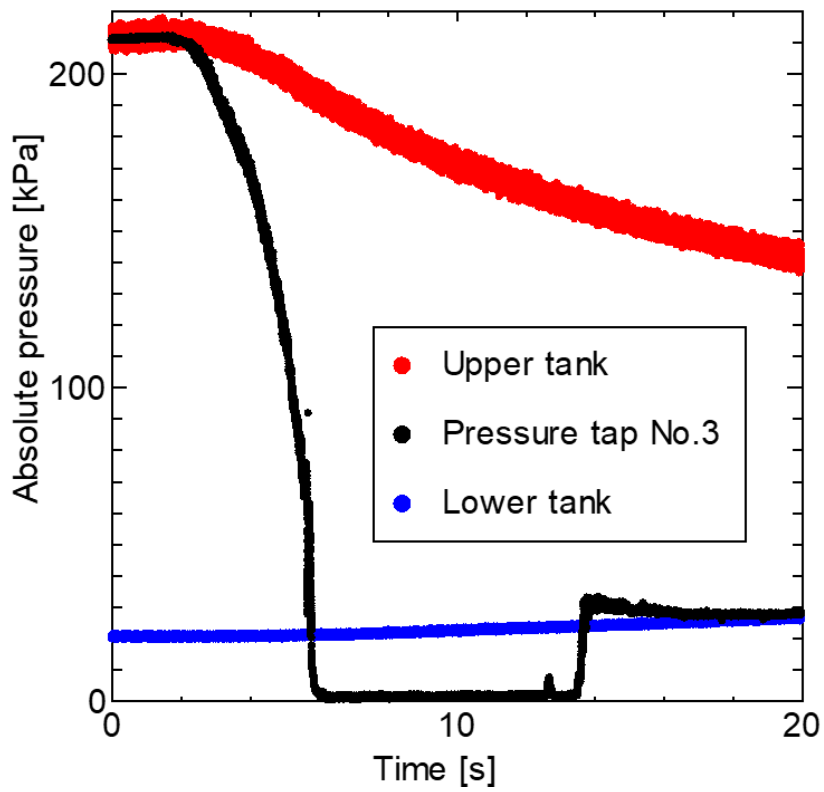


Figure 2.7. Example of quasi-steady flow.

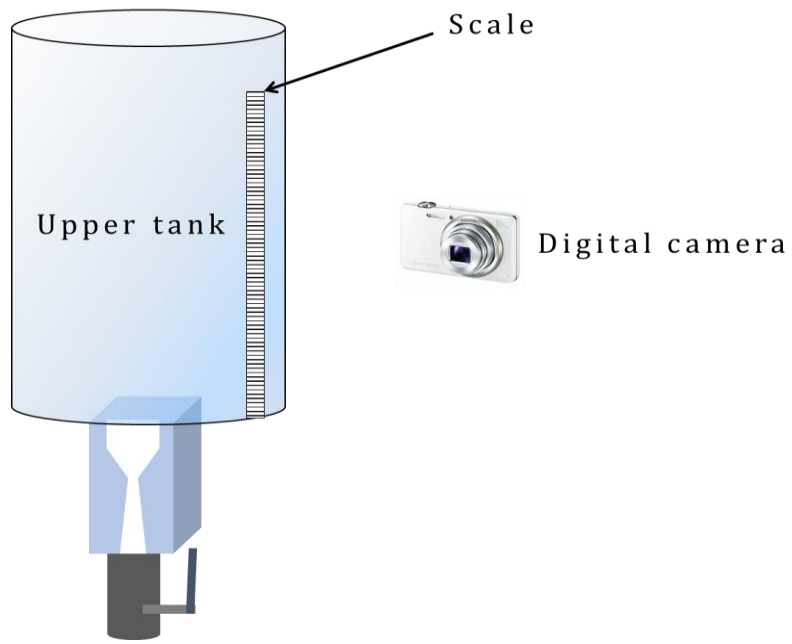


Figure 2.8. Scale of the upstream water tank.

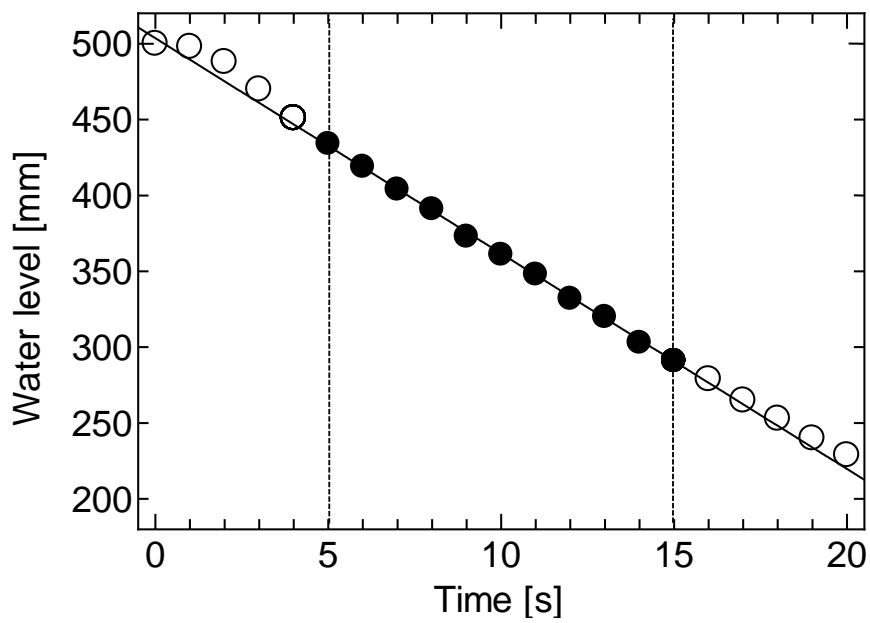


Figure 2.9. Example of time change of water level in the upper tank.

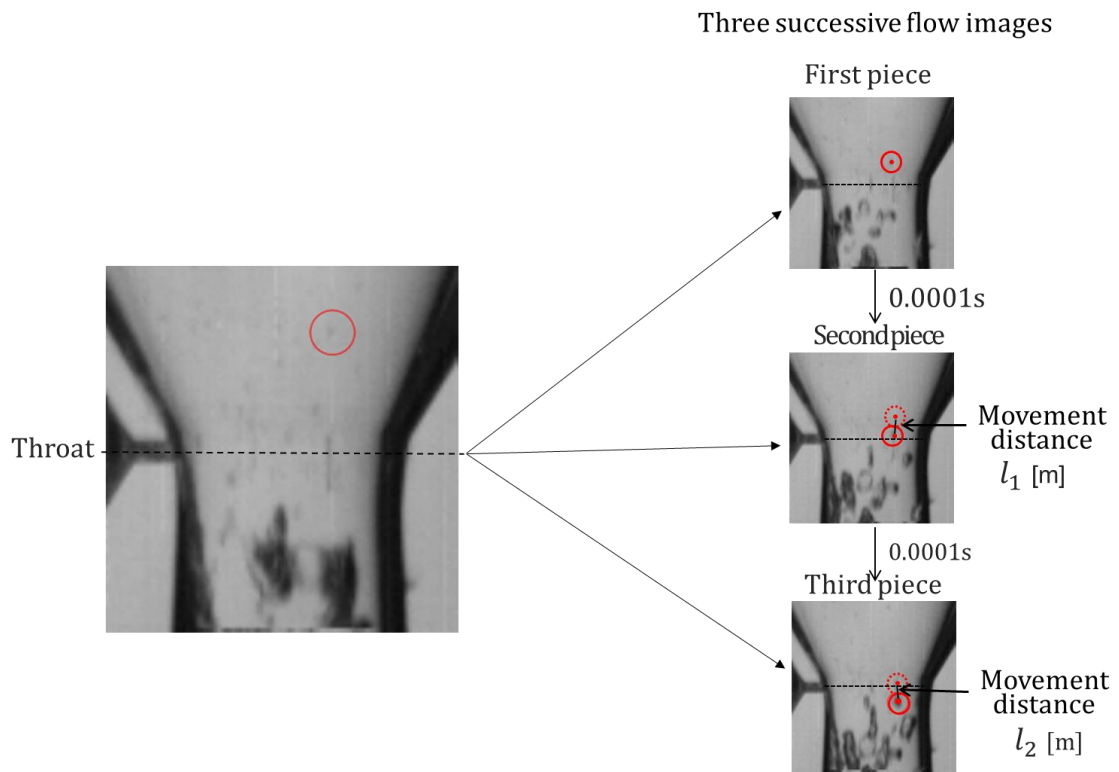


Figure 2.10. Three successive flow images at the throat.

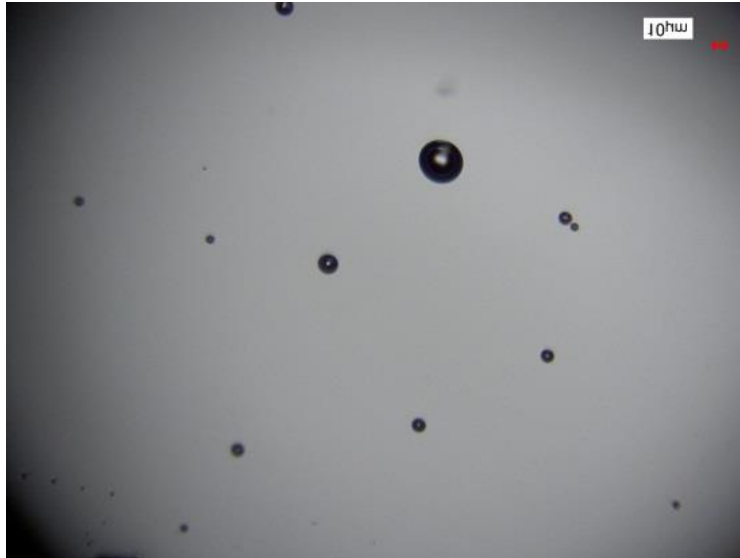


Figure 2.11. The photo of micro-bubble by the microscope.

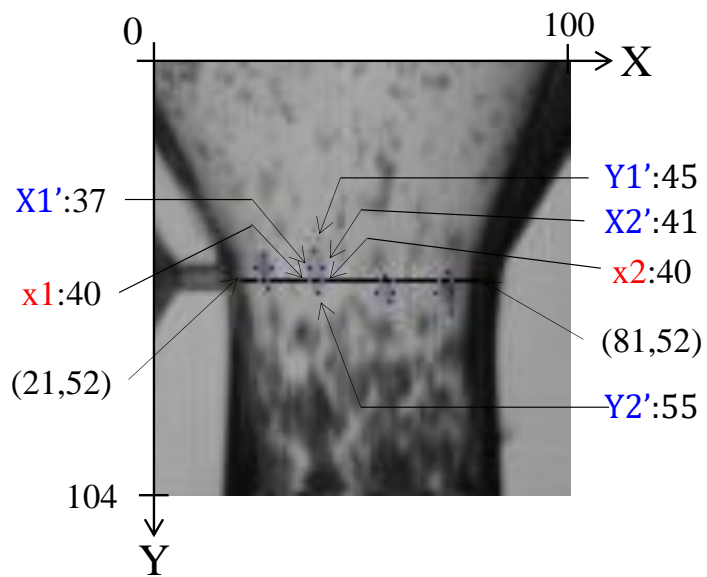


Figure 2.12. Example of bubble diameter measurement at the throat.

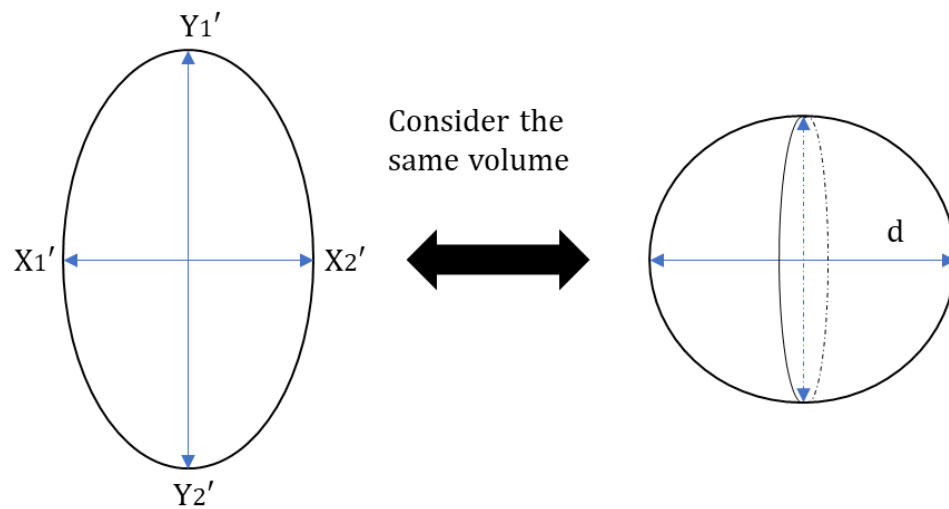


Figure 2.13. Equivalent bubble diameter.

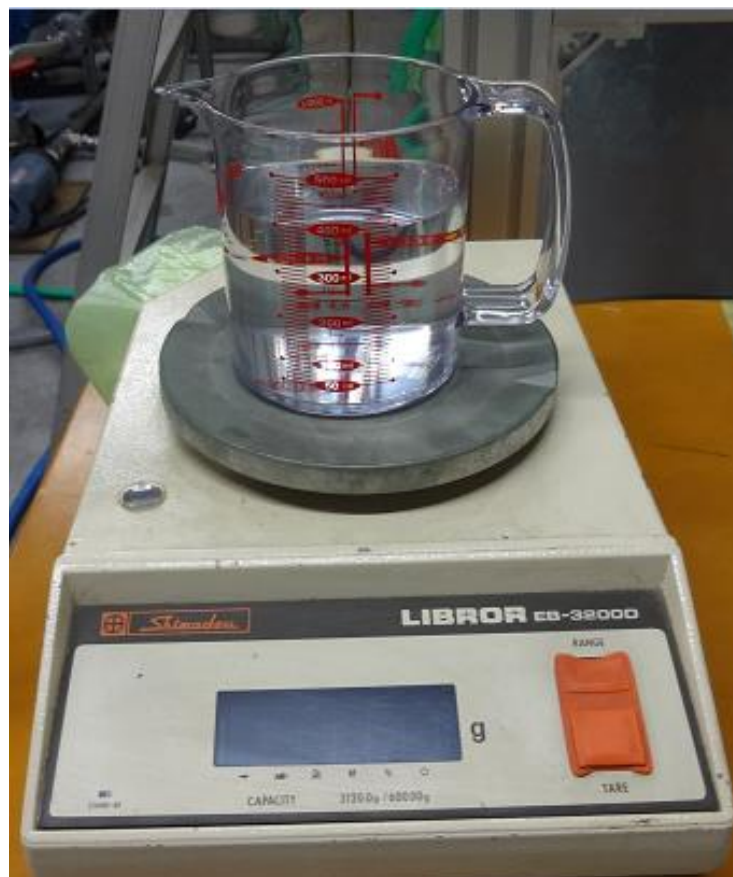


Figure 2.14. Measurement of void fraction for the micro-bubble generator process.

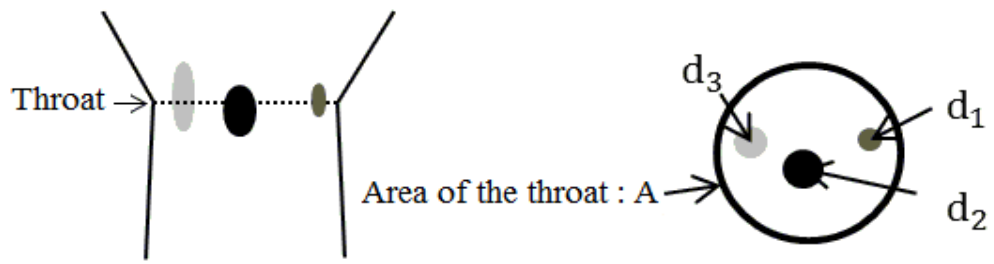


Figure 2.15. Schematic diagram of the instantaneous void fraction on cross section at the throat.

Chapter 3

Micro-Bubble Generator and Millimeter-Bubble Generator

3.1. Experimental procedure

3.1.1. Experiment with micro-bubble generator

A swirling-type of micro-bubble generator is a device that can generate high void fraction bubbly flows which are dominated by very small micro size bubbles shown in Fig. 3.1. Previous research was carried out by swirling-type micro-bubble generator. The micro-bubble generator used in this research was provided by Professor Harumichi Kyotoh (Yamada, 2005). The schematic micro-bubble generator with length 50 mm and width 25 mm is shown in Fig. 3.2. The micro-bubble generator includes a structure to swirl the gas and liquid flow under pressure into a circular vane channel to form a swirl-up flow at the periphery of divergent section and two-phase flow is provided as swirl-down flow. Swirling two-phase flow is controlled by the number of vanes, vane angle and vane channel depth of the vane swirler. Micro-bubble generation is enhanced by the vortex breakdown nozzle. The mechanism of vortex breakdown nozzle is induced by the coanda effect (Yamada, 2005). When a moving stream of fluid is contacted with a curved surface, it will tend to flow along the curvature of the surface rather than in a straight line. This phenomenon is coanda effect. Micro-bubble generator was connected with the static mixer (Fig. 3.3). The size of the static mixer of length and diameter are 100 cm and 2 cm. When the flow passes through the static mixer, it allows the gas to mix and dissolve into the water and the mixed water leads to the micro-bubble generator. The energy is needed for mixing of the gas into the pressure loss water when the fluid flows through the static mixer. The energy obtains by the pump-1 shown in Fig. 3.4.

The micro-bubble generator was installed in the upper tank, and nitrogen gas

was used as the gas phase and water was as the liquid phase. Firstly, the pressure of the nozzle, upper and lower tank were set up to 101 kPa (atmospheric pressure) and the result was recorded. Nitrogen gas was fed from the upper tank to the nozzle and the lower tank until to reach 190 kPa by a manometer and the data was also recorded. Then the gas was allowed to the atmosphere from the valve of the lower tank. These two steps were used for the calibration of the experimental data. After these two steps for calibration, the upper tank was supplied about 0.050 m³ water and pressurized by nitrogen gas according to the experimental condition. The lower tank was decompressed by using the water seal vacuum pump according to the experimental condition. The micro-bubbles were generated in the upper tank by the micro-bubble generator with the nitrogen gas from the cylinder (nitrogen gas cylinder in Fig. 3.4) and the water was circulated by the pump-1 (pump-1 in Figure 3.4). The micro-bubble generator was operated until the micro-bubbles generated fully. The experiment began by opening the valve downstream of the nozzle after setting the experimental condition.

3.1.2. Experiment with millimeter-bubble generator

Sintered alloy is used as a method to generate millimeter-bubbles shown in Fig. 3.5. Sintered alloy is an alloy which has many small holes. The nitrogen gas and water were used as working fluids. The millimeter-size bubbles are generated by using nitrogen gas. Nitrogen gas is injected into water through a sintered metal with 100 micrometer diameter of holes and millimeter-size bubbles are generated.

It was located near the inlet of the nozzle. The calibration steps and experimental procedure are the same as micro-bubble generator (section 3.1.1). The experiment began by opening the valve downstream of the nozzle (Fig. 3.6) after setting the experimental condition.

3.2. Experimental condition

The detail information of the experimental conditions is shown in Table 3.1. In the experimental conditions No.1 to No.6, the micro-bubble generator was used to generate the micro-bubbles. In the experimental condition No.1 the upper tank pressure P_U was atmospheric pressure (101 kPa) and lower tank pressure P_L was 50 kPa. The pressure difference P_D was 50 kPa. The experimental condition No.2 was also the upper tank pressure 101 kPa and lower tank pressure 20 kPa. The upper tank pressure of the experimental conditions No.3 and No.4 were set as constant 200 kPa, however the lower tank pressures were changed 101 kPa and 20 kPa. In the experimental conditions No.5 and No.6, the upper tank pressures were 301 kPa and lower tank pressures were set as 101 kPa and 20 kPa. The experimental conditions No.7 and No.8 used the millimeter-bubble generator. The upper tank pressures were set to atmospheric pressure and the lower tank pressure were changed to 50 kPa and 20 kPa.

3.3. Flow visualization

The flow pattern in the nozzle was taken by the high-speed camera. The flows images are over the entire nozzle and the close-up image at the throat. The image over the entire nozzle was taken at every 1ms to show the flow along the nozzle and is used to analyze the flow along the nozzle. The image at the throat was taken at every 0.1 ms to observe the magnification of the flow around the throat and to analyze the appearance of bubbles. The bubbles can be seen as a dark portion of the nozzle because the back light was scattered at the gas-liquid interface of a bubble and did not reach the video camera (Itamoto, 2011).

The flow under the experimental conditions No.1 to No.6 with micro-bubble generator and the experimental conditions No.7 and No.8 with millimeter-bubble

generator experiments were shown in Fig. 3.7. Under the experimental condition No.1 the dark part of the flow would be seen between the throat and the middle of the nozzle. The reason why the dark part was seen in the flow images was considered that the bubbles were expanded and the back light was covered by the large bubbles. Upstream of the throat, there were micro-bubbles but the back light could reach the high speed video camera because of small size of the bubbles. At the throat, the pressure decreased due to the high flow velocity caused by the small cross section of the flow channel. Therefore, micro-bubbles were expanded due to the low pressure at the throat. The pressure was low until the middle of the nozzle and increased in the latter half of the nozzle. The flow image corresponded to the pressure distribution, i.e., the flow image was dark due to the large bubbles until the middle of the nozzle and it was bright in the latter half of the nozzle. The same $P_U=101$ kPa and P_D changed to 80 kPa the dark park was observed from the throat to the exit of nozzle in the experimental condition No.2. When the P_U changed to 201 kPa and P_D was 100 kPa in the experimental condition No.3, the dark portion was obtained from the throat to the middle of nozzle. However, the dark section was observed along the downstream of the throat when P_D increased to 180 kPa in the experimental condition No.4. Even though the upper tank pressure was more increase to 301 kPa and the P_D was 200 kPa in the experimental condition No.5, the formation of dark part was almost the same with the experimental condition No.3 ($P_D=100$ kPa). When the P_D increased to 280 kPa in the experimental condition No.6, the dark part was observed from the throat to the exit of nozzle because the bubbles were large. Therefore, the bubble behavior depended on the upper tank pressure and lower tank pressure. Because the large bubbles were more observed when decreasing lower tank pressure in the case of the same upper tank pressure. The flow pattern of millimeter-bubble generator was also shown in Fig. 3.7. The more P_D increased to 80

kPa in the experimental condition No.8 the more millimeter-bubbles were observed at the diverging section than the experimental condition No.7. When the comparison of the flow pattern of the micro-bubble generator and millimeter-bubble generator, the supersonic flow with the micro-bubble was very homogeneous and stable compared with the millimeter-bubble flow.

3.4. Pressure profile along the nozzle

The pressure was measured with the sampling frequency (2 kHz) and the sampling number was 120000 points in 60 seconds. The average pressure was taken in quasi-steady state (ten seconds after starting the experiment). The data were taken from the seven pressure measuring taps of the main nozzle. The pressure profiles along the nozzle is the time average in the quasi-steady state. Some of the experiments the absolute pressure at the downstream of the nozzle is became negative. The reason why the value was negative may be that the pressure sensor was pulled by the flow and the measurement of the pressure could not be done correctly. In the case of negative pressure, it was not shown in the experimental results.

Figure 3.8 and Figure 3.9 show the pressure profiles along the nozzle under the experimental condition No.1 to No.6 with micro-bubble generator. In the experimental condition No.7 and No.8 of the millimeter-bubble generator experiments, the pressure could not be measured exactly because the pressure fluctuation was large. In the experimental condition No.1, the pressure kept low but it increased in the middle of the nozzle. That was why, after the throat the flow was expected to be supersonic flow and then it changed to subsonic flow from the middle of the nozzle. In the experimental condition No.2, the pressure kept it as a constant decreased pressure to the downstream of the throat. It was expected that supersonic flow condition. When the comparison of

the experimental condition No.1 and No.2, there were the same P_U and different P_L . However, the experimental condition No.1 was expected the combination of the supersonic and subsonic flow. Then, the experimental condition No.2 was only supersonic flow. Both of the two flow conditions were observed as supersonic flow with the same pressure at the throat. Therefore, we observed that even though the same P_U and different P_L of the experimental conditions with the supersonic flow, the pressure were not varied too much at the throat.

The experimental condition No.3 and No.4 were also the same $P_U=201$ kPa and different P_L as 101 kPa and 21 kPa. The pressure at the throat were almost the same with supersonic flow conditions. However, the experimental condition No.3 changed to subsonic flow because of increasing pressure from the middle of the nozzle. The pressure kept low but increased again in the middle of the nozzle, in the experimental condition No.5. It was considered that the flow was supersonic after the throat but it was changed to subsonic in the diverging section, based on the pressure distribution. The low pressure area of the experimental condition No.6 was larger than that of the experimental condition No.5. Between the two conditions, the pressure was the same in the upper tank but different in the lower tank. The lower pressure condition in the lower tank kept low pressure in the longer area. Based on keeping the low pressure in where the diverging section, the flow was expected as supersonic.

3.5. The comparison of the flow rate, liquid velocity and bubble velocity at the throat

The comparison of the flow rate, liquid velocity and bubble velocity at the throat for micro-bubble generator and millimeter-bubble generator experiments are shown in Fig. 3.10. The water level changed almost linearly with time and the flow rate can be obtained from the inclination of the water level to time. The result of the flow

rate was obtained by using Eq. (2.1). When increasing pressure difference between the upper tank and lower tank, which could cause the flow rate increased slightly. Furthermore, the averaged liquid velocity on the cross-sectional at the throat was obtained from the water flow rate.

The liquid velocity at the throat was also calculated by using the flow rate and the void fraction at the throat. The liquid velocity at the throat of the nozzle was calculated by using Eq. (2.2). As choking phenomenon occurs at the throat of the nozzle, the flow rate is no longer changed even by increasing the differential pressure between the upper tank and the lower tank as the experimental condition No.1 and No.2, the experimental condition No.3 and No.4, the experimental condition No.5 and No.6. Since the choking phenomenon has occurred, flow velocity reaches the sound speed at the throat of the nozzle. A single bubble velocity was obtained as an averaged velocity by using three successive flow images at the throat by using Eq. (2.3). The average bubble velocity was calculated as the average of 50 bubbles in each experimental condition by using Eq. (2.4).

The same upper tank pressure, difference lower tank pressure and increase the pressure difference of the experimental conditions No.1 and No.2, No.3 and No.4, No.5 and No.6 were almost the same flow rate, liquid velocity and bubble velocity at the throat. However, the flow rate, liquid velocity and bubble velocity were increased in the experimental conditions of No.2, No.4 and No.6, when increasing upper tank pressure, the same lower tank pressure and increasing the pressure difference. Therefore, the upper tank pressure and pressure difference depended on the flow rate and liquid velocity and bubble velocity at the throat. When the pressure difference increased 50 kPa to 80 kPa in the millimeter-bubble generator experiments of No.7 and No.8, the flow rate increased slightly and the difference of the bubble velocity and liquid velocity

at the throat also increased. The liquid velocity at the throat and the flow rate was not proportional to the differential pressure between the upper tank and the lower tank.

3.6. Measurement of bubble size distribution

The diameters of the micro-bubbles were measured when the micro-bubbles were fully generated in the upper tank at the atmospheric pressure for the micro-bubble generator experiments. For 65 bubbles, the equivalent diameter of bubbles was 7.313 μm and its standard deviation was 9.417 μm . The millimeter-size bubble diameter was measured by process images of high-speed camera. For 158 bubbles, the equivalent diameter of bubbles was 11.279 mm and its standard deviation was 15.554 mm. The distribution of the bubble diameter for micro-bubble and millimeter-size bubble are shown in Fig. 3.11 (a) and (b) respectively.

3.7. Void Fraction at the throat

The void fraction was measured when the bubbles were generated at the atmospheric pressure in the micro-bubble generator experiments. The water including micro-bubbles was taken 400 ml to 500 ml after micro-bubbles were generated fully from the upper tank. The mass and the water temperature were measured and instantaneous void fraction was calculated by using Eq. (2.7). The void fraction at the throat was obtained by Eq. (2.9) under the assumption of the velocity slip was not occurred at the throat in the calculation of the void fraction at the throat. When increasing pressure difference P_D , void fraction also increased as described in Fig. 3.12. The relative precision index of the void fraction measurement was 95% coverage. At the moment when millimeter-bubbles occurred in the water, it was assumed that there was no slip with the liquid phase. The instantaneous void fraction was calculated by using

Eq. (2.10). In experiment condition No.7, the average of the measurement of the initial void fraction of six times was 0.0078, and the standard deviation was 0.000035. In the experiment condition No.8, the average of the measurement of the initial void fraction of six times was 0.0078, and the standard deviation was 0.000020.

3.8. Velocity distribution along the nozzle

Liquid velocity distribution along the nozzle were calculated by using the Bernoulli equation represented in Eq. (2.29) based on the initial pressure, throat pressure and void fraction at the throat. The results are shown in Fig. 3.13 and Fig. 3.14. Figure 3.13 represents for the experimental condition No.1 to No.3. In the experimental condition No.1 and No.2 the same $P_U=101$ kPa and different P_L as 51 kPa and 21 kPa, the velocities at the throat were almost the same. However, the velocity of the experimental condition No.1 decreased from the pressure tap No.4 to the exit of nozzle because of the increasing pressure from that point. The velocity of the experimental condition No.2 kept constant until the exit of nozzle. In the experimental condition No.3, the velocity increased and then decreased from the pressure tap No.4 to the exit of nozzle.

Figure 3.14 shows for the experimental condition No.4 to No.6. In the experimental condition No.4, the velocity increased continuously from the throat to the exit of the nozzle because of decreasing pressure from the throat to the exit of nozzle. In the experimental conditions No.5 and No.6, the velocities were increase from the throat. However, the velocity of the experimental condition No.5 slightly decreased from the pressure tap No.6 because of the effect of the lower tank pressure.

3.9. The comparison of pressure distribution between the experimental and theoretical estimation of subsonic and supersonic flow

The pressure for the supersonic and subsonic conditions of each experiments were calculated by using Eq. (2.65). The experimental results of the pressure and void fraction at the throat were used for the calculation. However, the velocity ratio for each conditions were different. The velocity ratio was used the Eq. (2.60) for supersonic condition and the velocity ratio was used the Eq. (2.63) for subsonic condition. Figure 3.15 (a)-(f) represents the comparison of the pressure distribution along the diverging part between the experiment and theoretical estimation of the subsonic and the supersonic flow of the experimental condition No.1 to No.6. In the experimental condition No.1 the experimental pressure kept to supersonic condition downstream of the throat and then it closed to the subsonic condition from the middle to the exit of the nozzle. Its means that the pressure changed from supersonic to subsonic flow condition. The experimental pressure of the experimental condition No.2 was kept to supersonic pressure condition from the throat to the exit of the nozzle. Experimental conditions No.1 and No.2 were the same $P_U=101$ kPa but different $P_L=51$ kPa and 21 kPa. In these two experimental conditions when decreasing the lower tank pressure, the experimental pressure kept to the supersonic condition. In the experimental conditions No.3 and No.4, the pressure were also the same $P_U=201$ kPa but different $P_L=101$ kPa and 21 kPa. The experimental pressure of the experimental condition No.4 kept to supersonic condition to the exit of the nozzle. However, the pressure of the experimental condition No.3 kept to subsonic condition near the end of the nozzle. The pressure of the experimental condition No.6 was continuously decreased to the supersonic condition and the pressure of the experimental condition No.5 slightly increased at the end of the nozzle.

3.10. The comparison of liquid velocity and sound speed at the throat

The adiabatic sound speed and the isothermal sound speed assuming a homogeneous two-phase flow was calculated by Eq. (2.69) and (2.70), respectively. Figure 3.16 shows the result of the liquid velocity of the experimental value and the sound speeds calculated at the throat. The liquid velocities estimated by the experiment are larger than the isothermal sound speed and smaller than the adiabatic sound speed at experimental conditions No.1 to No.6. The real sound speed is also between the adiabatic and isothermal sound speed because the gas shows the polytrope change in the flow. Therefore, it can be estimated that the liquid velocity reached the sound speed at the throat and the flow became supersonic downstream of the throat.

3.11. Velocity slip ratio

Velocity slip ratio was calculated by Eq. (2.71). Figure 3.17 shows the result of velocity slip ratio of the experimental conditions No.1 to No.8 with micro-bubble generator process and millimeter-bubble generator process. When increasing pressure difference between the upper tank pressure and lower tank pressure, the less velocity slip ratio was observed in the experimental conditions No.1 to No.6. When the pressure difference was increased 150 kPa to 180 kPa in the millimeter-bubble generator process of the experimental conditions No.7 and No.8, the more millimeter-bubble was observed, and velocity slip ratio was increased.

3.12. The comparison of pressure loss and void-fraction at the throat

Pressure loss at the throat was calculated by using Eq. (2.77) of Lockhart and Martinelli method and compare with the void fraction at the throat. The results are shown in Fig. 3.18 and Fig. 3.19. When increasing pressure difference, void fraction

would increase, and pressure loss also increase. Because of increasing bubble formation at the throat.

3.13. Concluding remarks

In order to reduce the velocity slip and to improve the conversion efficiency of the supersonic nozzle, micro-bubble two-phase flow was attempted to be used as the working fluids. By the blow-down experiment of the micro-bubble generator and millimeter-bubble generator of the two-phase flow nozzle, the following findings were obtained:

- i. Based on the flow images, the pressure and velocity distribution, it was confirmed that the micro-bubble two-phase flow generated by using a vortex breakdown mechanism became supersonic in the diverging section in the nozzle.
- ii. In some cases, the flow changed to subsonic in the middle of the nozzle where the shock wave was observed.
- iii. The pressure could not measure correctly at the millimeter-bubble generator experiments because the pressure sensor was pulled by the flow. Therefore, the fluctuation of the pressure waves was too large. The bubble velocity increased when increasing pressure difference, it was caused the velocity slip increased.
- iv. In the throat of the nozzle, the velocity slip of micro-bubble was smaller than velocity slip of millimeter-bubble.
- v. The supersonic flow with the micro-bubble was very homogeneous and stable compared with the millimeter-bubble flow.

The study in Chapter 3 was reported in the reference,

1. Nakamura, K., Khine Tun Naung, Monji, H., Study on Supersonic Nozzle Flow with Micro Bubbles, *J. JSEM*, 14-Special Issue, s88-s93, 2014.
2. Hideaki Monji, Khine Tun Naung, Kentaro Nakamura, Rei Mikoshiha, Micro-Bubble Two-Phase Flow in Converging-Diverging Nozzle, *Japan-US Seminar on Two-Phase Dynamics*, May, 2015.
3. Khine Tun Naung, Kentaro Nakamura, Rei Mikoshiha, and Hideaki Monji, Study on Converging-Diverging Nozzle Flow with Micro Bubbles, 第9回新エネルギー技術シンポジウム, 2014年3月.

Table.3.1. Experimental conditions for the micro-bubble generator and millimeter-bubble generator.

Experimental condition	Method to generate micro-bubble	Upper tank pressure P_U [kPa]	Lower tank pressure P_L [kPa]	Pressure difference P_D [kPa]	CO ₂ rate [%]	N ₂ rate [%]
No.1	Micro-bubble generator	101	51	50	0	100
No.2			21	80		
No.3		201	101	100		
No.4			21	180		
No.5		301	101	200		
No.6			21	280		
No.7	Millimeter-bubble generator	101	51	50		
No.8			21	80		

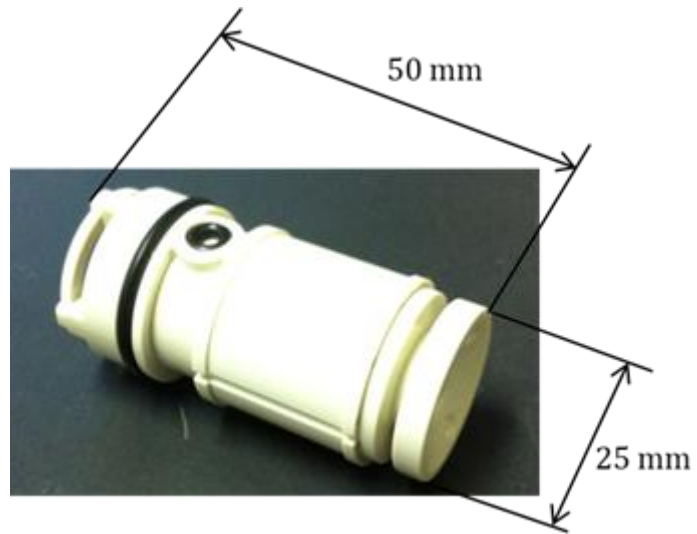


Figure 3.1. Micro-bubble generator.

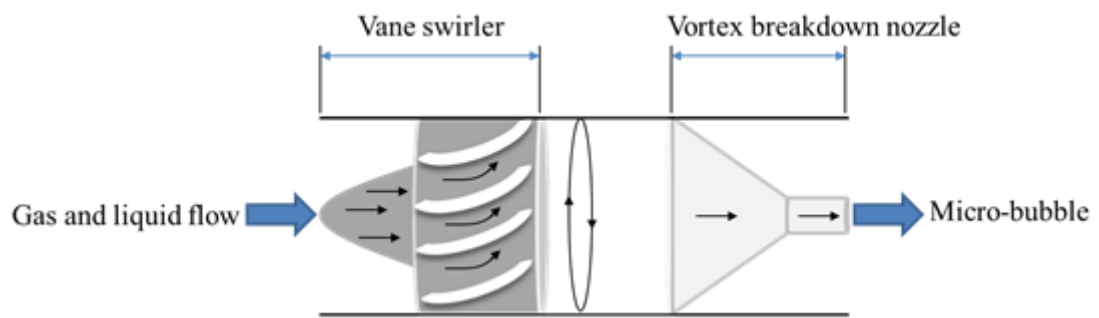


Figure 3.2 Schematic of micro-bubble generator



Figure 3.3. Static mixer.

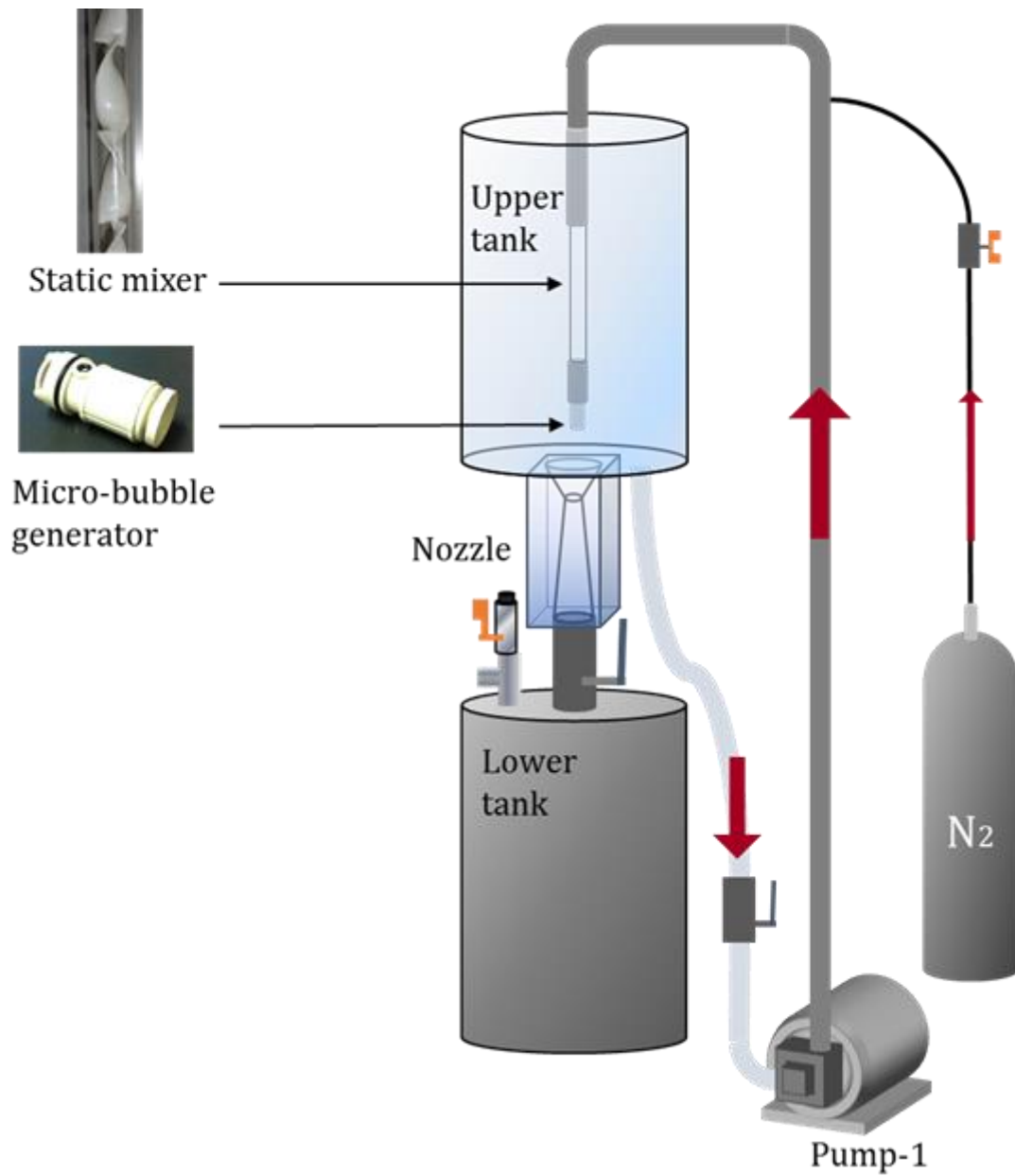


Figure 3.4. Experimental procedure by micro-bubble generator.



Figure 3.5. Sintered alloy.

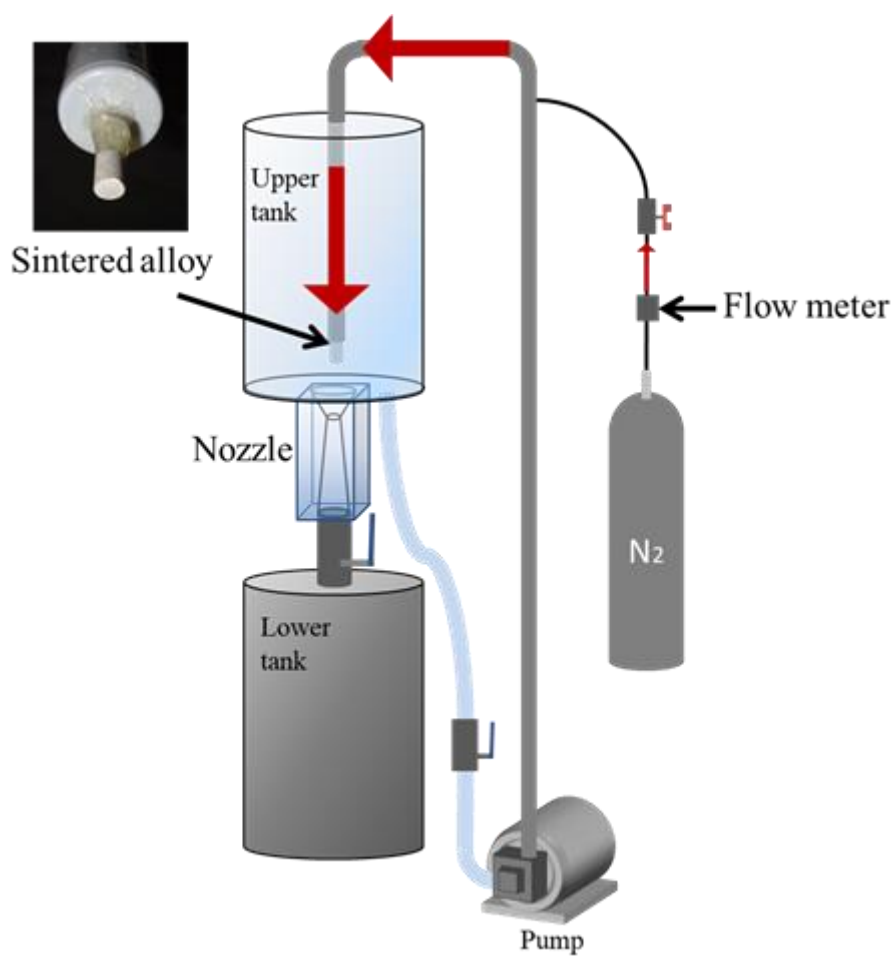


Figure 3.6. Experimental procedure by millimeter-bubble generator.



No.1

No.2

No.3

No.4



No.5

No.6

No.7

No.8

Figure 3.7. Flow pattern of the experimental conditions No.1 to No.8

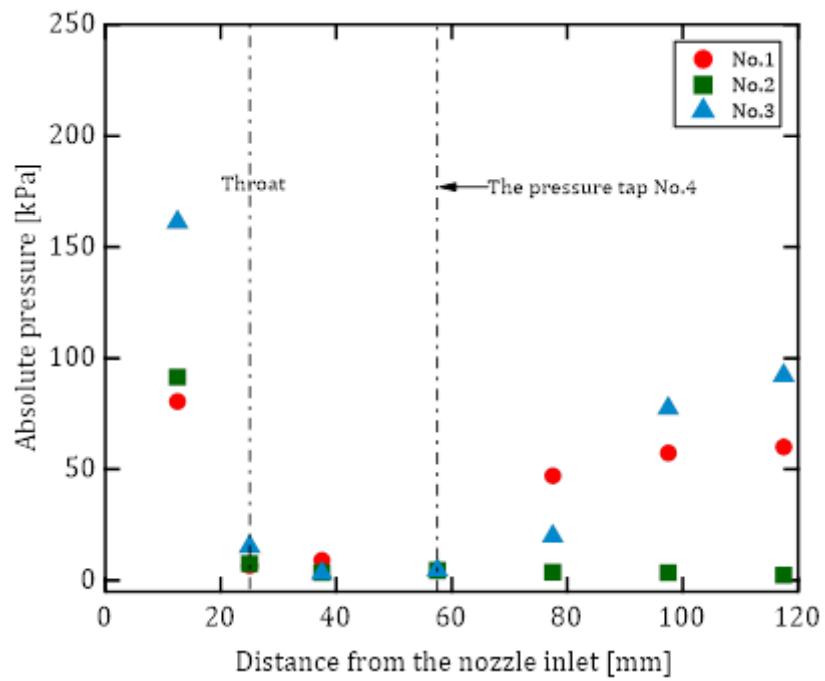


Figure 3.8. Pressure distribution along the nozzle of the experimental conditions No.1 to No.3.

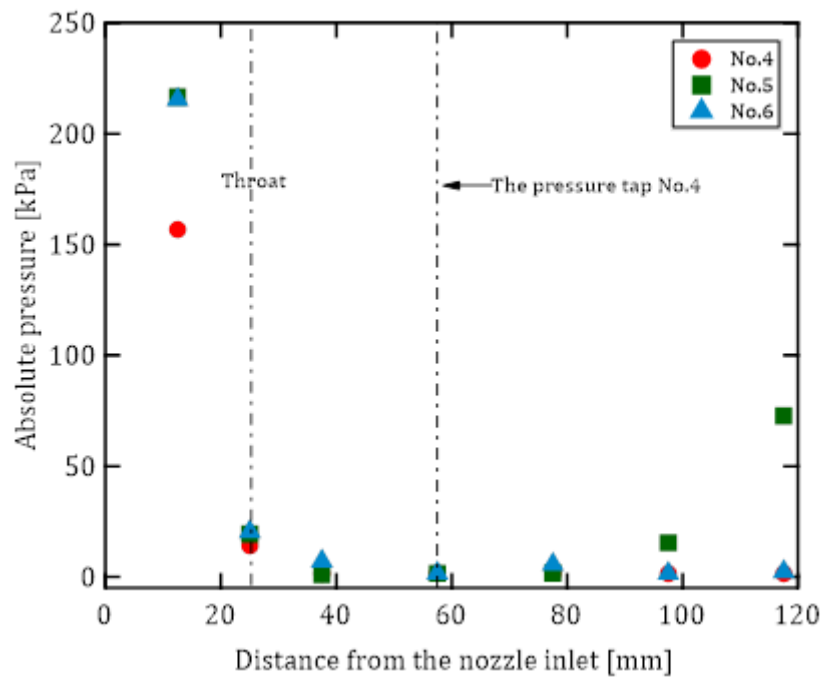


Figure 3.9. Pressure distribution along the nozzle of the experimental conditions No.4 to No.6.

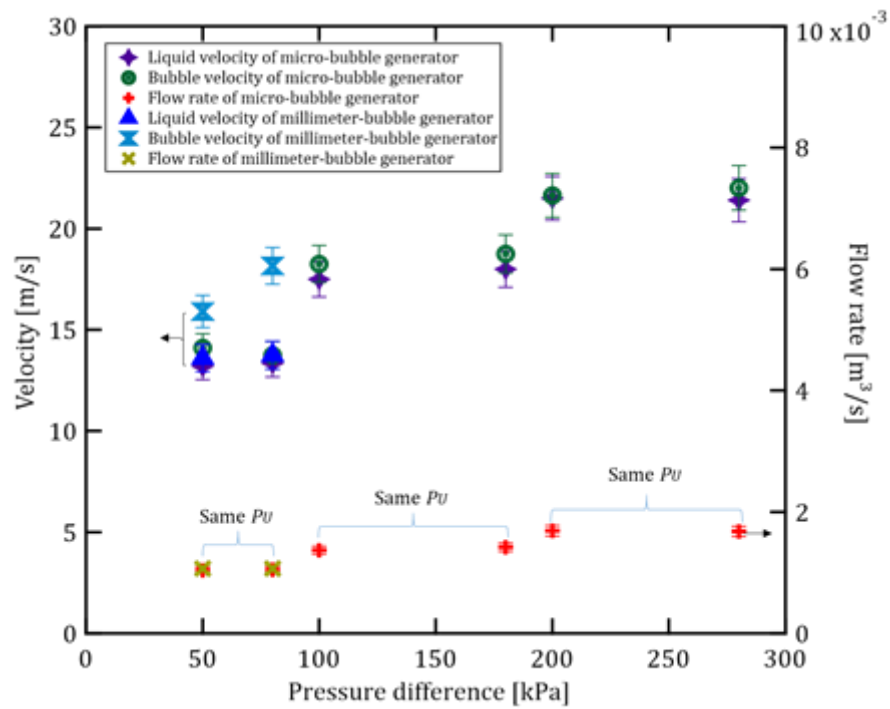
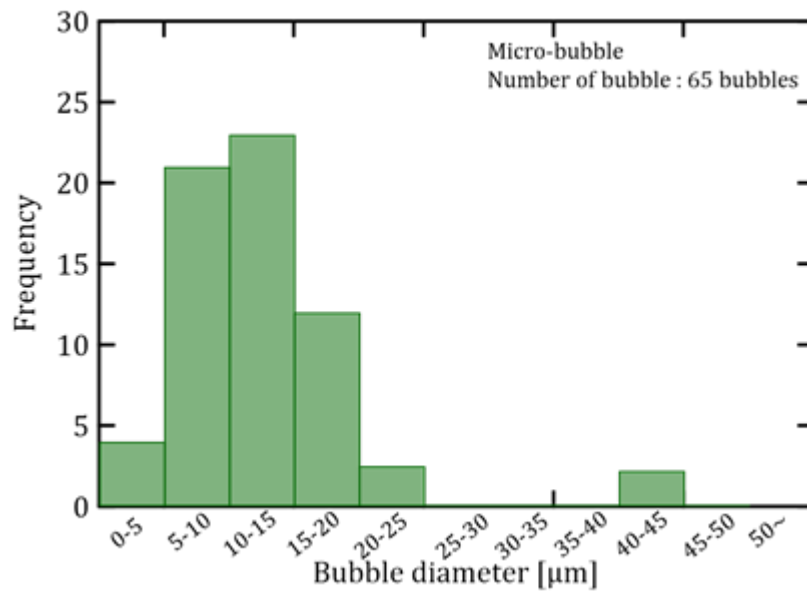
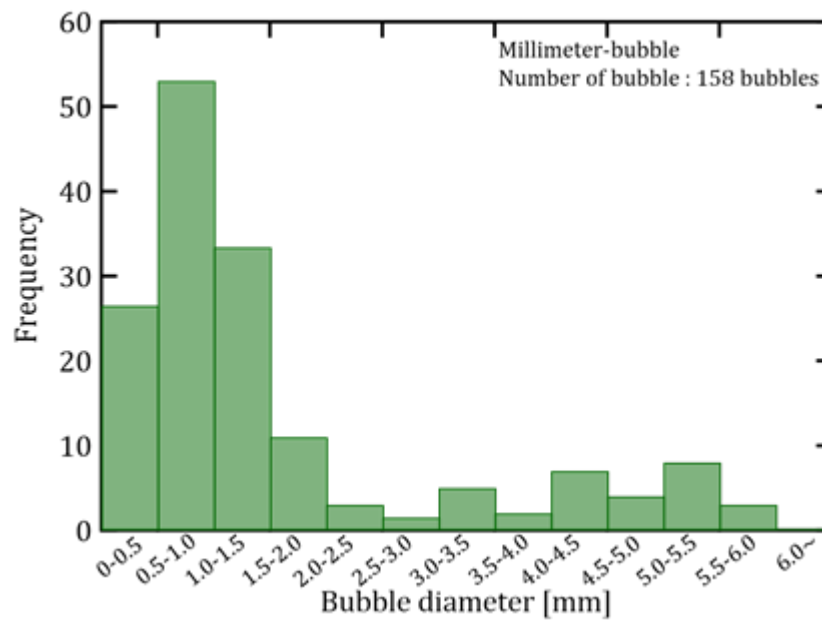


Figure 3.10. The comparison of flow rate, liquid velocity and bubble velocity at the throat of the experimental conditions No.1 ($P_D=50$ kPa), No.2 ($P_D=80$ kPa), No.3 ($P_D=100$ kPa), No.4 ($P_D=180$ kPa), No.5 ($P_D=200$ kPa), No.6 ($P_D=280$ kPa), No.7 ($P_D=50$ kPa) and No.8 ($P_D=80$ kPa).



(a) Micro-bubble



(b) Millimeter-bubble

Figure 3.11. Bubble size distribution of micro-bubble and millimeter-bubble.

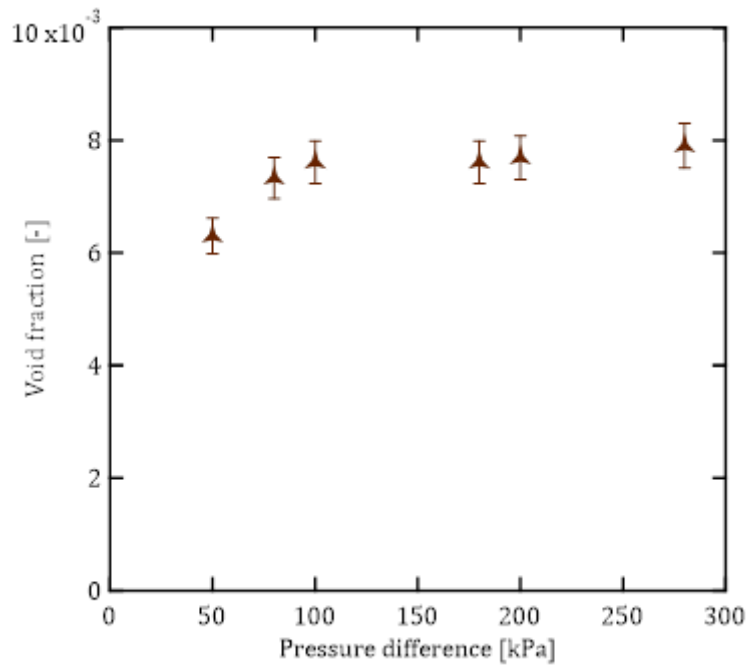


Figure 3.12. Void fraction at the throat of the experimental condition No.1 ($P_D=50$ kPa), No.2 ($P_D=80$ kPa), No.3 ($P_D=100$ kPa), No.4 ($P_D=180$ kPa), No.5 ($P_D=200$ kPa) and No.6 ($P_D=280$ kPa).

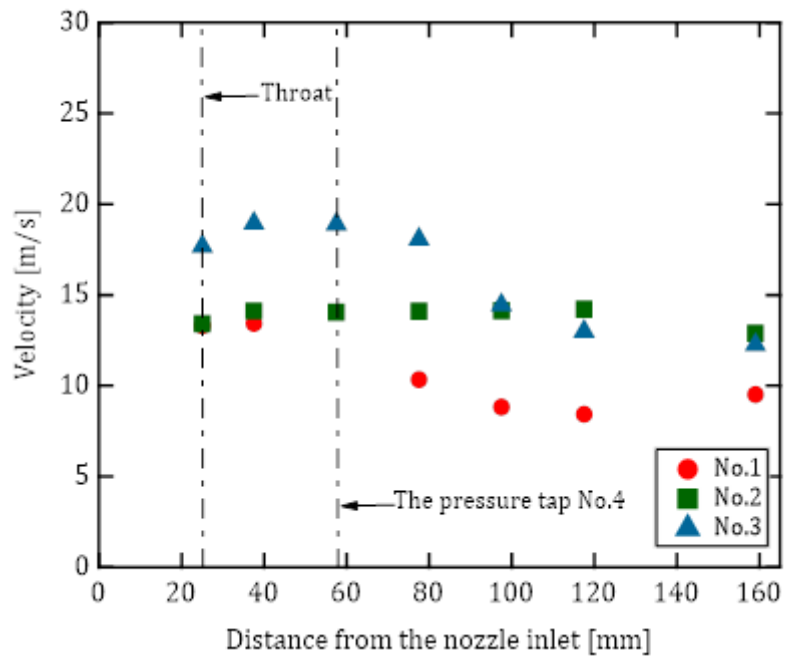


Figure 3.13. Liquid velocity distribution along the nozzle of the experimental conditions No.1 to No.3.

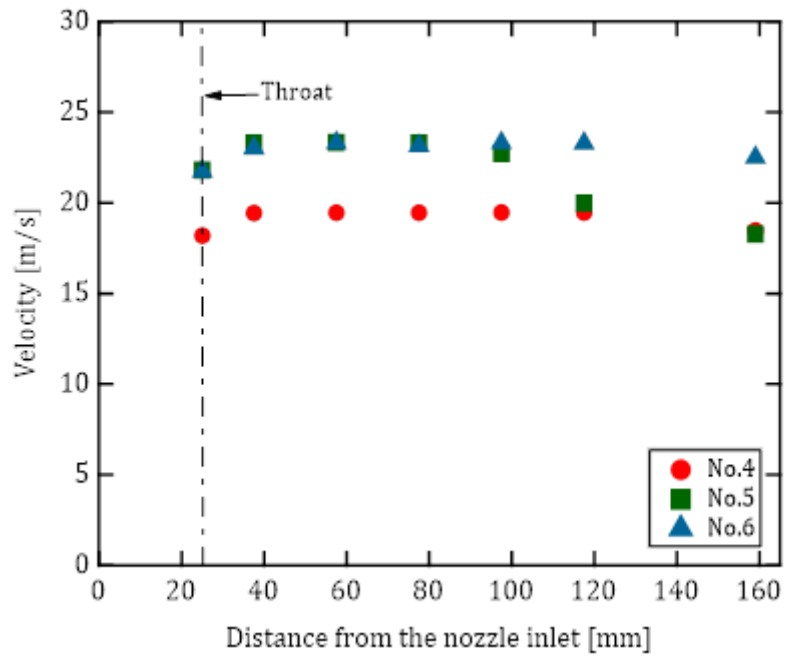
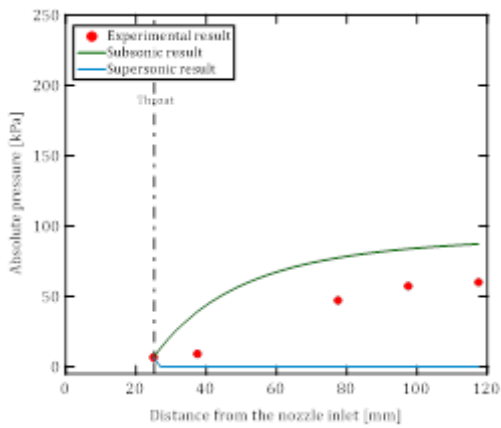
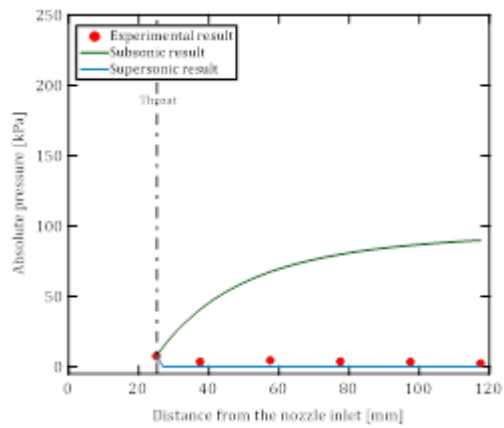


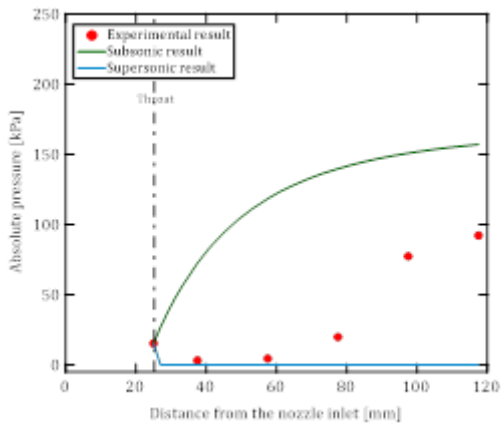
Figure 3.14. Liquid velocity distribution along the nozzle of the experimental conditions No.4 to No.6.



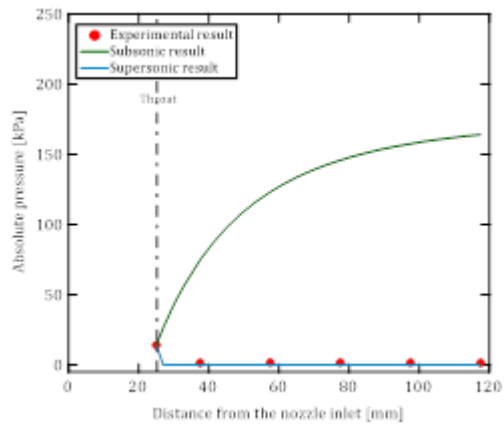
(a) Experimental condition No.1



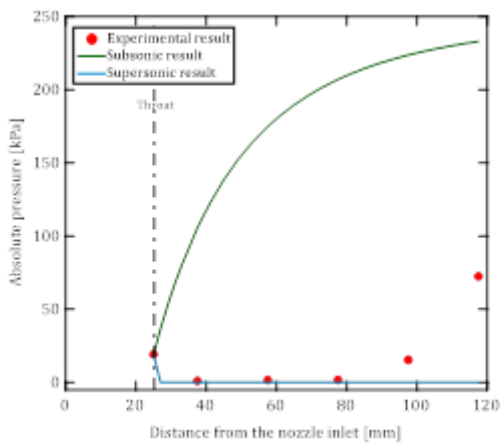
(b) Experimental condition No.2



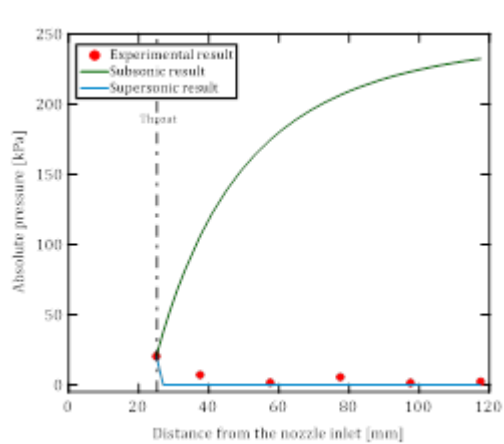
(c) Experimental condition No.3



(d) Experimental condition No.4



(e) Experimental condition No.5



(f) Experimental condition No.6

Figure 3.15. The comparison of pressure distribution between the experimental and theoretical estimation of subsonic and supersonic flow of the experimental conditions No.1 to No.6.

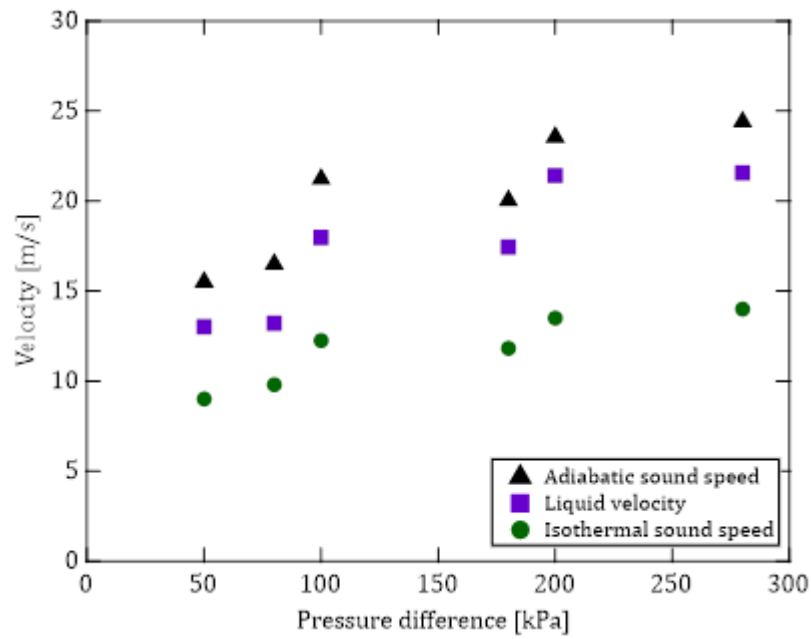


Figure 3.16. The comparison of liquid velocity and sound speed at the throat of the experimental condition No.1 to No.6.

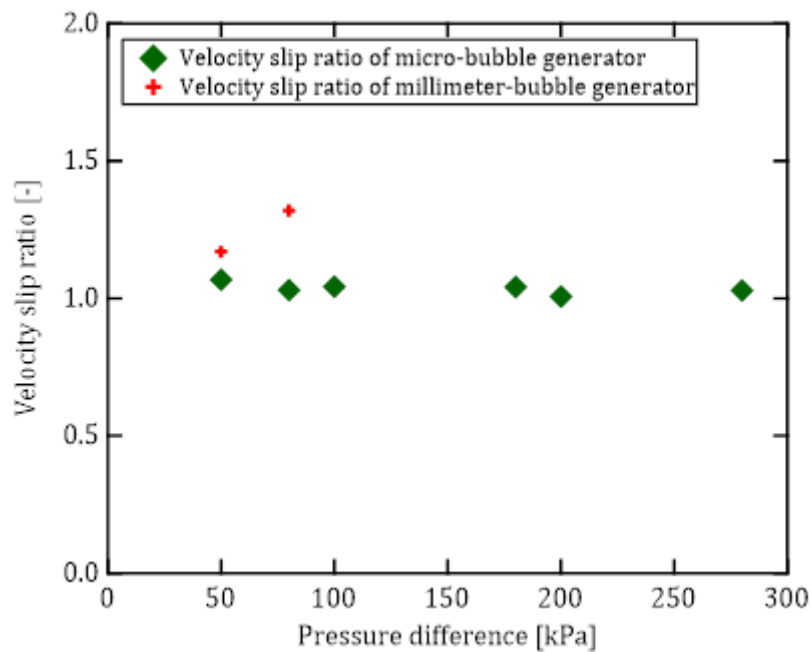


Figure 3.17. Velocity slip ratio of the experimental conditions No.1 ($P_D=50$ kPa), No.2 ($P_D=80$ kPa), No.3 ($P_D=100$ kPa), No.4 ($P_D=180$ kPa), No.5 ($P_D=200$ kPa), No.6 ($P_D=280$ kPa), No.7 ($P_D=50$ kPa) and No.8 ($P_D=80$ kPa).

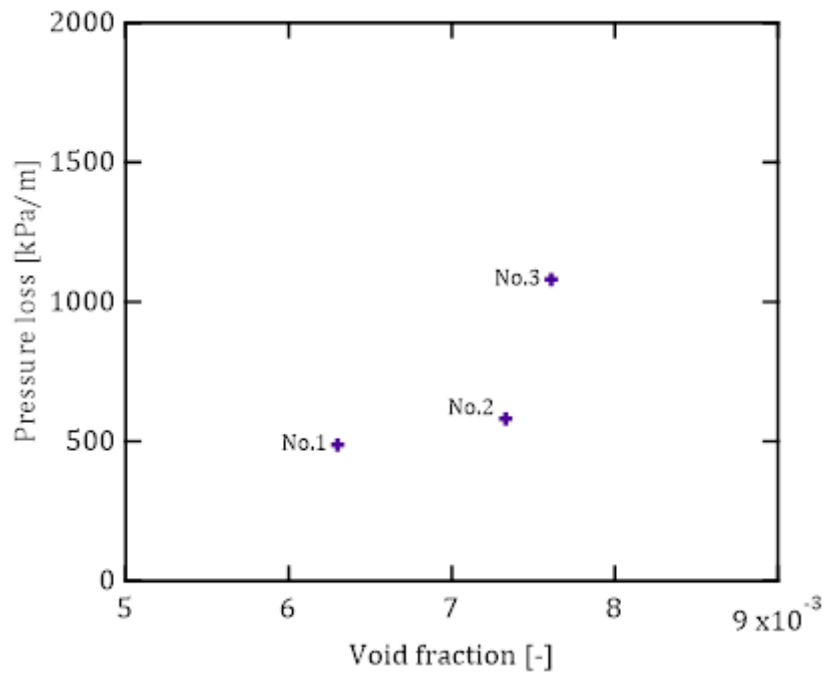


Figure 3.18. The comparison of void fraction and pressure loss at the throat of the experimental conditions No.1 to No.3.

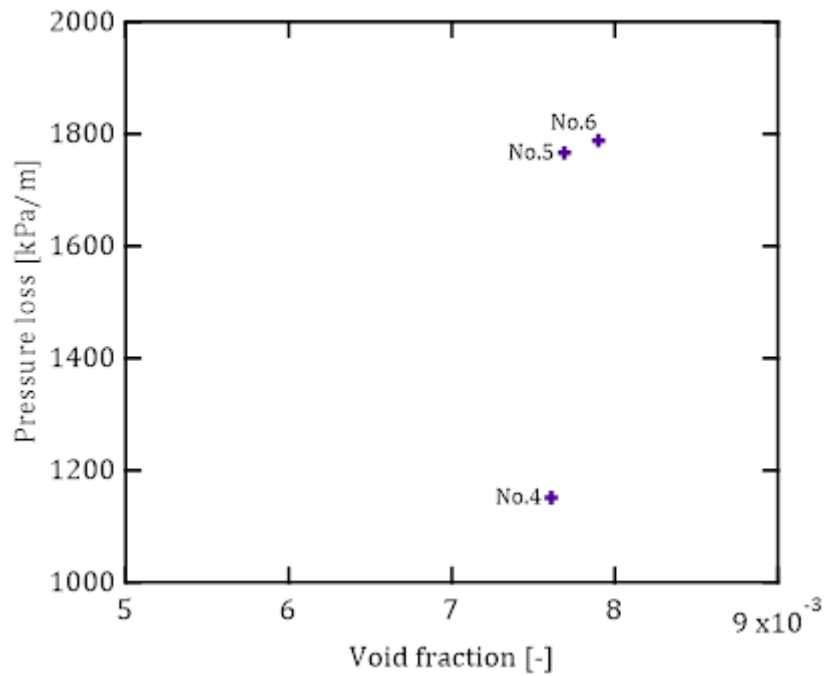


Figure 3.19. The comparison of void fraction and pressure loss at the throat of the experimental conditions No.4 to No.6.

Chapter 4

Pressurized Dissolution Method and Single-Phase Flow

4.1. Experimental procedure

The pressurized dissolution method is used to generate micro-bubbles. Micro-bubble will be appeared by reducing the pressure in a saturated liquid. The solubility of carbon dioxide is higher than nitrogen in the water. Therefore, carbon dioxide was chosen for the pressurized dissolution method in this experiment. It is referred to as the micro-bubble generation method and is depicted in Fig. 1.4 how to generate micro-bubbles as follow. After adding carbon dioxide and water into a tank, overhead high pressure is given into the tank. When the pressure decreases at the tank, micro-bubbles will come out from the liquid.

In pressurized dissolution method, the calibration steps are the same as micro-bubble generator (section 3.1). After the calibration process, the upper tank was supplied about 0.050 m³ water and depressurized until 21 kPa with the water seal vacuum pump. The upper tank was pressurized with the carbon dioxide gas to reach to 101 kPa. At that time the all of the pumps valve were closed. It was needed to make the depressurization and pressurization three times to reduce the tendency of result. After pressurizing and depressurizing three times, the pressure was adjusted to the desired pressure according to the experimental condition. While the carbon dioxide was mixing into the water by using the pump-1 to circulate the water letting in and out of the tank, it was also needed to supply carbon dioxide as the pressure was lost during mixing of water and carbon dioxide as represented in Fig. 4.1. When it reached to the saturated liquid phase, the pressure would rise again to desired pressure because it was mixed homogeneously. In the saturated liquid phase, it was needed to maintain the desired pressure without changing the pressure level in 30 seconds. If the lower tank pressure

was 101 kPa, the experiment could start at the unchangeable desired pressure. But the desired pressure of lower tank was below 101 kPa, it was needed to depressurize the lower tank pressure to get the desired pressure. Finally, the experiment was started by opening the valve under the nozzle after preparation of these steps. When the experiment finished, carbon dioxide was exited as an exhaust gas to the atmosphere by opening the leakage valve.

4.2. Experimental condition

The detail information for the experimental conditions of pressurized dissolution method and single-phase flow are shown in Table 4.1. Experimental condition No.9 was only for single-phase flow of the upper tank pressure was set 201 kPa and the lower tank pressure was set 101 kPa. Only nitrogen gas was used in this experiment. Experimental conditions No.10 to No.13 represented for the pressurized dissolution method with the upper tank and lower tank pressure were changing. The carbon dioxide was used in pressurized dissolution method.

4.3. Flow visualization

The flow image of single-phase flow and conventional pressurized dissolution method were shown in Figure 4.2. There was not observed bubble at the nozzle of the single-phase flow in the experimental condition No.9. In the conventional pressurized dissolution method of the experimental conditions No.10 to No.13, the bubbles were not generated upstream of the throat. Conversely, the bubble generation began at the throat and the gas phase was seen in the diverging section. At the throat, the flow was seen to be water single-phase flow or its void fraction was very little based on the images. Assuming the water single-phase flow and the atmospheric pressure at the throat, the

sound speed was estimated at about 1490 m/s. Even though upper tank or lower tank pressure increased or decreased the flow pattern did not change so much and the bubble did not appear at the throat of the nozzle in pressurized dissolution method.

4.4. Pressure profiles along the nozzle

Figure 4.3 shows the pressure distribution along the nozzle under the experimental condition No.9 of single-phase flow and the experimental conditions No.10 to No.13 of conventional pressurized dissolution method. As a reference, the experimental condition No.9 was only the water single phase flow. The flow might be subsonic because the pressure increased rapidly downstream of the throat. Generally, the sound speed in the water exceeds 1500 m/s under the atmospheric pressure. Therefore, it was subsonic flow in the experiment.

The pressure was increased along the nozzle after the throat in the experimental condition No.10. It was similar to the single-phase flow. The pressure in the experimental condition No.11 and No.12 was slightly increased from the throat to the end of the nozzle. Therefore, these experiments were a subsonic flow even though the micro-bubbles were generated in the nozzle. Under the experimental condition No.13, however, the pressure decreased just downstream of the throat. The decrease of the pressure after the throat is shown in case of a supersonic flow but the flow of the experimental condition No.13 was not identified as supersonic, because many bubbles were generated on the wall and the flow was as turbulent flow.

4.5. The comparison of the flow rate and liquid velocity at the throat

The comparison of the flow rate and liquid velocity at the throat are shown in Figure 4.4. In the single-phase flow of the experiment No.9, the flow rate and liquid

velocity were more increase than other experiment. Pressurized dissolution method of the experimental conditions No.10 to No.13 were not observed micro-bubble at the throat. However, the liquid velocity and flow rate are directly proportional to the pressure difference.

4.6. Velocity distribution along the nozzle

Only liquid velocity was observed in these experimental conditions. The results are shown in Fig. 4.5. In the single-phase flow of the experimental condition No.9, the liquid velocity decreased from the throat to the exit of the nozzle. The other experimental conditions were also decrease liquid velocity from the throat to the exit of the nozzle. All of the experiments were subsonic flow. The velocity decreasing was small because of the micro-bubbles were generated in pressurized dissolution method.

4.7. The comparison of pressure distribution between the experimental and theoretical estimation of subsonic and supersonic flow

Figure 4.6 (a)-(e) illustrates the comparison of the pressure distribution along the diverging part between the experiment and theoretical estimation of the subsonic and the supersonic flow of the experimental condition No.9 to No.13. The pressure distribution assuming the subsonic and supersonic flows are drawn by Eq. (2.66) based on the data at the throat. In the experimental condition No.9 of single-phase flow the experimental pressure closed to the subsonic condition. The experimental pressure of the experimental condition No.10 ($P_L=101$ kPa) was near to the subsonic condition. When the P_L decreased to 21 kPa and 51 kPa in the experimental conditions No.11 and No.12, the experimental pressure approached to the supersonic condition. The experimental result of the experimental condition No.13 also approached to the

supersonic condition. However, these three experimental conditions were not supersonic flow because of single phase flow were observed at the throat.

4.8. Concluding remarks

In order to reduce the velocity slip in the converging-diverging nozzle, use of micro-bubbles generated by the pressurized dissolution method was proposed. The results on the single-phase flow and pressurized dissolution method of the two-phase flow nozzle as discussed above were summarized as follows:

- i. There was not observed bubble at the nozzle of the single-phase flow. The pressure was immediately increased from the throat to the exit of the nozzle. The liquid velocity decreased from the throat to the exit of the nozzle. However, the flow rate and liquid velocity were high.
- ii. By the conventional pressurized dissolution method, the flow at the throat was almost a single-phase flow and the void fraction at the throat was almost zero.
- iii. In the case of pressurized dissolution method, the homogeneous micro-bubble was not obtained at the throat of the nozzle and the two-phase flow did not become supersonic according to the flow images, pressure and velocity distribution along the nozzle.

The study in Chapter 4 was reported in the reference,

1. Khine Tun Naung, Nakamura, K., Mikoshiba, R., Monji, H., Study on Generation of Supersonic Flow in a Converging-Diverging Nozzle by Modified Pressurized Dissolution Method, *J. JSEM*, **15**-Special Issue, s15-s20, 2015.
2. Khine Tun Naung, Kentaro Nakamura, Rei Mikoshiba, and Hideaki Monji, Study on Converging-Diverging Nozzle Flow with Micro Bubbles, 第9回新エネルギー

技術シンポジウム, 2014 年 3 月.

3. カイン トウン ナウン, 文字秀明, 加圧溶解法を用いた気液二相ノズル流れに対する溶存気体の影響, 日本混相流学会混相流シンポジウム 2014 講演論文集, 2014 年 7 月.

Table.4.1. Experimental conditions for the single-phase flow and pressurized dissolution method.

Experimental condition	Method to generate micro-bubble	Upper tank pressure P_U [kPa]	Lower tank pressure P_L [kPa]	Pressure difference P_D [kPa]	CO ₂ rate [%]	N ₂ rate [%]
No.9	Single-phase flow	201	101	100	0	100
No.10	Pressurized dissolution method		51	100	100	0
No.11			21	150		
No.12			101	180		
No.13			301	200		

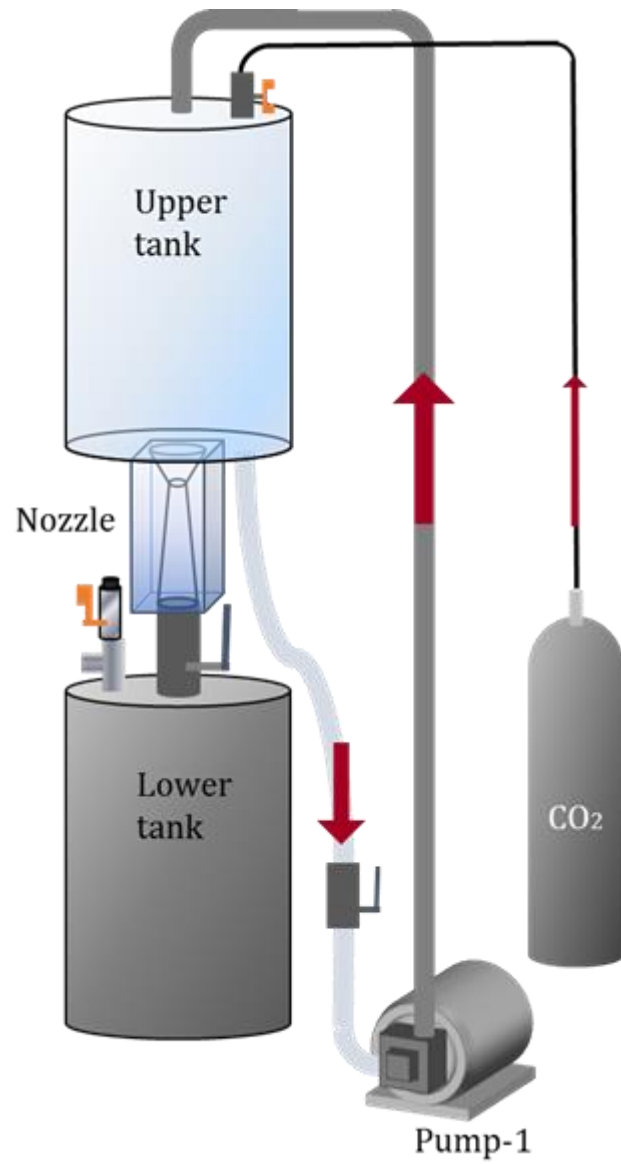
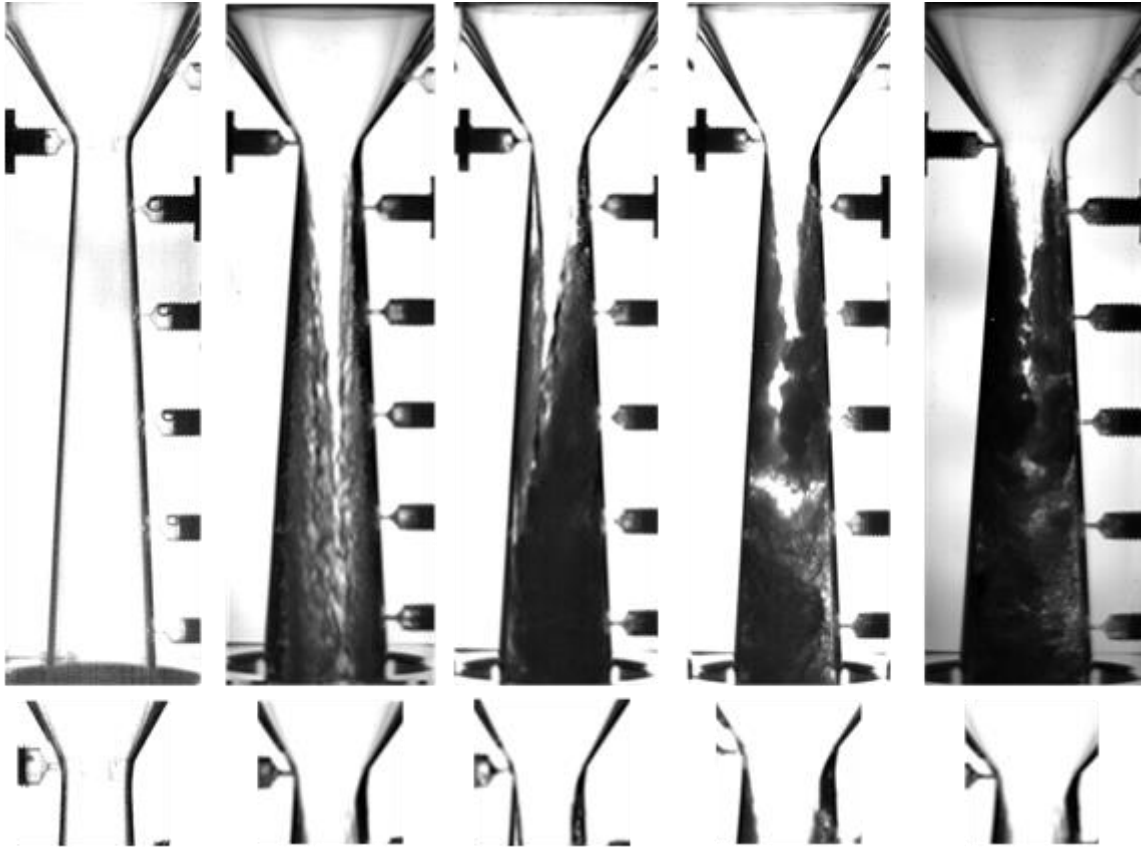


Figure 4.1. Experimental procedure by pressurized dissolution method.



No.9

No.10

No.11

No.12

No.13

Figure 4.2. Flow pattern at the experimental conditions No.9 to No.13.

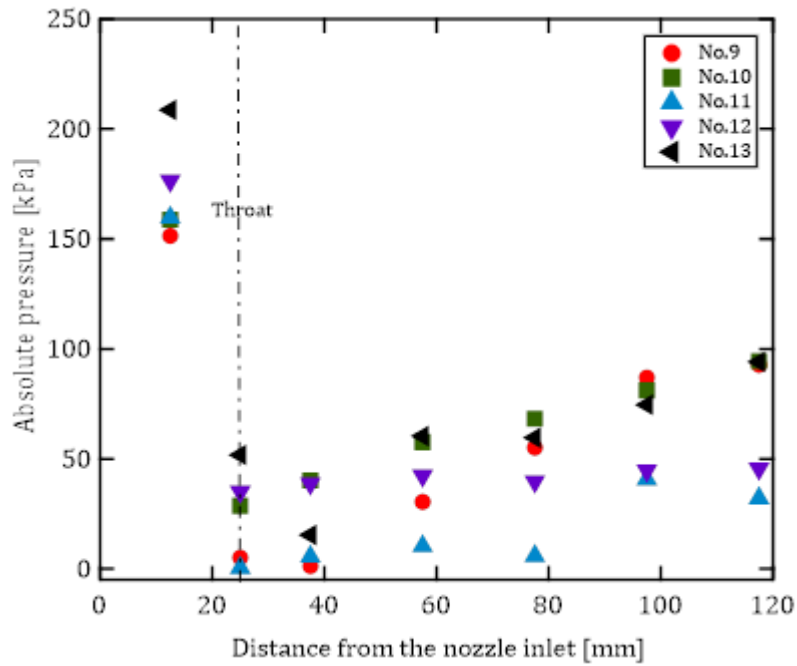


Figure 4.3. Pressure distribution along the nozzle of the experimental conditions No.9 to No.13.

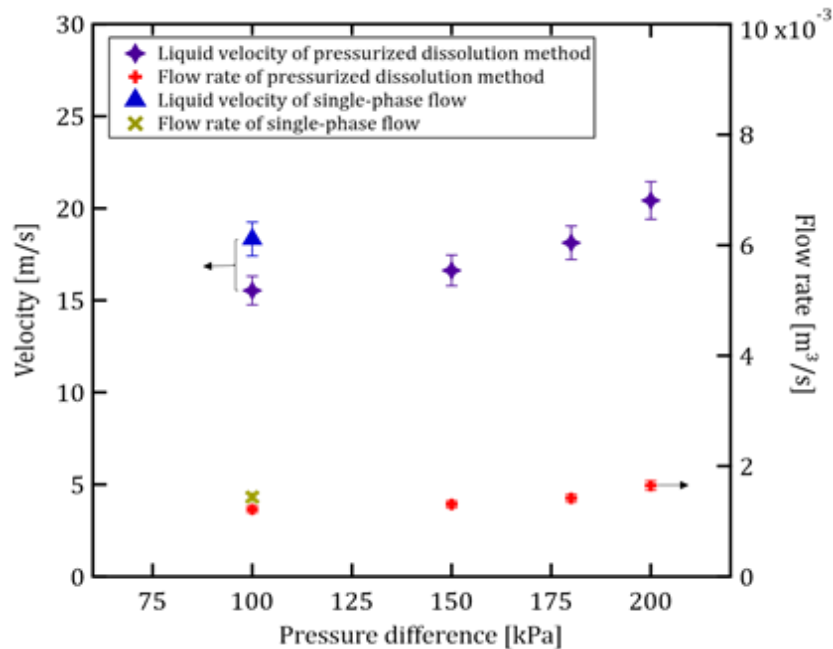


Figure 4.4. The comparison of flow rate, liquid velocity and bubble velocity at the throat of the experimental conditions No.9 ($P_D=100$ kPa), No.10 ($P_D=100$ kPa), No.11 ($P_D=150$ kPa), No.12 ($P_D=180$ kPa) and No.13 ($P_D=200$ kPa).

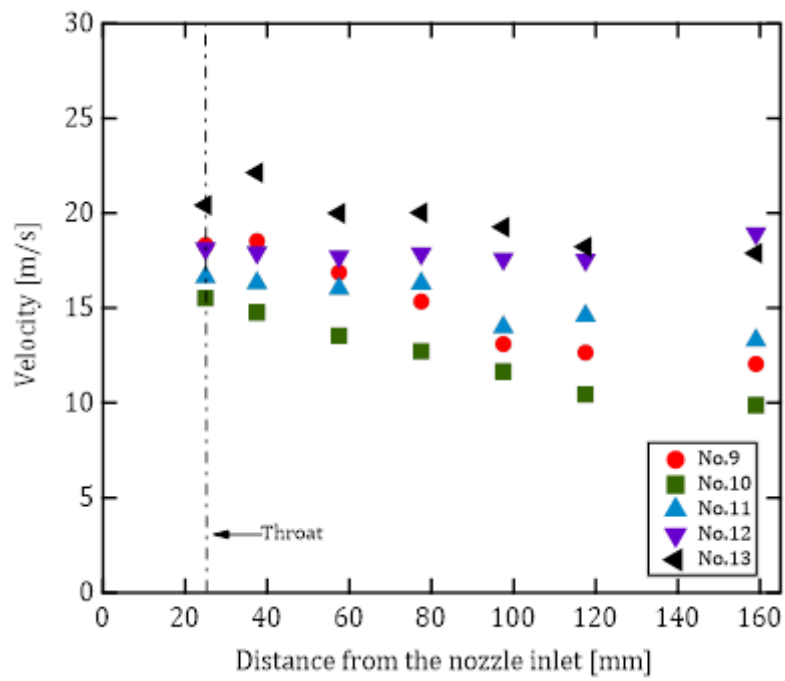
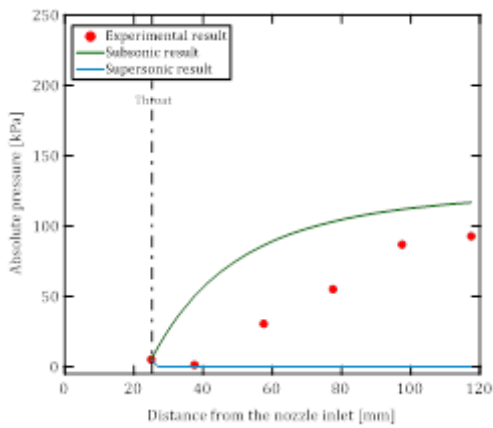
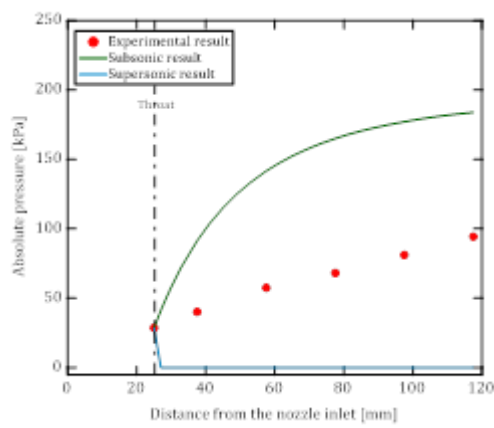


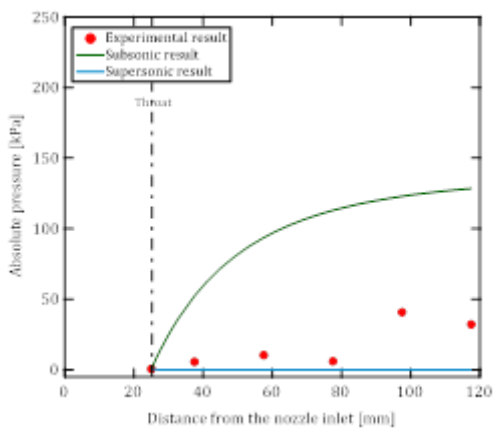
Figure 4.5. Velocity distribution along the nozzle of the experimental conditions No.9 to No.13.



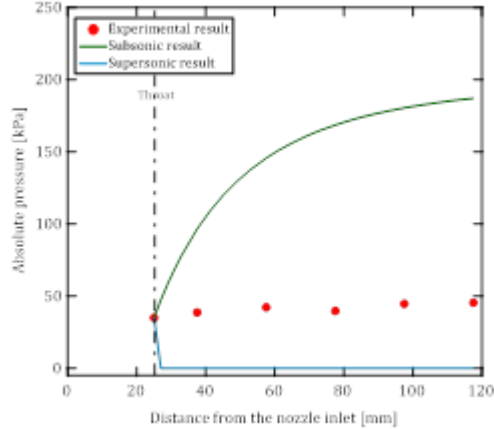
(a) Experimental condition No.9



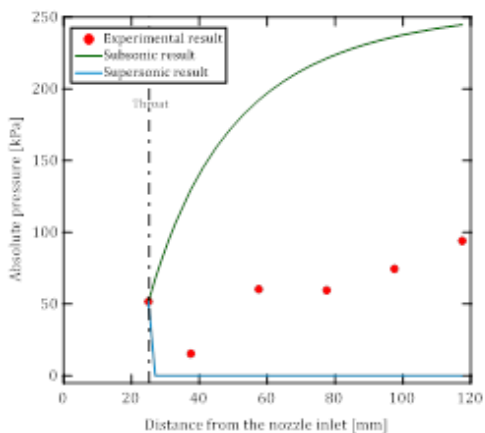
(b) Experimental condition No.10



(c) Experimental condition No.11



(d) Experimental condition No.12



(e) Experimental condition No.13

Figure 4.6. The comparison of pressure distribution between the experimental and theoretical estimation of subsonic and supersonic flow of the experimental conditions No.9 to No.13.

Chapter 5

Modification of Pressurized Dissolution Method with Orifice Plates

5.1. Experimental procedure

The pressurized dissolution method was modified by using the orifice plate. The pressure of the water was reduced at the orifice, and the micro-bubble was generated at the converging section of the nozzle. If the flow is gas-liquid two-phase flow at the throat, the sound velocity is very low and the flow will become supersonic easily after the throat (Nakamura, 2014). Therefore, it is expected that the flow becomes supersonic by the modified pressurized dissolution method. The generation of the supersonic flow in the converging-diverging nozzle is the main purpose of this study by using the modified pressurized dissolution method.

The orifice plates used in the modified pressurized dissolution method are made of alumina plate with 140 mm length and 140 mm width. Four types of orifice plate are shown in Fig. 5.1. The diameter of the hole of plate is 20 mm for orifice plate.1 (area is $3.142 \times 10^{-4} \text{ m}^2$). The orifice plate.2 has 7 holes of each 7 mm diameter (area is $2.694 \times 10^{-4} \text{ m}^2$). The orifice plate.3 has 19 holes of each 5 mm diameter (area is $3.730 \times 10^{-4} \text{ m}^2$). Orifice plate.4 has a hole of 40 mm diameter covered by a mesh (mesh number 16, wire diameter: 0.4 mm) (area is $12.566 \times 10^{-4} \text{ m}^2$).

The orifice was mounted at the exit of an upper tank or the inlet of the nozzle to reduce once the diameter of the flow channel. Figure 5.2 depicts schematic diagram of the modification of pressurized dissolution method with the orifice plate. The calibration process was the same as the micro-bubble generator (section 2.3). After the upper tank was supplied about 0.050 m^3 water, the pressure in the upper tank was set to atmospheric pressure. After deaeration of the upper tank, the upper tank was pressurized by N_2 and CO_2 gases shown in Fig. 5.3. N_2 and CO_2 gases were used as working fluids

in this study. Because the solubility of N_2 gas is very small comparing with that of the CO_2 gas, the effect of CO_2 gas was only considered in the pressurized dissolution method. The amount of the dissolving gas is proportional to the partial pressure of the gas. The total pressure in the upper tank was fixed at 201 kPa but the partial pressure of CO_2 dissolved gas rate changed as Table 5.1 in order to control the amount of the void fraction at the throat. The experimental condition was set in equilibrium state after mixing the water and the gases. After the experimental condition was set, the experiment was began by opening the valve downstream of the nozzle.

5.2. Experimental condition

The detail information for the experimental conditions of the modification of pressurized dissolution method with orifice plates are shown in Table 5.1. Experimental conditions No.14 to No.20 were modification of pressurized dissolution method with orifice plate.1 (one hole). The total pressure in the upper tank (201 kPa) and the lower tank (101 kPa) was set to be constant in the experimental conditions No.14 to No.18 but the partial pressure of CO_2 dissolved gas rate was changed in each experimental condition. The upper tank was filled with CO_2 and N_2 gases. The carbon dioxide gas dissolved well, but N_2 gas did not well. Nitrogen gas was fed to supply a shortage for the total pressure. The rate of CO_2 gas was decided by using Eq. (5.1). The reason for mixing together with CO_2 and N_2 was to change the amount of bubble at the throat in the nozzle. If there were changing the amount of bubble in the case of CO_2 , the upper tank pressure was needed to change. In these experiments were done without changing the upper tank and lower tank pressure, however, the amount of bubbles wanted to change. At that time, N_2 was used to adjust for total pressure.

$$CO_2 \text{ rate } [\%] = \frac{CO_2 \text{ partial pressure}}{\text{Upper tank pressure}} \times 100 \quad (5.1)$$

For example, in the case of 0% of CO₂, N₂ gas filled up to 100% (201 kPa) in the upper tank and there was no supplying of CO₂. In the case of 25% (50 kPa) of CO₂, the rate of the partial pressures of CO₂ and N₂ gas were supplied 25% (50 kPa) and 75% (151 kPa) to make the total pressure, respectively. The ratio of CO₂ or the dissolved gas rate was changed in the experiment to control the dissolved gas in the water. The experimental conditions No.19 and No.20 used the upper tank pressure ($P_U=201$ kPa) and the lower tank pressure changed 51 kPa and 21 kPa.

In the experimental conditions No.21 to No.23, the orifice plate.2 (7 holes) was used as the modification of pressurized dissolution method. The upper tank pressure was set 201 kPa and the lower tank pressure was changed as 101 kPa, 51 kPa and 21 kPa. The experimental condition No.24 with orifice plate.3 (19 holes) and the experimental condition No.25 with orifice plate.4 (mesh) were set upper tank pressure ($P_U=201$ kPa) and lower tank pressure ($P_L=101$ kPa).

5.3. Flow visualization

Figure 5.4 is represented the flow visualization of the experimental conditions No.14 to No.25. The experimental conditions No.14 to No.20 show that the bubble generation by the modified pressurized dissolution method with orifice plate.1. In there, the experimental conditions No.14 to No.18 depended on the CO₂ dissolved rate. The close-up images also show that the bubbles were stretched along the flow at the throat. When the rate of the partial pressures of CO₂ increased, the generation of bubbles was also increased in the experimental conditions No.14 to No.18. Therefore, the dark portion could be seen more in experimental condition No.18 than the experimental

conditions No.14 to No.17. When the lower tank pressure was more decreased, the micro-bubbles were more produced at the throat and diverging section in the experimental conditions No.19 and No.20.

The experimental conditions No.21 to No.23 are the flow pattern of orifice plate.2, the experimental condition No.24 is the flow pattern of orifice plate.3 and the experimental condition No.25 is the flow pattern of orifice plate.4 the modified pressurized dissolution method. The micro-bubble could be generated at the throat in the experimental condition No.21 more than the experimental conditions No.22 and 23. The experimental conditions No.24 and No.25 were observed less micro-bubble production in the nozzle.

5.4. Pressure profiles along the nozzle

Figure 5.5 represents the experimental conditions No.14 to No.20 of the modification of pressurized dissolution method with orifice plate.1. Among them the experimental conditions No.14 to No.18 were the same upper tank and lower tank pressure and different CO₂ rate. In these experimental conditions the pressure at the throat decreased, however, its increased along the nozzle. Because the pressure recovered in the diverging nozzle, the flow seemed subsonic in all experimental condition. In the experimental conditions No.19 and No.20, the pressure decreased along the nozzle after the throat, even if the fluid flowed in the diverging section. Therefore, there is possibility of supersonic flow. However, the pressure increased near the end of the nozzle. The difference pressure could effect on supersonic flow.

The experimental conditions No.21 to No.25 are the modification of pressurized dissolution method with orifice plate.2, plate.3 and plate.4 shown in Fig. 5.6. All the experiments were subsonic because the pressure was increasing from the throat

to the end of the nozzle. The pressure of the experimental condition No.21, No.22, No.23 and No.24 decreased from the throat to the pressure tap No.3 and rapidly increased to the exit of the nozzle. However, the experimental condition No.25 the pressure was measured only at the throat of the nozzle. The other pressure tap could not be measured correctly because of the fluctuation was too large.

5.5. The comparison of the flow rate, liquid velocity and bubble velocity at the throat

As illustrated in Fig. 5.7, the rate of the CO₂ increased from 0% to 100% in the modification of pressurized dissolution method with the orifice plate.1 of the experimental condition No.14 to No.18, the flow rate and bubble velocity were almost constant, the liquid velocity was slightly decreased. However, there was no micro-bubble generated at the throat in the experimental condition No.14 (CO₂ 0%). When the pressure difference was increased to $P_D=150$ kPa and $P_D=180$ kPa in the experimental conditions No.19 and No.20, the bubble and liquid velocity were almost the same and flow rate increased slightly in the experimental condition No.20 comparing with the experimental conditions No.19 as expressed in Fig. 5.8.

In Fig. 5.9, the experimental condition No.21 to No.23 used orifice plate.2 with the same upper tank pressure and different lower tank pressure. When the pressure difference increased 100 kPa, 150 kPa and 180 kPa, the flow rate and liquid velocity gradually increased and bubble velocity was almost closed to liquid velocity in the experimental condition No.22 ($P_D=150$ kPa). When the orifice was changed to orifice plate.3 and orifice plate.4 under the same pressure difference ($P_D=100$ kPa), flow rate was a little increase. In contrast, the liquid velocity and bubble velocity decreased from experimental condition No.24 to No.25 as shown in Fig. 5.10.

5.6. Measurement of bubble size distribution

The bubble diameter distribution was obtained by 20 images of the throat in 0.002 s by taking high speed camera in the modification of pressurized dissolution method. The image of the throat section is represented in Fig. 5.4. In the experimental condition No.14 (orifice plate.1, CO₂ 0%), the micro-bubble could not be observed at the throat. The distribution of the bubble diameter for the experimental condition No.15 to No.25 are shown in Fig. 5.11 (a) to (k), respectively. In the experimental condition No.15 (orifice plate.1, CO₂ 25%) 8 micro-bubbles were observed with the average value of equivalent diameter 300.8 μm and its standard deviation was 1.342 μm . The micro-bubbles in experimental condition No.16 (orifice plate.1, CO₂ 50%) were 23 bubbles and its equivalent diameter was 301.643 μm . The standard deviation was 3.729 μm . More micro-bubbles were generated at the experimental conditions No.17 (orifice plate.1, CO₂ 75%) and No.18 (orifice plate.1, CO₂ 100%) as 50 bubbles and 118 bubbles. The equivalent diameters were 328.125 μm and 356.556 μm respectively. The standard deviations were 6.756 μm and 10.055 μm . The more carbon dioxide dissolved, the more micro-bubble observed in these experimental conditions. When the pressure difference increased to 150 kPa (No.19) and 180 kPa (No.20) in the orifice plate.1, the same size of the bubbles was more observed than the other experimental conditions. The number of bubbles were 173 and 194. The equivalent diameters were 529.806 μm and 555.105 μm with standard deviation 8.283 μm and 8.643 μm respectively.

In the experimental condition No.21 (orifice plate.2, $P_D=100$ kPa) the number of bubbles was 161 bubbles, the equivalent diameter of bubbles was 604.237 μm and its standard deviation was 7.05 μm . 106 bubbles, equivalent diameter 403.533 μm and standard deviation 9.896 μm were observed in the experimental condition No.22 (orifice plate.2, $P_D=150$ kPa). 125 bubbles of the experimental condition No.23 (orifice plate.2,

$P_D=180$ kPa) had the equivalent diameter $552.976 \mu\text{m}$ and standard deviation $7.915 \mu\text{m}$. Total 45 bubbles were observed in the experimental condition No.24 (orifice plate.3, $P_D=100$ kPa) with equivalent diameter of bubbles $402.045 \mu\text{m}$ and standard deviation $2.548 \mu\text{m}$. In the experimental condition No.25 (orifice plate.4, CO_2 100%) the micro-bubble was observed 19 bubbles and its equivalent diameter was $203.167 \mu\text{m}$ and standard deviation was $3.215 \mu\text{m}$.

Furthermore, the time average equivalent bubble diameter of the bubbles and the number of bubbles passing the throat for a second were obtained. In Fig. 5.12 to Fig. 5.15, the left axis of ordinate denotes the equivalent bubble diameter at the throat and the right axis of ordinate, the number of bubbles passing the throat for a second. As describes in Fig. 5.12, the CO_2 dissolved gas rate increased, the equivalent bubble diameter was almost constant. Inversely the number of bubbles increased with the CO_2 dissolved gas rate in modification of pressurized dissolution method with orifice plate.1. When the pressure difference increased 150 kPa and 180 kPa in the experimental condition No.19 and No.20, the equivalent bubble diameter was almost constant and the number of bubbles increased as illustrated in Fig. 5.13. When the pressure difference increased in the experimental conditions No.21 ($P_D=100$ kPa) to No.23 ($P_D=180$ kPa) with orifice plate.2, the equivalent bubble diameter did not change so much. The least number of bubbles was observed, when the pressure difference increased to 150 kPa of the experimental condition No.22 as represented in Fig. 5.14. Figure 5.15 describes, the small equivalent bubble diameter and less number of bubbles were observed in the experimental conditions No.24 (orifice plate.3, $P_D=100$ kPa) and No.25 with (orifice plate.4, $P_D=100$ kPa).

5.7. Void fraction at the throat

Figure 5.16 gives the time average void fraction on the cross section of the throat was related to CO₂% in the experimental condition No.15 to No.18, the same pressure difference ($P_D=100$ kPa). If the CO₂% increased, the void fraction also increased. The pressure difference also influenced on the void fraction. The void fraction was observed 0.107 in the experimental condition No.19 ($P_D=150$ kPa). In the experimental condition No.20 ($P_D=180$ kPa) the void fraction was 0.118. The more pressure differenced with the upper tank and lower tank, the more void fraction obtained at the throat as shown in Fig. 5.17.

The result of the void fraction of the experimental conditions No.21 to No.23 used the orifice plate.2 represented in Fig. 5.18. In these experimental conditions, the void fraction was increased when the pressure difference increased. However, the void fraction in the experimental condition No.23 did not increase even if lower tank pressure decreased. Because the void fraction depended on not only lower tank pressure, but also the shape of the opening area of the orifice plate. The void fraction decreased at the same pressure difference ($P_D=100$ kPa) of the experimental condition No.24 (orifice plate.3) and No.25 (orifice plate.4) were shown in Fig. 5.19.

5.8. Velocity distribution along the nozzle

The results of the velocity distribution along the nozzle were obtained by Eq. (2.29) based on the pressure distribution of the experimental condition No.14 to No.20 with orifice plate.1 ($P_D=100$ kPa) are represented in Fig. 5.20. The experimental condition No.14 did not generate micro-bubble. Therefore, only liquid velocity observed in this experiment. The liquid velocity decreased from the throat to the exit of the nozzle. In the same pressure difference of the experimental conditions No.15 to

No.18, liquid velocities were obviously decreasing from the downstream of the throat along the nozzle. However, the liquid velocities of the experimental conditions No.19 ($P_D=150$ kPa) and No.20 ($P_D=180$ kPa) were increased from the throat to the exit of the nozzle.

The velocity distribution of the experimental conditions No.21 to No.24 is illustrated in Fig. 5.21. Among them, the experimental conditions with orifice plate.2 experiment of No.22 ($P_D=150$ kPa) was the highest velocity distribution than the other experimental conditions and gradually decreased to the exit of the nozzle. In the experimental condition No.23 ($P_D=180$ kPa), the velocity was also gradually decrease from the pressure measuring tap 5. In the experimental conditions No. 21 ($P_D=100$ kPa), liquid velocity distribution obviously decreased from the pressure measuring tap 4 to the exit. The experimental conditions No.24 (orifice plate.3, $P_D=100$ kPa) observed at the throat and decreasing velocities from the pressure tap No.6. The velocity along the nozzle of the experimental conditions No.25 (orifice plate.4, $P_D=100$ kPa) was not observed because the pressure at each the pressure could not be measured due to large fluctuation flow.

5.9. The comparison of pressure distribution between the experimental and theoretical estimation of subsonic and supersonic flow

The results of the theoretical estimation of subsonic and supersonic flow were calculated by Eq. (2.66) for the experimental conditions No.14 to No.25 are depicted in Fig. 5.22 (a)-(l). In the experimental conditions No.14 to No.18 with the same P_D of the orifice plate.1, the experimental pressures approached to the subsonic condition. The experimental pressure of the experimental conditions No.19 ($P_D=150$ kPa) and No.20 ($P_D=180$ kPa) of the orifice plate.1, closed to the supersonic condition and then it

increased to subsonic condition near the end of nozzle. When increasing P_D in the experimental condition No.21 to No.23 of the orifice plate.2, the experimental pressure closer to the supersonic condition. In the experimental condition No.23 of orifice plate.3, the experimental pressure was observed only in pressure measuring tap 6 and 7 that were closed to the subsonic condition. The experimental pressure only got at the throat in the experimental condition No.25 of the orifice plate.4.

5.10. The comparison of liquid velocity and sound speed at the throat

As illustrated in Fig. 5.23, in the experimental conditions No.15 to No.18, the liquid velocity did not reach the sound speed. It is expected to be subsonic. The liquid velocity at the throat were almost constant, however, increasing the CO₂ dissolved gas rate. The experimental conditions No.19 and No.20 reached the sound speed as described in Fig. 5.24. It could be estimated that the flow became supersonic condition. Figure 5.25 is represented the experimental conditions of No.21 to No.23 of the orifice plate.2 with almost constant liquid velocity at the throat. In the case of No.22, the liquid velocity closed to the sound speed because of increasing void fraction. The experimental conditions of No.24 and No.25, the liquid velocity was lower than the adiabatic and isothermal sound speeds as shown in Fig. 5.26.

5.11. Velocity slip ratio

Figure 5.27 and Figure 5.28 represents the experimental conditions No.15 to No.20 of the modification of pressurized dissolution method with orifice plate.1. When increasing the CO₂%, the velocity slip was slightly increased in the experimental conditions No.15 to No.18 as shown in Fig. 5.27. As illustrating in Fig. 5.28, the experimental conditions No.19 ($P_D=150$ kPa) was less velocity slip ratio and the

experimental conditions No.20 ($P_D=180$ kPa) was the least velocity slip ratio in the modification of pressurized dissolution method with orifice plate.1.

The experimental conditions No.21 to No.23 were the modification of pressurized dissolution method with orifice plate.2 (see in Fig. 5.29). Among them, when the pressure difference increased the velocity slip ratio also decreased. Figure 5.30 shows the result of the velocity slip ratio of the experimental conditions No.24 and No.25 with the same $P_D=100$ kPa. Higher velocity slip ratio got in these experimental conditions because of increasing bubble velocity at the throat, however, liquid velocities were almost similar.

5.12. The comparison of pressure loss and void fraction at the throat

The results of the comparison of pressure loss and void fraction at the throat are shown in Fig. 5.31 and Fig. 5.32. Figure. 5.31 represents the experimental conditions No.15 to No.20. When the amount of CO₂ rate increased, the void fraction also increased. Therefore, pressure loss also increased at the throat in the experimental conditions No.15 to No.18. When increasing pressure difference, void fraction would increase and pressure loss also increase in the experimental conditions No.19 and No.20. Figure. 5.32 illustrates the results of the comparison of pressure loss and void fraction at the throat of the experimental conditions No.21 to No.24. In these experimental conditions, No.21 and No.22 increased pressure loss and No.23 and No.24 decreased pressure loss. That is why, pressure loss is influenced by the void fraction.

5.13. Concluding remarks

The pressurized dissolution method was modified by four types of orifice plates to reduce the diameter of the flow channel and to generate more micro-bubble at

the throat. The results on the modification of pressurized dissolution method with orifice plates as discussed above were summarized as follows:

- i. In the case of modified pressurize dissolution method with the orifice plate.1 (area is $3.142 \times 10^{-4} \text{ m}^2$), as increasing the CO_2 dissolved gas rate, the void fraction increased and the liquid velocity decreased at the throat. The bubble velocity was almost constant. Therefore, the velocity slip between the bubble and the liquid increased. Based on the pressure and the flow velocity distribution along the nozzle and the liquid velocity at the throat, the liquid velocity did not reach the sound speed in all case.
- ii. When the pressure difference increased to the experimental condition No.19 ($P_D=150 \text{ kPa}$) and No.20 ($P_D=180 \text{ kPa}$), the pressure distribution decreased along the nozzle after the throat. However, the pressure increased near the end of the nozzle. The liquid velocities of the experimental conditions No.19 ($P_D=150 \text{ kPa}$) and No.20 ($P_D=180 \text{ kPa}$) were increased from the throat to the exit of the nozzle. It was seen that the liquid and bubble velocities were increase together. According to the pressure difference, the liquid velocity and flow rate were increased and the liquid velocity closed to the bubble velocity. The bubbles were more generated and void fraction was more increased. Therefore, pressure loss at the throat also increased. The liquid velocity reached the sound speed. The less velocity slip ratio was observed in these experimental conditions. Therefore, these experiments were expected to be supersonic flow.
- iii. Much micro-bubble could be generated in experimental condition No.22 ($P_D=150 \text{ kPa}$) at the throat comparing with the other experimental conditions with orifice plate.2 (area is $2.694 \times 10^{-4} \text{ m}^2$). In this experimental condition, the

formation of the number of bubbles at the throat was more than the other experimental conditions and the liquid velocity was lower. Because of the higher bubble formation and lower liquid velocity, the higher void fraction was observed in experimental condition No.22. In addition, it approached to the sound speed at the throat because of its void fraction. Therefore, the experimental condition design (7 holes with the diameter of 7 mm) was the most potential for supersonic flow because of its higher void fraction, the throat velocity was closed to the sound speed.

- iv. The orifice plate.3 (area is $3.730 \times 10^{-4} \text{ m}^2$) and orifice plate.4 (area is $12.566 \times 10^{-4} \text{ m}^2$) used to modify pressurized dissolution method. The void fraction and pressure loss were decreased in the experimental condition No.24. The less velocity slip ratio was observed in the experimental condition No.25. All the experimental conditions of orifice plate.3 and 4 were expected only subsonic flow.

The study in Chapter 5 was reported in the reference,

1. Khine Tun Naung, Rei Mikoshiba, Junhyuk Lee, Hideaki Monji, Effect of Orifice Shape and Dissolved Gas on Bubble Generation in Two-Phase Nozzle Flow by Pressurized Dissolution Method, *Advanced Experimental Mechanics*, Vol.1, pp.80-85, 2016.
2. Khine Tun Naung, Nakamura, K., Mikoshiba, R., Monji, H., Study on Generation of Supersonic Flow in a Converging-Diverging Nozzle by Modified Pressurized Dissolution Method, *J. JSEM*, **15**-Special Issue, s15-s20, 2015.
3. Rei Mikoshiba, Khine Tun Naung, Hideaki Monji, Micro-Bubble Flow in Converging-Diverging Nozzle Using Pressurized Dissolution Method - Effect of

Amount of Dissolved Gas -, *Proc. of 10th International Symposium on Advanced Science and Technology in Experimental Mechanics*/p.059, Nov, 2015.

4. カイン トウン ナウン, 文字秀明, 加圧溶解法を用いた気液二相ノズル流れに対する溶存気体の影響, 日本混相流学会混相流シンポジウム 2014 講演論文集, 2014 年 7 月.

Table.5.1. Experimental conditions for the modification of pressurized dissolution method with orifice plate.

Experimental condition	Modification type	Upper tank pressure P_U [kPa]	Lower tank pressure P_L [kPa]	Pressure difference P_D [kPa]	CO ₂ rate [%]	N ₂ rate [%]
No.14	Orifice plate.1	201	101	100	0	100
No.15					25	75
No.16					50	50
No.17					75	25
No.18			51	150	100	0
No.19						
No.20						
No.21	Orifice plate.2	201	101	100	100	0
No.22			51	150		
No.23			21	180		
No.24	Orifice plate.3	201	101	100	100	0
No.25	Orifice plate.4	201	101	100	100	0

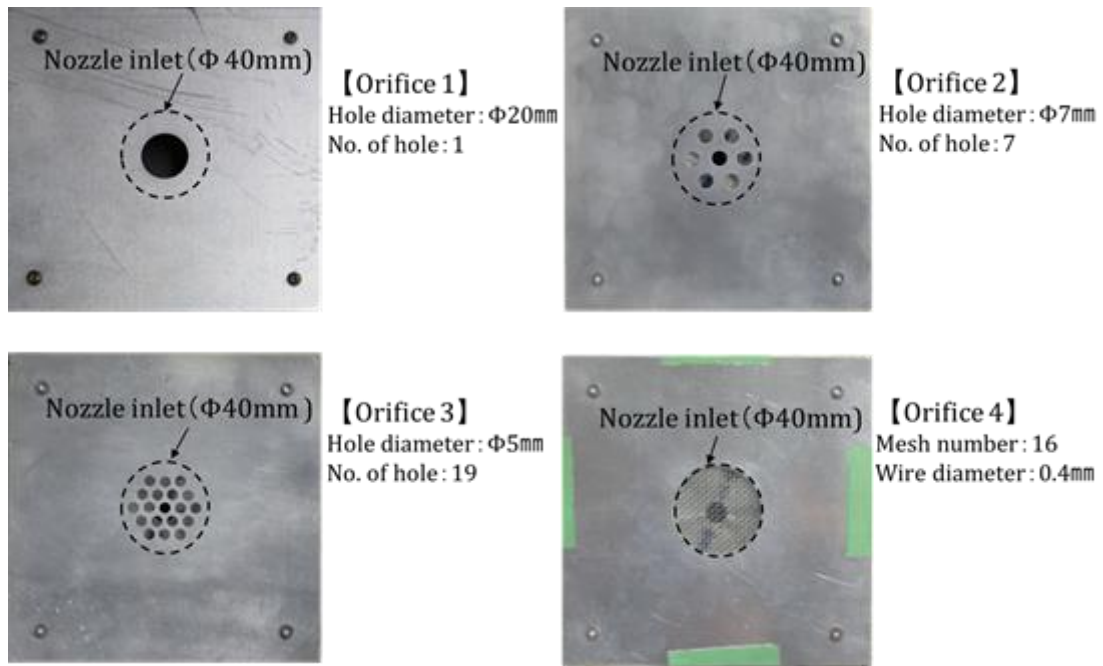


Figure 5.1. Orifice plates used in pressurized dissolution method.

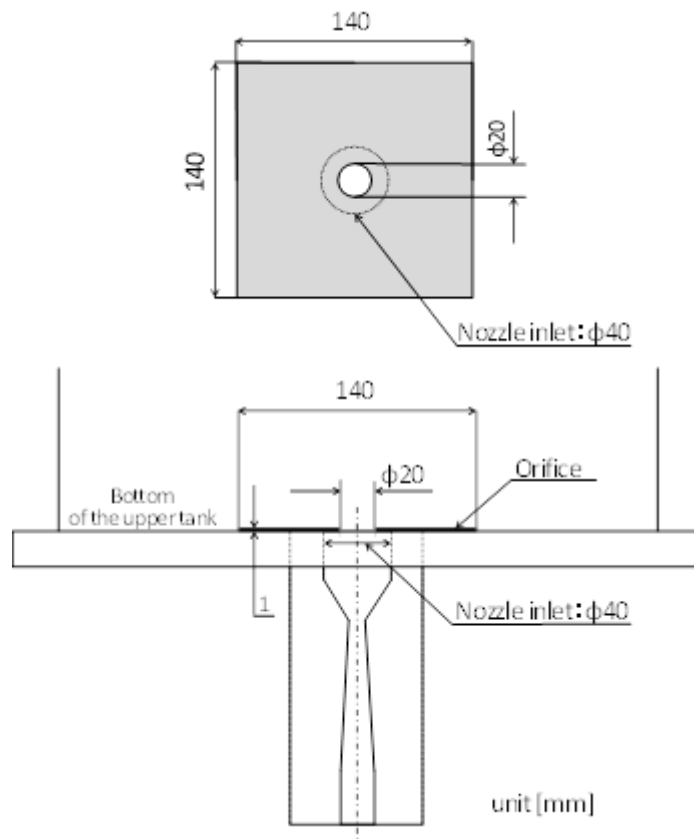


Figure 5.2. Schematic diagram of the modification of pressurized dissolution method with the orifice plate.

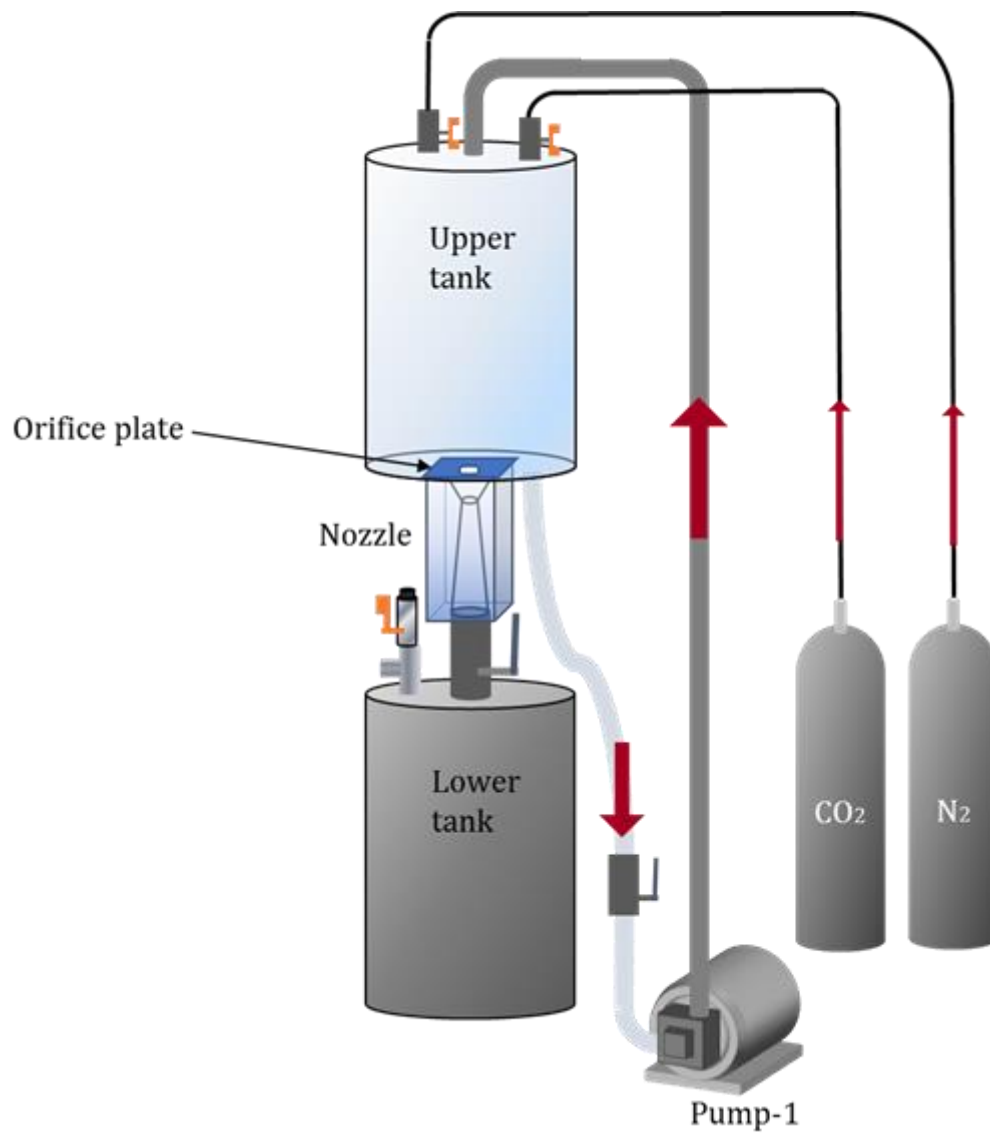


Figure 5.3. Experimental procedure by the modification of pressurized dissolution method with orifice plate.

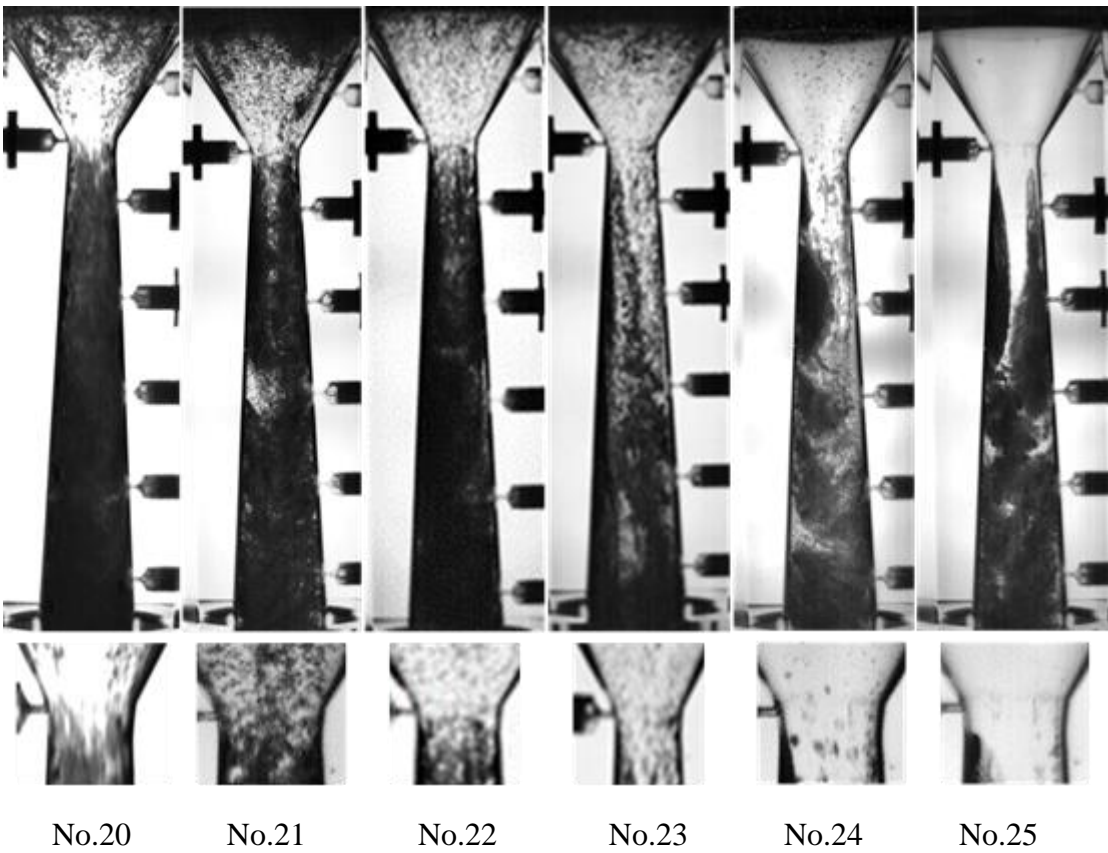
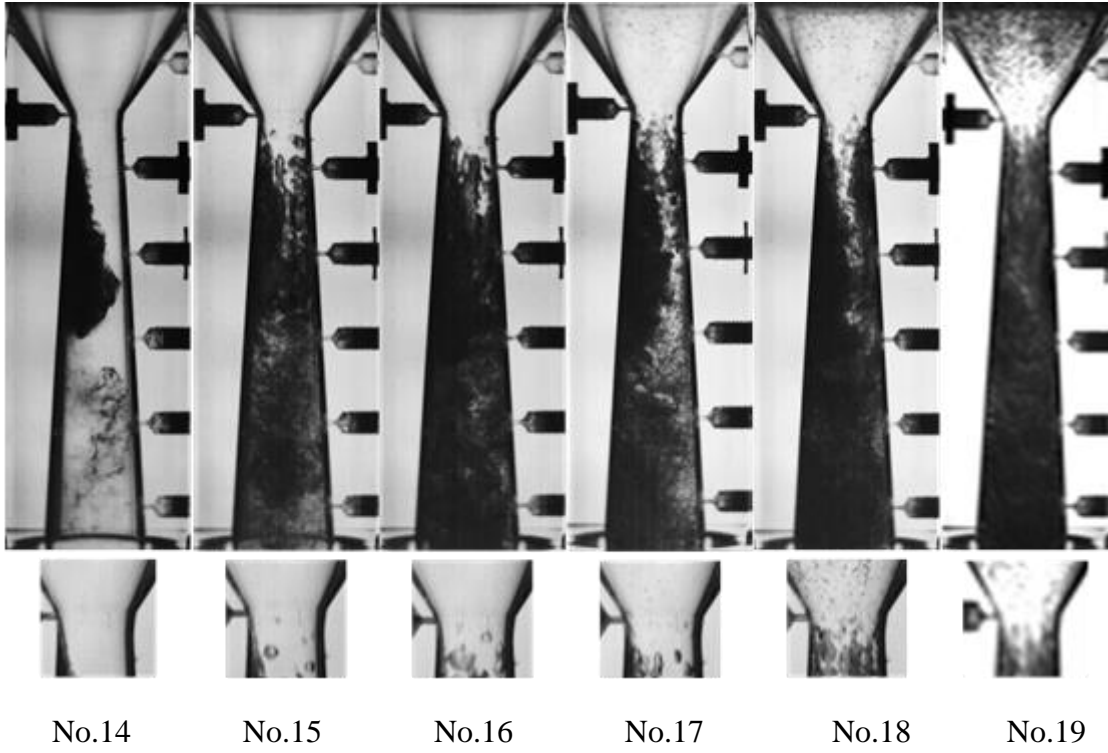


Figure 5.4. Flow pattern of the experimental conditions No.14 to No.25.

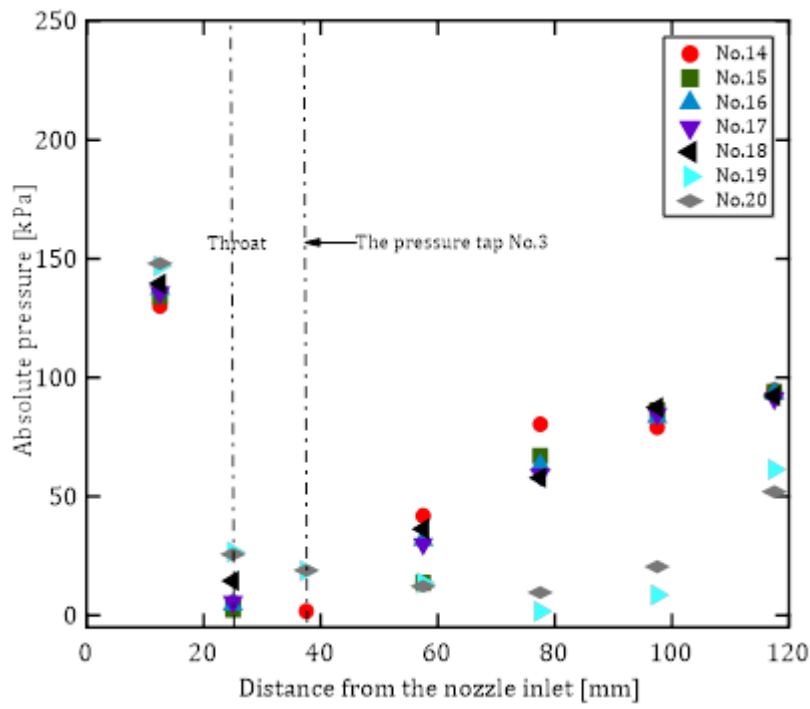


Figure 5.5. Pressure distribution along the nozzle of the experimental conditions No.14 to No.20.

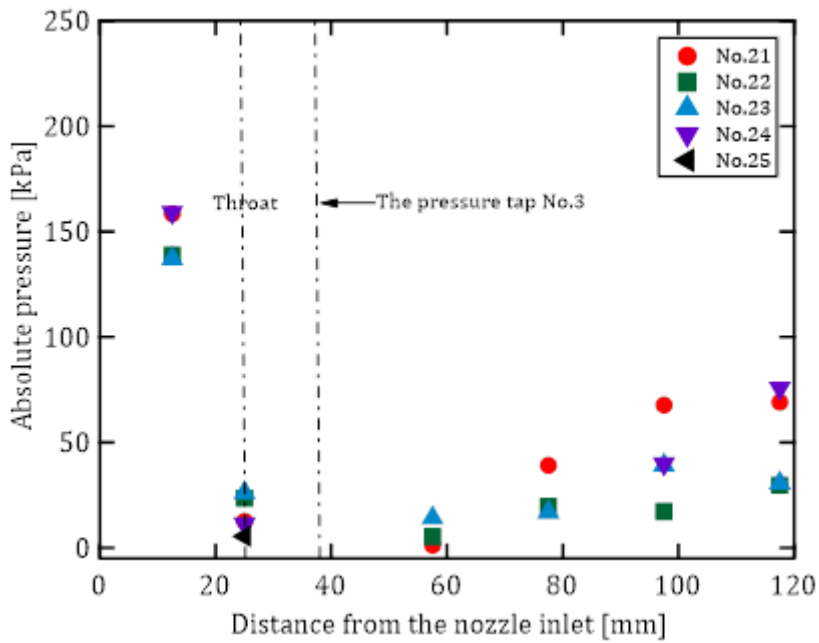


Figure 5.6. Pressure distribution along the nozzle of the experimental conditions No.21 to No.25.

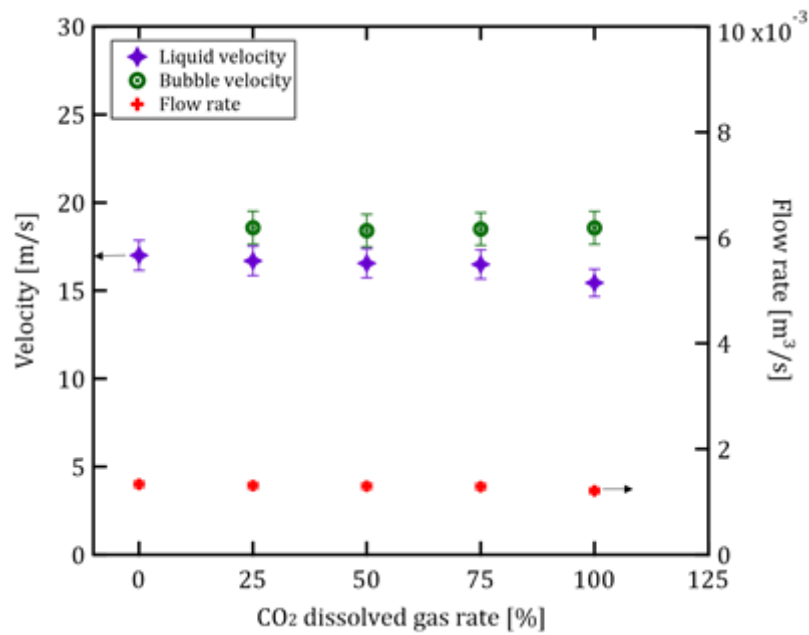


Figure 5.7. The comparison of flow rate, liquid velocity and bubble velocity at the throat of the experimental conditions No.14 (CO₂ 0%), No.15 (CO₂ 25%), No.16 (CO₂ 50%), No.17 (CO₂ 75%) and No.18 (CO₂ 100%) in orifice.1.

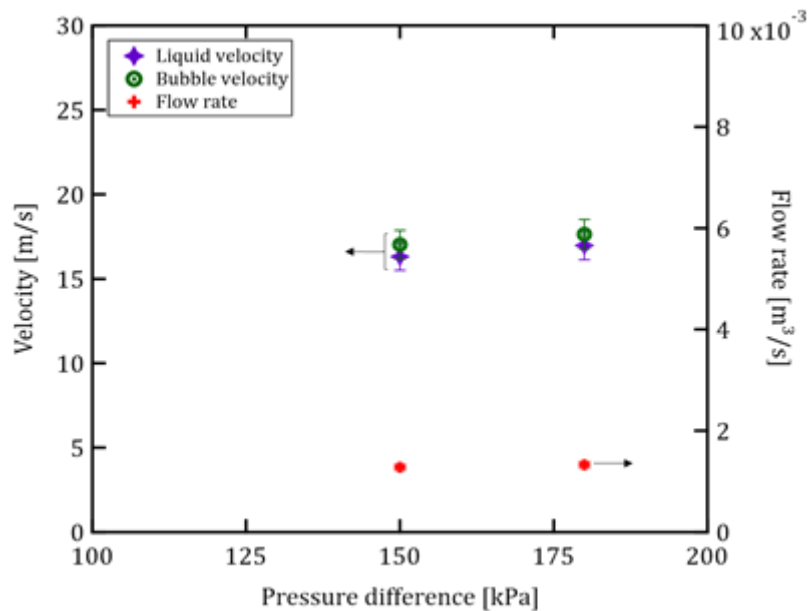


Figure 5.8. The comparison of flow rate, liquid velocity and bubble velocity at the throat of the experimental conditions No.19 ($P_D=150$ kPa) and No.20 ($P_D=180$ kPa) in orifice.1.

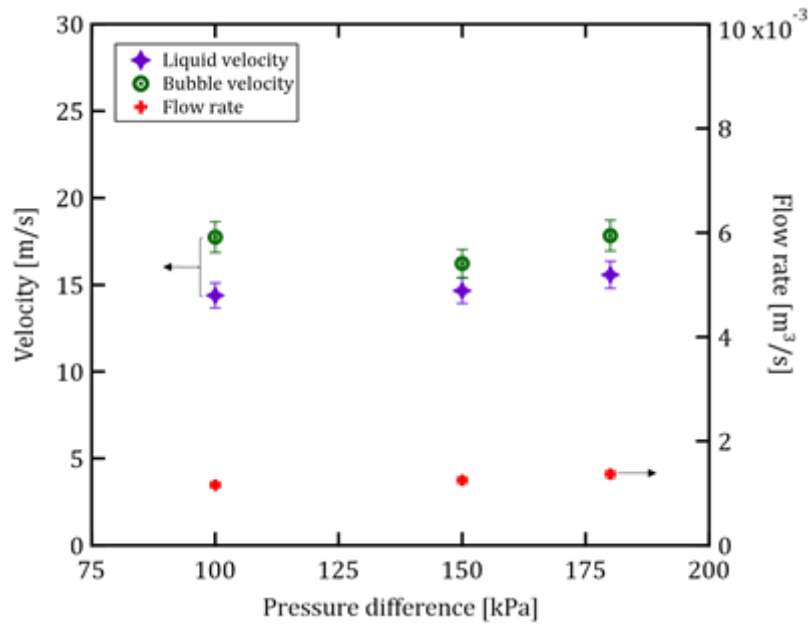


Figure 5.9. The comparison of flow rate, liquid velocity and bubble velocity at the throat of the experimental conditions No.21 ($P_D=100$ kPa), No.22 ($P_D=150$ kPa) and No.23 ($P_D=180$ kPa) in orifice.2.

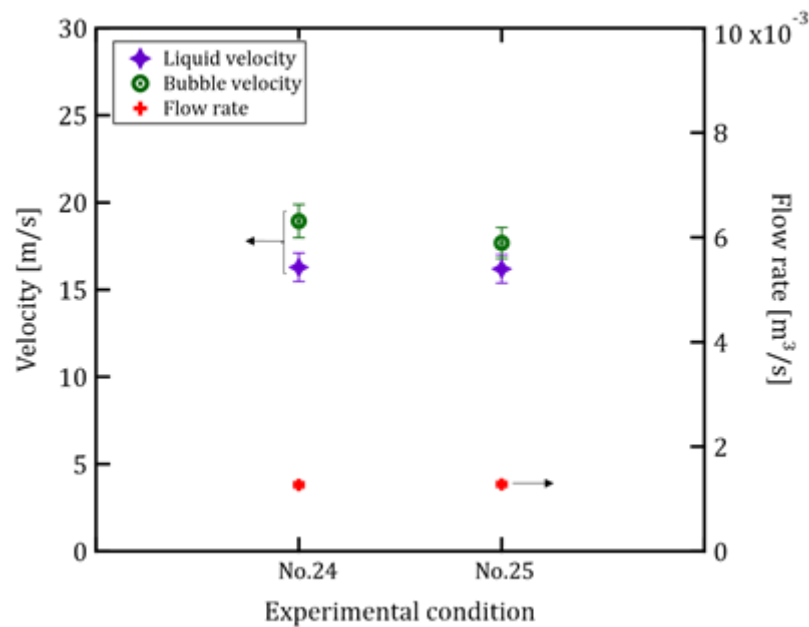
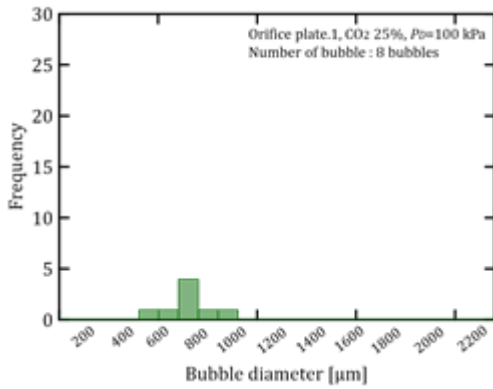
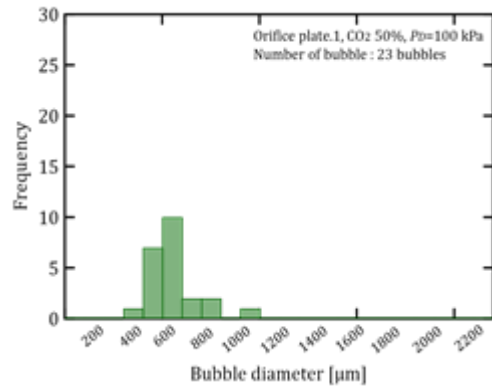


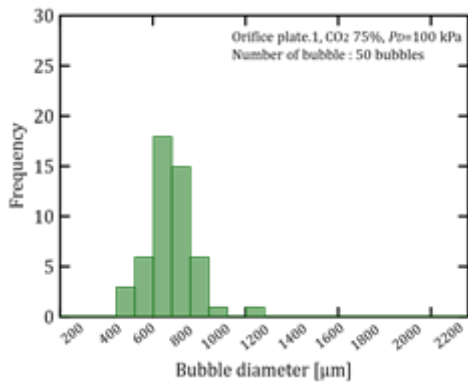
Figure 5.10. The comparison of flow rate, liquid velocity and bubble velocity at the throat of the experimental conditions No.24 ($P_D=100$ kPa) orifice.3 and No.25 ($P_D=100$ kPa) orifice.4.



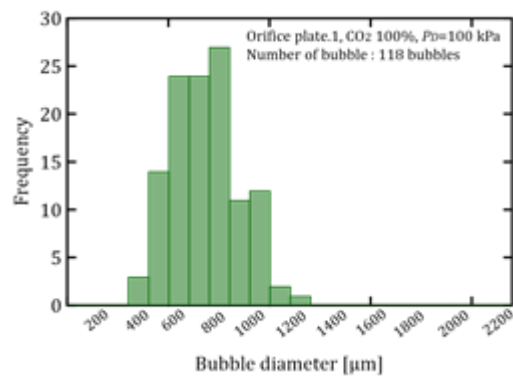
(a) Experimental condition No.15



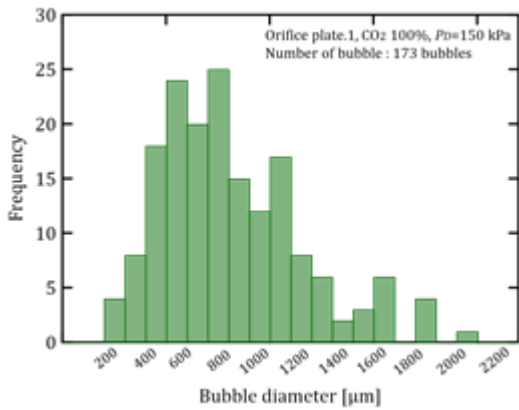
(b) Experimental condition No.16



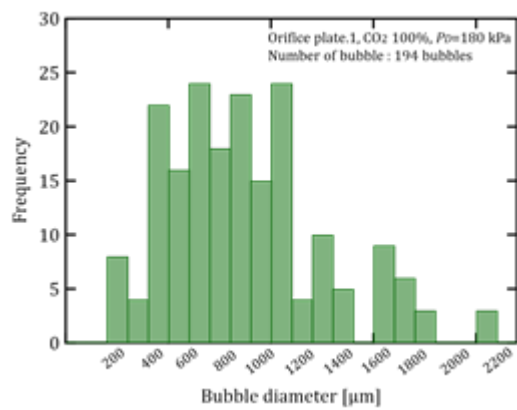
(c) Experimental condition No.17



(d) Experimental condition No.18

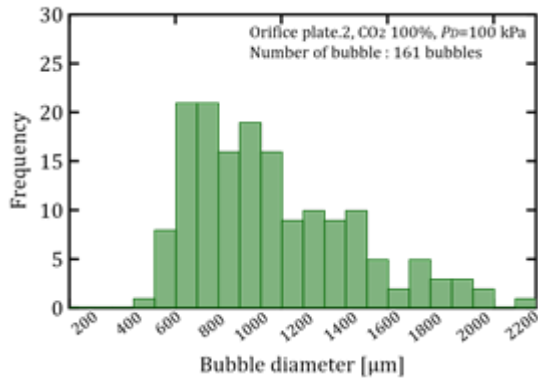


(e) Experimental condition No.19

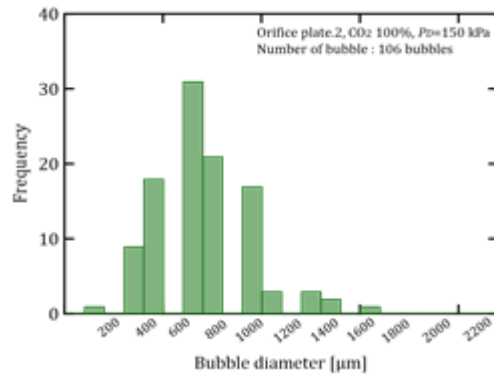


(f) Experimental condition No.20

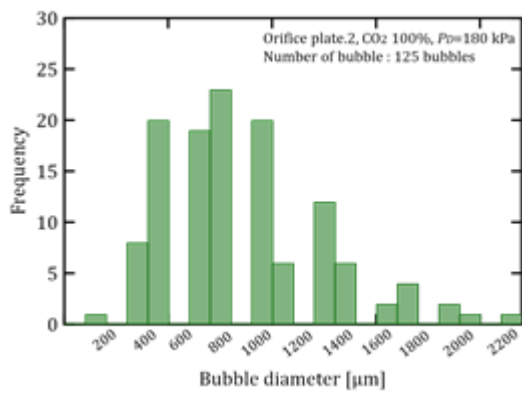
Figure 5.11. Bubble size distribution of the experimental conditions No.15 to No.25.



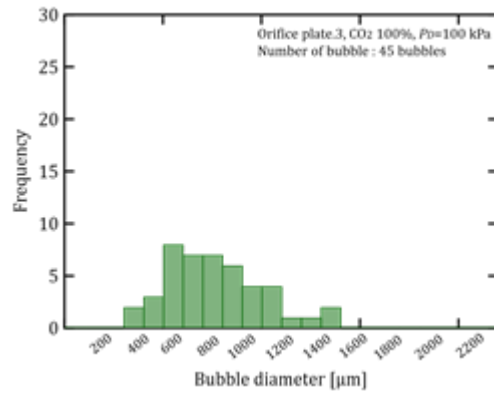
(g) Experimental condition No.21



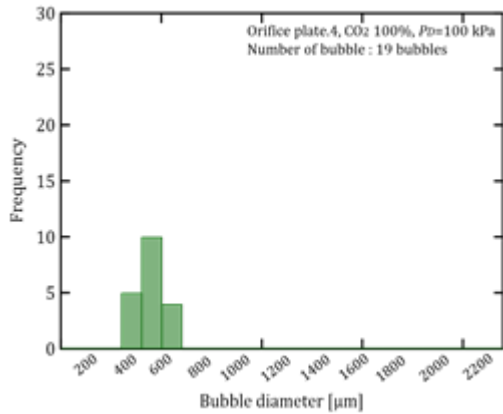
(h) Experimental condition No.22



(i) Experimental condition No.23



(j) Experimental condition No.24



(k) Experimental condition No.25

Figure 5.11. Bubble size distribution of the experimental conditions No.15 to No.25.

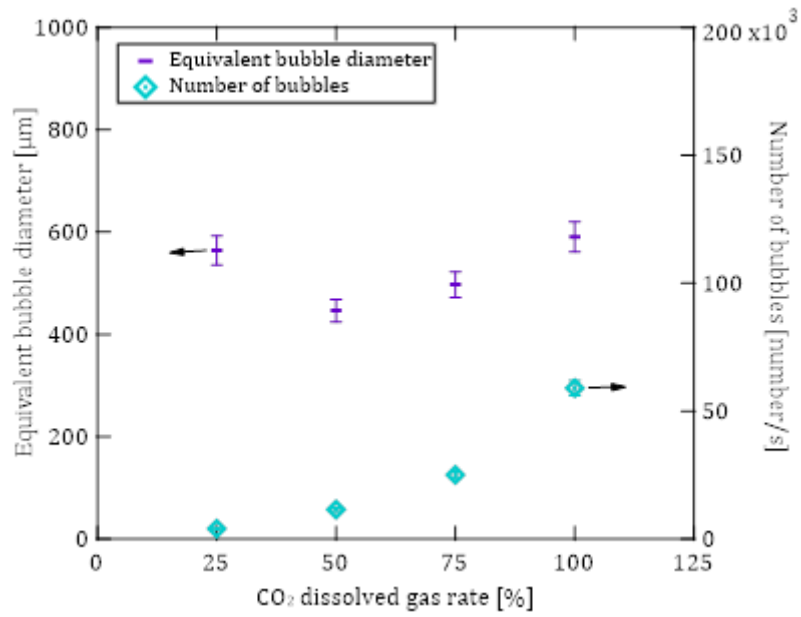


Figure 5.12. Equivalent of bubble diameter and number of bubbles of the experimental conditions No.14 (CO₂ 0%), No.15 (CO₂ 25%), No.16 (CO₂ 50%), No.17 (CO₂ 75%) and No.18 (CO₂ 100%) in orifice.1 with $P_U=201$ kPa, $P_L=101$ kPa and $P_D=100$ kPa.

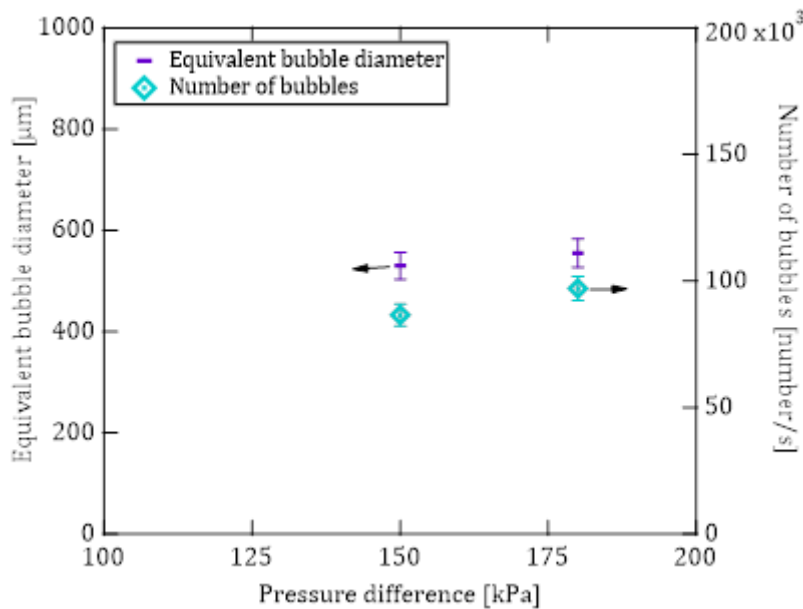


Figure 5.13. Equivalent of bubble diameter and number of bubbles of the experimental conditions No.19 ($P_U=201$ kPa, $P_L=50$ kPa and $P_D=150$ kPa) and No.20 ($P_U=201$ kPa, $P_L=20$ kPa and $P_D=180$ kPa) in orifice.1.

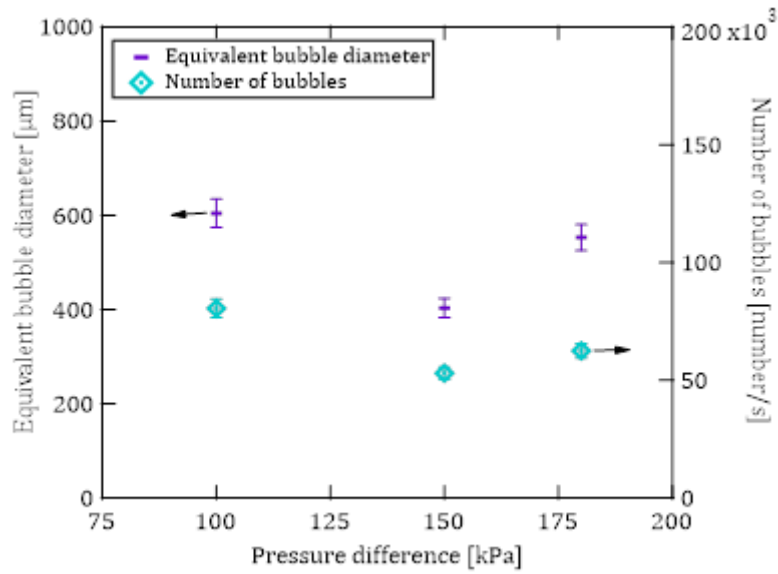


Figure 5.14. Equivalent of bubble diameter and number of bubbles of the experimental conditions No.21 ($P_U=201$ kPa, $P_L=50$ kPa and $P_D=150$ kPa), No.22 ($P_U=201$ kPa, $P_L=50$ kPa and $P_D=150$ kPa) and No.23 ($P_U=201$ kPa, $P_L=50$ kPa and $P_D=150$ kPa) in orifice.2.

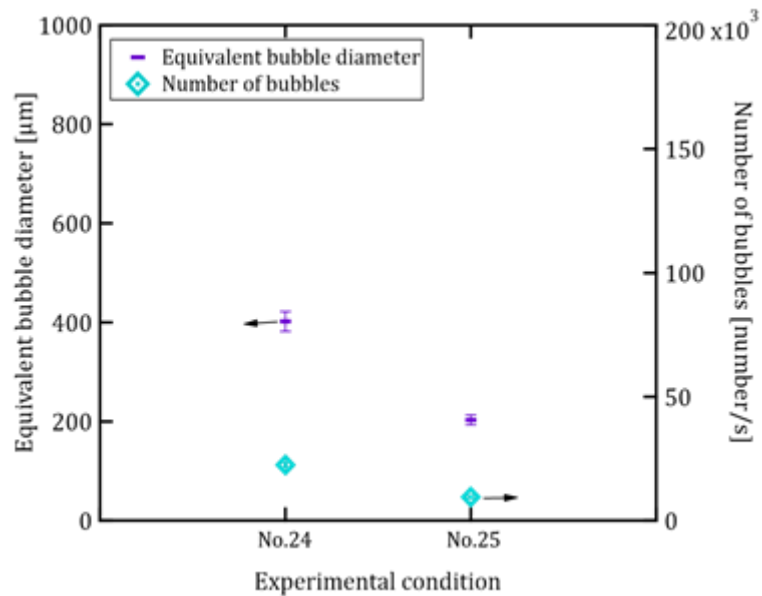


Figure 5.15. Equivalent of bubble diameter and number of bubbles of the experimental conditions No.24 orifice.3 and No.25 orifice.4 with $P_U=201$ kPa, $P_L=101$ kPa and $P_D=100$ kPa.

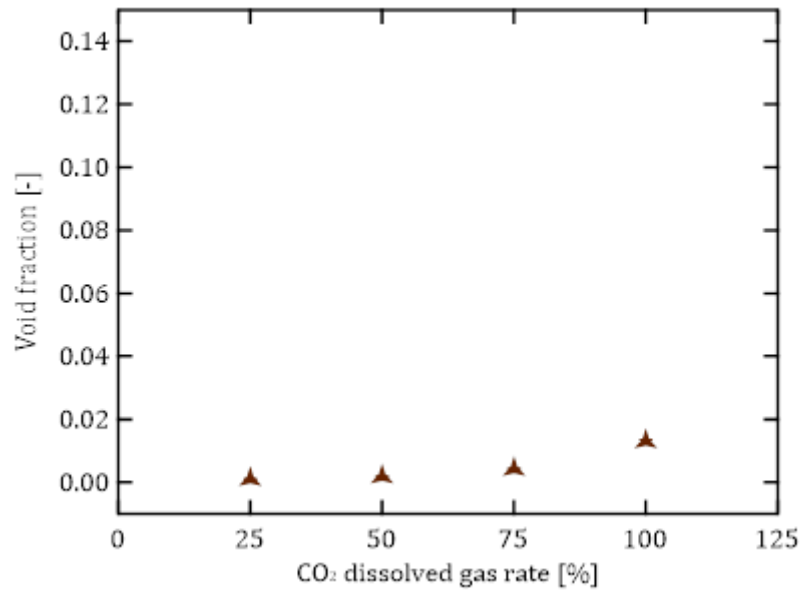


Figure 5.16. Void fraction at the throat of the experimental conditions No.15 (CO₂ 25%), No.16 (CO₂ 50%), No.17 (CO₂ 75%) and No.18 (CO₂ 100%) in orifice.1.

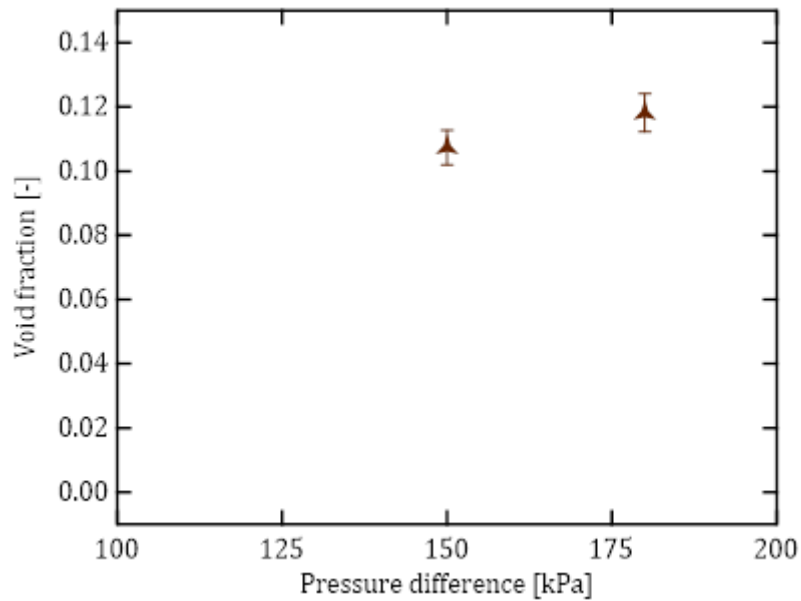


Figure 5.17. Void fraction at the throat for the experimental conditions No.19 ($P_D=150$ kPa) and No.20 ($P_D=180$ kPa) in orifice.1.

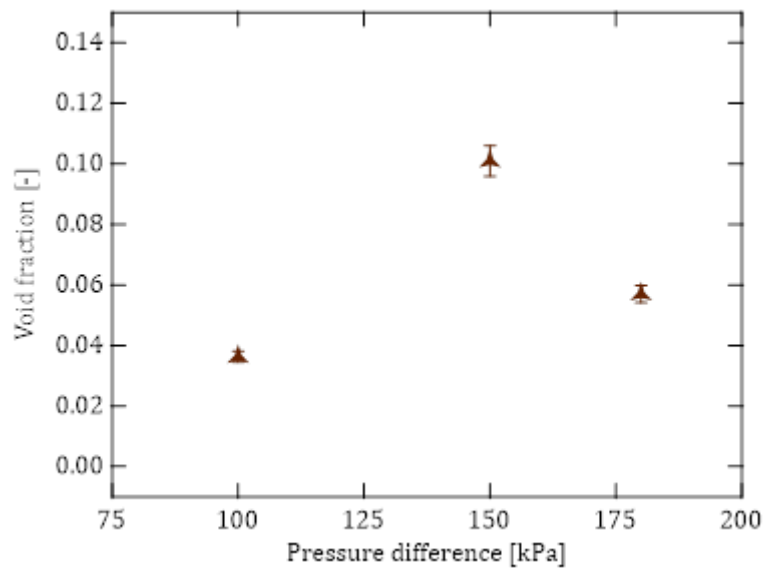


Figure 5.18. Void fraction at the throat of the experimental conditions No.21 ($P_D=100$ kPa), No.22 ($P_D=150$ kPa) and No.23 ($P_D=180$ kPa) in orifice.2.

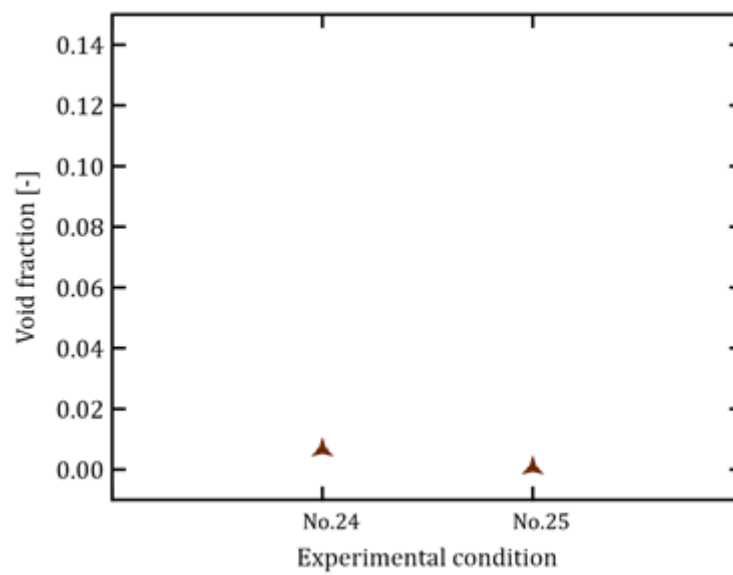


Figure 5.19. Void fraction at the throat of the experimental conditions No.24 ($P_D=100$ kPa) orifice.3 and No.25 ($P_D=100$ kPa) orifice.4.

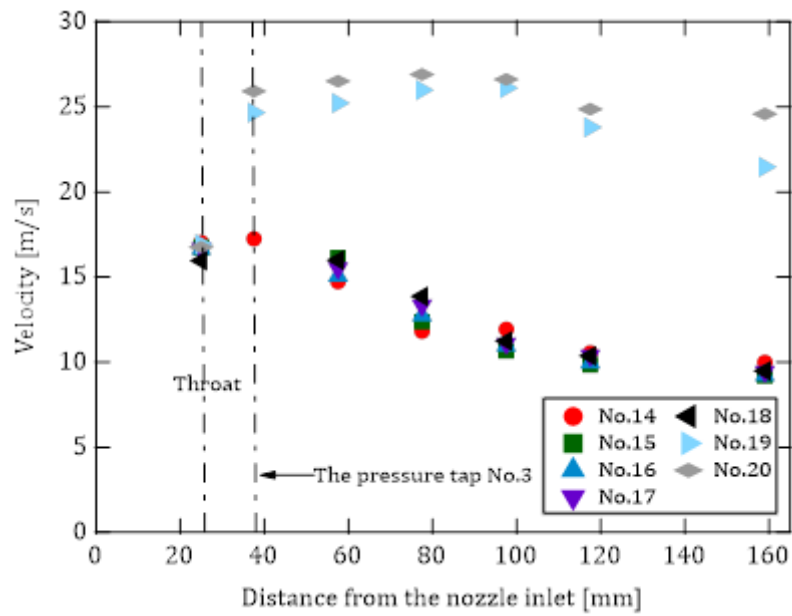


Figure 5.20. Velocity distribution along the nozzle of the experimental conditions No.14 to No.20.

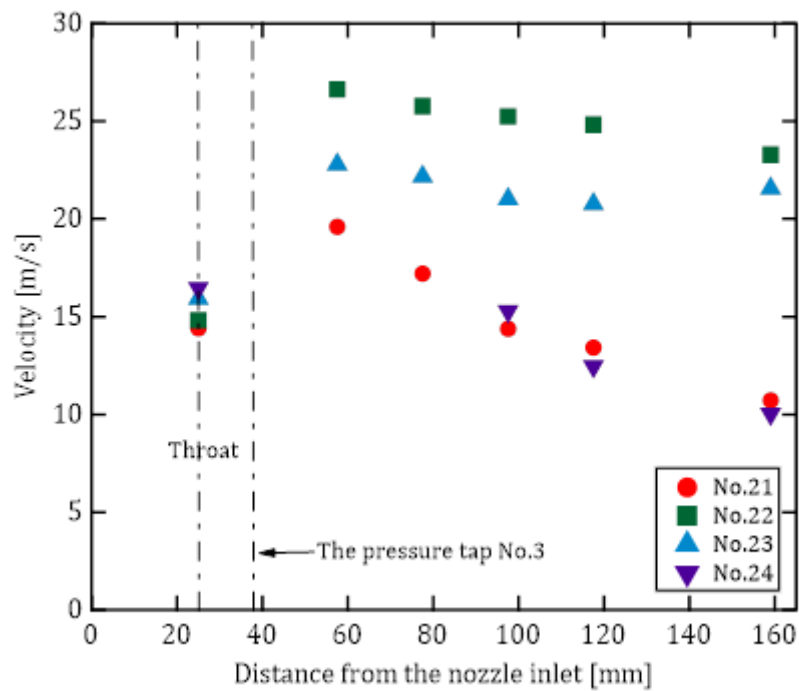
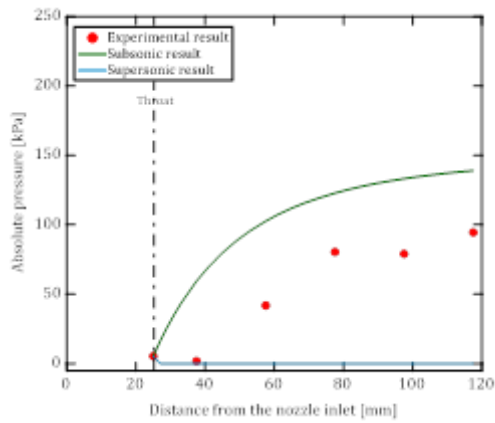
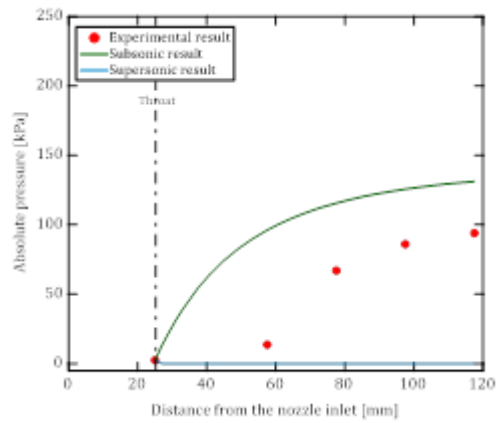


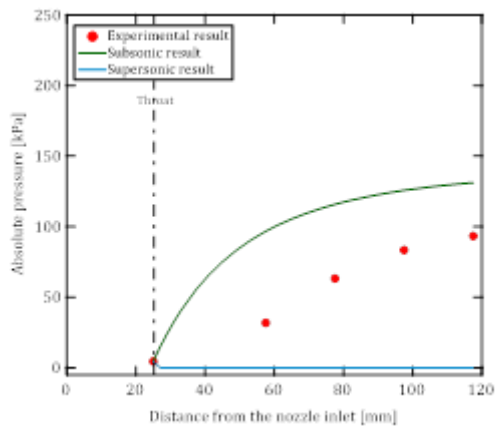
Figure 5.21. Velocity distribution along the nozzle of the experimental conditions No.21 to No.24.



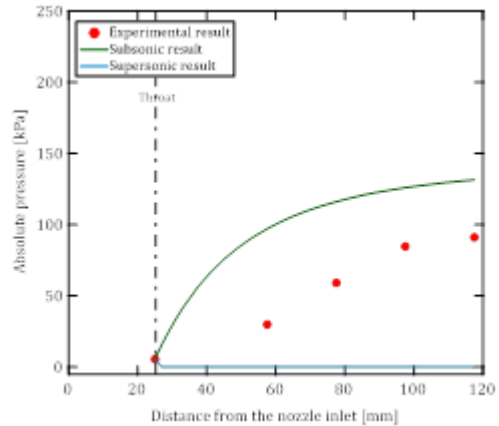
(a) Experimental condition No.14



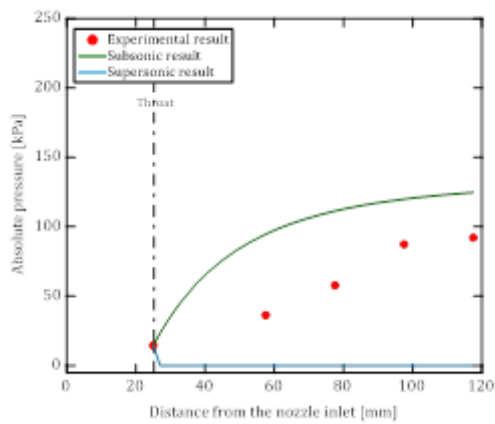
(b) Experimental condition No.15



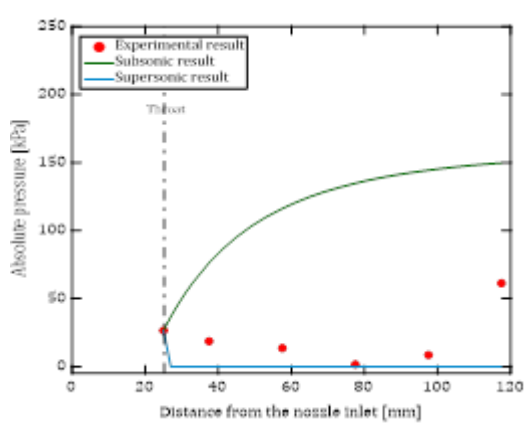
(c) Experimental condition No.16



(d) Experimental condition No.17

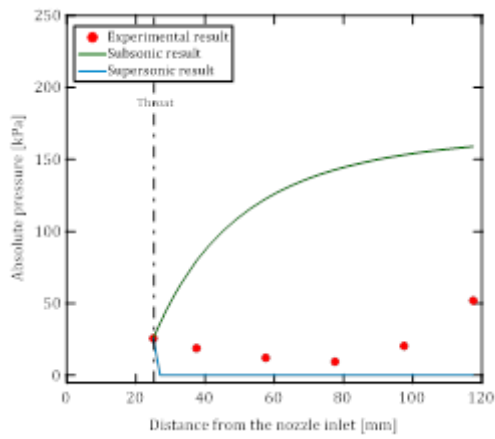


(e) Experimental condition No.18

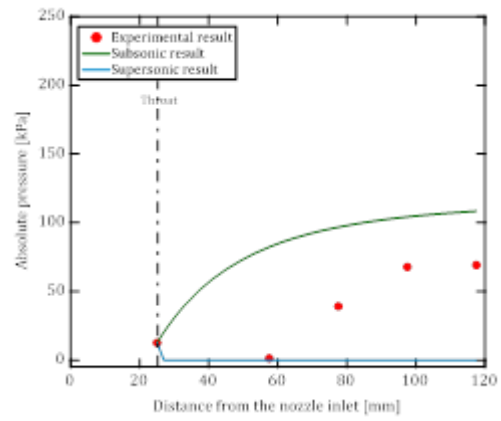


(f) Experimental condition No.19

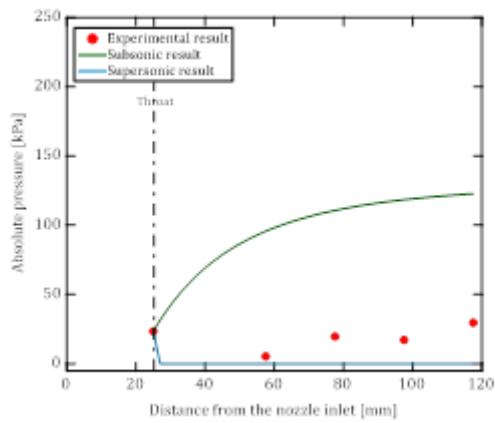
Figure 5.22. The comparison of pressure distribution between the experimental and theoretical estimation of subsonic and supersonic flow of the experimental conditions No.14 to No.25.



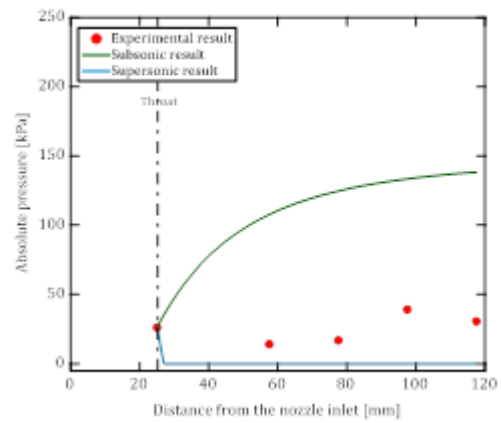
(g) Experimental condition No.20



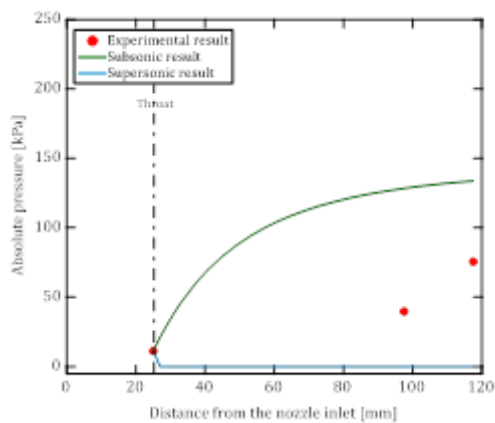
(h) Experimental condition No.21



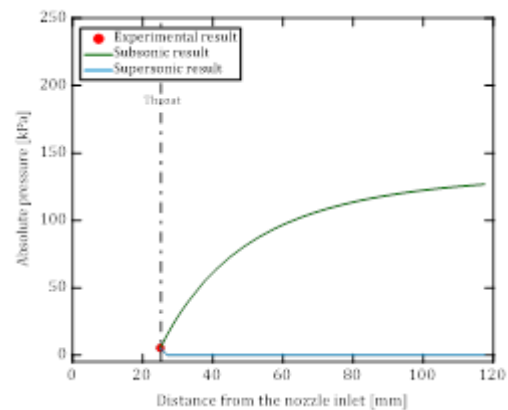
(i) Experimental condition No.22



(j) Experimental condition No.23



(k) Experimental condition No.24



(l) Experimental condition No.25

Figure 5.22. The comparison of pressure distribution between the experimental and theoretical estimation of subsonic and supersonic flow of the experimental conditions No.14 to No.25.

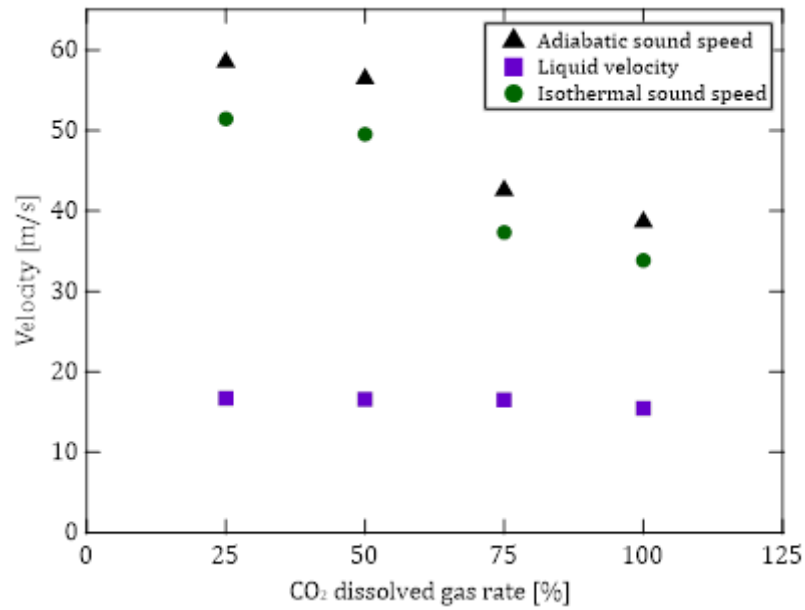


Figure 5.23. The comparison of liquid velocity and sound speed at the throat of the experimental conditions No.15 (CO₂ 25%), No.16 (CO₂ 50%), No.17 (CO₂ 75%) and No.18 (CO₂ 100%) in orifice.1.

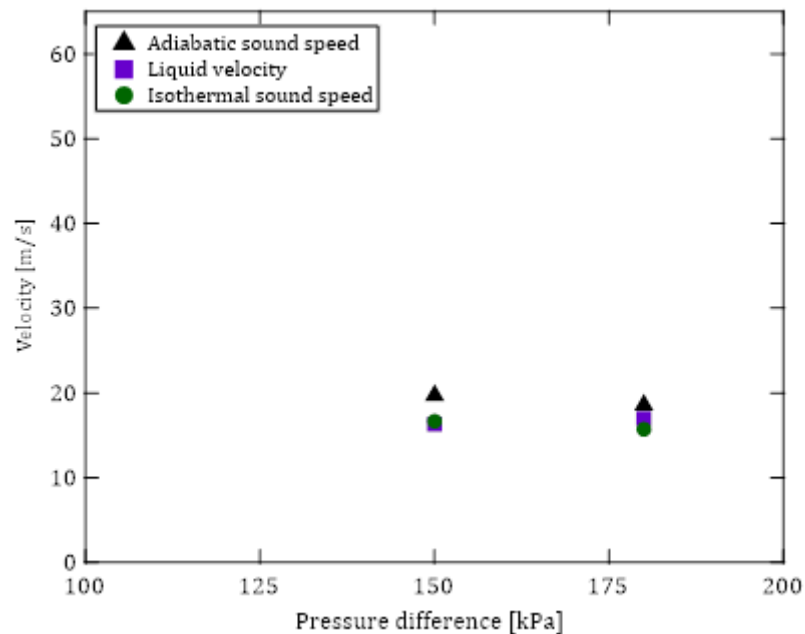


Figure 5.24. The comparison of liquid velocity and sound speed at the throat of the experimental conditions No.19 ($P_D=150$ kPa) and No.20 ($P_D=180$ kPa) in orifice.1.

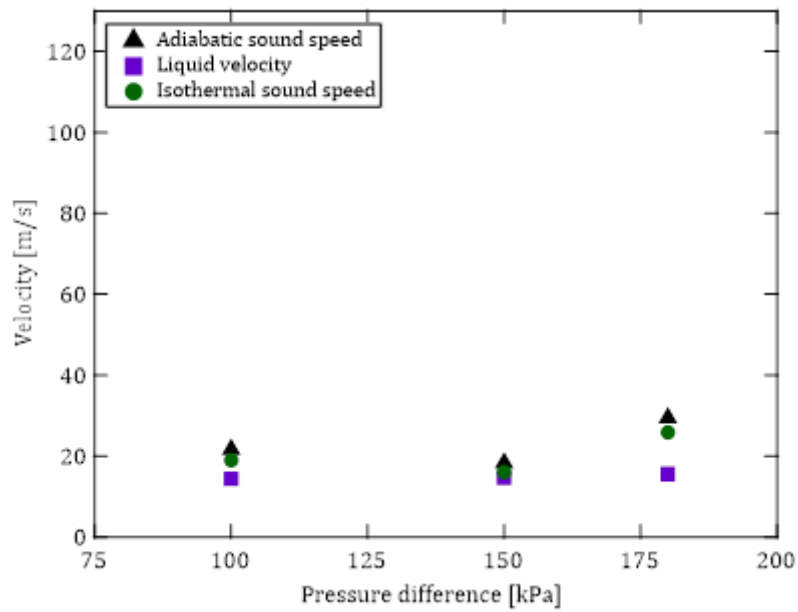


Figure 5.25. The comparison of liquid velocity and sound speed at the throat of the experimental conditions No.21 ($P_D=100$ kPa), No.22 ($P_D=150$ kPa) and No.23 ($P_D=180$ kPa) in orifice.2.

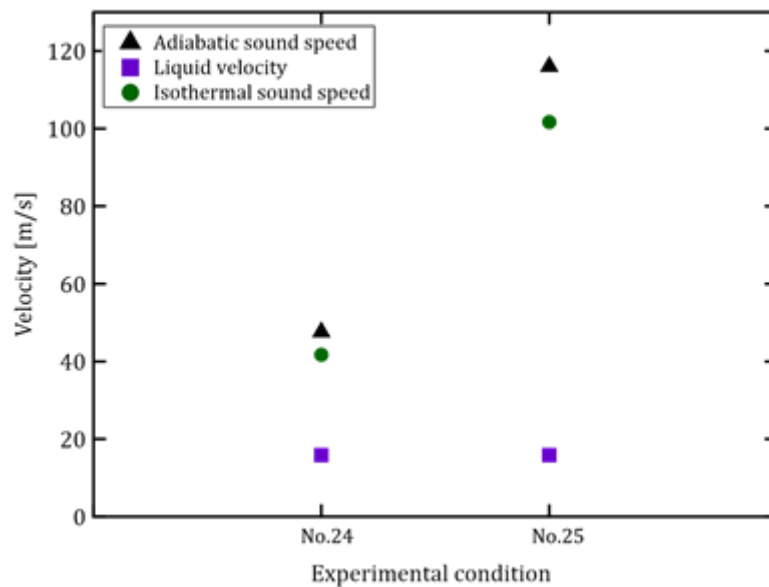


Figure 5.26. The comparison of liquid velocity and sound speed at the throat of the experimental conditions No.24 ($P_D=100$ kPa) orifice.3 and No.25 ($P_D=100$ kPa) orifice.4.

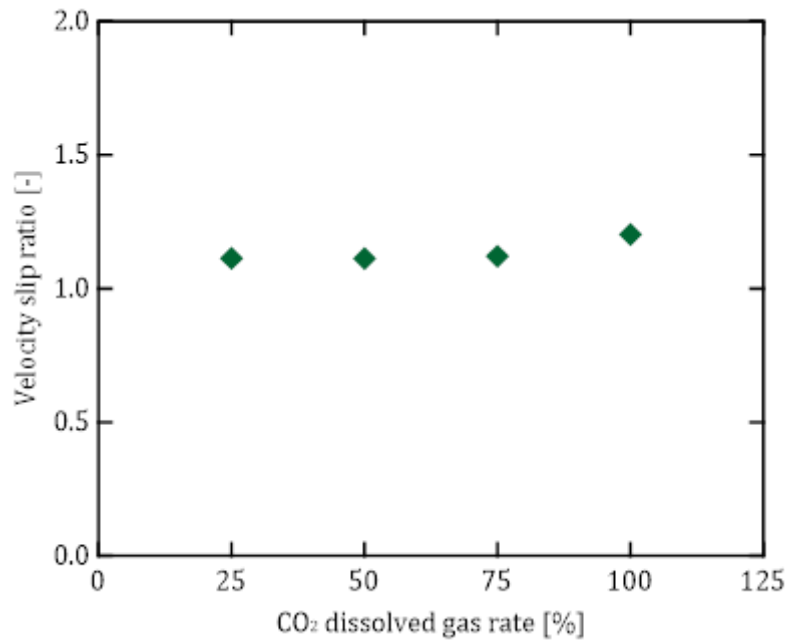


Figure 5.27. Velocity slip ratio of the experimental conditions No.15 (CO₂ 25%), No.16 (CO₂ 50%), No.17 (CO₂ 75%) and No.18 (CO₂ 100%) in orifice.1 with $P_D=100$ kPa.

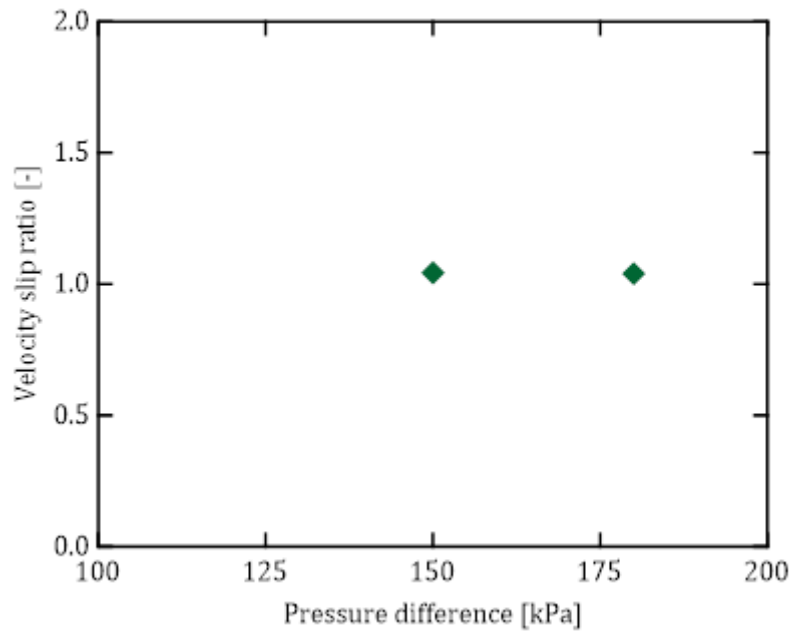


Figure 5.28. Velocity slip ratio of the experimental conditions No.19 ($P_D=150$ kPa) and No.20 ($P_D=180$ kPa) in orifice.1 with CO₂ rate 100%.

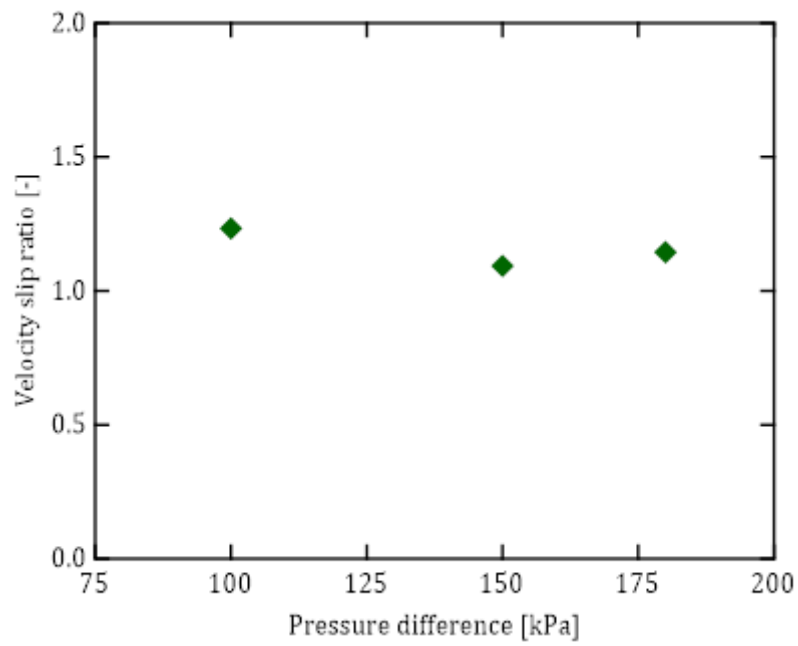


Figure 5.29. Velocity slip ratio of the experimental conditions No.21 ($P_D=100$ kPa), No.22 ($P_D=150$ kPa) and No.23 ($P_D=180$ kPa) in orifice.2 with CO₂ rate 100%.

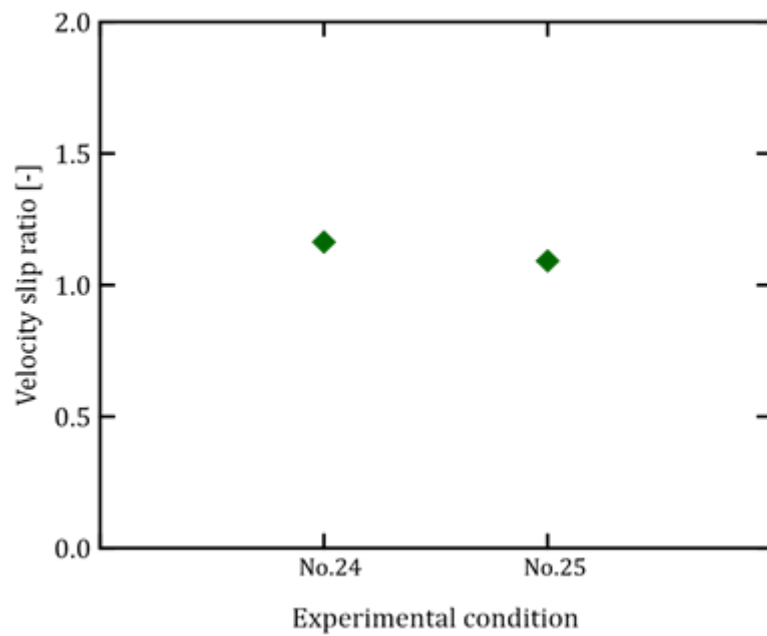


Figure 5.30. Velocity slip ratio of the experimental conditions No.24 ($P_D=100$ kPa) orifice.3 and No.25 ($P_D=100$ kPa) orifice.4 with CO₂ rate 100%.

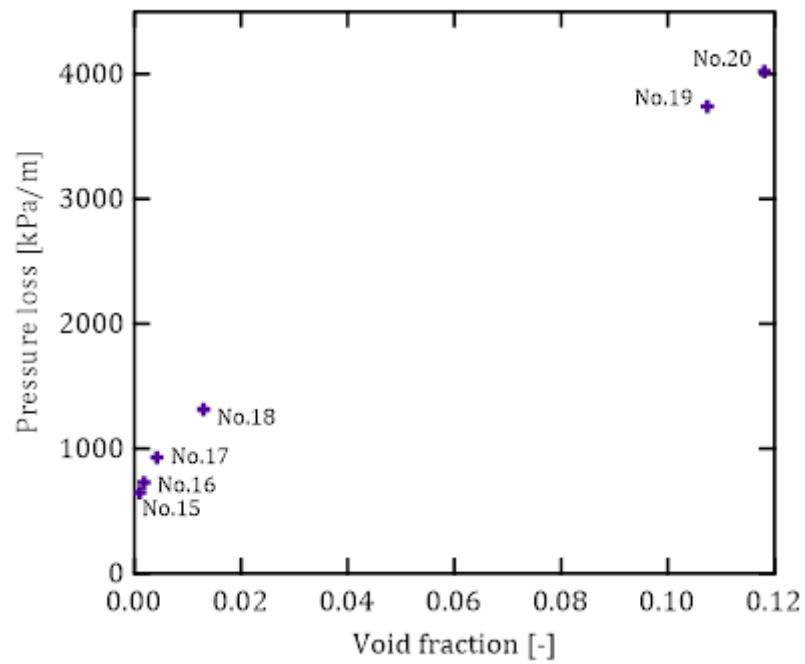


Figure 5.31. The comparison of pressure loss and void fraction of the experimental conditions No.15 to No.20.

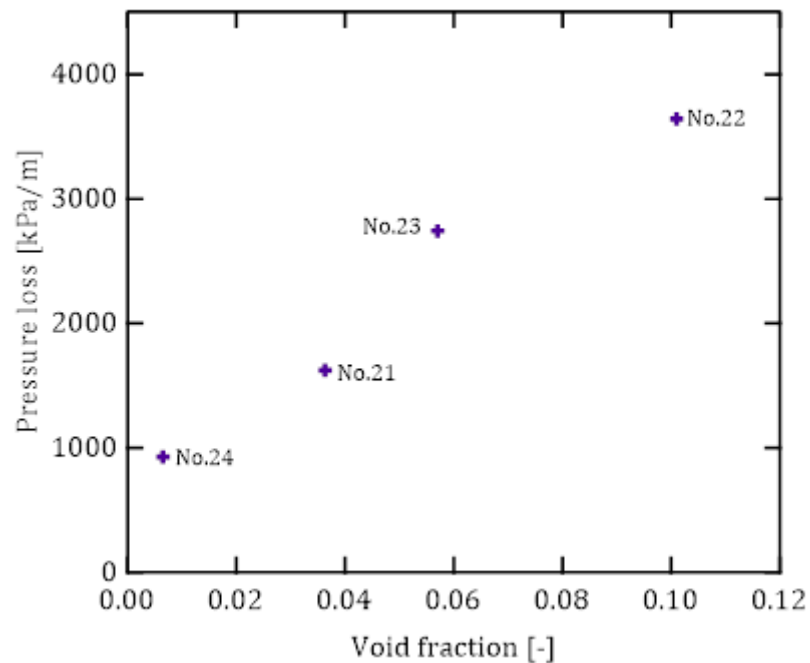


Figure 5.32. The comparison of pressure loss and void fraction of the experimental conditions No.21 to No.24.

Chapter 6

Modification of Pressurized Dissolution Method with Connecting Two Nozzles

6.1. Experimental procedure

In the modification of pressurized dissolution method with orifice plates, the supersonic flow was observed. However, the formation of micro-bubble was less. Therefore, in this chapter connecting two nozzles were used to generate more micro-bubbles in the converging section of the main nozzle. A front nozzle is used to generate micro-bubbles. Photo of the front nozzle is shown in Fig. 6.1. The diameter of both the inlet and the outlet of the front nozzle is 40 mm and the diameter of the throat is 10 mm. The lengths of the converging and diverging parts are 40 mm and 60 mm respectively. Photo and schematic diagram of the connecting two nozzles is shown in Fig. 6.2. The front nozzle is connected with the main nozzle to generate more micro-bubble in the converging section of the main nozzle. The experimental procedure steps are almost the same with the modification of pressurized dissolution method with the orifice (section 5.1). After three times of pressurizing and depressurizing, the pressure of the upper and the lower tanks were adjusted to the desired pressure according to the experimental condition. While the carbon dioxide gas and the nitrogen gas were mixing into the water by using the pump-1 to circulate the water letting in and out of the tank, it was also needed to supply carbon dioxide and nitrogen as the total pressure shown in Fig. 6.3. When it reached to the saturated liquid phase, the experiment was began by opening the valve downstream of the nozzle.

6.2. Experimental condition

The detail information of the experimental conditions is shown in Table 6.1. In the experimental conditions No.26 to No.40 were the modification of pressurized

dissolution method with connecting two nozzles was used. In these experimental conditions, the upper tank pressure was kept at 201 kPa and only the lower tank pressure was changed according to the experimental conditions. In the experimental conditions No.26 to No.30, the lower tank pressure was 101 kPa and pressure difference was 100 kPa. Even if the total pressure in the upper tank and the lower tank was set to be constant in the experimental conditions No.26 to No.30, the partial pressure of CO₂ was changed with N₂ in each experimental condition to examine the effect of CO₂ gas on two-phase flow of connecting two nozzles. In the experimental conditions No.31 to No.35, the lower tank pressure was 51 kPa and pressure difference was 150 kPa. In the experimental conditions No.36 to No.40 the lower tank pressure is 21 kPa and pressure difference is 180 kPa.

6.3. Flow visualization

Figure 6.4 (a)-(c) show flow in case of the modification of pressurized dissolution method with connecting two nozzles. Among the experimental conditions No.26 to No.30 (see Fig. 6.4 (a)), most micro-bubbles were formed in No.30 (CO₂ 100%). The formation of micro-bubbles was observed much in 50% CO₂, in the experimental conditions No.31 to No.35 (see Fig. 6.4 (b)). In the experimental conditions No.36 to No.40 (see Fig. 6.4 (c)), the micro-bubbles can be formed even in 0% CO₂ conditions because they may come from the dissolved N₂ gas. Therefore, in these experimental conditions the upper tank pressure 201 kPa and lower tank pressure 21 kPa was the preferable conditions for the micro-bubble formation.

6.4. Pressure profiles along the nozzle

The results of the pressure profiles along the nozzle in the case of the

modification of pressurized dissolution method with connecting two nozzles represented in Fig. 6.5 to 6.7. In case of the experimental conditions No.26 to No.30 ($P_U=201$ kPa, $P_L=101$ kPa, $P_D=100$ kPa), the flow may be subsonic which was estimated based on the increasing pressure distribution is shown in Fig. 6.5. In the experimental conditions No.31 to No.34 ($P_U=201$ kPa, $P_L=51$ kPa, $P_D=150$ kPa), the pressure decreased downstream the throat, but it turns to increase on the way of the diverging part of the nozzle. The experimental conditions No.35 showed high pressure at the throat illustrated in Fig. 6.6. Figure 6.7 describes the experimental conditions No.36 to No.38 have low pressure downstream the throat. In the experimental conditions No.39 and No.40 the pressure increased from the throat to the exit of the nozzle. The pressure distribution was less fluctuated when the amount of CO₂ gas increased.

6.5. The comparison of the flow rate, liquid velocity and bubble velocity at the throat

Figure 6.8 to Figure 6.10 depict the comparison of the flow rate, liquid velocity and bubble velocity at the throat in the case of the modification of the pressurized dissolution method with connecting two nozzles from the experimental conditions No.26 to No.40. When the CO₂% increased from 0% to 75% in the experimental conditions No.26 to No.30, the flow rate and liquid velocity were constant. However, micro-bubbles were not generated at the throat in the experimental conditions No.26 to No.28. The flow rate, liquid velocity and bubble velocity decreased in the experimental conditions No.29 (CO₂ 75%) to No.30 (CO₂ 100%).

The experimental conditions No.31 to No.35 were the same pressure difference as 150 kPa shown in Figure 6.9. In these experimental conditions the flow rate and liquid velocity at the throat were almost constant with CO₂% increased. The bubble velocity was gradually increased, when the CO₂% increased. However, the liquid

velocity and bubble velocity were decreased in experimental condition No.35 (CO₂ 100%), even though CO₂% increased.

The experimental conditions No.36 to No.40 were the pressure difference was constant with 180 kPa, but the amount of CO₂ changed 0% to 100% as represented in Fig. 6.10. The flow rate and liquid velocity were constant and bubble velocity was slightly increase, when CO₂% increased. In the experimental conditions No.37 and No.38, the liquid velocity was almost the same as the bubble velocity. In the experimental conditions No.36, No.39 and No.40, the bubble velocity was higher than liquid velocity.

6.6. Measurement of bubble size distribution

Figure 6.11 (a)-(i) illustrates bubble diameter distributions of the experimental condition No.29 to No.39. There is no micro-bubble generation at the throat in the experimental conditions No.26 to No.28. Total 252 bubbles were observed in the experimental condition No.29 (CO₂ 75%, $P_D=100$ kPa) with the equivalent diameter of bubbles 385.5 μm and its standard deviation 30.29 μm . The lower tank pressure was decreased to 51 kPa with the same upper tank pressure in this connecting two nozzles experiments in the experimental conditions No.31 to No.34. For the experimental conditions No.31 (CO₂ 0%), No.32 (CO₂ 25%), No.33 (CO₂ 50%) and No.34 (CO₂ 75%) the results of the bubbles were 115 bubbles, 185 bubbles, 321 bubbles and 348 bubbles, the results of the equivalent diameter were 453.833 μm , 480.781 μm , 607.643 μm and 608.286 μm and the results of the standard deviation were 11.191 μm , 15.849 μm , 21.571 μm and 17.778 μm respectively. The bubble formation of the experimental condition No.35 (CO₂ 100%) was too much. Therefore, in this experimental condition the bubble behavior could not be observed. In the experimental condition No.36 (CO₂

0%, $P_D=180$ kPa) the micro-bubble was observed 87 bubbles and its equivalent diameter was $378.625 \mu\text{m}$ and standard deviation was $9.304 \mu\text{m}$. For 135 bubbles, the equivalent diameter of bubbles was $603.214 \mu\text{m}$ and its standard deviation was $9.867 \mu\text{m}$ in the experimental condition No.37 (CO_2 25%, $P_D=180$ kPa). In the experimental conditions No.38 (CO_2 50%, $P_D=180$ kPa) and No.39 (CO_2 75%, $P_D=180$ kPa) the bubbles were 330 bubbles and 349 bubbles, the equivalent diameters were $607.857 \mu\text{m}$ and $608.31 \mu\text{m}$ and the standard deviation were $17.732 \mu\text{m}$ and $18.618 \mu\text{m}$.

Consequently, the results of the equivalent bubble diameter and number of bubbles passing at the throat for a second were shown in Fig. 6.12 to Fig. 6.14. In these experiments CO_2 dissolved gas rate was increased, the equivalent bubble diameter and the number of bubbles increased. However, in the experimental conditions No.33 (CO_2 50%) and No.34 (CO_2 75%) with $P_D=150$ kPa, the equivalent bubble diameter was almost constant. And the equivalent bubble diameter was also constant, in the experimental conditions No.37 (CO_2 25%), No.38 (CO_2 50%) and No.39 (CO_2 75%) with $P_D=180$ kPa.

6.7. Void fraction at the throat

In the experimental conditions No.30, No.35 and No.40, the void fraction could not be calculated because the expansion of micro-bubbles were observed in the converging section of the main nozzle. Therefore, much number of big bubbles covered the micro-bubbles to see clearly. The void fractions at the throat are shown in Fig. 6.15 to Fig. 6.17. Only the value of the void fraction was observed in the experimental condition No.29 (CO_2 75%) with $P_D=100$ kPa as shown in Fig. 6.15. Figure 6.16 depicts the void fraction at the throat for the experimental condition No.31 to No.35 with $P_D=150$ kPa. The void fraction increased when the amount of CO_2 increased in

these experiments. In $P_D=180$ kPa, the void fraction at the throat increased as increasing the amount of CO₂ in the experimental condition No.36 to No.40 was represented in Fig. 6.17.

6.8. Velocity distribution along the nozzle

Compare the void fraction at the throat between the cases using the orifice and the connecting nozzle. In the experimental condition No.19, the orifice plate.1 was used and the void fraction at the throat was 0.11 (see Fig. 5.17). In the experimental condition No.22, the orifice plate.2 was used and the void fraction at the throat was also 0.11 (see Fig. 5.18). On the other hand, in case of the connecting nozzle under the same pressure conditions or the experimental condition No.35, the void fraction was too high and could not be measured by the image processing. Even if in the low CO₂% rate case, the void fraction was 0.11 at the throat (see Fig. 6.16). Because the pressure at the converging part of the main nozzle in the connecting nozzle was lower than that in the orifice plate.1 case, it is estimated that more air bubbles were generated in the case of the connecting nozzle (see Fig.5.5 and Fig. 6.5). Comparison between the experimental condition No.20 (orifice plate.2) and No.40 (the connecting nozzles) shows the similar result. Therefore, compared with the case where an orifice is used, the connecting nozzle can obtain high void fraction flow.

Estimated liquid velocity distribution along the nozzle by Eq. (2.28) was shown in Fig. 6.18 and Fig. 6.19. Figure 6.8 represents the experimental conditions No.31 to No.34 with the same pressure difference $P_D=150$ kPa. The experimental conditions of No.31 (CO₂ 0%) and No.32 (CO₂ 25%), liquid velocities were decrease from the pressure tap No.5. The liquid velocity was decrease from the pressure tap No.6 in the experimental condition No.33 (CO₂ 50%). In the experimental condition No.34 (CO₂

75%), the liquid velocity was decrease from the pressure tap No.4.

Figure 6.19 illustrates the experimental conditions No.36 to No.39 with the same pressure difference $P_D=180$ kPa. The liquid velocity was almost constant from the pressure tap No.3 in the experimental condition No.36 (CO₂ 0%). In the experimental conditions No.37 (CO₂ 25%), liquid velocity was slightly decrease from the pressure tap No.4. In the experimental conditions No.38 (CO₂ 50%), liquid velocity was increase from the throat and decrease from the pressure tap No.5.

6.9. The comparison of pressure distribution between the experimental and theoretical estimation of subsonic and supersonic flow

The theoretical results of the subsonic and the supersonic conditions were calculated by Eq. (2.65). Figure 6.20 (a)-(k) represents the comparison of the pressure distribution along the diverging part between the experiment and theoretical estimation of the subsonic and the supersonic flow of the experimental conditions No.30 to No.40. The experimental conditions No.26 to No.29 were not plotted in the figures because of the pressure were not obtained exact data at the throat. The experimental result in the experimental condition No.30 ($P_D=101$ kPa) closed to the subsonic condition. In the experimental conditions No.31 to No.35 with the same pressure difference ($P_D=150$ kPa), the experimental pressures approached to the subsonic condition. The experimental conditions No.36 to No.40 were the same pressure difference ($P_D=180$ kPa). In these experiments all of the experimental pressure were low because of the lower tank pressure was 21 kPa. However, the experimental pressure of the experimental condition No.38 was expected to be closed with the supersonic condition. When increasing CO₂ % with the same pressure difference P_D , the pressure estimated in the subsonic condition moved far away from the experimental result.

6.10. The comparison of liquid velocity and sound speed at the throat

The comparison of the experimental results with calculation results estimated by Eq. (2.68) of adiabatic sound speed and Eq. (2.69) of isothermal sound speed at the throat of the experimental conditions No.31 to No.40 were represented in Fig. 6.21 and Fig. 6.22. The experimental condition No.29 could not calculate the sound speed because the pressure was not measured properly at the throat. The experimental condition No.30, No.35 and No.40 also could not calculate the sound speed because the void fraction was not obtained. In the experimental conditions No.31 to No.35, liquid velocities did not reach the sound speed at the throat. Therefore, the flow in these experimental conditions may be subsonic flow shown in Fig. 6.21. In Fig. 6.22, only the liquid velocity at the throat of the experimental condition No.38 (CO₂ 50%, $P_D=180$ kPa) reached the sound speed. Therefore, the experimental condition No.38 was estimated to be supersonic flow. Experimental conditions No.36, No.37 and No.39 maybe subsonic flow.

6.11. Velocity slip ratio

Figure 6.23 to Figure 6.25 give the result of the velocity slip ratio of the experiments of the modification of pressurized dissolution method with connecting two nozzles. According to Fig. 6.23, there were no results in the experimental conditions No.26 to No. 28 because of the micro-bubble could not generate at the throat in these experiments. In the experimental conditions No.31 to No.35 with the same pressure difference ($P_D=150$ kPa), the velocity slip ratio was not proportional to the amount of CO₂. The velocity slip ratios decreased from CO₂ 0% to 50%, and then it increased to 100% because of the bubble velocity was higher at the throat, as shown in Fig. 6.24. The experimental conditions No.38 (CO₂ 50%) was the least velocity slip in the case of

same pressure difference ($P_D=180$ kPa) of the experimental conditions No.36 to No.40 was represented in Fig. 6.25.

6.12. The comparison of pressure loss and void fraction at the throat

The variations of pressure loss estimated by Eq. (2.76) and void fraction at the throat of the nozzle are illustrated in Fig. 6.26 and Fig. 6.27. Figure. 6.26 represents the experimental condition No.31 to No.34. When increasing CO_2 rate from the experimental conditions No.31 to No.34, the void fraction also increased. Therefore, pressure loss also increased at the throat. Because void fraction was directly proportional with pressure loss. Figure 6.27 describes the results of the comparison of pressure loss and void fraction at the throat of the experimental condition No.36 to No.39. In these experimental conditions, pressure loss increased with void fraction because generation of bubbles were more observed from the experimental condition No.36 to No.39.

6.13. Concluding remarks

Two connecting nozzles were used to generate more micro-bubbles from the converging section of the nozzle. The results on the modification of pressurized dissolution method with connecting two nozzles as discussed above were summarized as follows:

- i. Two nozzles were connected to modify the pressurized dissolution method. The fraction of carbon dioxide (CO_2) to the total gas was changed in order to study its effect on the generation of micro-bubbles. The micro-bubbles can be generated much when the carbon dioxide percentage increased. The pressure is less fluctuated in case of the lower percentage of CO_2 . However, the bubbles

can be generated much even in low percentage of CO₂ in case of low pressure in the lower tank. Therefore, the micro-bubbles can be generated much when the outlet pressure reduces much. It proves that the outlet pressure condition in converging-diverging nozzles is also important to generate micro-bubbles.

- ii. The experimental condition No.30, No.35, No.39 and No.40 has more micro-bubbles formation than the experimental condition No.38 but the supersonic flow was not obtained. Therefore, there is a proper condition to obtain the supersonic flow. In the study, the proper condition was a low pressure at the outlet of the nozzle and the middle amount of the dissolved gas.
- iii. In the experimental conditions No.30, No.35 and No.40 the bubbles were formed too much to identify the flow characteristics.
- iv. Comparing with the orifice, the connecting nozzle makes many bubbles under the same pressure condition.

The study in Chapter 6 was reported in the reference,

1. Khine Tun Naung, Hideaki Monji, Supersonic Flow Conditions for Two Connecting Two-Phase Flow Nozzle in Pressurized Dissolution Method, *Advanced Experimental Mechanics*, Vol.3, pp. 92-97, 2018.
2. Khine Tun Naung, Hideaki Monji, 超音速ノズルのための加圧溶解法によるマイクロバブル生成の最適条件, 第 22 回動力・エネルギー技術シンポジウム講演論文集/p.B111, 2017 年 6 月.
3. カイン トウン ナウン, 文字秀明, 修正された溶解法による超音速二相流の実現可能性, 日本実験力学会講演論文集 2016 年度年次講演会/pp.202-203, 2016 年 9 月.

Table.6.1. Experimental conditions for the modification of pressurized dissolution method with connecting two nozzles.

Experimental condition	Modification type	Upper tank pressure P_U [kPa]	Lower tank pressure P_L [kPa]	Pressure difference P_D [kPa]	CO ₂ rate [%]	N ₂ rate [%]
No.26	Connecting two nozzles	101	101	100	0	100
No.27					25	75
No.28					50	50
No.29					75	25
No.30					100	0
No.31		51	51	150	0	100
No.32					25	75
No.33					50	50
No.34					75	25
No.35					100	0
No.36		21	21	180	0	100
No.37					25	75
No.38					50	50
No.39					75	25
No.40					100	0

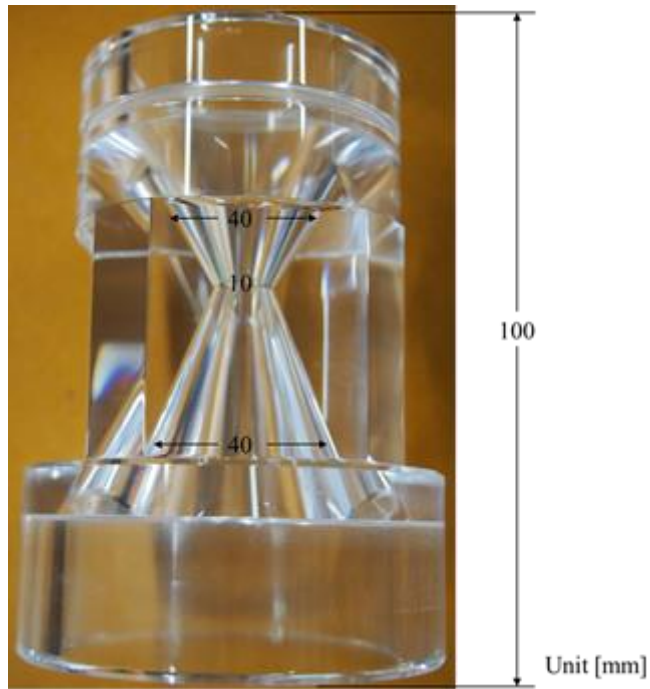


Figure 6.1. Photo of the front nozzle.

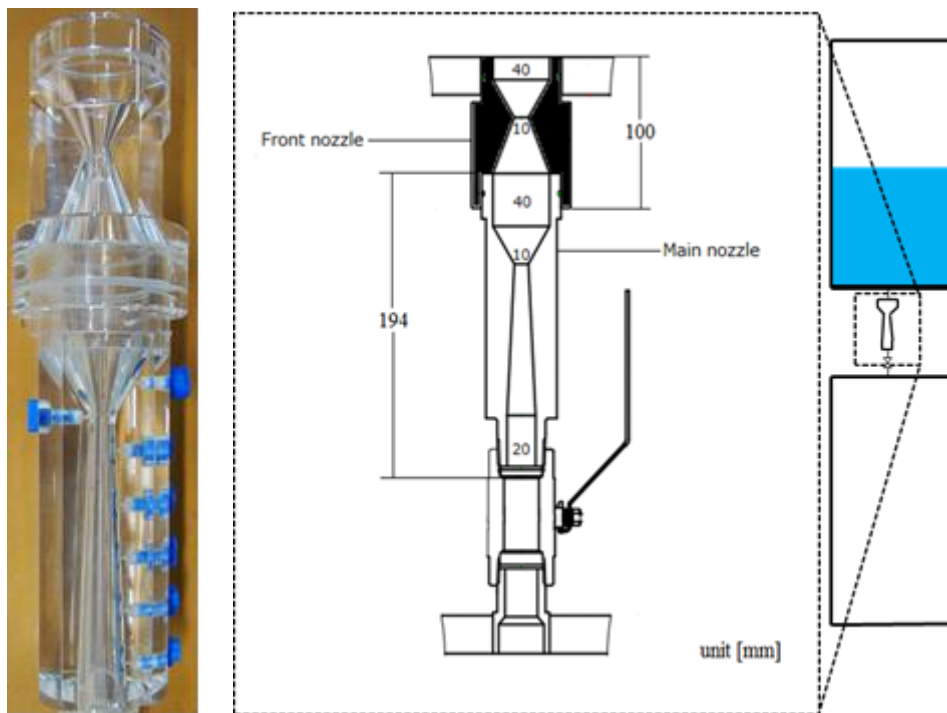


Figure 6.2. Photo and schematic diagram of the modification of pressurized dissolution method with connecting two nozzles.

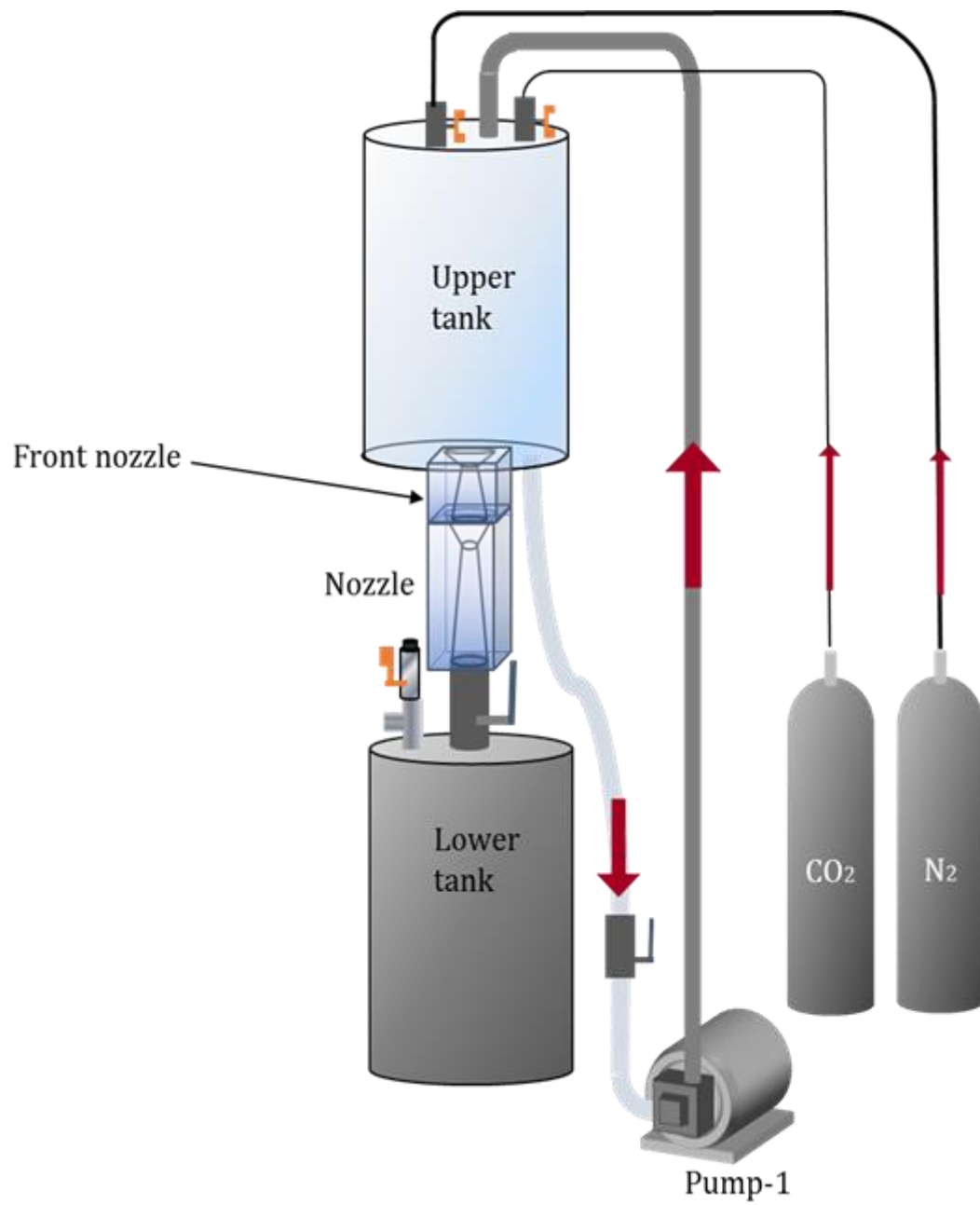
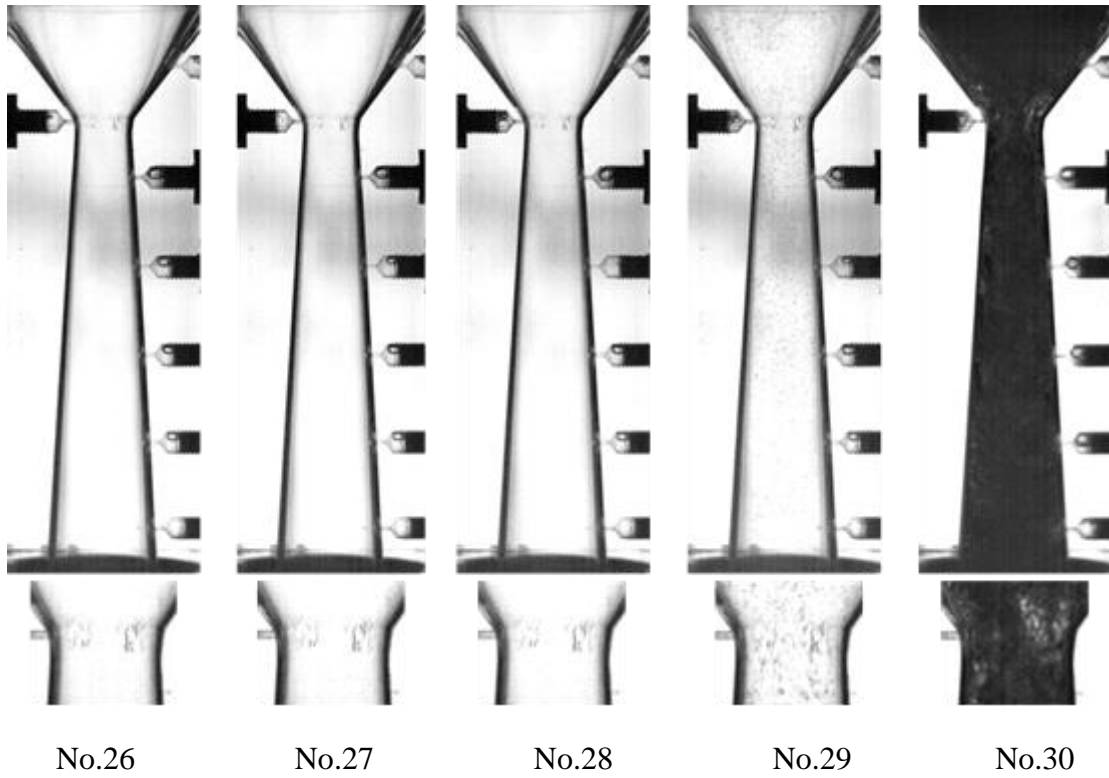
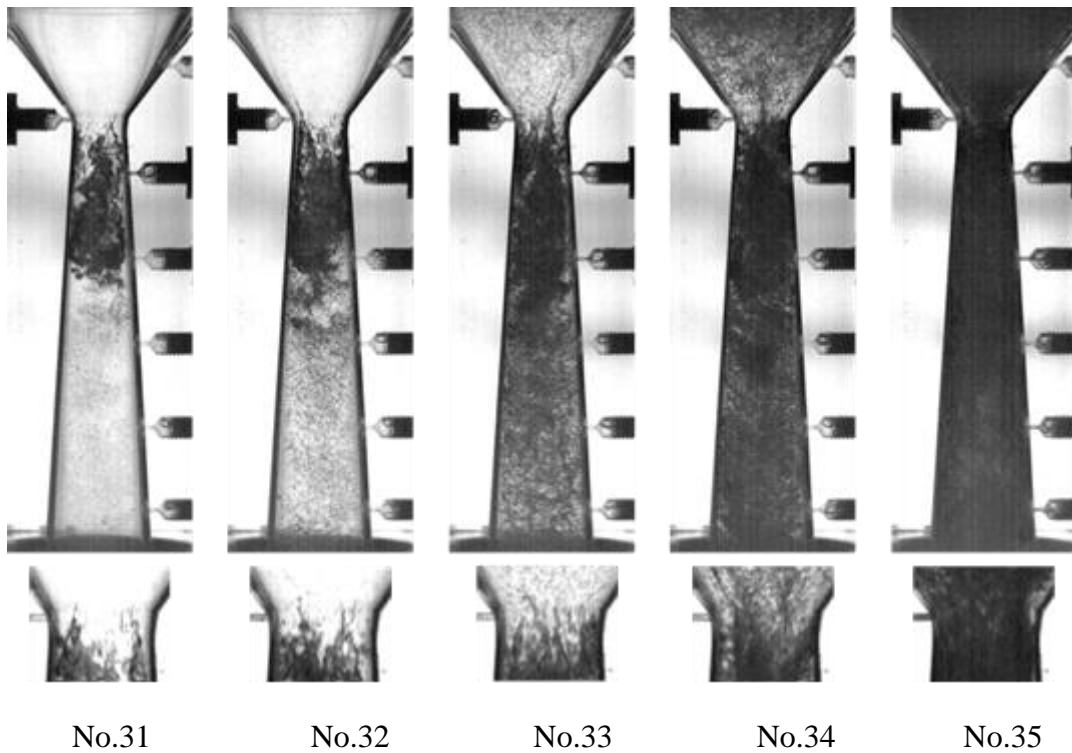


Figure 6.3. Experimental procedure for the modification of pressurized dissolution method with connecting two nozzles.

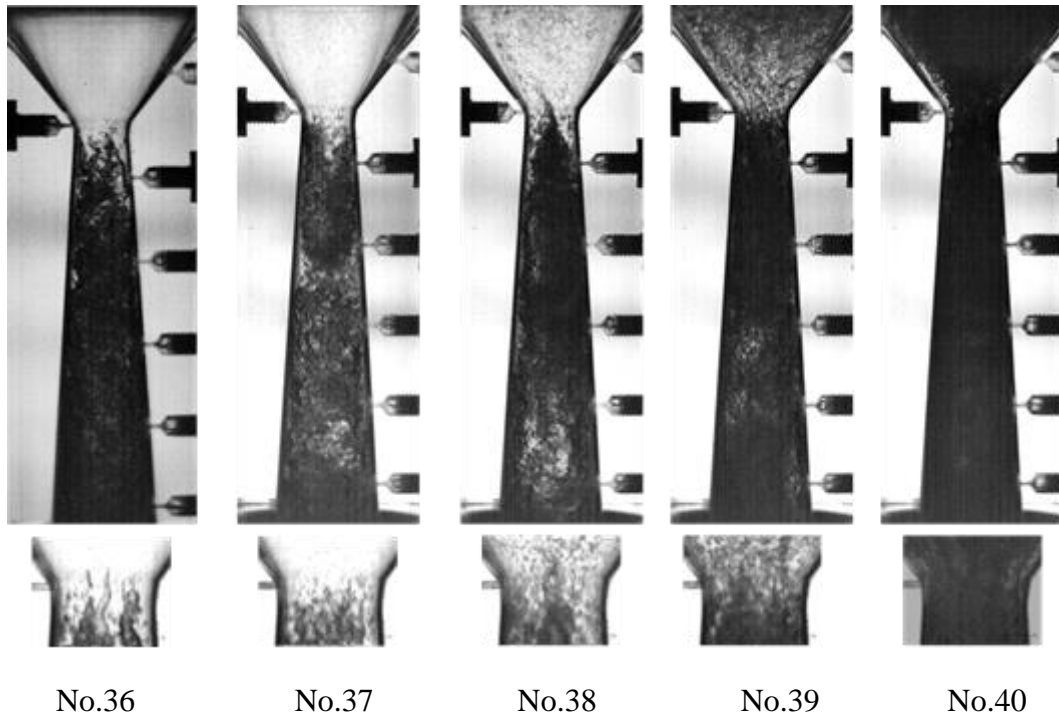


(a) $P_U=201$ kPa, $P_L=101$ kPa, $P_D=100$ kPa



(b) $P_U=201$ kPa, $P_L=51$ kPa, $P_D=150$ kPa

Figure 6.4. Flow pattern of the experimental conditions No.26 to No.35.



(c) $P_U=201$ kPa, $P_L=21$ kPa, $P_D=180$ kPa

Figure 6.4. Flow pattern of the experimental conditions No.36 to No.40.

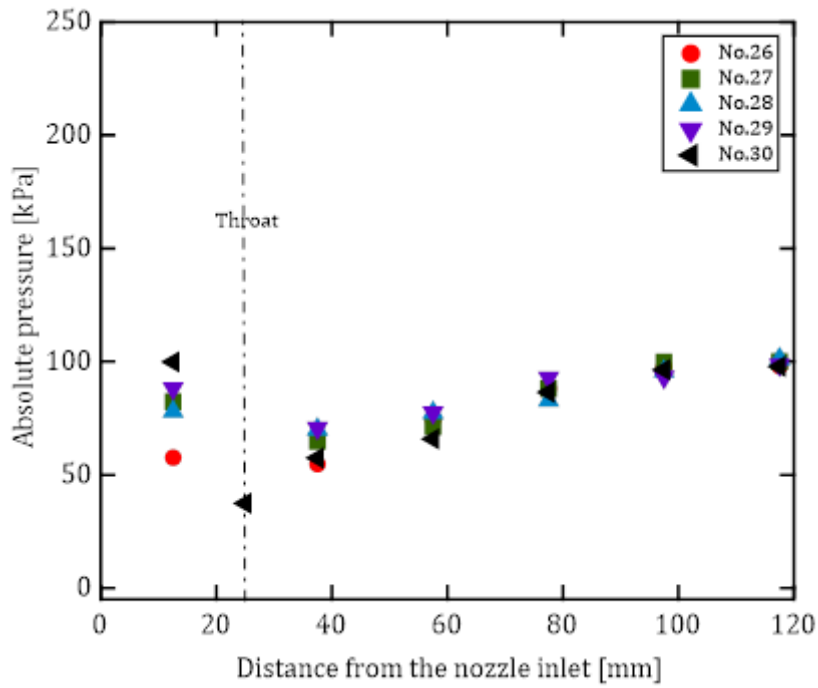


Figure 6.5. Pressure distribution along the nozzle of the experimental condition No.26 to No.30 ($P_U=201$ kPa, $P_L=101$ kPa, $P_D=100$ kPa).

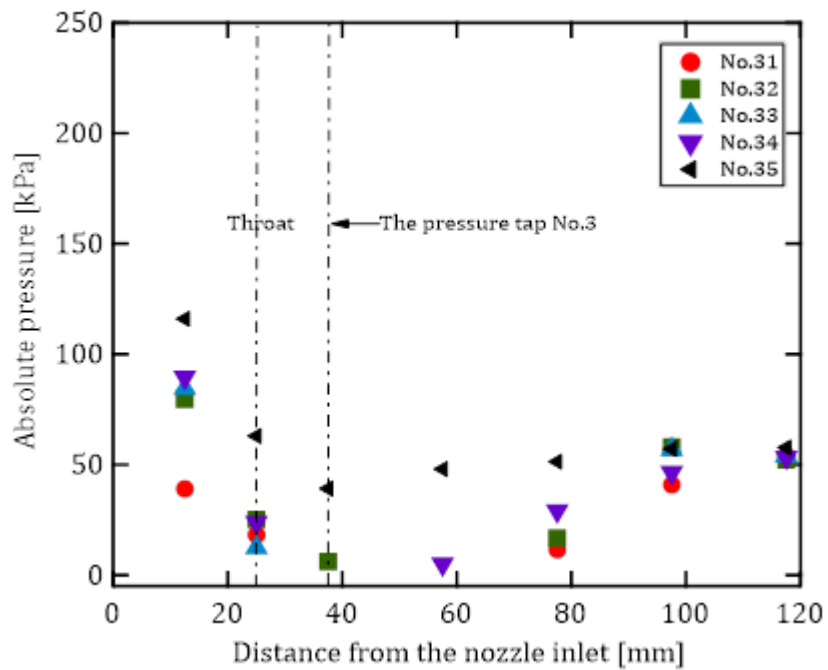


Figure 6.6. Pressure distribution along the nozzle of the experimental conditions No.31 to No.35 ($P_U=201$ kPa, $P_L=51$ kPa, $P_D=150$ kPa).

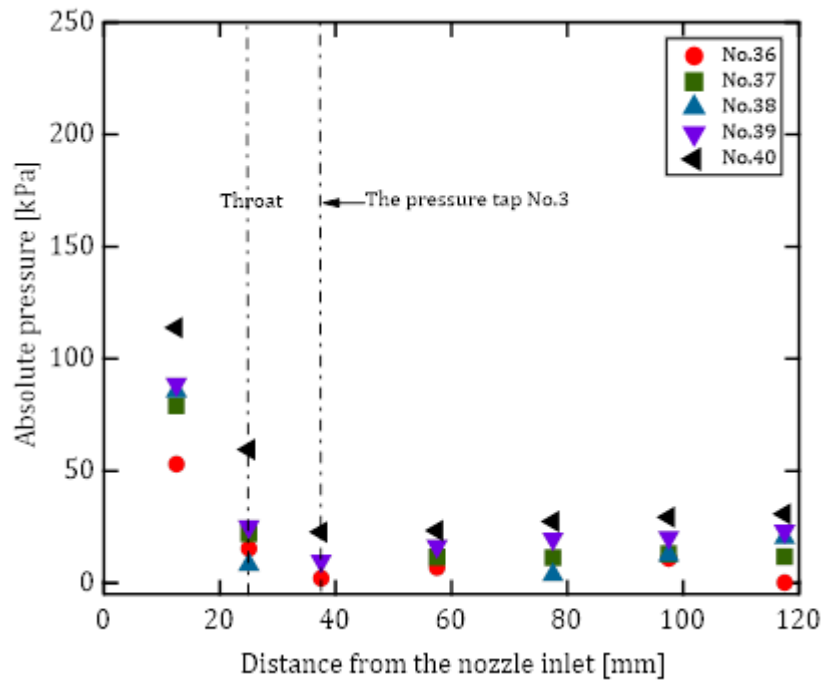


Figure 6.7. Pressure distribution along the nozzle of the experimental conditions No.36 to No.40 ($P_U=201$ kPa, $P_L=21$ kPa, $P_D=180$ kPa).

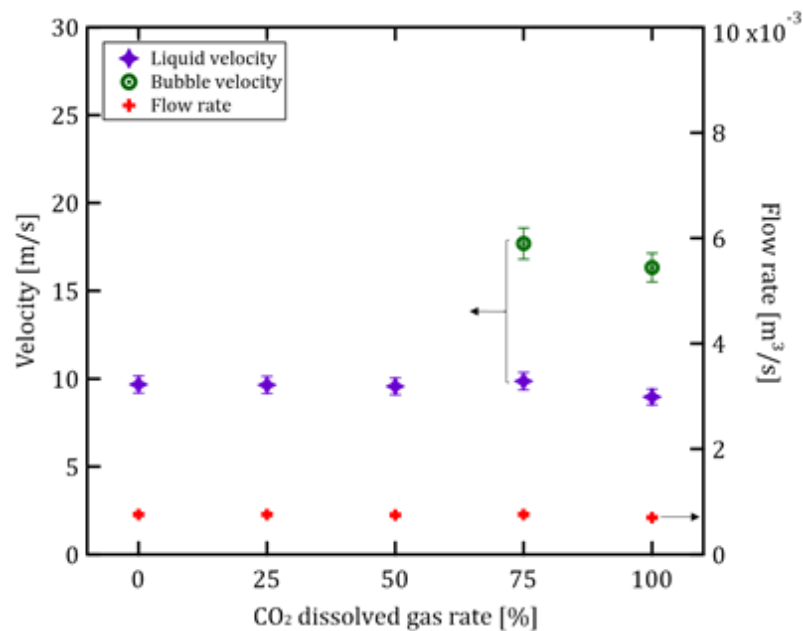


Figure 6.8. The comparison of flow rate, liquid velocity and bubble velocity at the throat of the experimental conditions No.26 (CO₂ 0%), No.27 (CO₂ 25%), No.28 (CO₂ 50%), No.29 (CO₂ 75%) and No.30 (CO₂ 100%) with the same $P_D=100$ kPa.

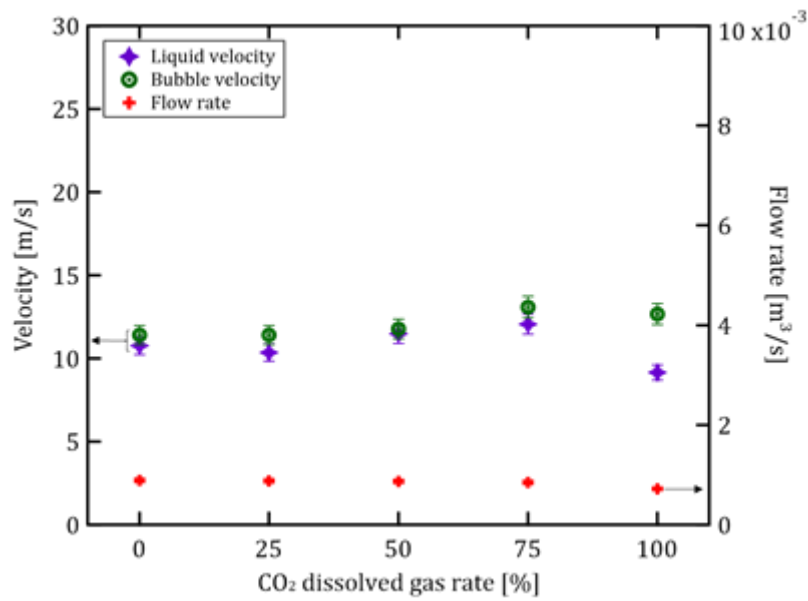


Figure 6.9. The comparison of flow rate, liquid velocity and bubble velocity at the throat of the experimental conditions No.31 (CO₂ 0%), No.32 (CO₂ 25%), No.33 (CO₂ 50%), No.34 (CO₂ 75%) and No.35 (CO₂ 100%) with the same $P_D=150$ kPa.

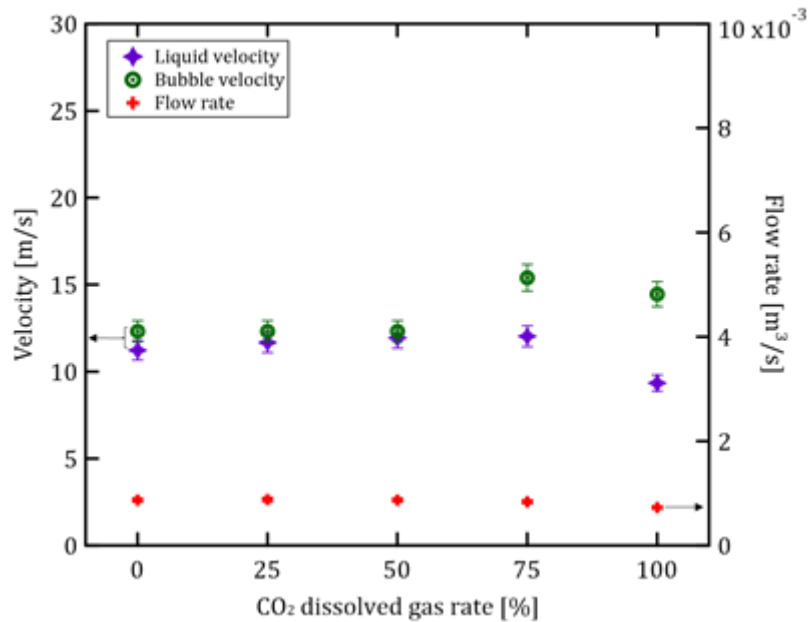
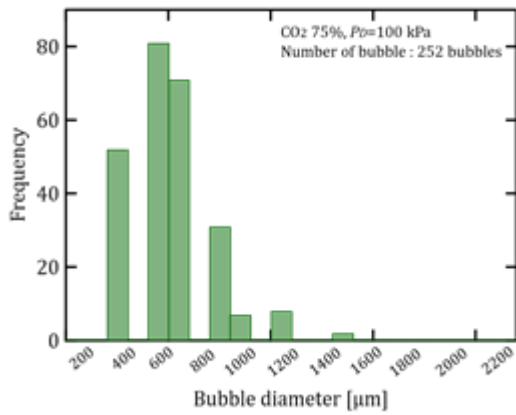
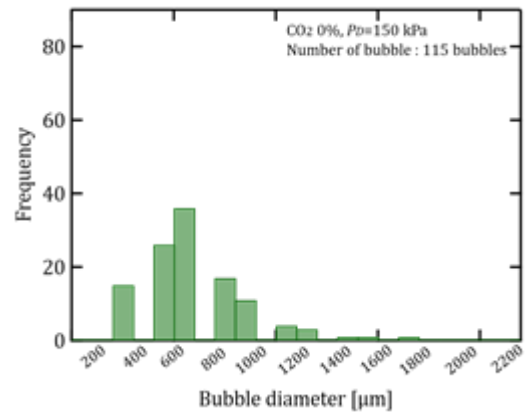


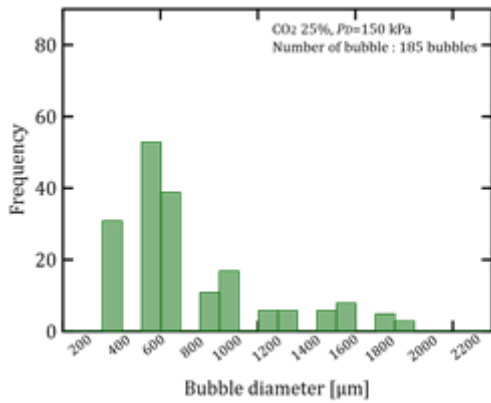
Figure 6.10. The comparison of flow rate, liquid velocity and bubble velocity at the throat of the experimental conditions No.36 (CO₂ 0%), No.37 (CO₂ 25%), No.38 (CO₂ 50%), No.39 (CO₂ 75%) and No.40 (CO₂ 100%) with the same $P_D=180$ kPa.



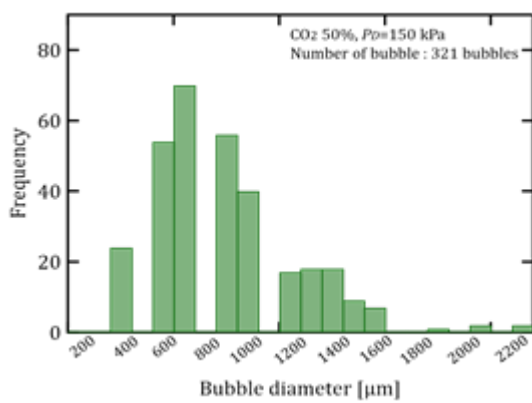
(a) Experimental condition No.29



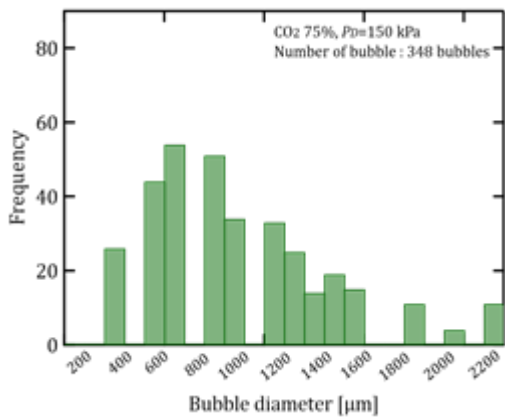
(b) Experimental condition No.31



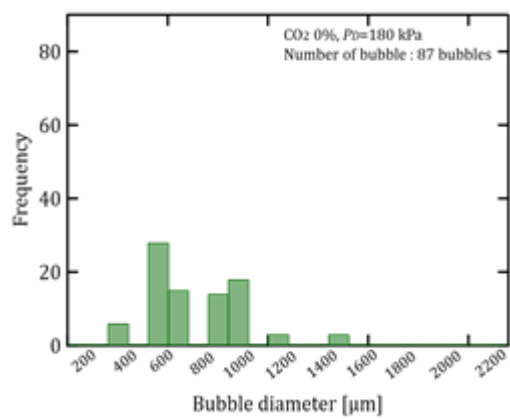
(c) Experimental condition No.32



(d) Experimental condition No.33

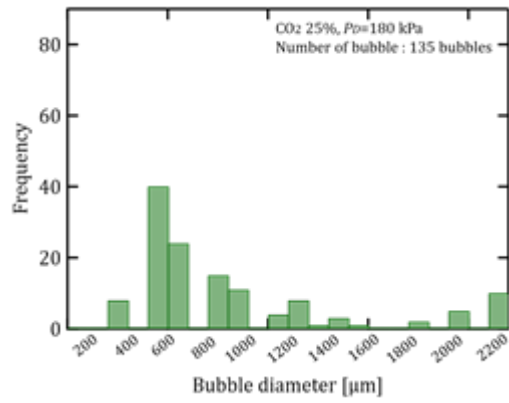


(e) Experimental condition No.34

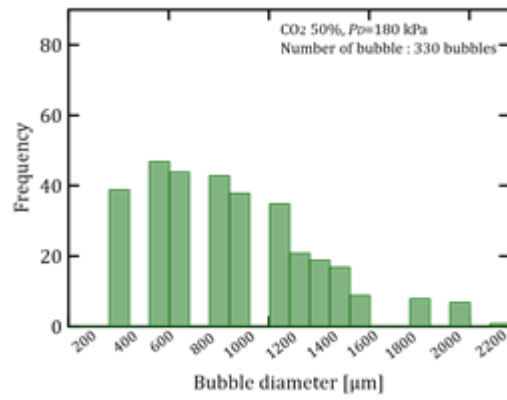


(f) Experimental condition No.36

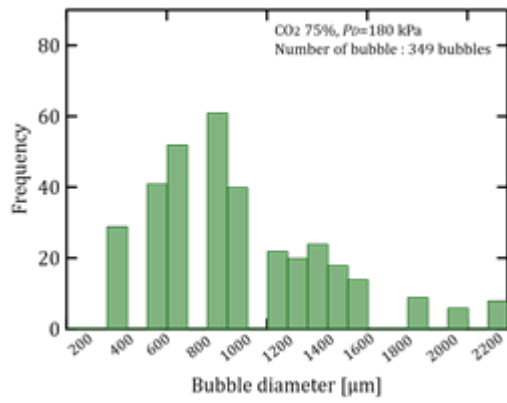
Figure 6.11. Bubble size distribution of the experimental conditions No.29 to No.39.



(g) Experimental condition No.37



(h) Experimental condition No.38



(i) Experimental condition No.39

Figure 6.11. Bubble size distribution of the experimental conditions No.29 to No.39.

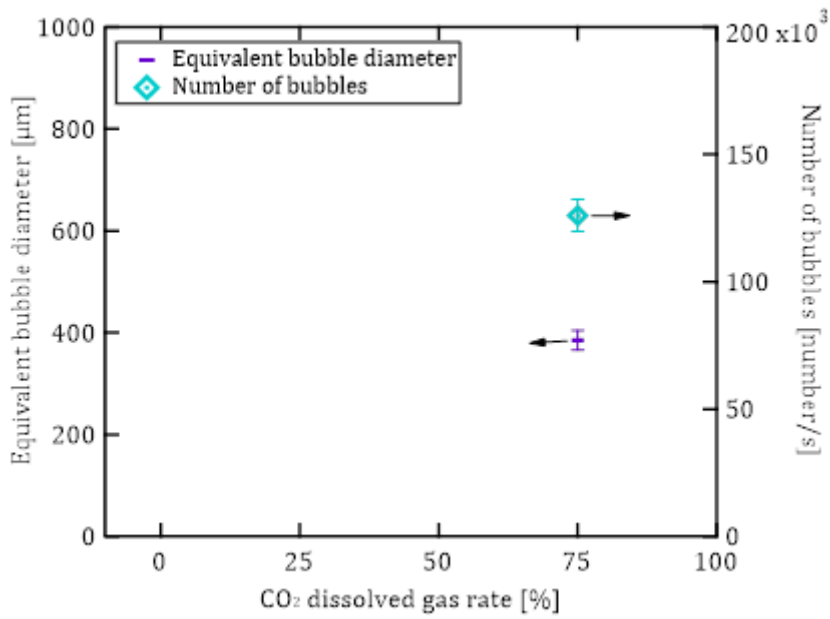


Figure 6.12. Equivalent of bubble diameter and number of bubbles of the experimental conditions No.26 (CO₂ 0%), No.27 (CO₂ 25%), No.28 (CO₂ 50%), No.29 (CO₂ 75%) and No.30 (CO₂ 100%) with the same $P_D=100$ kPa.

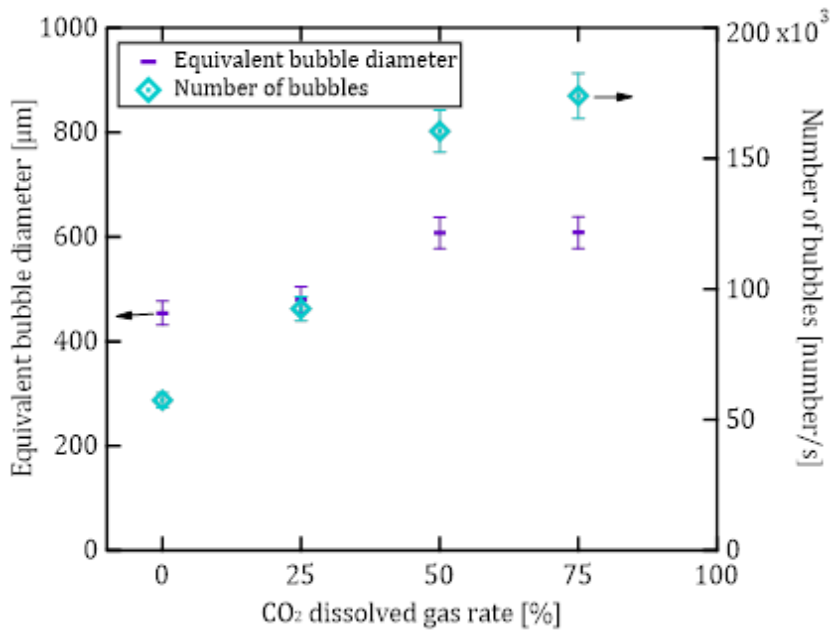


Figure 6.13. Equivalent of bubble diameter and number of bubbles of the experimental conditions No.31 (CO₂ 0%), No.32 (CO₂ 25%), No.33 (CO₂ 50%), No.34 (CO₂ 75%) and No.35 (CO₂ 100%) with the same $P_D=150$ kPa.

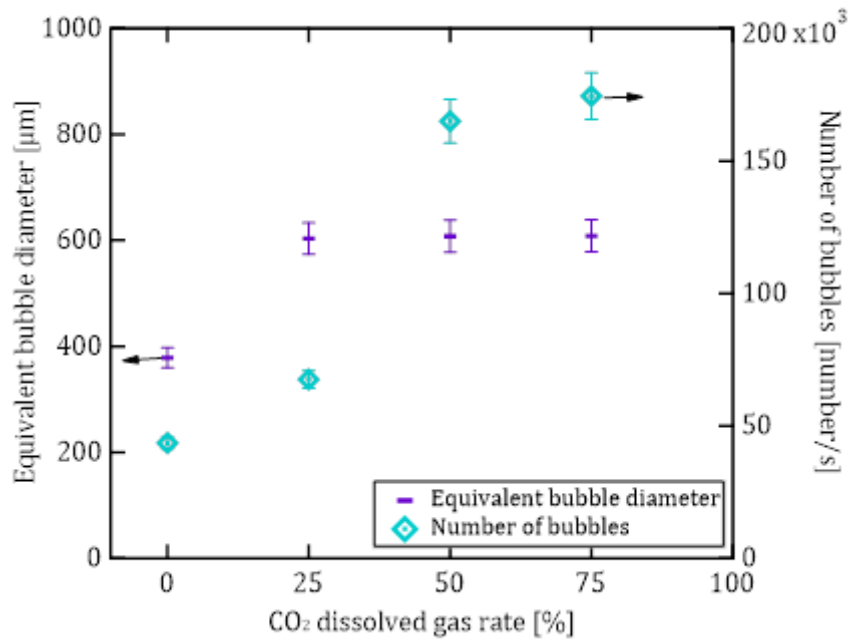


Figure 6.14. Equivalent of bubble diameter and number of bubbles of the experimental conditions No.36 (CO₂ 0%), No.37 (CO₂ 25%), No.38 (CO₂ 50%), No.39 (CO₂ 75%) and No.40 (CO₂ 100%) with the same $P_D=180$ kPa.

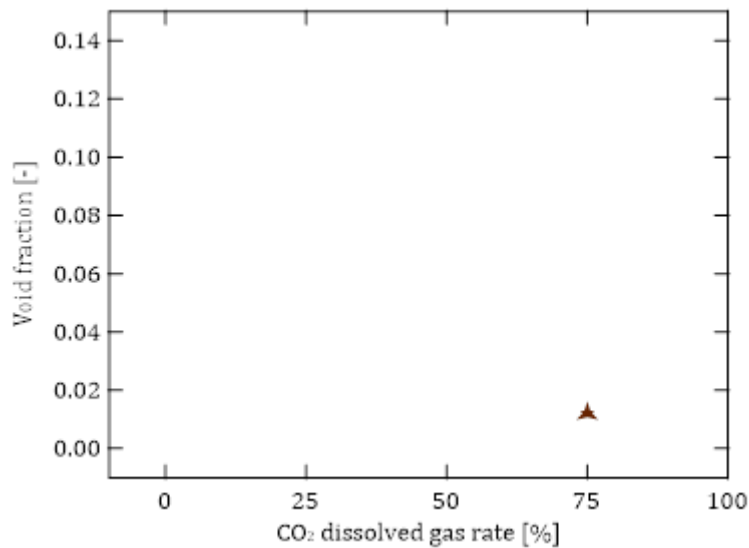


Figure 6.15. Void fraction at the throat of the experimental conditions No.26 (CO₂ 0%), No.27 (CO₂ 25%), No.28 (CO₂ 50%), No.29 (CO₂ 75%) and No.30 (CO₂ 100%) with the same $P_D=100$ kPa.

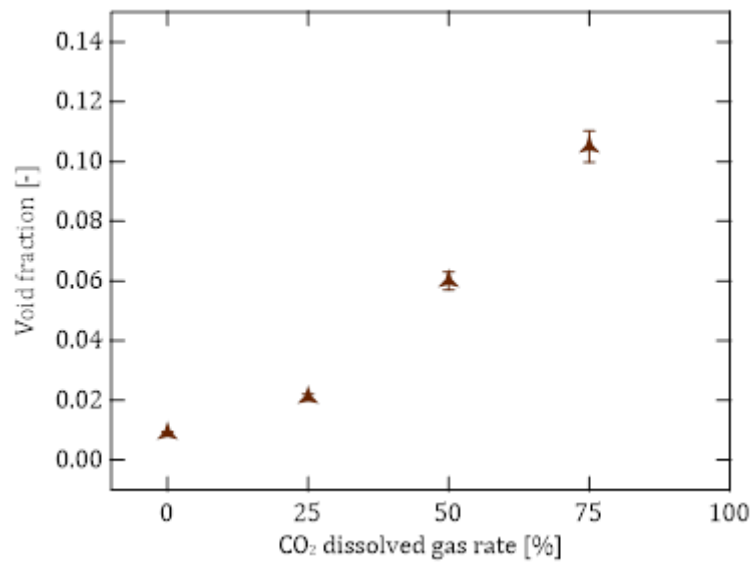


Figure 6.16. Void fraction at the throat of the experimental conditions No.31 (CO₂ 0%), No.32 (CO₂ 25%), No.33 (CO₂ 50%), No.34 (CO₂ 75%) and No.35 (CO₂ 100%) with the same $P_D=150$ kPa.

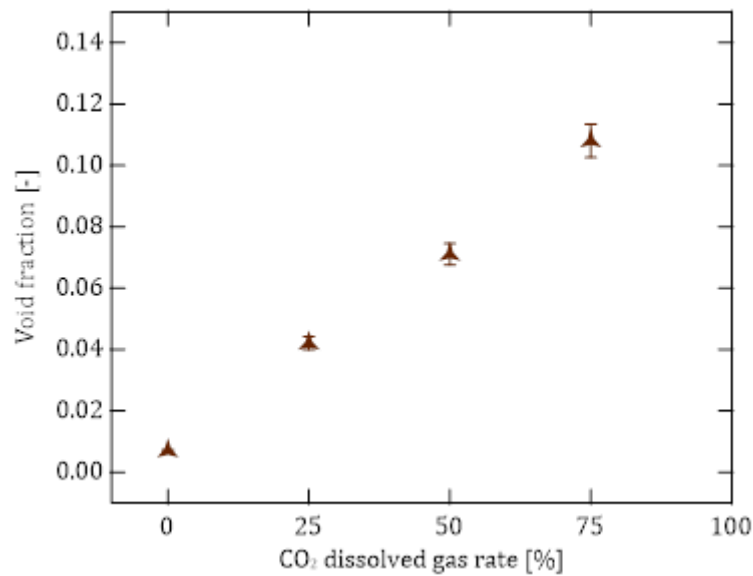


Figure 6.17. Void fraction at the throat of the experimental conditions No.36 (CO₂ 0%), No.37 (CO₂ 25%), No.38 (CO₂ 50%), No.39 (CO₂ 75%) and No.40 (CO₂ 100%) with the same $P_D=180$ kPa.

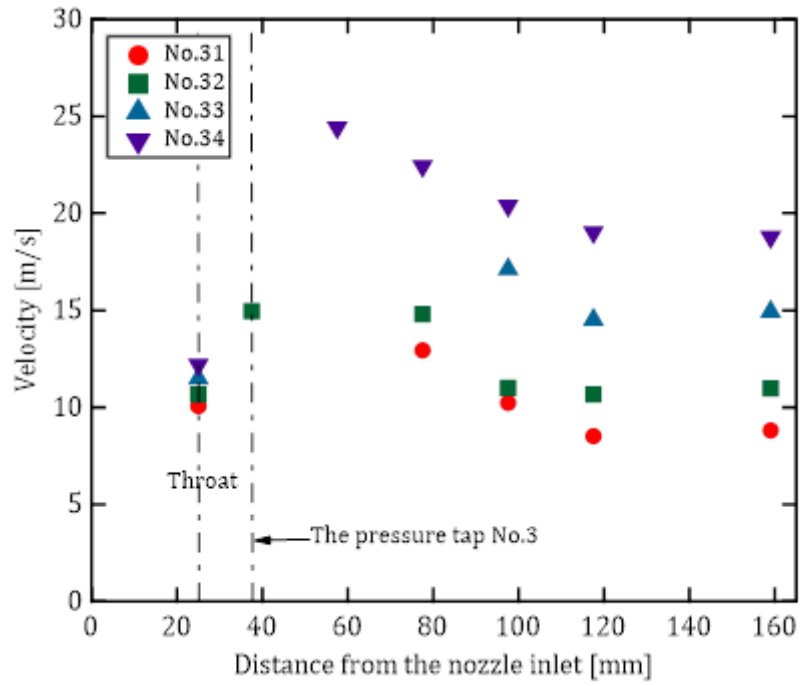


Figure 6.18. Velocity distribution along the nozzle of the experimental condition No.31 to No.34 ($P_U=201$ kPa, $P_L=51$ kPa, $P_D=150$ kPa).

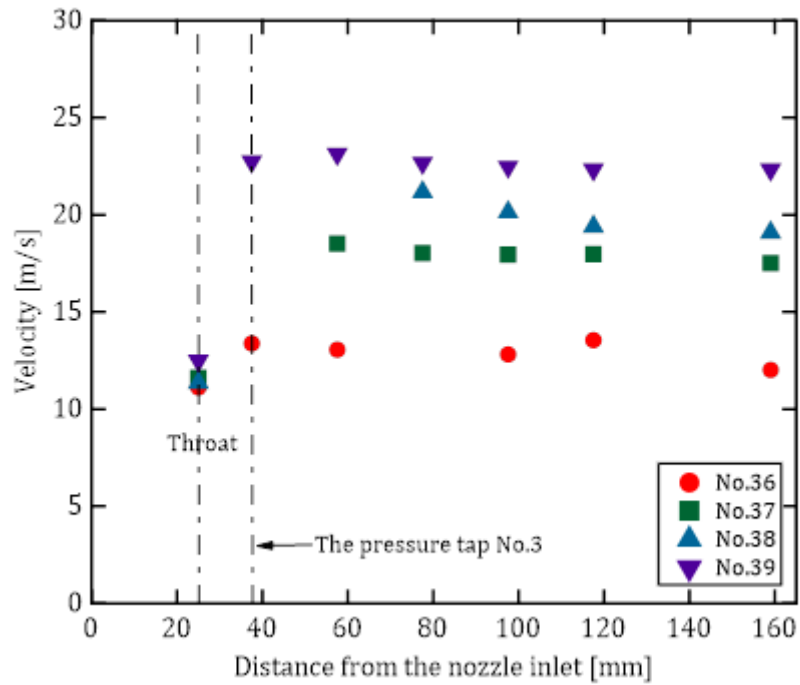
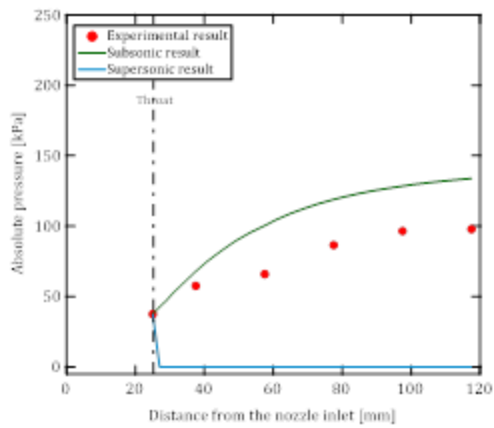
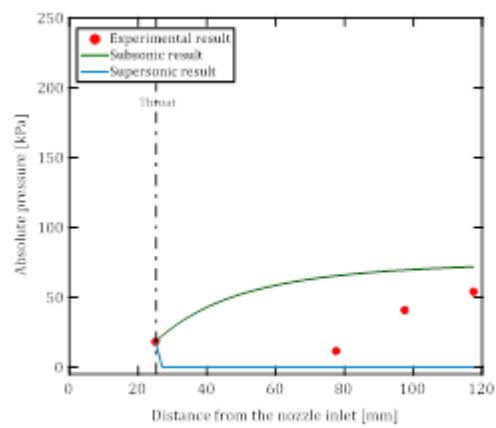


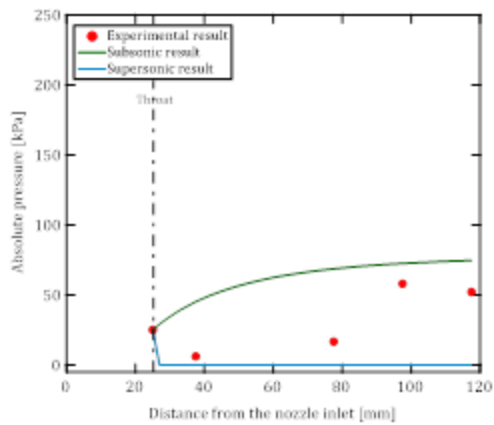
Figure 6.19. Velocity distribution along the nozzle of the experimental condition No.36 to No.39 ($P_U=201$ kPa, $P_L=21$ kPa, $P_D=180$ kPa).



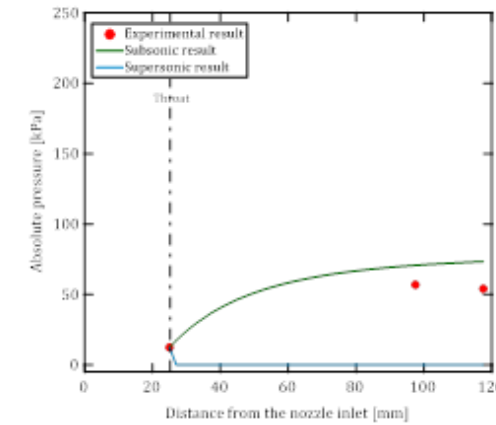
(a) Experimental condition No.30



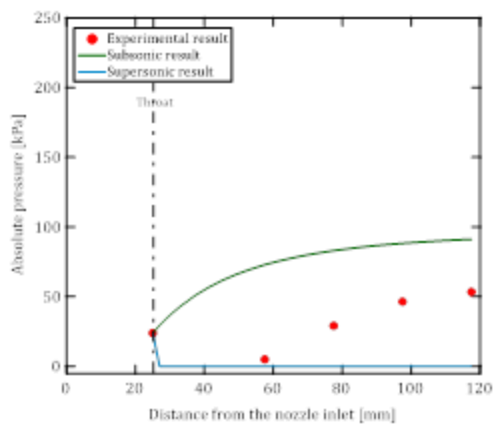
(b) Experimental condition No.31



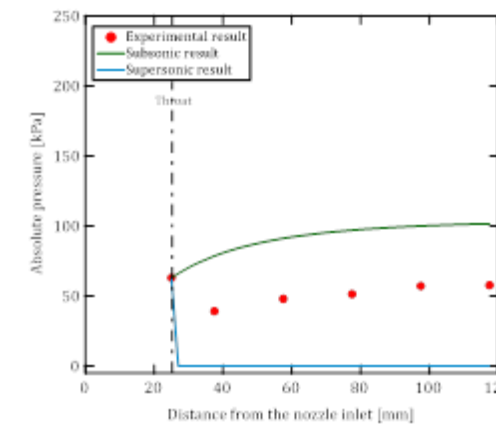
(c) Experimental condition No.32



(d) Experimental condition No.33

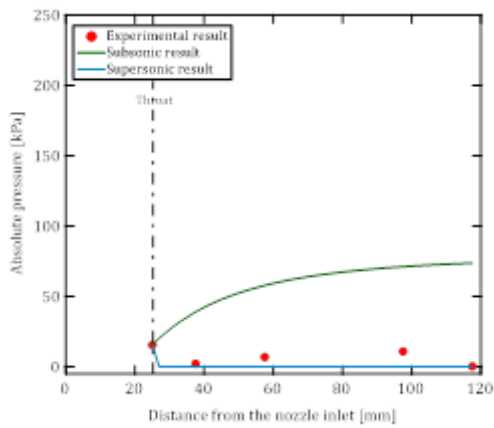


(e) Experimental condition No.34

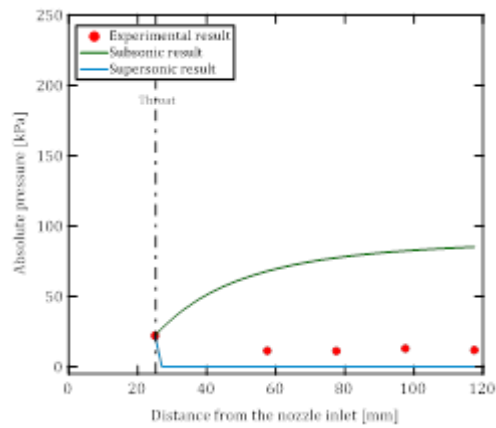


(f) Experimental condition No.35

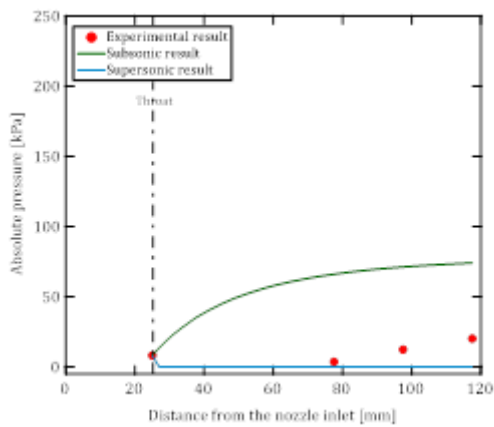
Figure 6.20. The comparison of pressure distribution between the experimental and theoretical estimation of subsonic and supersonic flow of the experimental conditions No.30 to No.40.



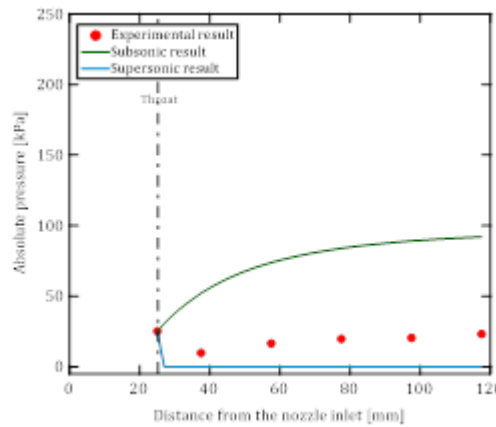
(g) Experimental condition No.36



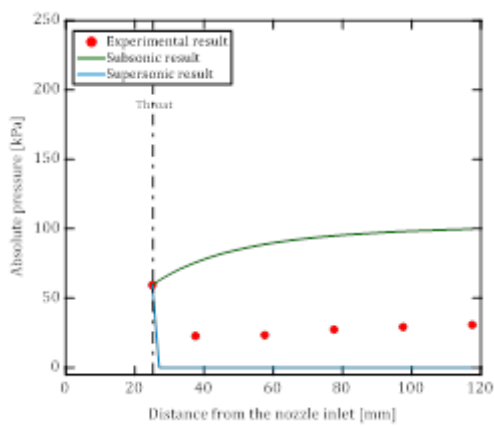
(h) Experimental condition No.37



(i) Experimental condition No.38



(j) Experimental condition No.39



(k) Experimental condition No.40

Figure 6.20. The comparison of pressure distribution between the experimental and theoretical estimation of subsonic and supersonic flow of the experimental conditions No.30 to No.40.

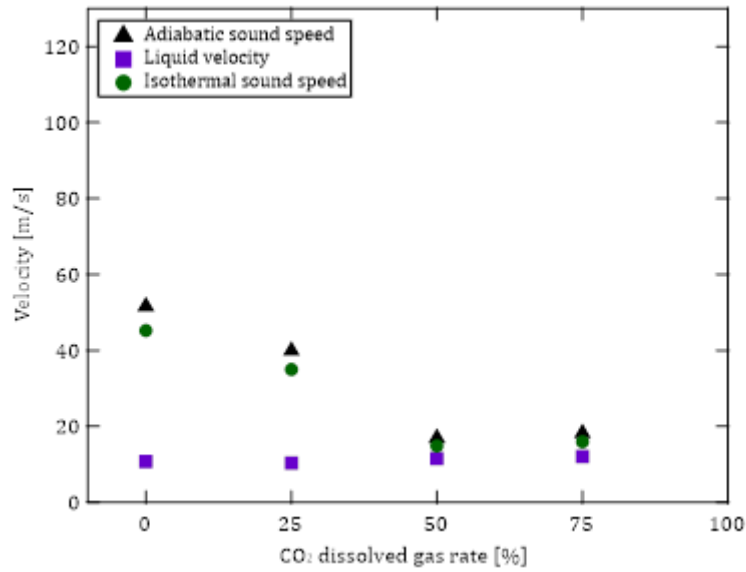


Figure 6.21. Experimental value and sound speed at the throat for the experimental conditions No.31 (CO₂ 0%), No.32 (CO₂ 25%), No.33 (CO₂ 50%) and No.34 (CO₂ 75%) with the same $P_D=150$ kPa.

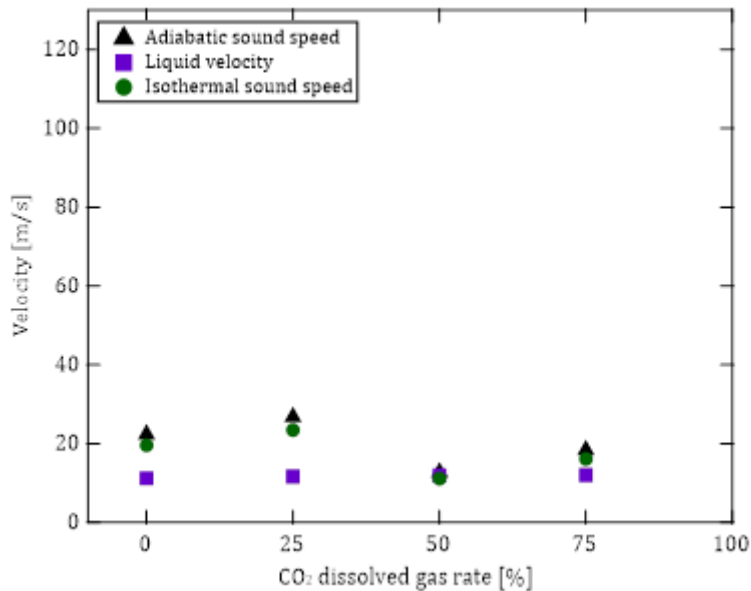


Figure 6.22. Experimental value and sound speed at the throat of the experimental conditions No.36 (CO₂ 0%), No.37 (CO₂ 25%), No.38 (CO₂ 50%) and No.39 (CO₂ 75%) with the same $P_D=180$ kPa.

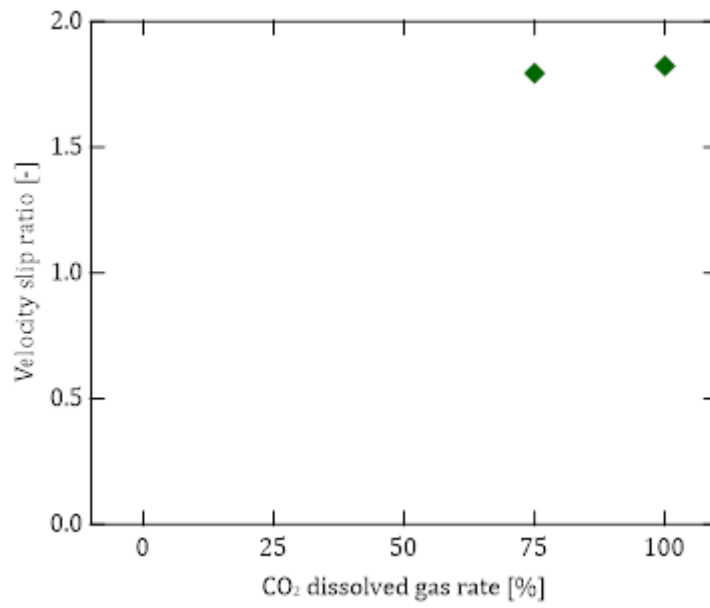


Figure 6.23. Velocity slip ratio of the experimental conditions No.29 (CO₂ 75%) and No.30 (CO₂ 100%) with the same $P_D=100$ kPa.

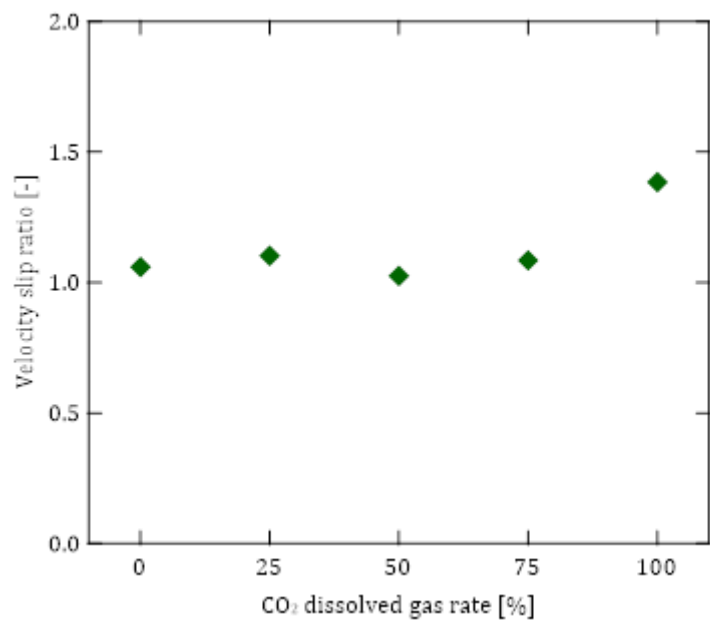


Figure 6.24. Velocity slip ratio of the experimental conditions No.31 (CO₂ 0%), No.32 (CO₂ 25%), No.33 (CO₂ 50%), No.34 (CO₂ 75%) and No.35 (CO₂ 100%) with the same $P_D=150$ kPa.

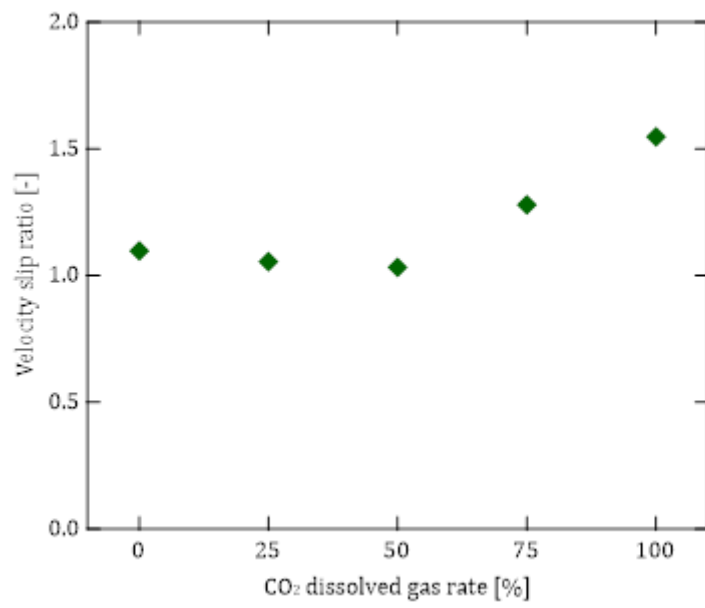


Figure 6.25. Velocity slip ratio of the experimental conditions No.36 (CO₂ 0%), No.37 (CO₂ 25%), No.38 (CO₂ 50%), No.39 (CO₂ 75%) and No.40 (CO₂ 100%) with the same $P_D=180$ kPa.

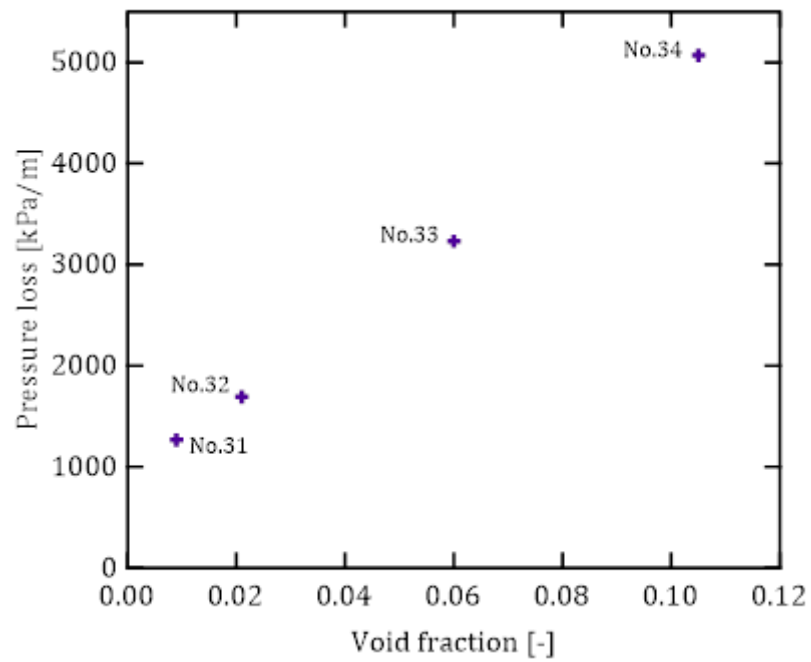


Figure 6.26. The comparison of pressure loss and void fraction at the throat of the experimental conditions No.31 to No.34 with the same $P_D=150$ kPa.

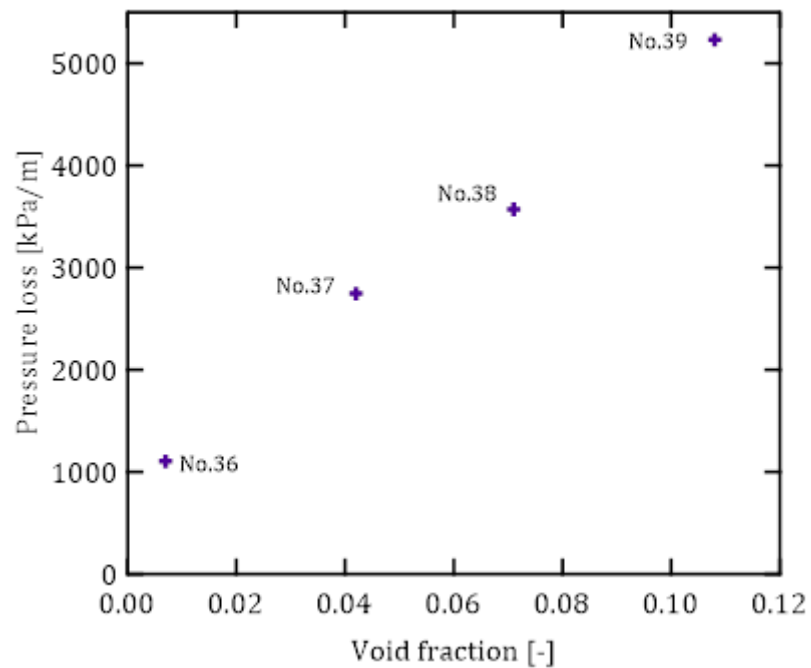


Figure 6.27. The comparison of pressure loss and void fraction at the throat of the experimental conditions No.36 to No.39 with the same $P_D=180$ kPa.

Chapter 7

The Comparison of Flow Conditions

In this research the sound speed varied however the liquid velocity at the throat was almost constant. It is easy to get supersonic flow if the sound speed at the throat is low. There was a problem to reduce the sound speed. The sound speed at the throat depends on the void fraction and the pressure at the throat as Eq. (7.1). The high void fraction or low pressure at the throat only can reduce the sound speed. On the other hand, by the energy equation of Eq. (7.2), if the flow generates more bubble at the throat, the void fraction will increase, and pressure loss also will increase. Therefore, the liquid cannot flow well. In contrast, if the flow generates less bubble at the throat, the liquid velocity will high, the void fraction will decrease, and the sound speed will increase. Therefore, the flow cannot obtain the supersonic flow. However, the experiments with higher void fraction observed that pressure loss also increased. Therefore, the flow could not reach the sound speed. The middle amount of void fraction and low pressure at the throat was better condition to obtain the supersonic flow. Here, the middle void fraction is about 0.1. In the experimental conditions No. 30, No. 35, and No. 40, the void fraction could not be measured by the image processing, but it was estimated that the void fraction exceeded 0.15. Under these conditions, the flow did not reach the sound speed at the throat section.

$$a_{iso} = \sqrt{\frac{P}{\alpha(1-\alpha)\rho_L}} \quad (7.1)$$

$$\frac{1}{2}\rho_1 u_1^2 + p_1 + \frac{\alpha_0}{(1-\alpha_0)} p_0 \ln p_1 + \rho_1 g x = \frac{1}{2}\rho_2 u_2^2 + p_2 + \frac{\alpha_0}{(1-\alpha_0)} p_0 \ln p_2 + \Delta E_{Loss} \quad (7.2)$$

7.1. Supersonic flow with increasing void fraction

In the experimental condition No.19 and No.20, the orifice plate.1 was used for modification of pressurised dissolution method as described in Fig. 7.1. In these experiments the same upper tank pressure $P_U=201$ kPa and lower tank pressure P_L changed as 51 kPa and 21 kPa. The pressure difference were $P_D=150$ kPa and $P_D=180$ kPa. The results are shown in Fig. 7.2. The micro-bubbles were generated in the converging section. Therefore, the high void fractions were obtained. However, the pressure at the throat was higher than other experiments. That higher void fraction could decrease sound speed as expressed in Eq. (7.1). Therefore, the liquid velocity reached the sound speed at the throat with decreasing velocity slip and bubble velocities and liquid velocities were flowed together at the throat. The flow of the experimental conditions No.19 and No.20 were expected to be supersonic flow.

7.2. Supersonic flow with decreasing throat pressure

As represented in the Fig. 7.3, the experimental condition No.38 was modification of pressurized dissolution method with connecting two nozzles with $P_U=201$ kPa, $P_L=21$ kPa, pressure difference $P_D=180$ kPa and CO₂ 50%. According to the results of the Fig. 7.4, in this experiment, middle amount of bubbles were generated at the throat of the nozzle because middle amount of CO₂ dissolved gas rate. Therefore, the void fraction obtained the middle amount. The less pressure at the throat was observed. In the experiments with connecting two nozzles throat pressure could decrease because of effect of the front nozzle. The pressure loss at the throat was also lower than that in the experimental condition No.39. If the void fraction increased, pressure loss would increase according to the Eq. (7.2). Therefore, the flow of the experimental condition No.39 could not flow well because of the increasing pressure

loss at the throat. However, the liquid velocities of these two experimental conditions did not change too much. The bubble velocity at the throat was obviously higher than the liquid velocity. The pressure loss of the experimental condition No.38 was more reduce than the pressure loss of the experimental condition No.39. The bubble velocity was almost similar to liquid velocity at the throat. Therefore, the velocity slip ratio decreased at the throat. However, the liquid velocity of all experiments were almost the same. Because of decreasing pressure at the throat and middle amount of void fraction could reduce the sound speed at the throat. Therefore, liquid velocity easily reached the sound speed at the throat. The flow of the experimental condition No.38 was expected to be supersonic flow.

7.3. Subsonic flow with increasing pressure loss at the throat of the nozzle

The experimental condition No.35 was modification of pressurized dissolution method with connecting two nozzles with $P_U=201$ kPa, $P_L=51$ kPa, pressure difference $P_D=150$ kPa and CO₂ 100% is shown in Fig. 7.5. In Fig. 7.6, the liquid velocity decreased and bubble velocity was slightly increase. Therefore, the velocity slip increased in the experimental condition No.35. As expresses in the schematic diagram of Fig. 7.7, when the pressure difference fed to the nozzle the flow would start (a) and it changed to (c) to get supersonic flow. If much bubbles were generated at the throat, the void fraction would increase and the pressure loss also would increase (b). Therefore, the flow could not flow well to reach supersonic flow. The flow would only be subsonic flow.

7.4. Subsonic flow with increasing pressure loss at the exit of the nozzle


When the comparison of the supersonic and subsonic flow of the experimental

conditions No.19 (orifice plate.1) and No.39 (connecting two nozzles), in these experiments were the same $P_U=201$ kPa and different P_L as 51 kPa and 21 kPa as represented in Fig. 5.8. Both of the experiments were generated micro-bubbles from the converging section of the nozzle. The pressure at the throat were almost the same. In Fig. 7.9, void fraction at the throat of the experimental condition No.19 was slightly higher than the experimental condition No.39. Because CO₂ dissolved gas rate in experimental condition No.19 was 100% and only 75% dissolved gas rate in experimental condition No.39. Lower liquid velocity was observed in the experimental condition No.39 because of the increasing pressure loss at the exit of the nozzle due to the decreasing lower tank pressure as shown in schematic diagram of Fig. 7.10. Therefore, only the experimental condition No.19 reached the sound speed at the throat. The experimental condition No.39 was subsonic flow because of the increasing pressure loss at the throat.

7.5. Concluding remarks

The results on the comparison of the supersonic flow conditions as discussed above were summarized as follows:

- i. Much amount of bubbles prevented the flow due to the large pressure loss.
- ii. Bubble generation also depended on the CO₂ dissolved gas rate and lower tank pressure.
- iii. Decreasing lower tank pressure could generate the supersonic flow in the orifice plate.1.
- iv. The lowest throat pressure and middle amount of void fraction could obtain supersonic flow in the connecting two nozzles.

	Experimental condition	No.14	No.15	No.16	No.17	No.18	No.19	No.20
	Upper tank absolute pressure P_U [kPa]	201	201	201	201	201	201	201
Lower tank absolute pressure P_L [kPa]	101	101	101	101	101	101	51	21
Pressure difference P_D [kPa]	100	100	100	100	100	100	150	180
CO ₂ rate [%]	0	25	50	75	100	100	100	100
N ₂ rate [%]	100	75	50	25	0	0	0	0

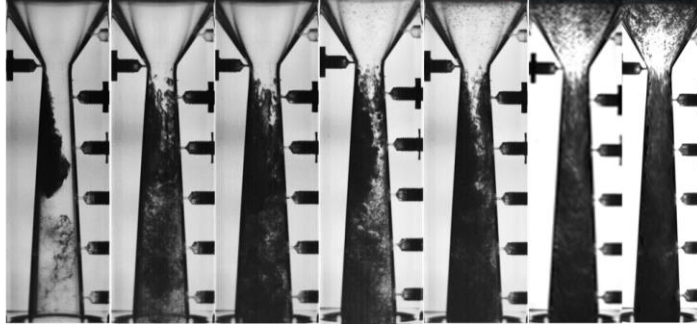


Figure 7.1. Experimental conditions and flow pattern of the orifice plate.1.

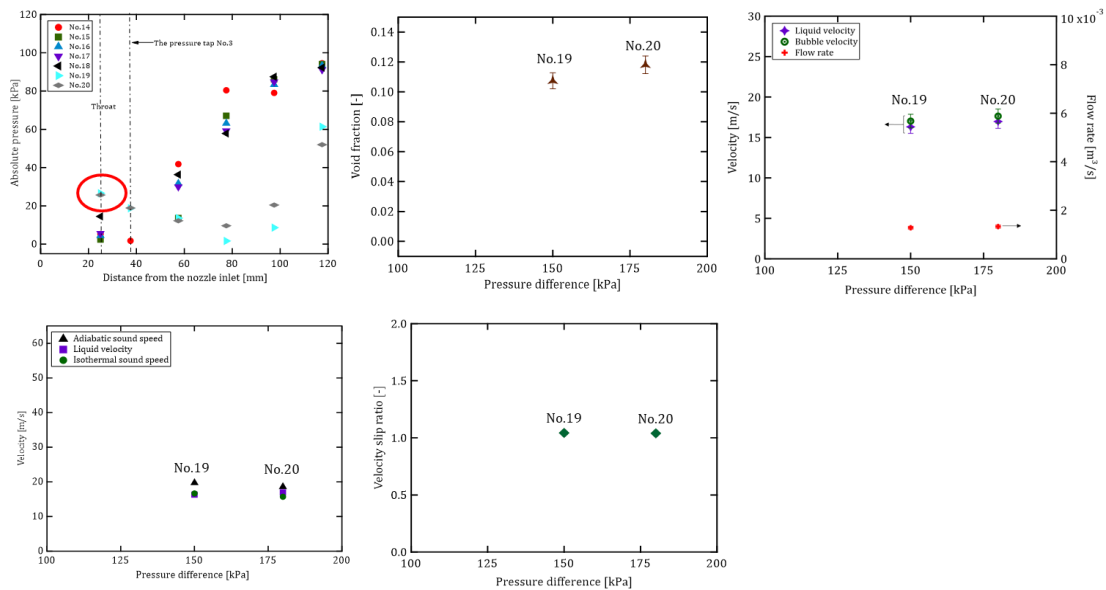


Figure 7.2. The results of the experimental conditions No.19 and No.20 with orifice plate.1.

Experimental condition	No.36	No.37	No.38	No.39	No.40
Upper tank absolute pressure P_U [kPa]	201	201	201	201	201
Lower tank absolute pressure P_L [kPa]	21	21	21	21	21
Pressure difference P_D [kPa]	180	180	180	180	180
CO ₂ rate [%]	0	25	50	75	100
N ₂ rate [%]	100	75	50	25	0

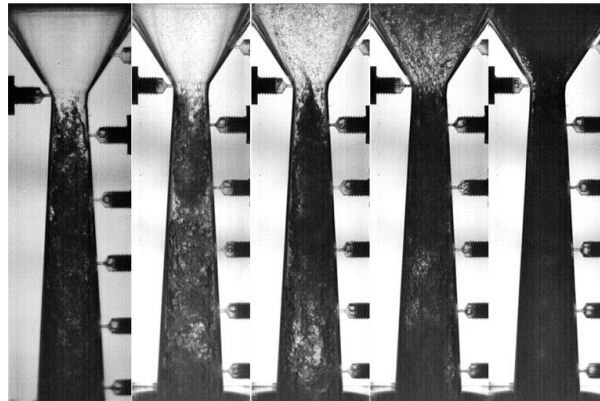


Figure 7.3. Experimental conditions and flow pattern of the connecting two nozzles with $P_D=180$ kPa.

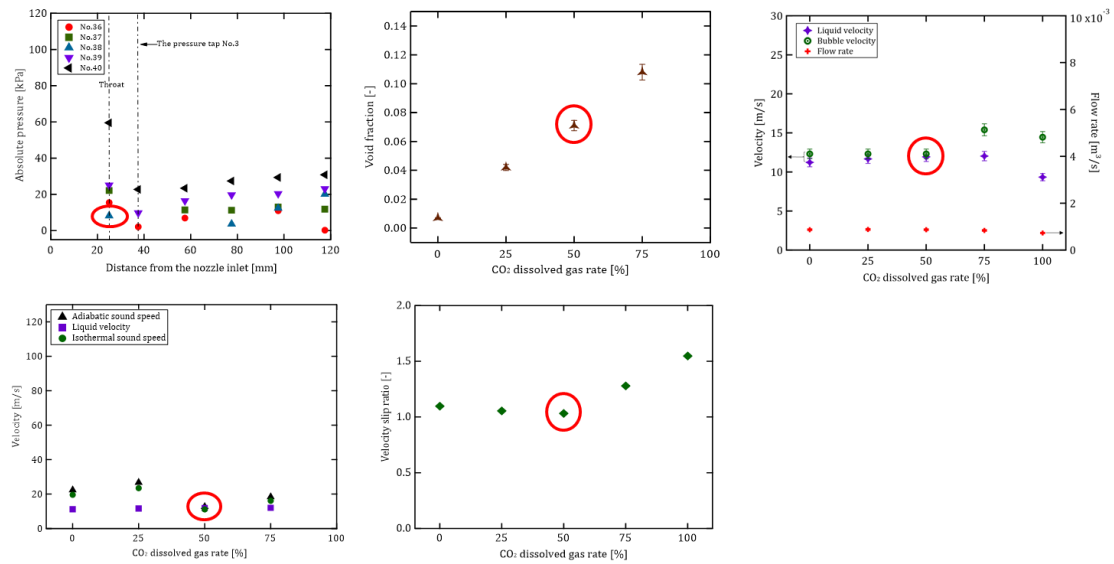


Figure 7.4. The results of the experiments with connecting two nozzles with $P_D=180$ kPa.

Experimental condition	No.31	No.32	No.33	No.34	No.35
Upper tank absolute pressure P_U [kPa]	201	201	201	201	201
Lower tank absolute pressure P_L [kPa]	51	51	51	51	51
Pressure difference P_D [kPa]	150	150	150	150	150
CO ₂ rate [%]	0	25	50	75	100
N ₂ rate [%]	100	75	50	25	0

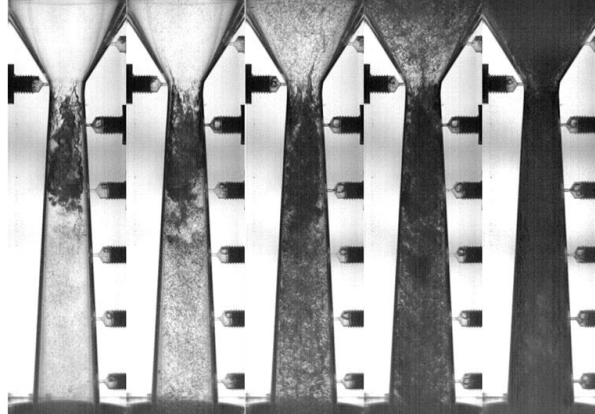


Figure 7.5. Experimental conditions and flow pattern of the connecting two nozzles with $P_D=150$ kPa.

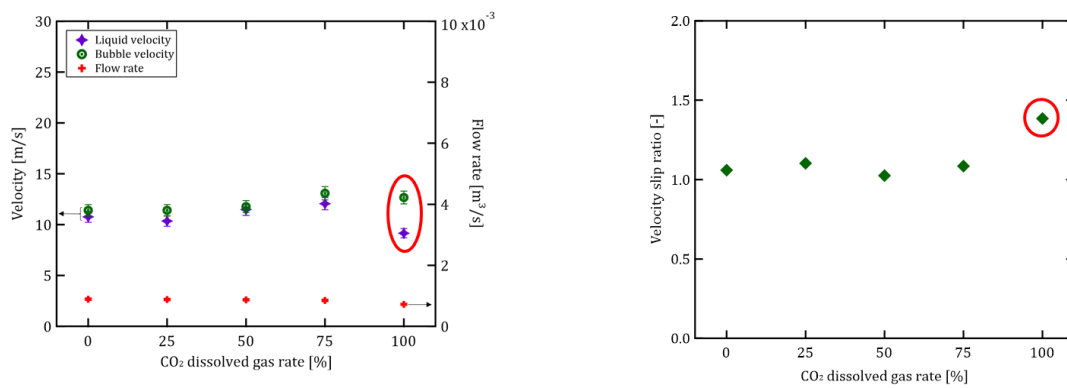


Figure 7.6. The results of the experiments with connecting two nozzles with $P_D=150$ kPa.

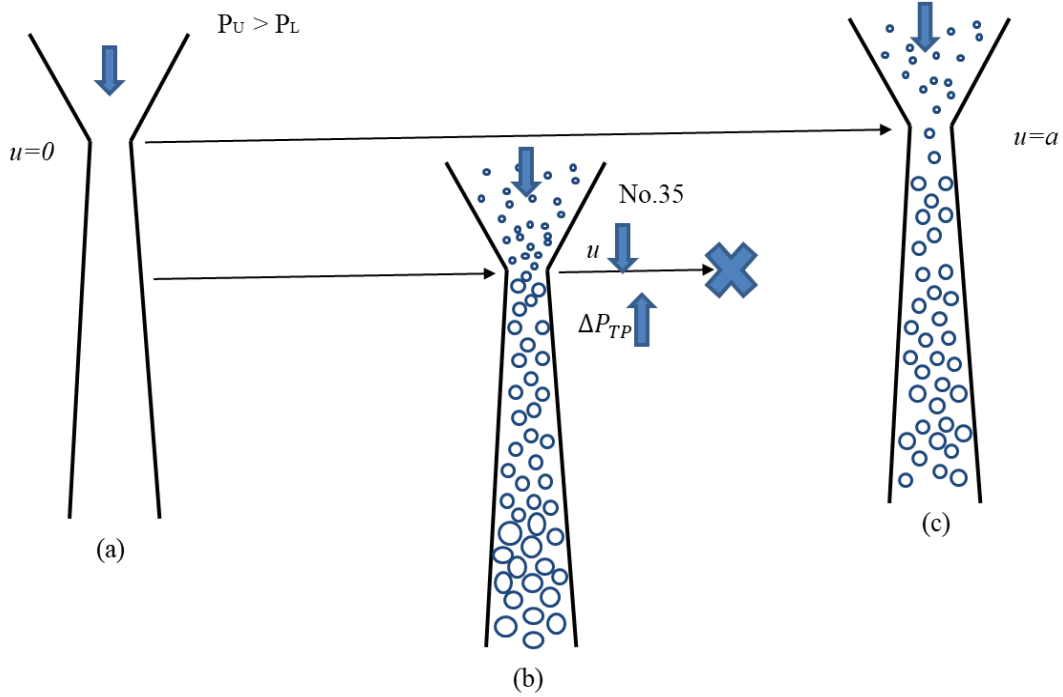


Figure 7.7. Schematic diagram of the experimental condition No.35.

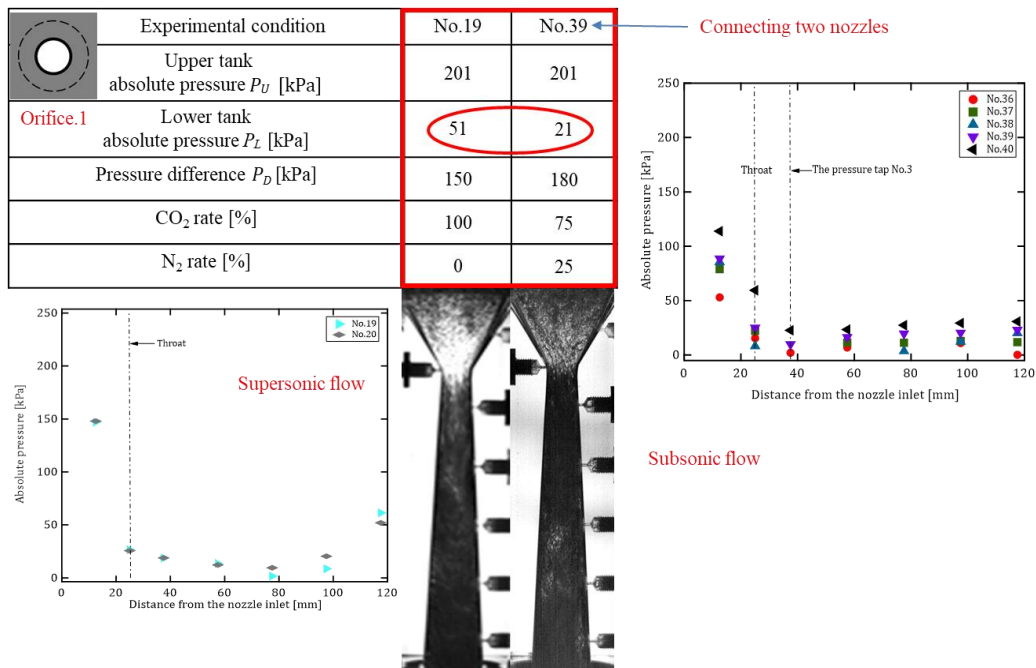


Figure 7.8. Comparison of the experimental conditions No.19 and No.39.

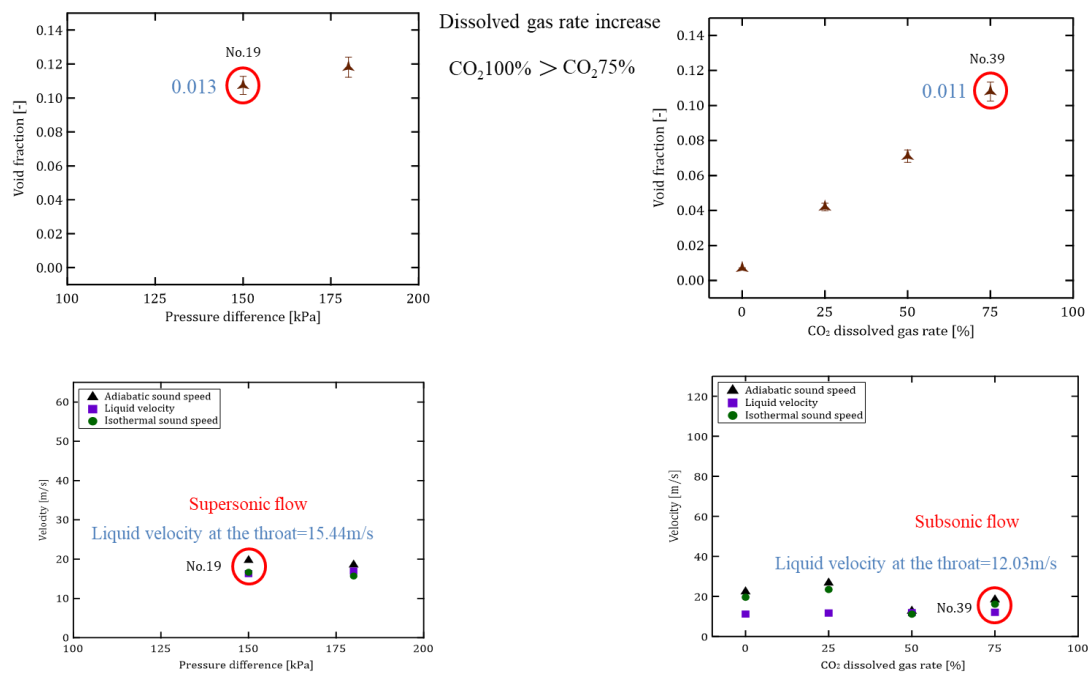


Figure 7.9. The results of the comparison of the experimental conditions No.19 and No.39.

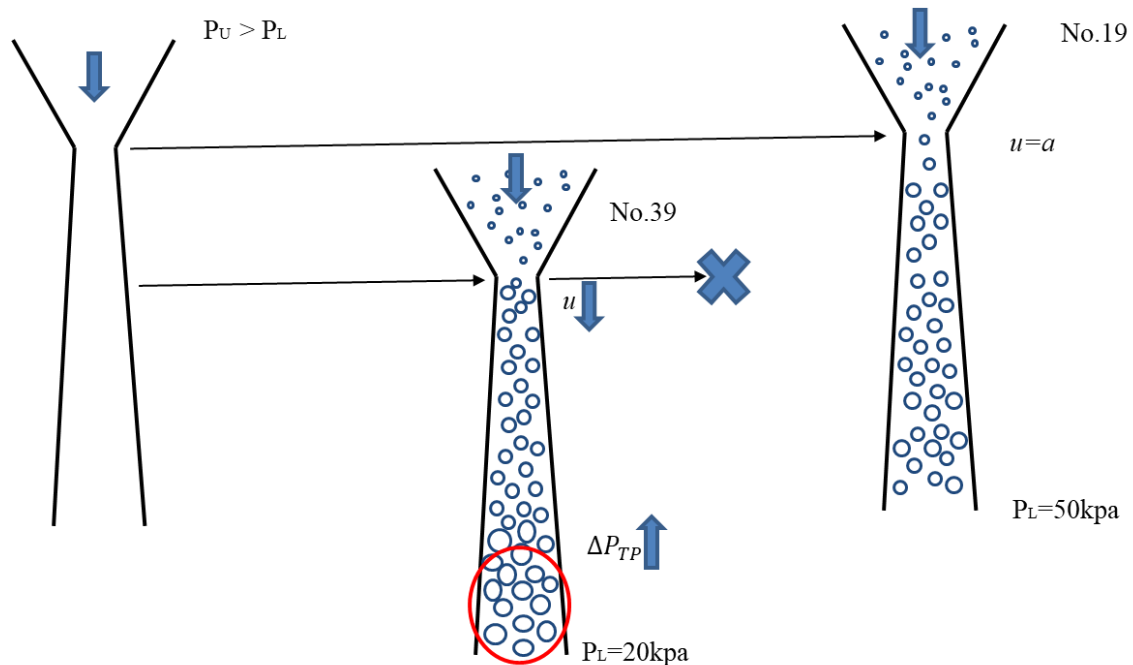


Figure 7.10. Schematic diagram of the experimental conditions No.19 and No.39.

Chapter 8

Conclusion

In order to reduce the velocity slip and to improve the conversion efficiency of the converging-diverging nozzle, micro-bubble two-phase flow was attempted to be used as the working fluids. The micro-bubbles were generated by the micro-bubble generator or the pressurized dissolution method. Millimeter-bubble generator and single-phase flow were used as a reference.

Based on the flow images, the pressure distribution and characteristics of micro-bubbles, it was confirmed that the micro-bubble two-phase flow generated by using a vortex breakdown mechanism became supersonic flow in the diverging section of the nozzle. In some cases, the flow changed to subsonic in the middle of the nozzle where the shock wave was observed. The supersonic flow with the micro-bubbles was very stable with low velocity slip ratio and homogeneous flow compared with the millimeter-bubble flow.

By the conventional pressurized dissolution method, however, the homogeneous micro-bubble was not obtained at the throat and bubbly flow in the diverging section of the nozzle. The subsonic flow was observed in the diverging nozzle. In the case of pressurized dissolution method, the micro-bubbles were not generated at the throat and the flow did not become supersonic flow. Therefore, in this study the pressurized dissolution method was also studied with more pressure difference with the upper tank and lower tank. However, these studies also were not observed the supersonic flow. Therefore, this method was modified by the four type of orifices.

In the case of the modification by using the orifice plate.1, the flow in the diverging nozzle was subsonic flow when the upper tank pressure and lower tank pressure were set to 201 kPa and 101 kPa with $P_D=100$ kPa. In order to examine the

effect of the amount of the dissolved gas on the pressurized dissolution method, the amount of CO₂ in the water at the upper tank was changed. As increasing the amount of CO₂, the void fraction increased, and the bubble velocity increased at the throat. The liquid velocity was almost constant. Therefore, the velocity slip between the bubble and the liquid increased. The amount of CO₂ could affect the generation of bubble. The more the amount of CO₂ was, the higher amount of bubbles appeared. When the amount of bubble was much, the bubble velocity became fast and it led to the large difference between the liquid velocity and bubble velocity. The larger velocity difference inhibited the reducing of velocity slip and it prevents the formation of supersonic flow. Based on the pressure distribution and velocity distribution along the nozzle the experimental conditions were only subsonic flow. Furthermore, the flow velocity did not reach the sound speed in all cases. Therefore, the pressure difference P_D was increased 150 kPa and 180 kPa to perform the supersonic flow. In these experiments the flow was estimated to be supersonic flow because the liquid velocity reached the sound speed and reduced velocity slip ratio. The liquid velocities were decreased along the nozzle. The micro-bubble could be generated at the throat in supersonic flow more than in subsonic flow. Therefore, the value of void fraction is higher in supersonic flow than in subsonic flow.

The pressurized dissolution method was also modified by orifice plate.² and the pressure difference P_D was increased to 100 kPa, 150 kPa and 180 kPa. The experimental condition of $P_D=150$ kPa was more potential to perform the supersonic flow because of its higher void fraction, the liquid velocity at the throat was close to the sound speed and low velocity slip ratio. Only subsonic flow was observed in the experiments of orifice plates.³ and 4.

The supersonic flow was observed in the upper cases of the modification of pressurized dissolution method with orifice plates. However, to get the homogeneous micro-bubble supersonic two-phase flow, the pressurized dissolution method was also modified by two connecting nozzles. In these experiments the upper tank pressure was 201 kPa when the flow passed through the front nozzle the pressure could decrease at the inlet of main nozzle and bubbles were more generated. The total amount of CO₂ gas rate was also changed in these experiments in order to study its effect on the generation of micro-bubbles. The micro-bubbles could be generated much when the CO₂% increased. The bubbles could be generated much even in lower percentage of CO₂ in case of low pressure in the lower tank 51 kPa and 21 kPa. Therefore, the micro-bubbles could be generated much when lower tank pressure reduced more (pressure difference more increased). It proves that the lower tank pressure condition in converging-diverging nozzles was also important to generate micro-bubbles.

In this study, we found out limitation on the amount of micro-bubbles. The experimental condition ($P_D=180$ kPa, CO₂ 50%) had the most possibility to perform supersonic flow because of the liquid velocity reaches the adiabatic and isothermal sound speed. The pressure at the throat could reduce and middle amount of void fraction was observed. Therefore, there was a proper condition to obtain the supersonic flow. In the study, the proper condition was a low pressure at the throat of the nozzle and the middle amount of the dissolved gas.

Under the same pressure difference conditions, the liquid velocity was almost the same at the throat. Therefore, it is important to reduce the sound speed to generate a supersonic flow. The supersonic flow was generated in high void fraction cases, because of low sound speed. However, the flow was subsonic under too high void fraction cases. Because much amount of bubbles prevented the flow due to the large pressure loss.

The supersonic flows were observed in the orifice plate.1 and connecting two nozzles. In the case of orifice plate.1, $P_D=150$ kPa and 180 kPa with CO₂ 100% were obtained supersonic flow with high void fraction. Therefore, velocity slip ratio was slightly high. In the case of connecting two nozzles, $P_D=180$ kPa with CO₂ 50% was obtained supersonic flow with medium void fraction. Therefore, velocity slip ratio was slightly lower than orifice plate.1. If high velocity slip ratio is obtained at the throat of the nozzle, the efficiency of the nozzle will be low. Therefore, in this two cases of the supersonic flow conditions, connecting two nozzles was the most proper condition to reduce velocity slip with micro-bubbles.

In future, pressurized dissolution method should be modified with different ways to generate homogeneous supersonic flow. If it not modifies with another way, the upper tank pressure should be higher, and the lower tank pressure should be lower in these experiments. For example, the upper tank pressure is 401 kPa or 501 kPa and lower tank pressure is 0 kPa. It will be generating more homogeneous supersonic flow. However, this experimental apparatus was designed not able too high pressure in the upper tank. Therefore, it is dangerous for this experimental apparatus. It should make to resist high pressure in the upper tank. Liquid Metal MHD power plant also used high pressure. If more homogeneous supersonic flow can generate, it will more useful in the Liquid Metal MHD power plant to reduce velocity slip.

The simulation method remains as a big challenge. Simultaneous measurement of the two-phase flow nozzle can effective to study for the supersonic flow with much micro-bubble.

Acknowledgments

Special acknowledges go to the following people who contributed this dissertation to be completed. First of all, I would like to express my deepest gratitude to my academic supervisor, Professor Hideaki Monji for permitting to undertake this research under his guidance, invaluable advice and providing all the research facilities. In addition, he widened my horizons and reinforced my understanding of the micro-bubbles in the supersonic two-phase flow nozzle as well as related fields of study and for exhorting to finish this course.

I also would like to pay grateful to the members of supervisory committee; Professor Yutaka Abe, Professor Makihito Nishioka, Professor Hideaki Monji, Associate Professor Akiko Kaneko and Dr. Cheong Kar Hooi for their offering of valuable comments, helpful advices and constructive discussions on my thesis. My heartfelt thanks are also due to the Hirose International Scholarship Foundation, Japan for providing financial support during my study period. I would like to mention my appreciation all my lab-mates: seniors and juniors for their understanding and cooperation throughout the work and all others who directly and indirectly contributed towards the success of this research work. Finally, I would like to extend my deepest gratitude to my devoted parents: U Maung Kyan and Daw Hnin Wai and my brothers and sisters who fulfill whatever I needs and give me never ending love and encouragement which have been helpful in my research. Last but not the least; I have the honors to pay my respect to all my teachers from kindergarten to university.

References

1. Barclay, F. J., Ledwidge, T. J., & Cornfield, G. C. (1969, September): Some experiments on sonic velocity in two-phase one-component mixtures and some thoughts on the nature of two-phase critical flow, In Proceedings of the Institution of Mechanical Engineers, Conference Proceedings (Vol. 184, No. 3, pp. 185-194). Sage UK: London, England: SAGE Publications.
2. Branover, H., Lykoudis, P.S. and Yakhot, A. (1983): Liquid-Metal Flows and Magnetohydrodynamics, American Institute of Aeronautics and Astronautics, Inc, New York.
3. Choi, J. K., Wu, X., & Chahine, G. L. (2014, November): Bubble Augmented Propulsion with a Convergent-Divergent Nozzle. In Proc. 30th Symposium on Naval Hydrodynamics.
4. Hanafizadeh, P., Ghanbarzadeh, S., Gheimasi, A. N., & Saidi, M. H. (2010, January): Experimental investigation of air-water two phase flow regime in vertical mini pipe, In ASME 2010 8th International Conference on Nanochannels, Microchannels, and Minichannels collocated with 3rd Joint US-European Fluids Engineering Summer Meeting (pp. 1411-1417). American Society of Mechanical Engineers.
5. Hosokawa, S., Tanaka, K., Tomiyama, A., Maeda, Y., Yamaguchi, S. and Ito, Y., (2009): Measurement of micro bubbles generated by a pressurized dissolution method, In Journal of Physics: Conference Series (Vol. 147, No. 1, p. 012016). IOP Publishing.
6. Ishii, R., Umeda, Y., Murata, S. and Shishido, N., (1993): Bubbly flows through a converging-diverging nozzle, Physics of Fluids A: Fluid Dynamics, 5(7),

pp.1630-1643.

7. Itamoto, Y. and Monji, H. (2011): Error of Optical Measurement on Dispersed Two-Phase Flow, Proc. of 6th International Symposium on Advanced Science and Technology in Experimental Mechanics, No.082.
8. Jamalabadi, M. Y. A. (2018): Electromagnetohydrodynamic two-phase flow-induced vibrations in vertical heated upward flow, Journal of Computational Design and Engineering.
9. Kaushik, S. C., Verma, S. S., & Chandra, A. (1995): Solar-assisted Liquid Metal MHD power generation: A state of the Art Study, Heat Recovery Systems & CHP, Vol. 15, No. 7, pp. 675-689.
10. Karplus, H. B., (1958): The velocity of sound in a liquid containing gas bubbles, Res. Develop. Rep. C00-248, 22 pp., Atomic Energy Commission, Chicago, III.
11. Kentaro Nakamura, Khine Tun Naung and Hideaki Monji, 3-6 November (2013): Study on supersonic nozzle flow with micro bubbles, Proc. of the 8th International Symposium on Advanced Science and Technology in Experimental Mechanics, No.079, Sendai.
12. Kieffer, S. W. (1977): Sound speed in liquid-gas mixtures: Water-air and water-steam, Journal of Geophysical research, 82(20), 2895-2904.
13. 日本流体力学会 (1989): 混相流体の力学, 朝倉書店.
14. Kuo, J.T. and Wallis, G.B., (1988): Flow of bubbles through nozzles, International Journal of Multiphase Flow, 14(5), pp.547-564.
15. Lockhart, R. W., & Martinelli, R. C. (1949): Proposed correlation of data for isothermal two-phase, two-component flow in pipes, Chem. Eng. Prog, 45(1), 39-48.
16. Maeda, Y., Hosokawa, S., Taya, C., Tomiyama, A., Yamaguchi, S. and Ito, Y., 24-4

- (2010): Diameter and Number Density of Micro-Bubbles Generated by a Pressurized Dissolution Method (in Japanese), *Japanese Journal of Multiphase Flow*, 462-469.
17. Mallock, H. R. A. (1910): The damping of sound by frothy liquids, *Proc. R. Soc. Lond. A*, 84(572), 391-395.
 18. Mc William, D., & Duggins, R. K. (1969, September): Speed of sound in bubbly liquids, In *Proceedings of the Institution of Mechanical Engineers, Conference Proceedings (Vol. 184, No. 3, pp. 102-107)*. Sage UK: London, England: SAGE Publications.
 19. 松本雅至, 井上欣也, 安富友香, 小橋好充, 松村恵理子, 神田睦美, & 千田二郎. (2013): 直接噴射方式におけるノズル内キャビテーションが噴霧特性に及ぼす影響 (第 2 報: 供試液体中の溶存空気濃度を変化させた際の衝撃加速度と噴流の関係), *日本機械学会論文集 B 編*, 79(806), 2160-2169.
 20. Mich, P. Davis, May (2008): Experimental investigation of the cavitation of aviation fuel in a converging-diverging nozzle, Graduate program in aerospace and mechanical engineering, Notre Dame, Indiana.
 21. Nakagawa, M., Berana, M. S., & Kishine, A. (2009): Supersonic two-phase flow of CO₂ through converging-diverging nozzles for the ejector refrigeration cycle, *International journal of refrigeration*, 32(6), 1195-1202.
 22. Nakagawa, M., Takeuchi, H., & Nakajima, M. (1998, June): Performance of two-phase ejector in refrigeration cycle, In *Proceedings of the 3rd International Conference on Multiphase Flow*, Lyon, France (Vol. 382, pp. 1-8).
 23. Ohnari, H., Takahashi, M., Himuro, S. and Shakutsui, H. 16-2 (2002): Roles of Micro Bubble Technique in Multiphase Flow (in Japanese), *Japanese Journal of Multiphase Flow*, 130-137.

24. Rajeev Parmar, Subrata Kumar Majumder, 20, December (2012): Microbubble generation and microbubble-aided transport process intensification-A-state-of-the-art report, Department of chemical engineering, Indian Institute of Technology Guwahati, Guwahati 781039, Assam, India.
25. Sato, Y. and Sekoguchi, K., (1975): Liquid velocity distribution in two-phase bubble flow, *International Journal of Multiphase Flow*, 2(1), pp.79-95.
26. Serizawa, A., Inui, T., Yahiro, T. and Kawara, Z., (2003) September: Laminarization of micro-bubble containing milky bubbly flow in a pipe, In *The 3rd European-Japanese Two-phase Flow Group Meeting*, Certosa di Pontignano.
27. Shatat, M.M., Yanase, S., Takami, T. and Hyakutake, T., (2009): Drag Reduction Effects of Micro-Bubbles in Straight and Helical Pipes, *Journal of Fluid Science and Technology*, 4(1), pp.156-167.
28. Shatat, M.M., Yanase, S., Takami, T. and Hyakutake, T., (2009): Pressure Drop Characteristics of Water Flow with Micro-bubbles Through Helical Pipes.
29. Soteriou, C., Andrews, R., & Smith, M. (1995): Direct injection diesel sprays and the effect of cavitation and hydraulic flip on atomization, *SAE transactions*, 128-153.
30. Toma, T., Yoshino, K. and Morika, S (1986): Mechanism of Velocity Slip and Associated Turbulence in a Accelerating Nozzle Flow of Bubbly Liquid, *Proc. Of Ninth Int. Conf. on Magnetohydrodynamic Electrical Power Generation*, 722-732.
31. Toma, T., Yoshino, K. and Morioka, S., (1988): Fluctuation characteristics of bubbly liquid flow in converging-diverging nozzle, *Fluid dynamics research*, 2(4), p.217.
32. Wang, Y.C. and Chen, E., (2002): Effects of phase relative motion on critical bubbly flows through a converging-diverging nozzle, *Physics of Fluids*, 14(9),

pp.3215-3223.

33. Wu, X., Choi, J. K., Nye, A. L., & Chahine, G. L. (2015): Effect of Nozzle Type on the Performance of Bubble Augmented Waterjet Propulsion. In Proceedings of the 4th International Symposium on Marine Propulsors, pp. 122-134.
34. Yamada, Y., Sakairi, N., Kaneko, K., Kyotoh, H (2005): The micro bubble generation due to the vortex breakdown (in Japanese), JSFM, 1-5.
35. Žun, I., (1990): The mechanism of bubble non-homogeneous distribution in two-phase shear flow, Nuclear engineering and design, 118(2), pp.155-162.

Publications

Journal articles

5. Khine Tun Naung, Hideaki Monji, Supersonic Flow Conditions for Two Connecting Two-Phase Flow Nozzle in Pressurized Dissolution Method, *Advanced Experimental Mechanics*, Vol.3, pp. 92-97, 2018.
6. Khine Tun Naung, Rei Mikoshiba, Junhyuk Lee, Hideaki Monji, Effect of Orifice Shape and Dissolved Gas on Bubble Generation in Two-Phase Nozzle Flow by Pressurized Dissolution Method, *Advanced Experimental Mechanics*, Vol.1, pp.80-85, 2016.
7. Khine Tun Naung, Nakamura, K., Mikoshiba, R., Monji, H., Study on Generation of Supersonic Flow in a Converging-Diverging Nozzle by Modified Pressurized Dissolution Method, *J. JSEM*, **15**-Special Issue, s15-s20, 2015.
8. Nakamura, K., Khine Tun Naung, Monji, H., Study on Supersonic Nozzle Flow with Micro Bubbles, *J. JSEM*, **14**-Special Issue, s88-s93, 2014.

Proceedings of international conference/symposium

1. Rei Mikoshiba, Khine Tun Naung, Hideaki Monji, Micro-Bubble Flow in Converging-Diverging Nozzle Using Pressurized Dissolution Method - Effect of Amount of Dissolved Gas -, *Proc. of 10th International Symposium on Advanced Science and Technology in Experimental Mechanics*/p.059, Nov, 2015.

2. Hideaki Monji, Khine Tun Naung, Kentaro Nakamura, Rei Mikoshihba, Micro-Bubble Two-Phase Flow in Converging-Diverging Nozzle, *Japan-US Seminar on Two-Phase Dynamics*, May, 2015.

National conference

4. Khine Tun Naung, Hideaki Monji, 超音速ノズルのための加圧溶解法によるマイクロバブル生成の最適条件, 第 22 回動力・エネルギー技術シンポジウム講演論文集/p.B111, 2017 年 6 月.
5. カイン トウン ナウン, 文字秀明, 修正された溶解法による超音速二相流の実現可能性, 日本実験力学会講演論文集 2016 年度年次講演会/pp.202-203, 2016 年 9 月.
6. 文字秀明, カイン トウン ナウン, マイクロバブルの超音速ノズル流れの詳細観察, 日本実験力学会, 2015 年 8 月.
7. カイン トウン ナウン, 文字秀明, 加圧溶解法を用いた気液二相ノズル流れに対する溶存気体の影響, 日本混相流学会混相流シンポジウム 2014 講演論文集, 2014 年 7 月.
8. Khine Tun Naung, Kentaro Nakamura, Rei Mikoshihba, and Hideaki Monji, Study on Converging-Diverging Nozzle Flow with Micro Bubbles, 第 9 回新エネルギー技

術シンポジウム, 2014年3月.

9. Khine Tun Naung, Hayato Tajima, Hideaki Monji, Analytical Study on Supersonic Two-Phase Flow Nozzle, 茨城講演会講演論文集, *Ibaraki district conference/2012(20)/pp.85-86*, Aug, 2012.

APPENDIX A

THE EFFECT OF NOZZLE DESIGN ON TWO-PHASE FLOW

A. The Effect of Nozzle Design on Two-Phase Flow

Many bubbles were generated from the pressure measuring taps of the throat in the experiment of nozzle I (with pressure measuring taps). Therefore, the void fraction was deviated and the flow was not become homogeneous. To avoid this problem in this chapter the flow was studied by using nozzle II (without pressure measuring taps). The photo of nozzle II is shown in Fig. 2.4 (b). The shape of the nozzle II was the same as nozzle I. The pressurized dissolution method was used and the influence of dissolved gas was investigated by changing the partial pressure of CO₂ in the upstream tank as in Section 5.2 of Chapter 5. However, modification method of orifices and connecting nozzle were not provided for all experimental conditions in this chapter. The changing of water temperatures were neglected under each experimental condition.

A.1. Experimental condition with nozzle II

Table A.1 represents the experimental conditions with nozzle II, the same experimental condition with modification of pressurized dissolution method with orifice plate.1 of the experimental conditions No.14 to No.18 (see Table.5.1). Table A.1 (a) represents the upper tank pressure 201 kPa and lower tank pressure 101 kPa. Table A.1 (b), (c) and (d) are also the same upper tank pressure 201 kPa and lower tank is changing 61 kPa, 51 kPa and 21 kPa respectively.

A.1.1. Acquisition of flow image

The flow images of the nozzle were taken by the high speed camera. The photographing speed was 1000 Hz and the exposure time was 50 μ s. The captured images were shown in Fig. A.1. The generation of micro-bubbles were homogeneously increased with CO₂% increased. However, less micro-bubbles were generated in these

experimental conditions than the same experimental of modification of pressurized dissolution method even if the CO₂ % increased. This might be due to the effect of orifice plates and front nozzle.

According to Fig. A.1, the brightness sharply increases from the middle of the nozzle to the exist. From the result of the PIV measurement (to be discussed in section A.3) brightness of bubbles were observed from the throat because of the water was separated from the nozzle wall surface. Therefore, it was considered that the flow reattached in the section where the brightness sharply brightens, and it was caused by the wake of the reattachment flow. The image of flow pattern is shown in Fig. A.2 as an example when the CO₂ partial pressure ratio is 0%. The luminance value distribution in the flow direction was calculated from image processing in order to examine the change of luminance value in the nozzle. When the exposure time of the high-speed camera was set at 50 μ s, the brightness of the photographed image was uneven. For this reason, the images were captured with an exposure time of 150 μ s was used as the image for calculating the luminance value distribution. A schematic diagram of the image processing method is shown in Fig. A.3. The luminance value distribution was calculated by subtracting the background image of the high speed camera, before the image of the experiment did not start. The luminance value of the x direction was calculated by using Eq. (A.1) and taken average value. The average luminance value of the x direction was taken along the vertical direction (z direction). B_z represents the luminance value of a certain z coordinate, and B_{zi} represents the average luminance value of a certain x coordinate. Also, the same image processing was applied to 400 capture images and averaged. The calculation result of the luminance value distribution is shown in Fig. A.4. According to the Figs. A.1 and A.4, the smaller the CO₂ partial pressure ratio was, the brighter luminance section were observed. That was probably

because of the amount of bubbles increased as the CO₂ partial pressure ratio increased. Also, in the CO₂ partial pressure ratio of 0% in Fig. A.4, the location where the flow reattachment and the luminance value increases were corresponded (see the red line in Fig. A.4). Therefore, if a place where the luminance value becomes large was defined as a reattachment point, that was difference in luminance due to a change in the CO₂ partial pressure ratio. However, the difference amount of the bubble formation remarkably appeared downstream of the red line. Also, when the CO₂ partial pressure ratio was large, it was difficult to understand where the luminance increased due to bubble generation, but from Fig. A.4 it could be seen that the reattachment point moves downstream as CO₂ increased.

$$B_z = \frac{\sum_{i=1}^n B_{zi}}{n} \quad (\text{A.1})$$

A.1.2. Two-phase flow rate

The flow rate of the two nozzles were calculated by using Eq. (2.17). The calculation result are shown in Fig. A.5. As shown in Fig. A.5, when the CO₂ partial pressure ratio increased, the liquid phase flow rate decreased. That was considered to be due to the increase of friction loss in two-phase flow as the amount of bubble formation increased when the CO₂ partial pressure ratio increased. In addition, compared to the case of nozzle I (with pressure measuring hole), the liquid flow rate decreased.

A.2. The effect of the lower tank pressure

Experiments were performed with the lower tank pressure P_L reduced to 61 kPa, 51 kPa and 21 kPa, from the experimental conditions of Table A.1 (a) (101 kPa,

atmospheric pressure). The upper tank pressure was fixed at 201 kPa. Experimental conditions are shown in Tables A.1 (a) to (d).

A.2.1. Acquisition of flow image

The flow images in the nozzle were taken by the high speed camera. Fig. A.7 to Fig. A.9 show the captured images along the nozzle II of each experimental conditions. At the CO₂ partial pressure ratio of 0%, the luminance value distribution for each lower tank pressure was calculated by image processing as the same procedure represented in Section A.1.1. The results are shown in Fig. A.10 to Fig. A.14. The result of the lower tank pressure of 101 kPa was used from the section A.1.1. In order to know how to effect of the lower tank pressure on the flow condition, the same CO₂ 0% of dissolution gas rate but different lower tank pressure 101 kPa (see in Fig. A.1) and 61 kPa (see in Fig. A.7) was compared as represented in Fig. A.6. According to the Fig. A.6, it can be seen that the reattachment point moved to the downstream as the lower tank pressure decreased. Also, from the change of the luminance value of the lower tank pressure of 101 kPa and the lower tank pressure of 61 kPa in Fig. A.10, it can be seen that the reattachment point moved to downstream.

Figure A.8 shows the flow in the nozzle when the lower tank pressure is more decreased (lower tank pressure $P_L=51$ kPa). From the results of partial pressure ratio of CO₂ 0% in Fig. A.7, Fig. A.8 and Fig. A.10, it can be seen that the reattachment point moves further downstream in the case where the lower tank pressure is 51 kPa than in the case where the lower tank pressure is 61 kPa. Also, as shown in Fig. A.8, when the CO₂ partial pressure ratio is 75% and 100%, the reattachment point can not be formed in the nozzle, and a thing like a water pillar is formed from the throat to the nozzle outlet. Consider the reason why the reattachment point could not be formed when the

CO₂ partial pressure ratio was 75% and 100%, when the reducing of the lower tank pressure moves the reattachment point downstream at all CO₂ partial pressure ratios. When the lower tank pressure is 51 kPa and the CO₂ partial pressure ratio is 0%, the reattachment point is near to the outlet of the nozzle from Fig. A.8 and Fig. A.10. From Section A.1.1, the reattachment point moved further downstream at the same lower tank pressure, as the CO₂ partial pressure ratio increased. Therefore, when the lower tank pressure is 51 kPa, the reattachment point exists in the nozzle when the CO₂ partial pressure ratio is 0%, 25%, 50%. When the CO₂ partial pressure ratio is 75% and 100%, there was no reattachment point because it moved further downstream. Furthermore, when the lower tank pressure was decreased to ($P_L=21$ kPa), as shown in Fig. A.9, there was no reattachment point inside the nozzle under all the experimental conditions. This is probably that the reattachment point moved to the downstream side from the nozzle outlet under all conditions due to the lower tank pressure decreased.

Therefore, the lower tank pressure could transit from the reattachment flow to the separated flow was examined by CO₂ partial pressure ratio experiments respectively. The experimental results are shown in Fig. A.15. However, the black dot is a reattachment flow, and the x dot is a separated flow which did not exist in the nozzle. Figure A.10 also shows the luminance value distribution when the CO₂ partial pressure ratio was 0%, in which the smallest value of luminance was observed at the lower tank pressure 41 kPa that would reattachment flow moved to the outlet of the of the nozzle. Also from Fig. A.10, it can be seen that when the CO₂ partial pressure ratio is 0% and the lower tank pressure which is the limit of the reattachment flow is 41 kPa, the reattachment point is closest to the nozzle outlet. In addition, as shown in Fig. A.15, it can be seen that as the CO₂ partial pressure ratio becomes larger, the region where reattachment flows becomes narrower. Figures A.16 to A.20 show the condition of flow

in the nozzle in the CO₂ partial pressure ratio when the lower tank pressure is changed.

A.2.2. Liquid phase flow rate

The liquid phase flow rate was calculated for all the experimental conditions represented in Table A.1 (a), (b), (c), (d). The results of the flow rate were taken for only one time because in all the experimental conditions had 95% of confidence interval. In Fig. A.21, the experimental results of the flow rate for only one time are plotted. The liquid flow rates were hardly changed in the range of reattachment flow, at all CO₂ partial pressure ratios even when the lower tank pressure was changed in the Fig. A.15 and Fig. A.21. The liquid flow rates were abruptly decreases in the range of separated flow, at all CO₂ partial pressure ratios, when the decreasing the lower tank pressure, and furthermore, when the lower tank pressure was decreased to 21 kPa, the liquid flow rate increased. It was thought that due to the increasing of fraction loss.

Therefore, it was considered that as the CO₂ partial pressure ratio was smaller, the region where a constant liquid flow rate could be observed wider. Matsumoto (2013) reported that when the liquid was sprayed from the nozzle to the atmospheric pressure, the separated flow occurred inside the nozzle because the pressure inside the nozzle was greatly lower than the atmospheric pressure. While flow in the nozzle was separated in the case of hydraulic flip the exit pressure was lower than the atmospheric pressure was measured in the nozzle (Soteriou, 1995). Therefore, it was considered that the flow rate decreased when the flow became a separated flow in this research under the influence of the lower tank pressure. In all the experimental conditions of the same lower tank pressure, the liquid phase flow rate decreased as the CO₂ partial pressure ratio increased because of the increasing the amount of bubble formation in two-phase flow.

A.3. PIV measurement

A.3.1. Over view of PIV measurement

Particle Image Velocimetry (PIV) is a non-intrusive laser optical measurement technique for research and diagnostics into flow, turbulence, microfluidics, spray atomization and combustion processes. Which is a method of measuring the fluid velocity by taking correlation of two images at appropriate timing irradiating with laser beam to a flow field in which tracer particles are mixed. We investigated the velocity field of the reattachment flow and the separated flow field and the condition of the flow inside the nozzle by using PIV measurement.

A schematic diagram of the PIV measurement system is shown in Fig. A.22. The laser used for PIV measurement is an Nd-YaG laser (Nano L50-100 PIV manufactured by Litoron). In this experimental apparatus, when the laser was irradiated from the same height as the nozzle a shadow was formed in the nozzle, that was inconvenience of the experimental apparatus. Therefore, irradiation light from the laser was changed in optical path by the mirror and a laser sheet was formed at the center of the nozzle obliquely downward. The laser sheet diffused onto the sheet by the cylindrical lens. Photographing was carried out using a high-speed camera from the side of the nozzle.

The high-speed camera and the two lasers were connected through a pulse generator (manufactured by Quantum Composers). The timing of the shooting and the irradiation of the laser light could be controlled by the signal of the pulse generator. In this experiment, the exposure time of the high-speed camera was set to 100 μs and the interval between the two laser beams was set to 20 μs and it was repeated at a cycle of 80 Hz. The timing chart is shown in Fig. A.23. Fluorescent particles (density 1500 kg/m^3 , average particle diameter 10 μm) coated with rhodamine B were used as laser

particles. This particle had an excitation spectrum peak at around 540 nm and a fluorescence spectrum peak at around 580 nm. Since the wavelength of the laser light was 532 nm, by using a high pass filter that transmits about 560 nm or more, the laser light was blocked and only the image of the fluorescent laser particle was photographed.

The experimental conditions are shown in Table A.2. PIV measurement was carried out when the CO₂ partial pressure ratio was 0% and the downstream tank pressure was 40 kPa and 35 kPa, and the state of flow when transitioning from the reattachment flow to the separated flow was investigated.

A.3.2. Experimental result

Figure A.24 shows the flow in the nozzle taken by the high-speed camera. In the photographed image, the white glossy portion was a fluorescent laser particle. As shown in Fig. A.24, it could be seen that in both conditions, downstream of the throat section, the flow was separating and flowing without attaching to the wall surface. In the reattachment flow, the flow attached to the wall further downstream and droplets existed upstream, whereas the flow was not reattaching because the flow was pulled off from the nozzle exit.

According to the PIV measurement, the flow velocity distribution in the vertical direction and the cross-sectional average flow velocity from the nozzle inlet to the throat section were calculated. The calculation formula is expressed by the Eq. (A.2). The flow velocity distribution for vertical direction was taken by the time average value obtained from 250 images.

$$u_L = \frac{\int u_L(r)2\pi r dr}{A} \quad (A.2)$$

The cross sectional average flow velocity value was calculated by dividing the result of experimental average flow velocity calculated from Eq. (A.2) and the flow rate was measured from the experiment by the cross section. Then PIV measurement result and calculation result were compared. The reattachment flow is shown in Fig. A.25, the seperated flow is shown in Fig. A.26 and the results of both were shown together. From Fig. A.25 and Fig. A.26, the average cross section flow velocity almost agreed with PIV measurement result. Therefore, the PIV measurement result in this experiment was judged to be valid.

Figure A.27 shows the flow velocity at the center of the nozzle obtained by PIV measurement. However, the flow velocity was the time average value of the flow velocity obtained from 250 images. The flow speed became faster at both conditions slightly downstream from the throat section. This was considered to be caused by contraction of flow. In addition, as a whole, the flow velocity was faster in the lower tank pressure of 41 kPa, reattachment flow compared with 36 kPa, seperated flow. This was consistent with the decrease in flow rate due to flow transitions in Fig. A.21.

In the result of the lower tank pressure of 41 kPa in Fig. A.27, the flow velocity abruptly decreased downstream of the throat part was because the refraction of the laser light did not accurately correlate, and the distance from the nozzle inlet 60 mm It was considered that the rapid decreased of the flow velocity in the ambient due to the influence of downstream adherence (see red dotted line in Fig. A.27). As a result of the lower tank pressure of 36 kPa, it was found that the flow rate sharply decreased near the distance of 75 mm from the nozzle inlet. It had less brightness than the photographed image of PIV by the high-speed camera, it was considered that correlation could not be obtained each other.

The flow velocity distribution in the perpendicular direction to the flow was measured at 0.65 mm downstream from the nozzle inlet, throat section and at the middle of two places (51 mm and 64 mm downstream from the throat section) in the nozzle. However, the flow velocity distribution in the direction perpendicular to the flow is the time average value obtained from 250 images. The reattachment flow is shown in Fig. A.28, and the separated flow is shown in Fig. A.29. However, the flow velocity distribution in the throat section is black line, and the flow velocity distribution of 0.65 mm downstream from the throat section is shown simultaneously with red line. As shown in Fig. A.28 and Fig. A.29, the nozzle inlet was a developed flow, whereas in the throat section the flow was not developed. In both conditions, it could be seen that the flow path was narrowed by the contraction flow and the flow velocity was faster than the throat section at a position slightly downstream from the throat section. From Fig. A.28, it could be seen that the reattachment flow path flowed with the same width as the contraction flow. On the other hand, in the separated flow, as shown in Fig. A.29, it was understood that the flow path flowed with the same width as the throat section.

The flow rate in the inspection area of 6.5 mm, 7.8 mm, 9.1 mm, 10.4 mm, 11.7 mm, 13 mm in width at the nozzle center was calculated in the nozzle flow direction from the Eq. (A.3). Here, the width of 6.5 mm, which was the minimum value of the inspection zone width, was set to be about the same as the width of the contraction flow. Figure A.30 represents the outline of the inspection area width, Fig. A.31 shows the result of the reattachment flow, and Fig. A.32 shows the case of separated flow. In Fig. A.31 and Fig. A.32, the flow rate increased as the inspection zone width changed upstream from the throat section. That was cause because of the liquid flowed between the end of the inspection area width and the nozzle wall surface. The fact that the flow rate abruptly decreased downstream from the throat section was because it could not be

accurately measured due to the refraction of the laser light and the flow rate sharply decreased at the nozzle exit from the center of the spreading nozzle section because of the luminance was low in PIV measurement and accurate measurement was not possible. Therefore, the more interesting in the result was the ambient of the distance of 50 mm from the nozzle inlet in Fig. A.31 and Fig. A.32. As shown in Fig. A.31 and Fig. A.32, it could be seen that even if the inspection area width increased, the flow rate did not change with a certain width. That means the liquid did not flow between the inspection zone width and the nozzle wall surface when the width was over a certain width, and it was understood that the flow was separated downstream from the throat section. In addition, in the reattachment flow, the flow rate did not change when the inspection zone width was 7.8 mm or more, whereas in the flow not adhering, the inspection zone width did not change with 9.8 mm or more. Therefore, it was considered that the reattachment flow was narrower in the width of the jet than the separated flow.

$$Q_L = \int u_L(r) 2\pi r dr \quad (A.3)$$

A.4. Concluding remarks

The result on the effect of nozzle design on two-phase flow as discussed above were summarized as follows:

- i. When pressurized dissolution method was used, there was a difference in bubble formation when changing the partial pressure of dissolved gas. In particular, the difference remarkably appeared downstream of the reattachment point.
- ii. In the reattachment flow, the liquid flow rate became constant even if the lower tank pressure was decreased. In the separated flow, the liquid flow rate was

sharply decrease from the reattachment flow then when the lower tank pressure was more decrease, the flow rate would increase.

- iii. As the partial pressure of dissolved gas increases, the area of reattachment flow narrowed.

Table.A.1. Experimental conditions of pressurized dissolution method with lower tank pressure changing.

(a) $P_L=101$ kPa

Experimental condition	Water temperature [°C]	Upper tank pressure P_U [kPa]	Lower tank pressure P_L [kPa]	Pressure difference P_D [kPa]	CO ₂ rate [%]	N ₂ rate [%]
1-a	18.8	201	101	100	0	100
1-b	18.8				25	75
1-c	18.8				50	50
1-d	19.8				75	25
1-e	19.0				100	0

(b) $P_L=61$ kPa

Experimental condition	Water temperature [°C]	Upper tank pressure P_U [kPa]	Lower tank pressure P_L [kPa]	Pressure difference P_D [kPa]	CO ₂ rate [%]	N ₂ rate [%]
2-a	17.0	201	61	140	0	100
2-b	16.5				25	75
2-c	16.5				50	50
2-d	18.8				75	25
2-e	18.8				100	0

(c) $P_L=51$ kPa

Experimental condition	Water temperature [°C]	Upper tank pressure P_U [kPa]	Lower tank pressure P_L [kPa]	Pressure difference P_D [kPa]	CO ₂ rate [%]	N ₂ rate [%]
3-a	19.0	201	51	150	0	100
3-b	20.0				25	75
3-c	20.0				50	50
3-d	20.0				75	25
3-e	20.0				100	0

(d) $P_L=21$ kPa

Experimental condition	Water temperature [°C]	Upper tank pressure P_U [kPa]	Lower tank pressure P_L [kPa]	Pressure difference P_D [kPa]	CO ₂ rate [%]	N ₂ rate [%]
4-a	17.0	201	21	180	0	100
4-b	16.9				25	75
4-c	16.9				50	50
4-d	16.9				75	25
4-e	18.8				100	0

Table.A.2. Experimental conditions of pressurized dissolution method for PIV measurement.

Experimental condition	Water temperature [°C]	Upper tank pressure P_U [kPa]	Lower tank pressure P_L [kPa]	Pressure difference P_D [kPa]	CO ₂ rate [%]	N ₂ rate [%]
1	18.2	201	41	160	0	100
2	18.2		36	165		

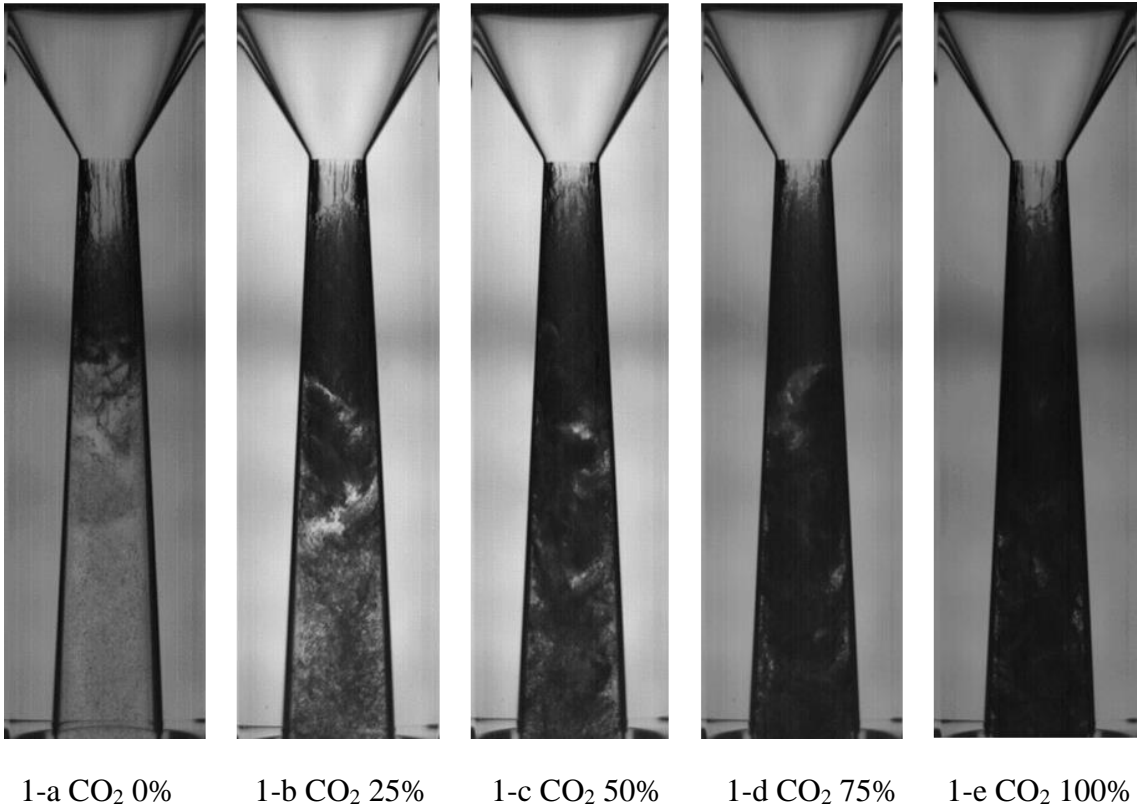


Figure A.1. Flow pattern with changing rate of CO₂ ($P_L=101$ kPa).

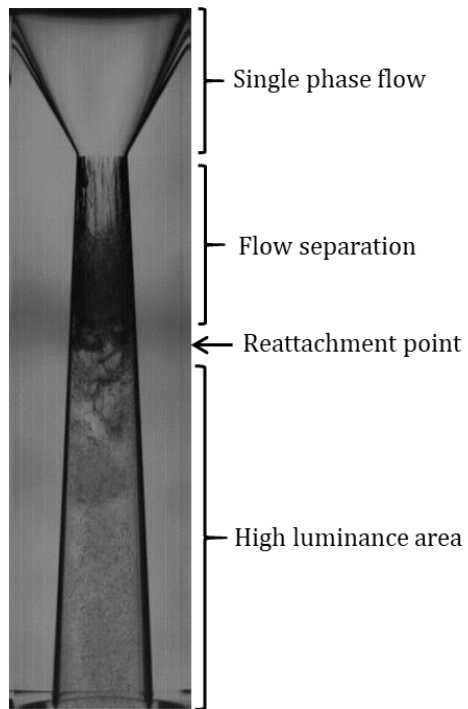


Figure A.2. Image of the flow pattern (CO₂ 0%).

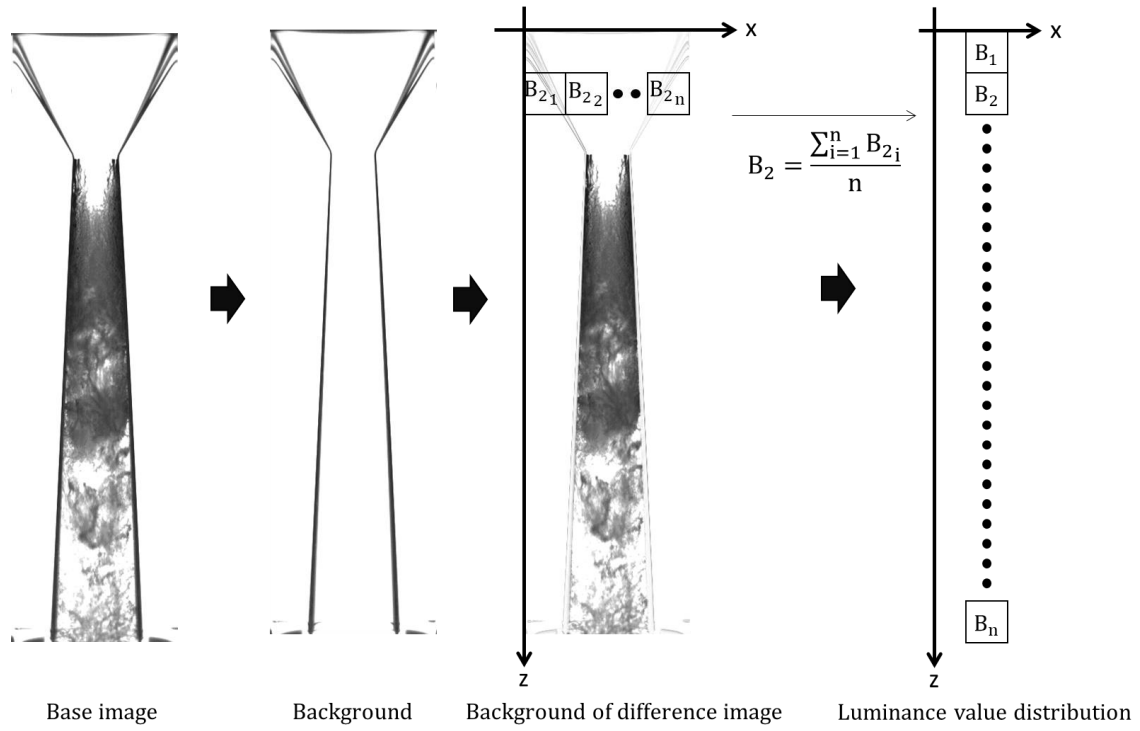


Figure A.3. Image processing method of brightness value.

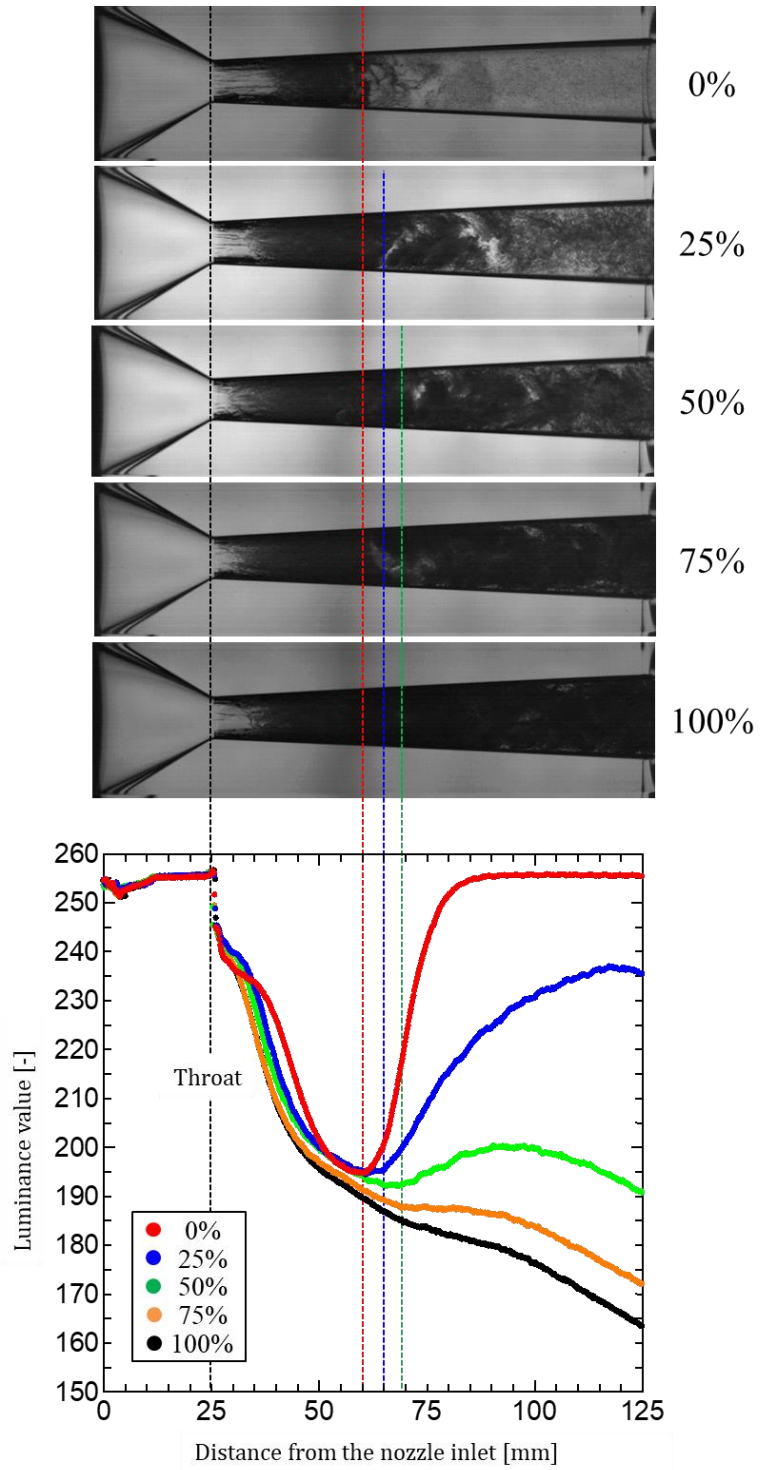


Figure A.4. Luminance value distribution when changing CO₂ partial pressure ratio.

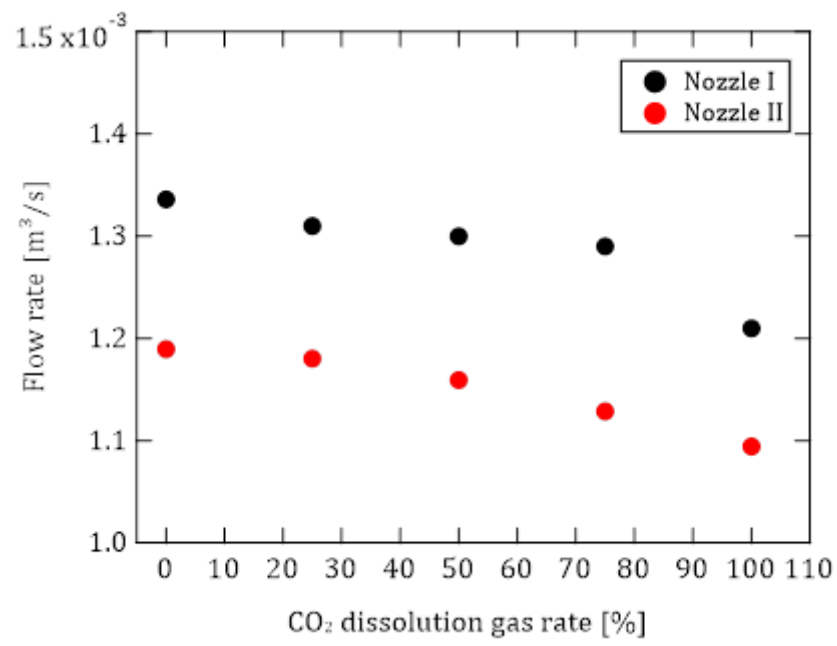


Figure A.5. Comparison of flow rate.



(1) $P_L=101$ kPa



(2) $P_L=61$ kPa

Figure A.6. Comparison of flow pattern with the same CO_2 0% of dissolution gas rate.



2-a CO_2 0%



2-b CO_2 25%



2-c CO_2 50%

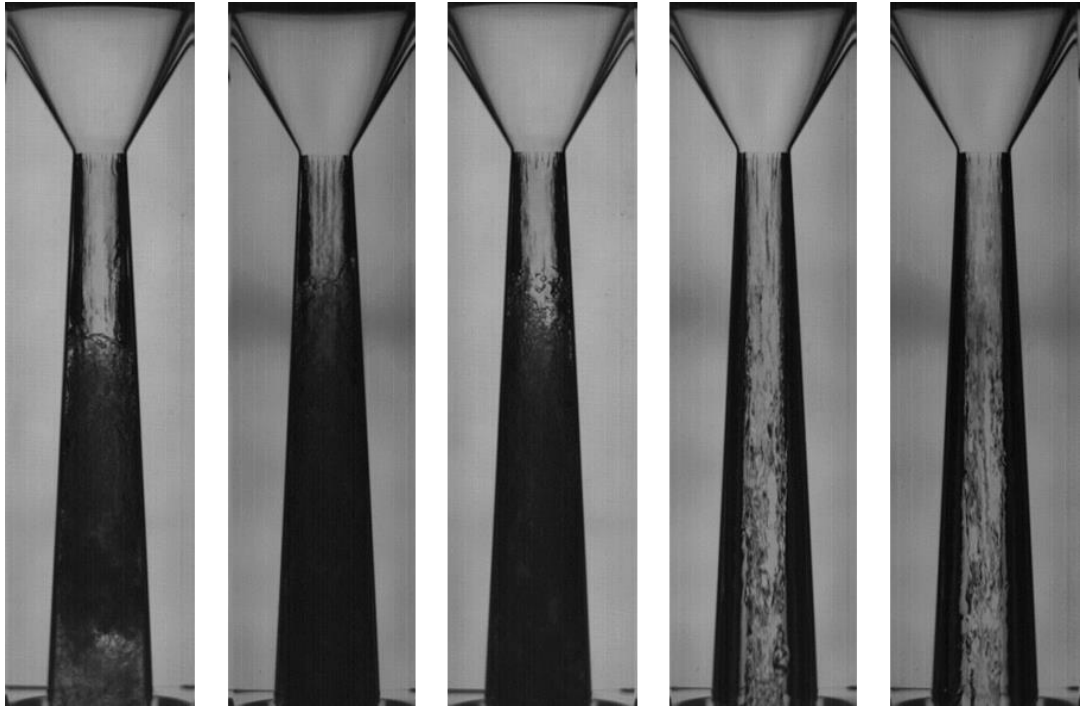


2-d CO_2 75%



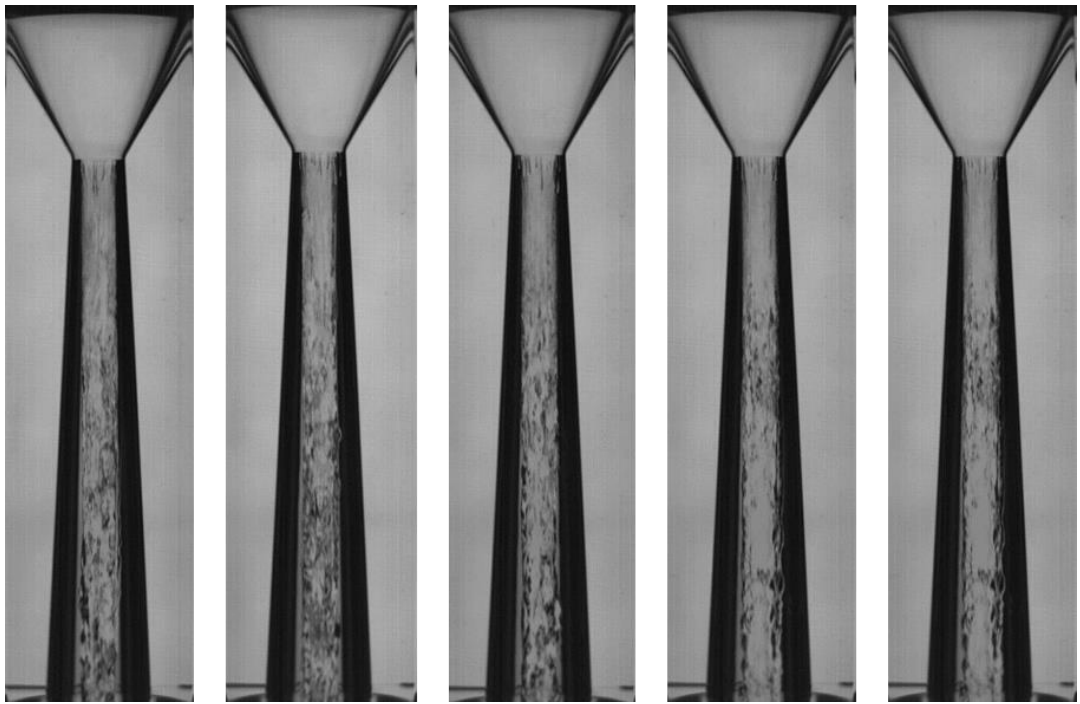
2-e CO_2 100%

Figure A.7. Flow pattern with changing rate of CO_2 ($P_L=61$ kPa).



3-a CO₂ 0% 3-b CO₂ 25% 3-c CO₂ 50% 3-d CO₂ 75% 3-e CO₂ 100%

Figure A.8. Flow pattern with changing rate of CO₂ ($P_L=51$ kPa).



4-a CO₂ 0% 4-b CO₂ 25% 4-c CO₂ 50% 4-d CO₂ 75% 4-e CO₂ 100%

Figure A.9. Flow pattern with changing rate of CO₂ ($P_L=21$ kPa).

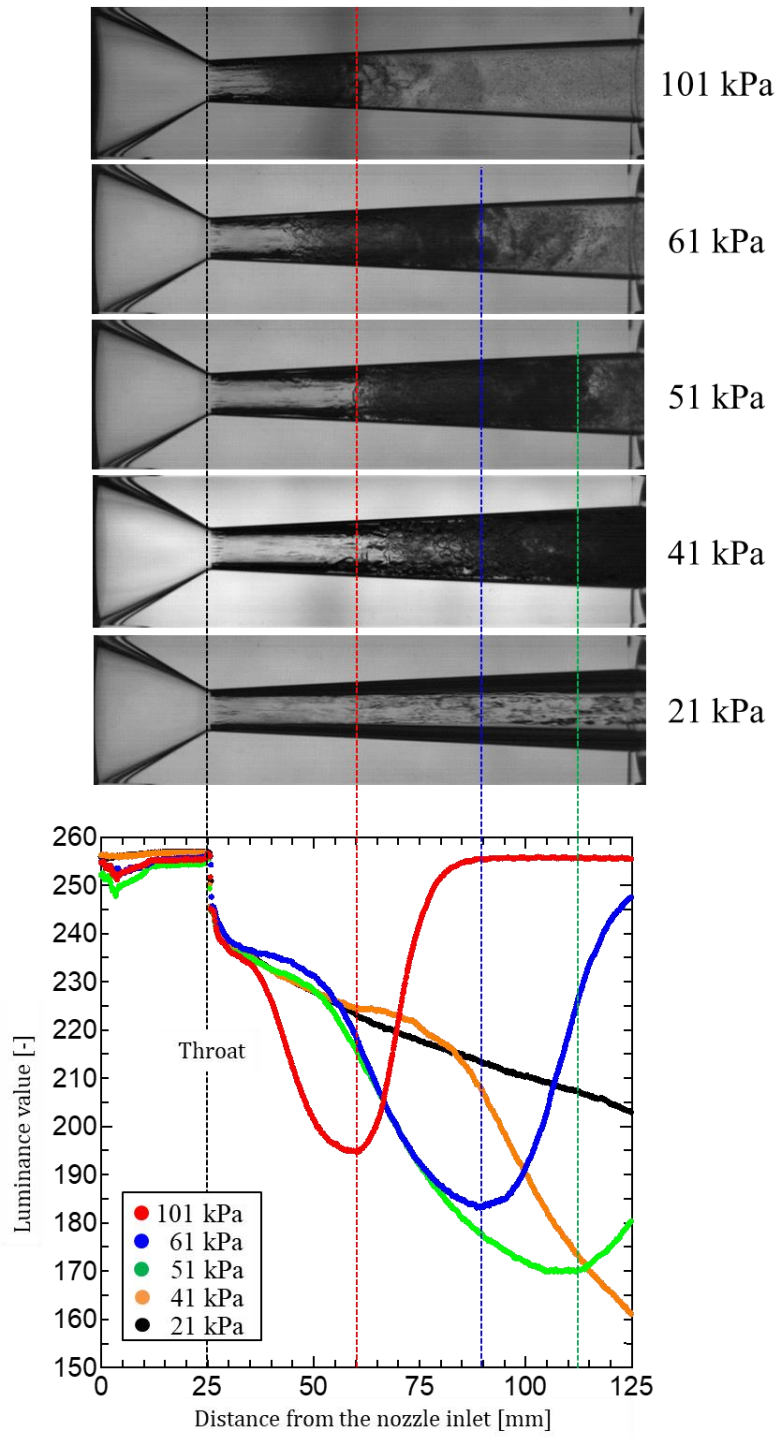


Figure A.10. Luminance value distribution with the lower tank pressure changing (CO₂ 0%)

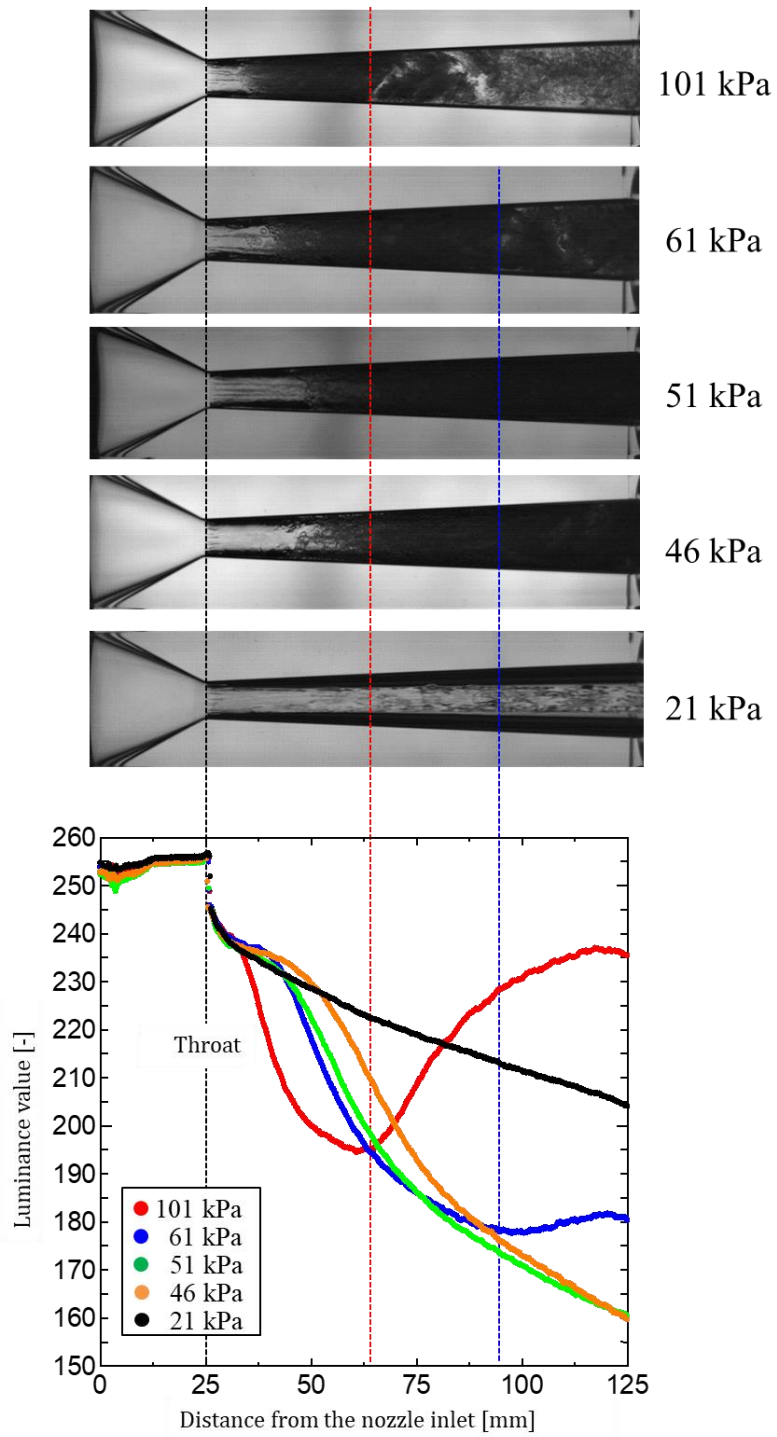


Figure A.11. Luminance value distribution with the lower tank pressure changing (CO₂ 25%)

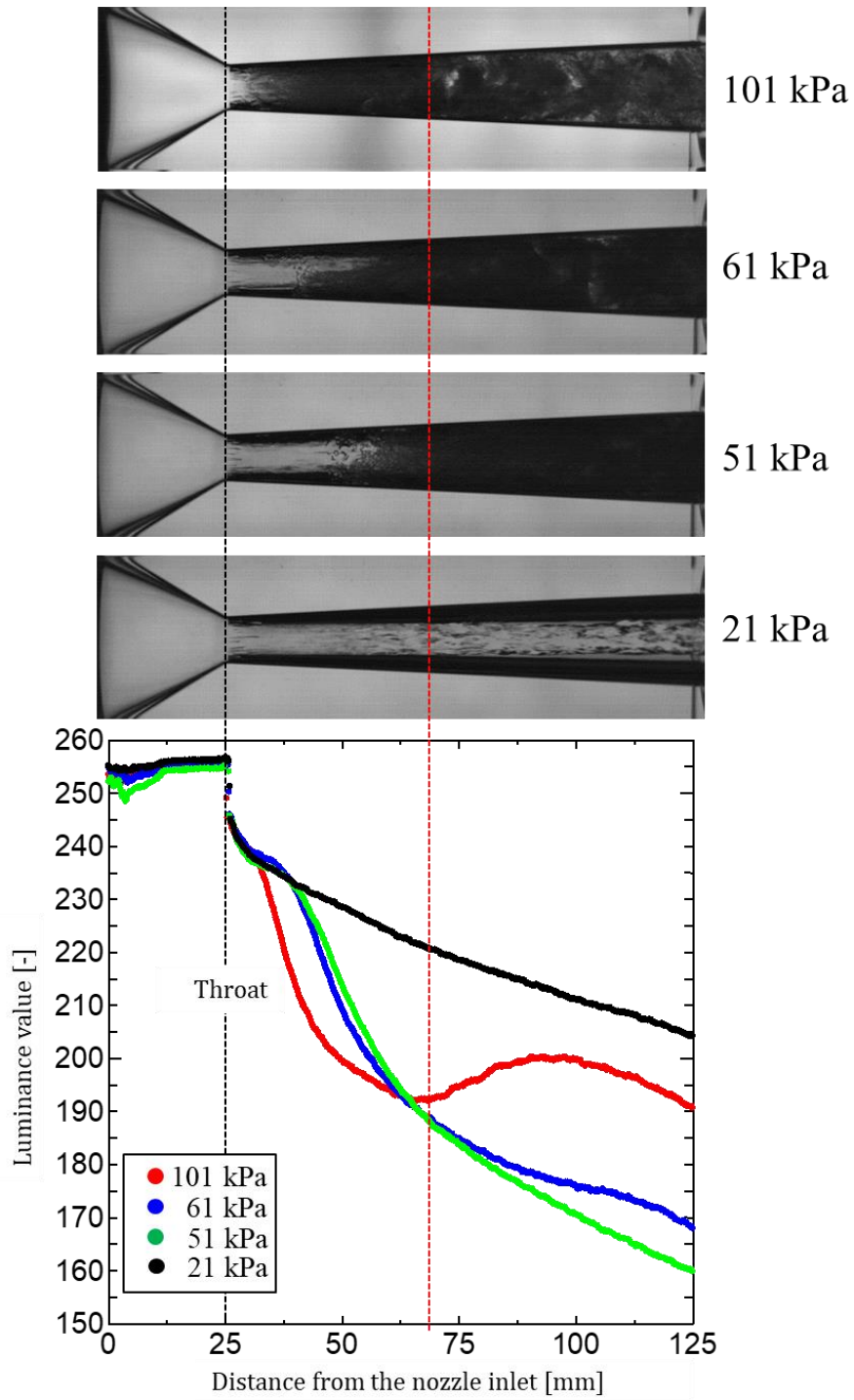


Figure A.12. Luminance value distribution with the lower tank pressure changing (CO₂ 50%)

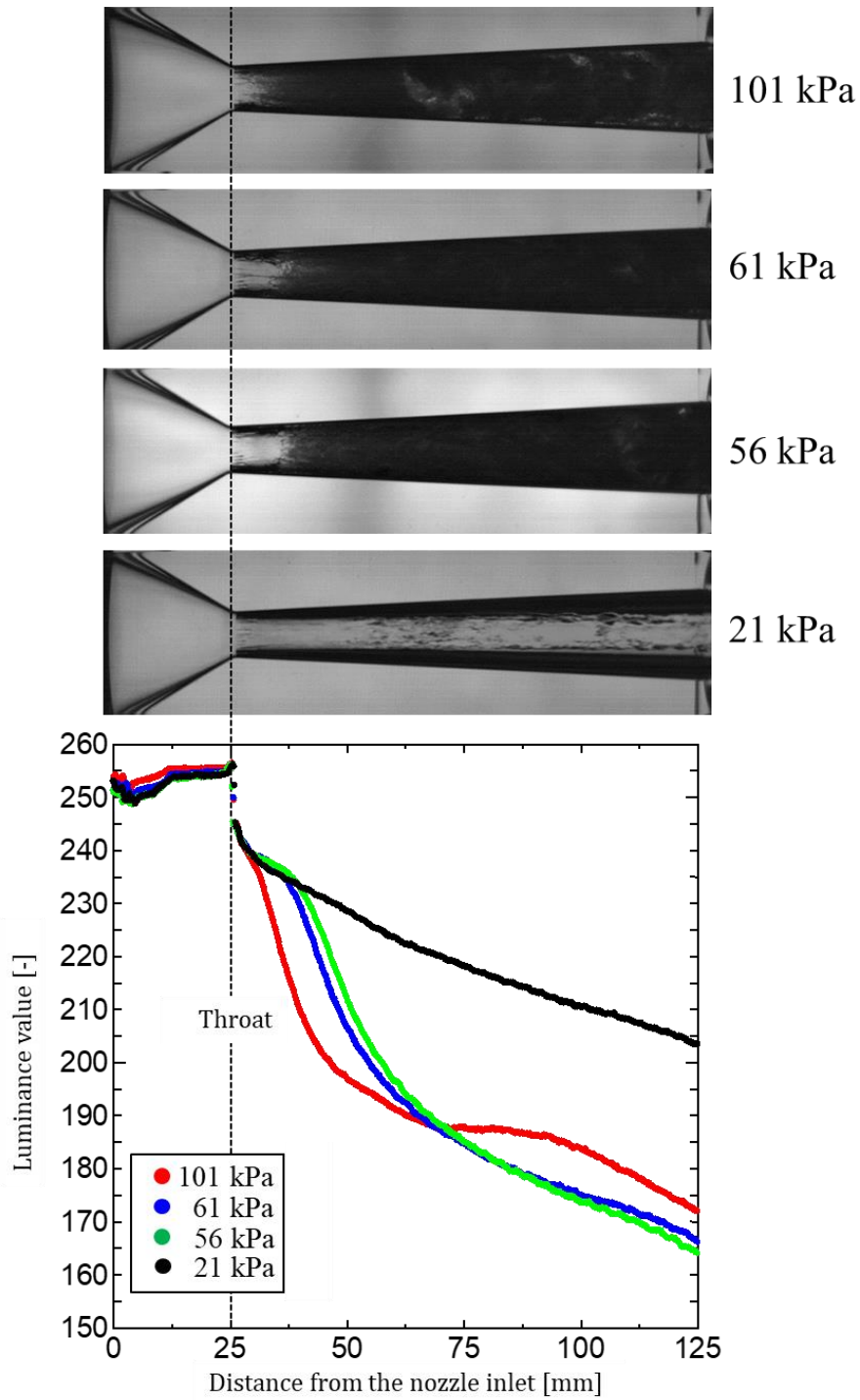


Figure A.13. Luminance value distribution with the lower tank pressure changing (CO₂ 75%)

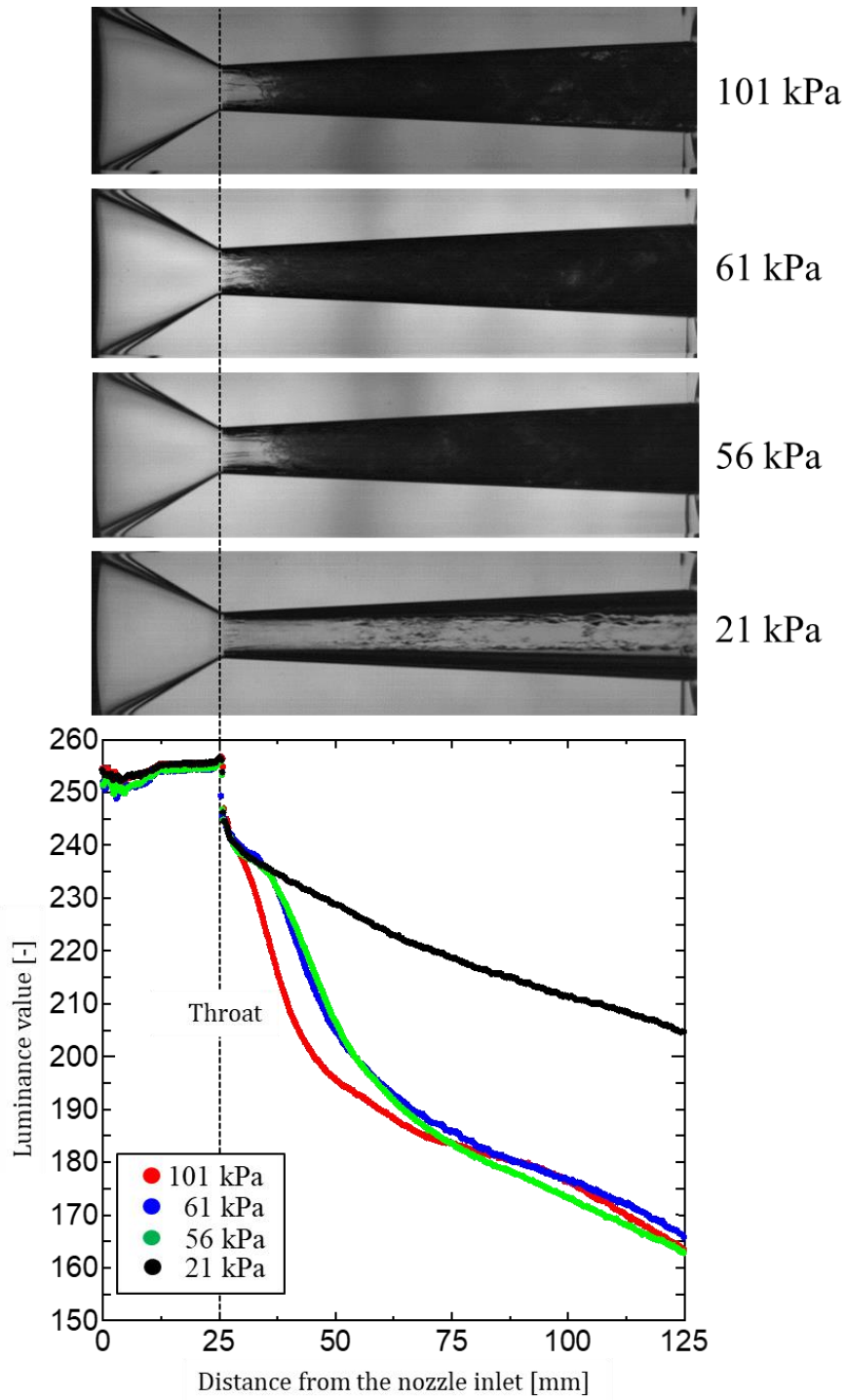


Figure A.14. Luminance value distribution with the lower tank pressure changing (CO_2 100%).

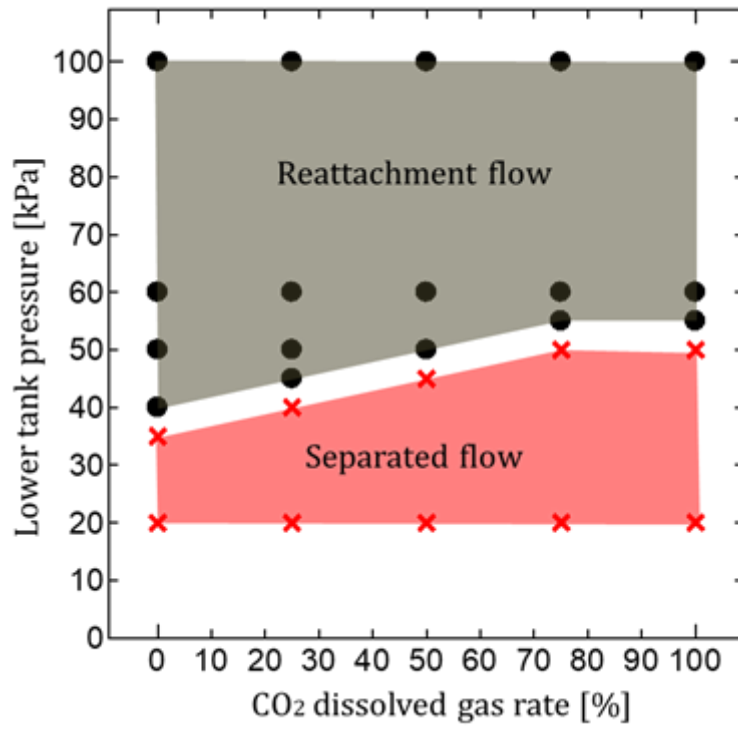
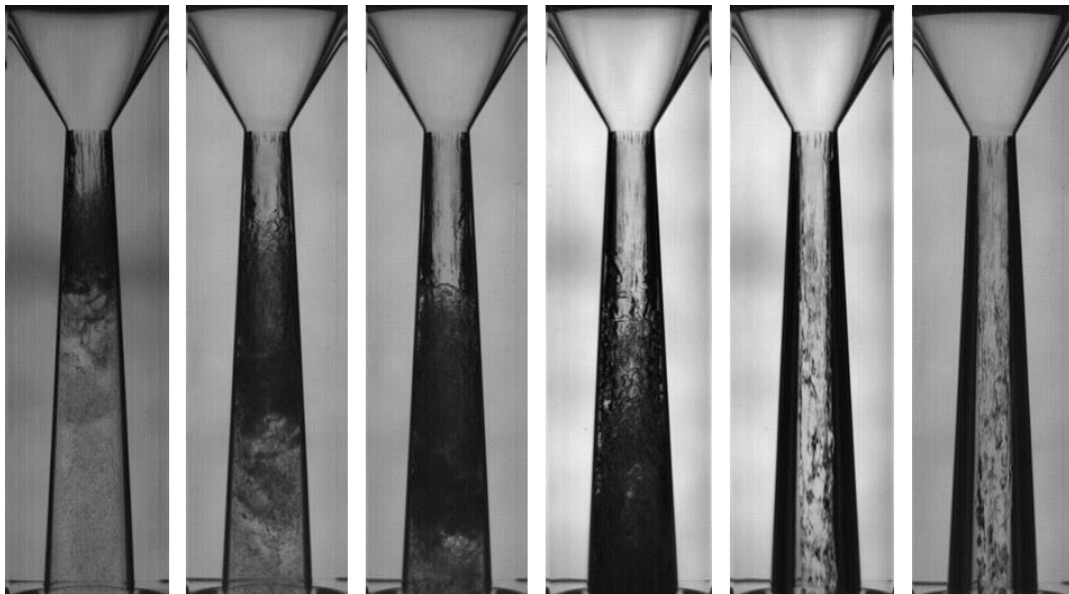
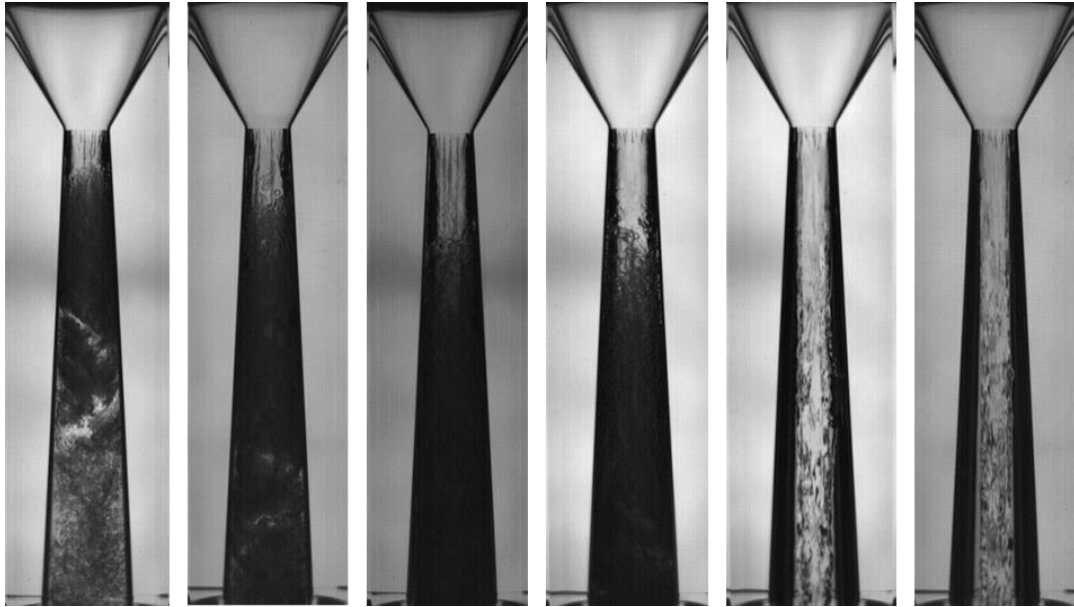


Figure A.15. Flow transition with changing the lower tank pressure and dissolved gas rate.



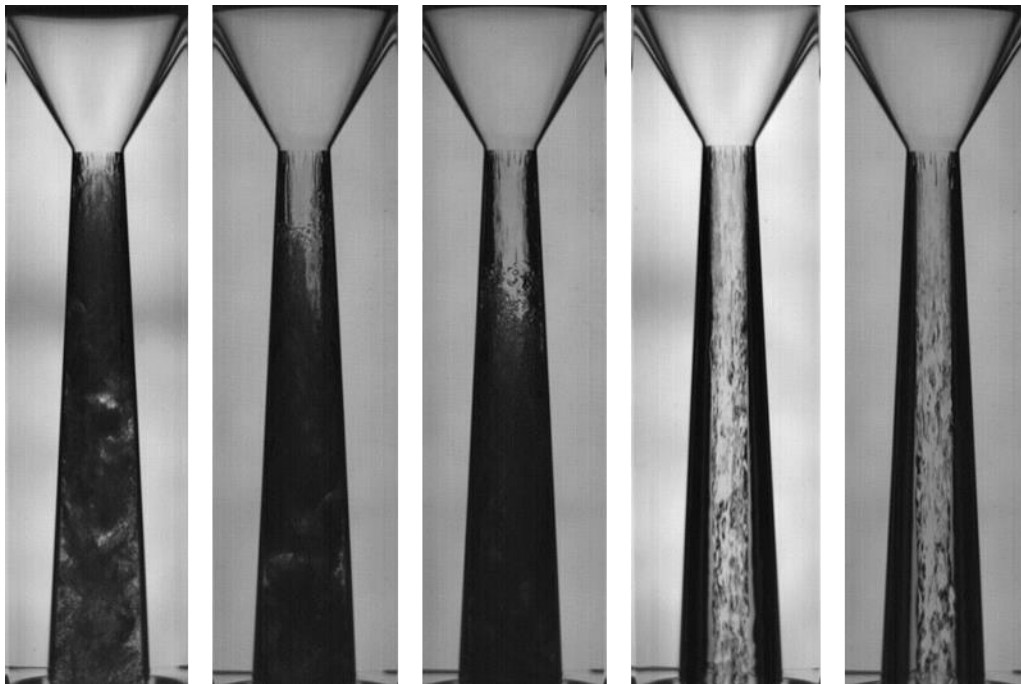
(1) 101 kPa (2) 61 kPa (3) 51 kPa (4) 41 kPa (5) 36 kPa (6) 21 kPa

Figure A.16. The flow pattern with lower tank pressure changing (CO₂ 0%).



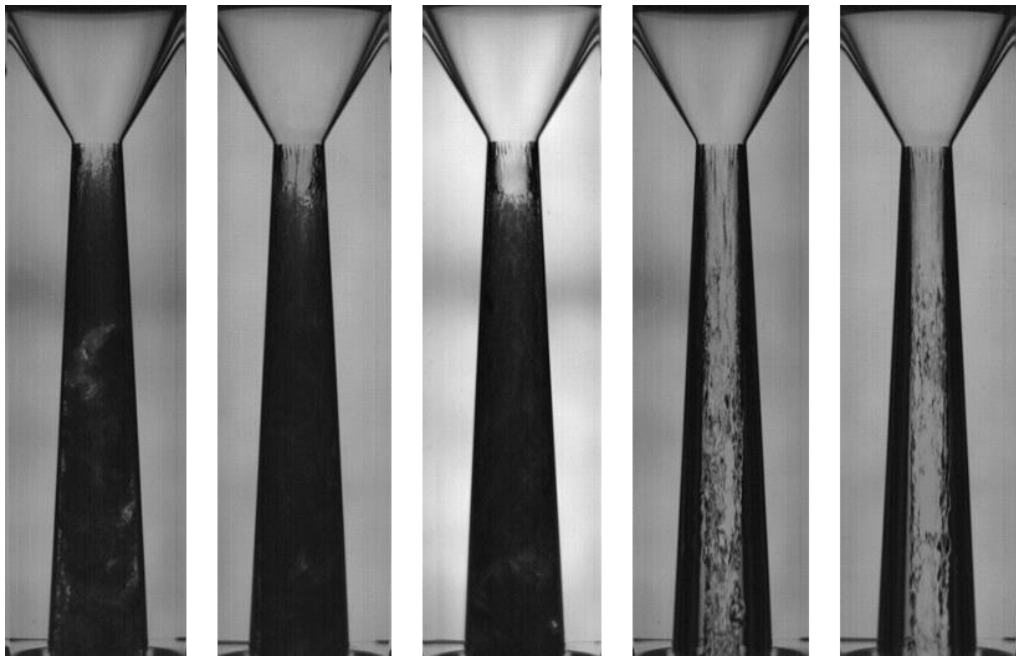
(1) 101 kPa (2) 61 kPa (3) 51 kPa (4) 41 kPa (5) 36 kPa (6) 21 kPa

Figure A.17. The flow pattern with lower tank pressure changing (CO₂ 25%).



(1) 101 kPa (2) 61 kPa (3) 51 kPa (4) 46 kPa (5) 21 kPa

Figure A.18. The flow pattern with lower tank pressure changing (CO₂ 50%).



(1) 101 kPa (2) 61 kPa (3) 51 kPa (4) 46 kPa (5) 21 kPa

Figure A.19. The flow pattern with lower tank pressure changing (CO₂ 75%).



(1) 101 kPa (2) 61 kPa (3) 51 kPa (4) 46 kPa (5) 21 kPa

Figure A.20. The flow pattern with lower tank pressure changing (CO₂ 100%).

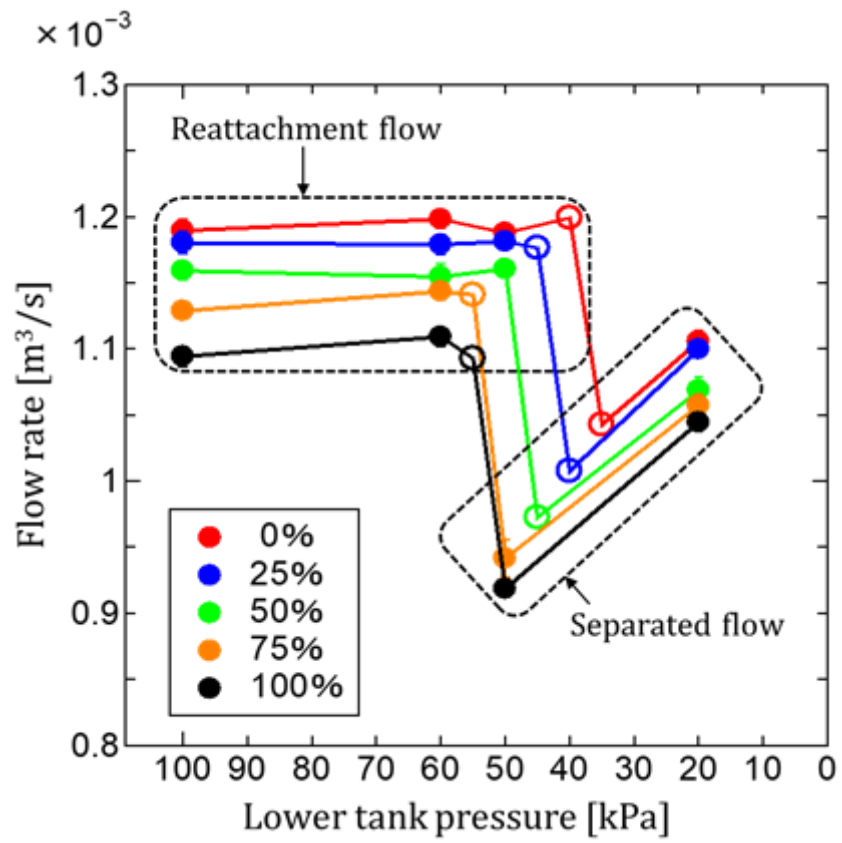


Figure A.21. The flow rate with lower tank pressure changing.

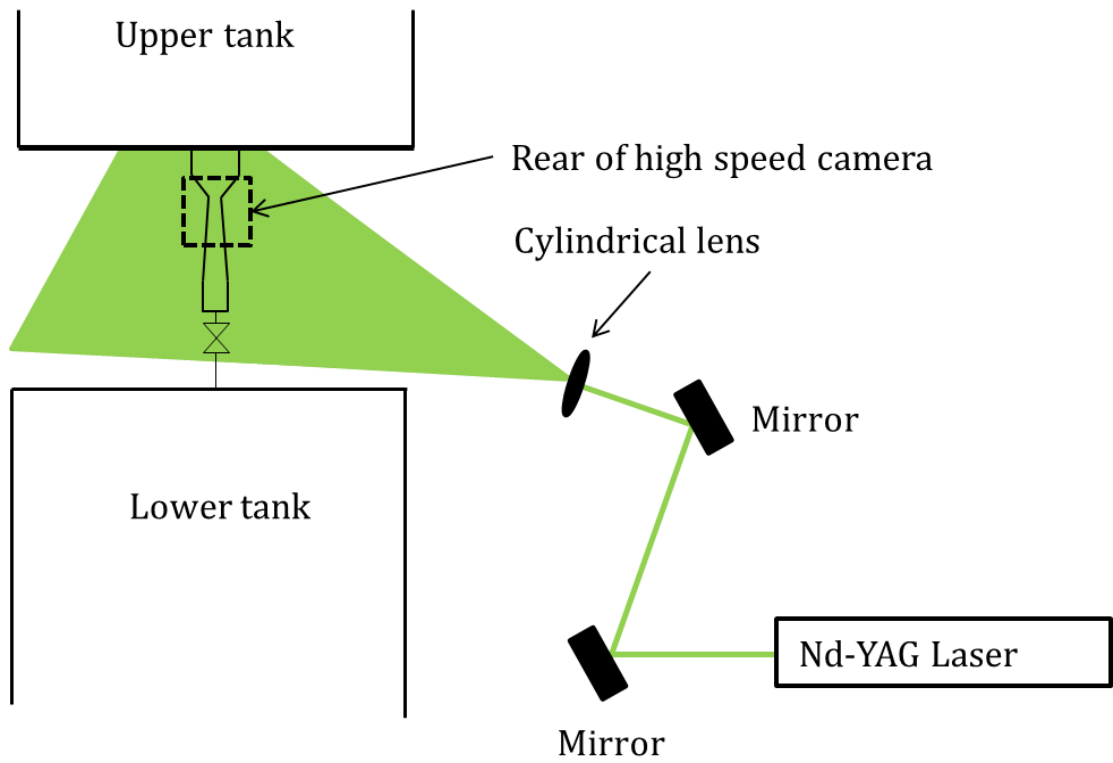


Figure A.22. Schematic depicting a typical PIV system.

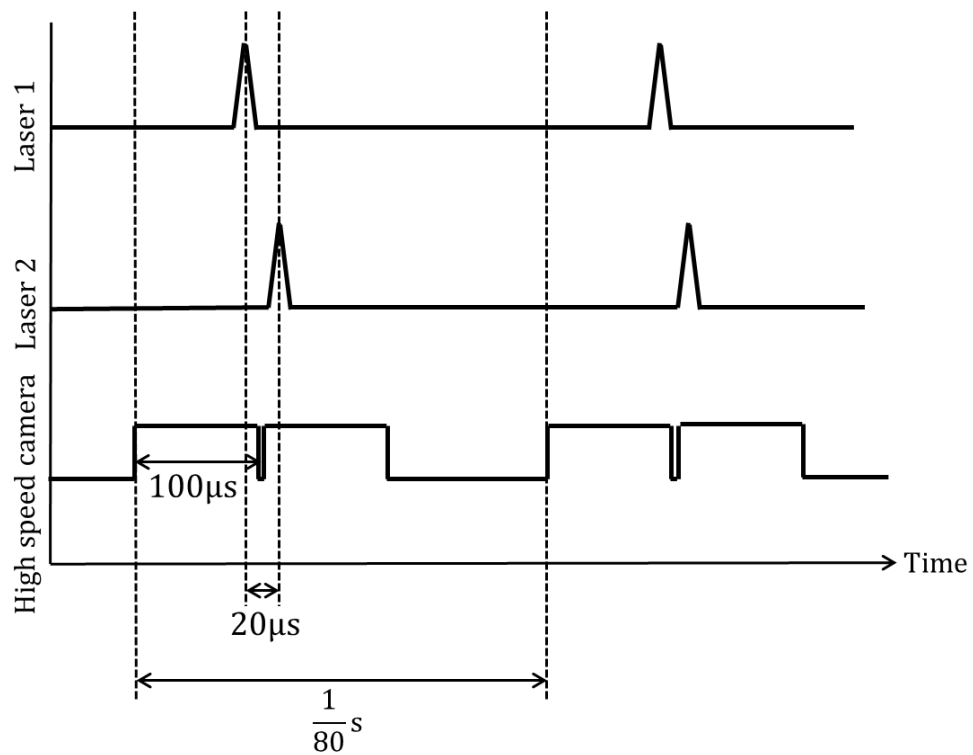


Figure A.23. Timing chart of PIV measurement.

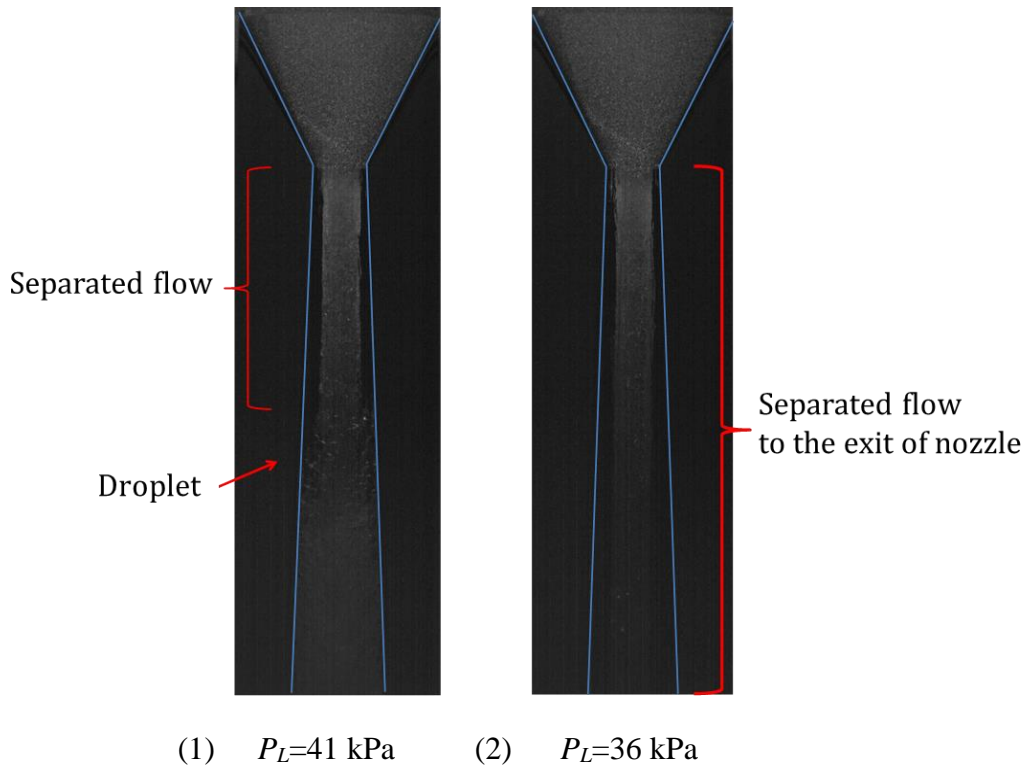


Figure A.24. The images taken by high speed camera.

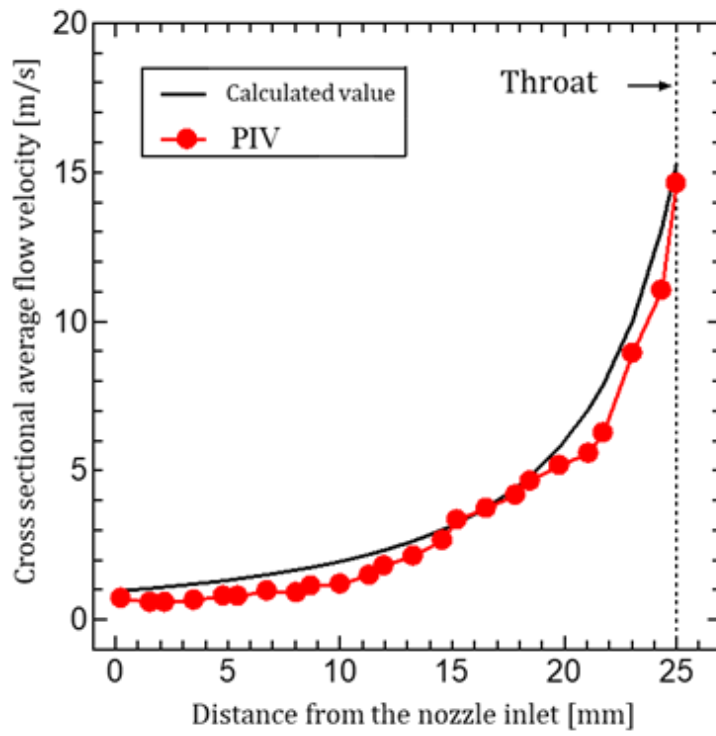


Figure A.25. Comparison of PIV and calculated result of flow velocity ($P_L=41$ kPa).

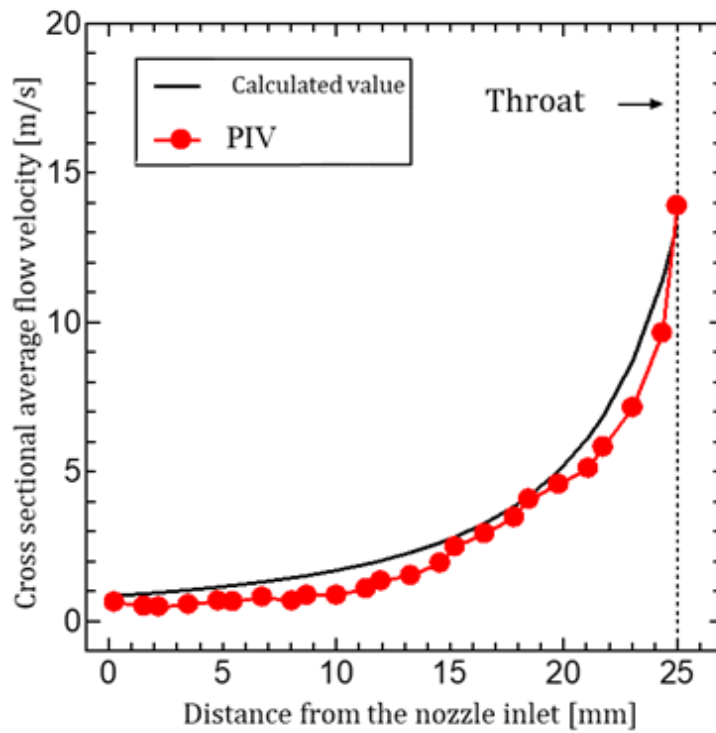


Figure A.26. Comparison of PIV and calculated result of flow velocity ($P_L=36$ kPa).

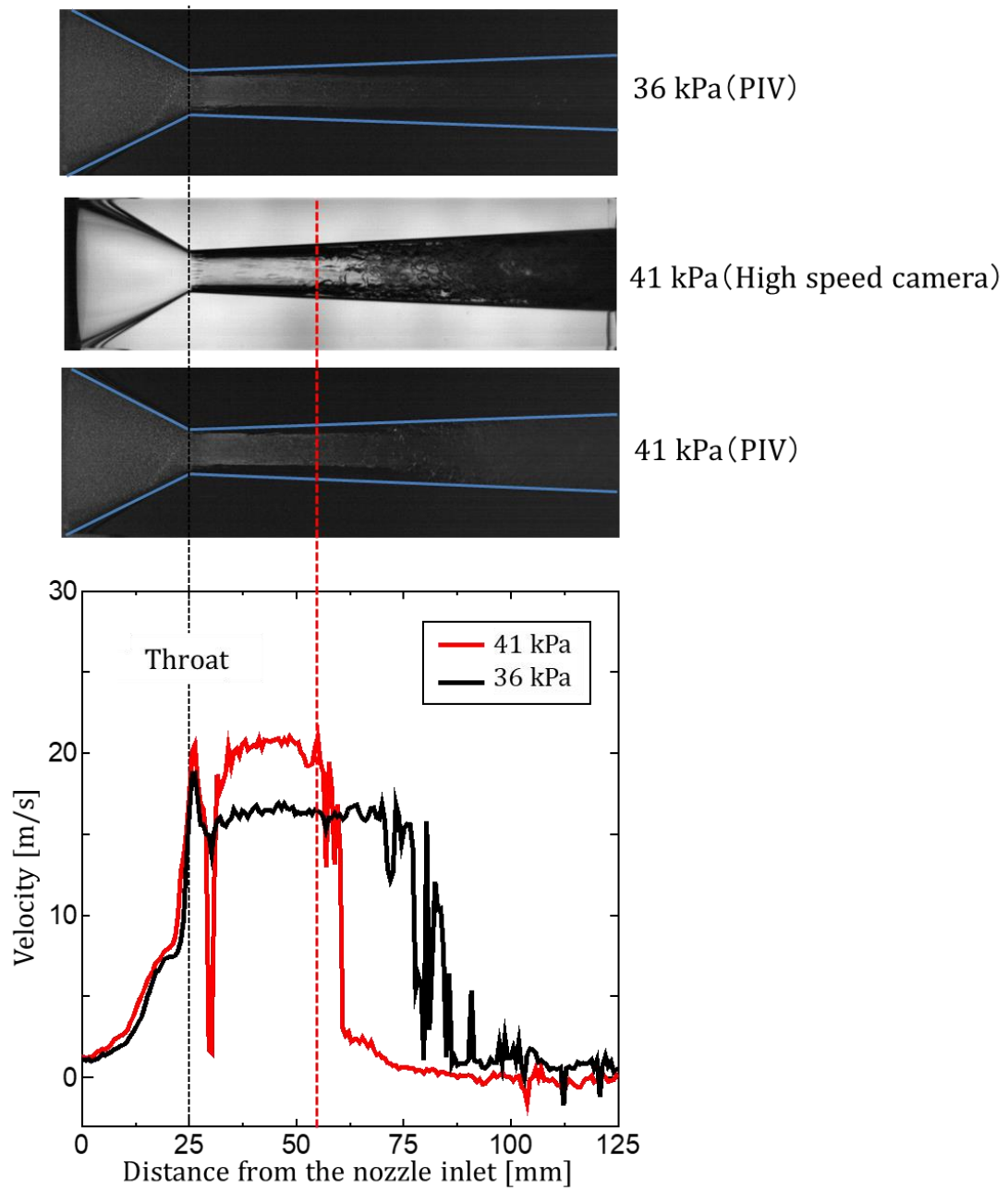


Figure A.27. Velocity result from PIV measurement.

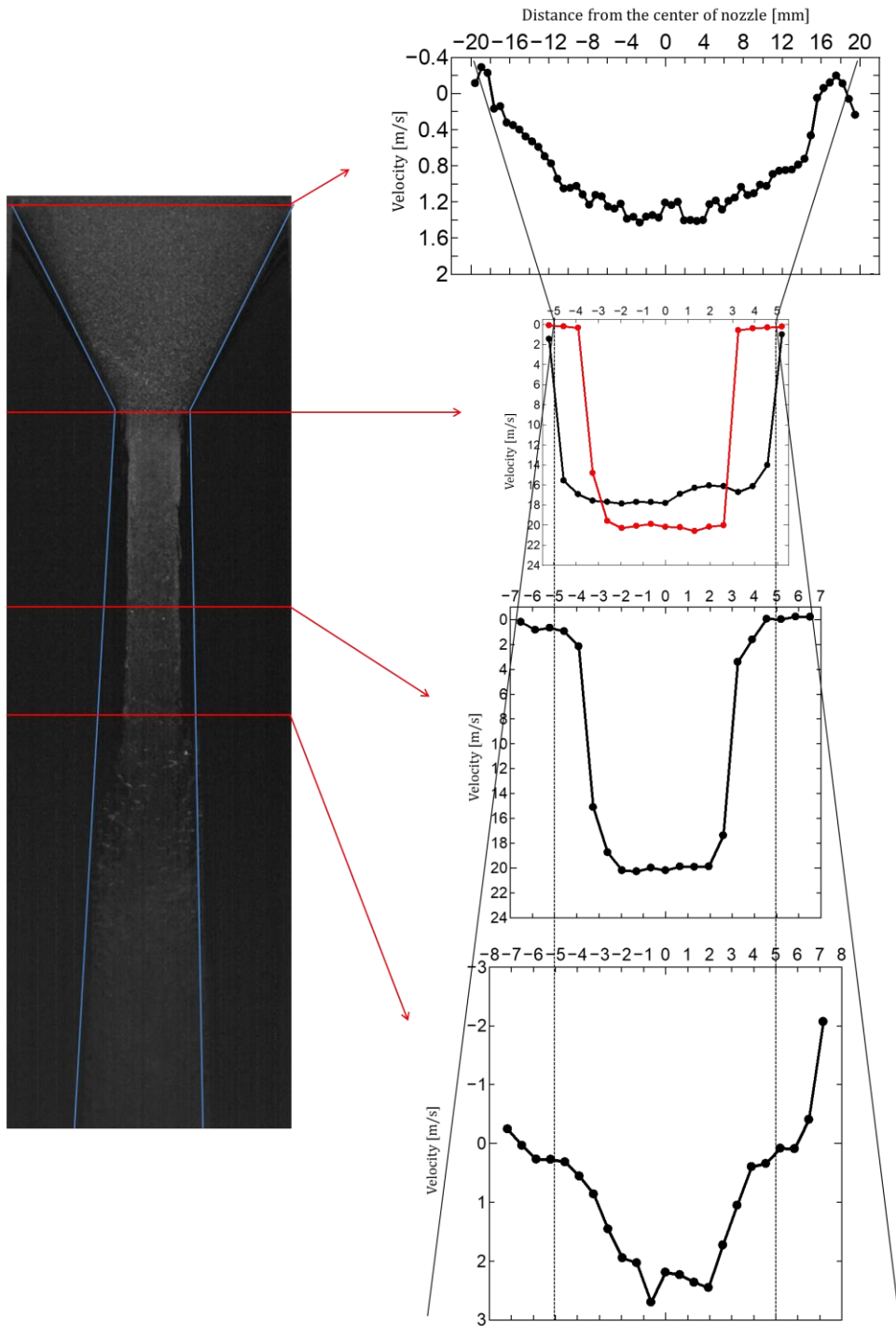


Figure A.28. Flow velocity distribution of the reattachment flow ($P_L=41$ kPa).

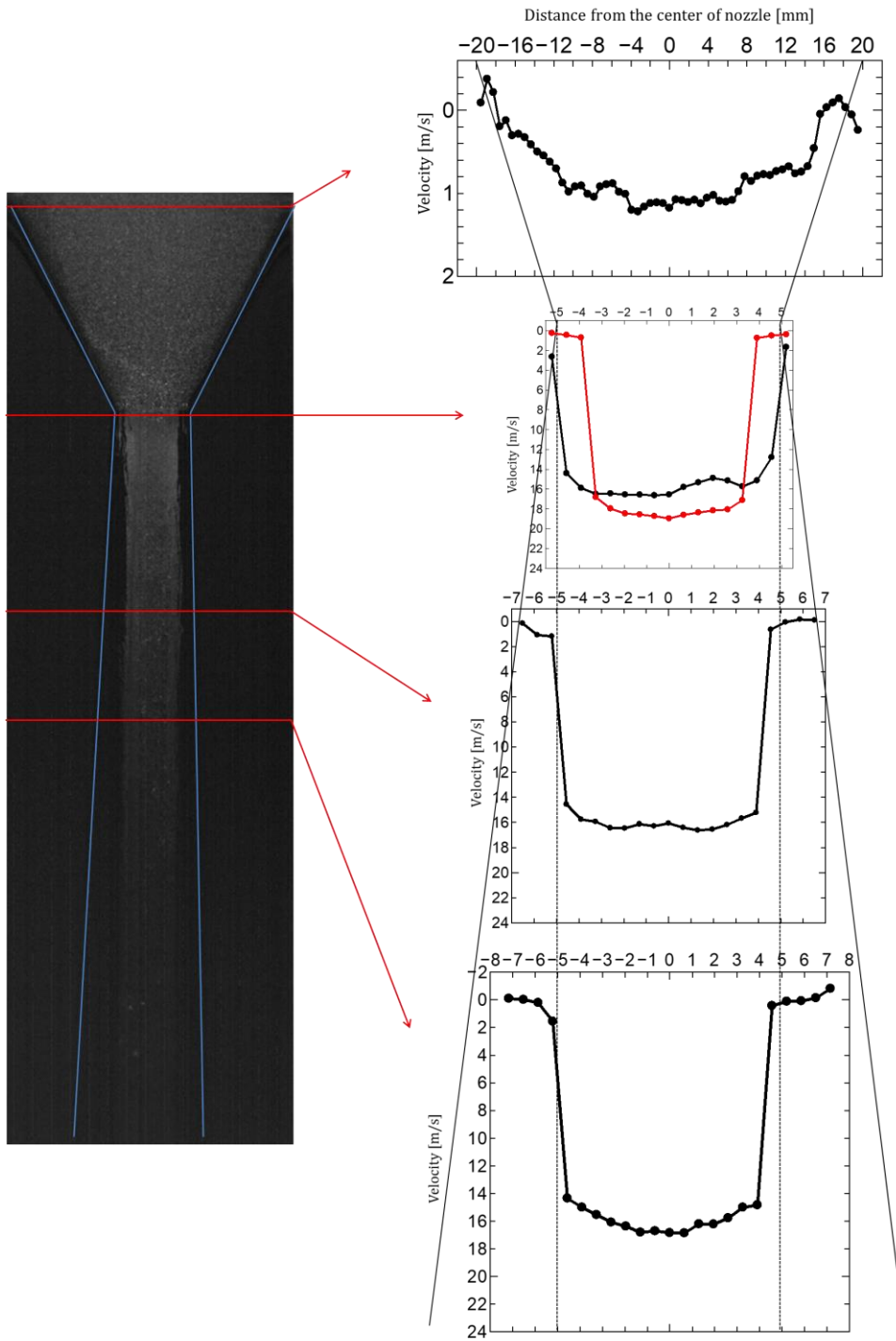


Figure A.29. Flow velocity distribution of the separated flow ($P_L=36$ kPa).

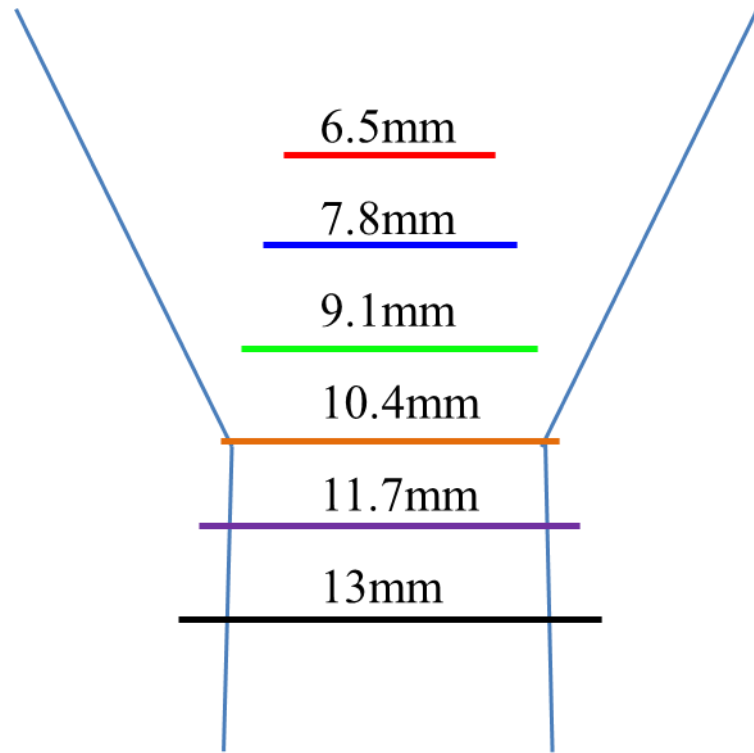


Figure A.30. Inspection of the cross sectional width of the flow measurement.

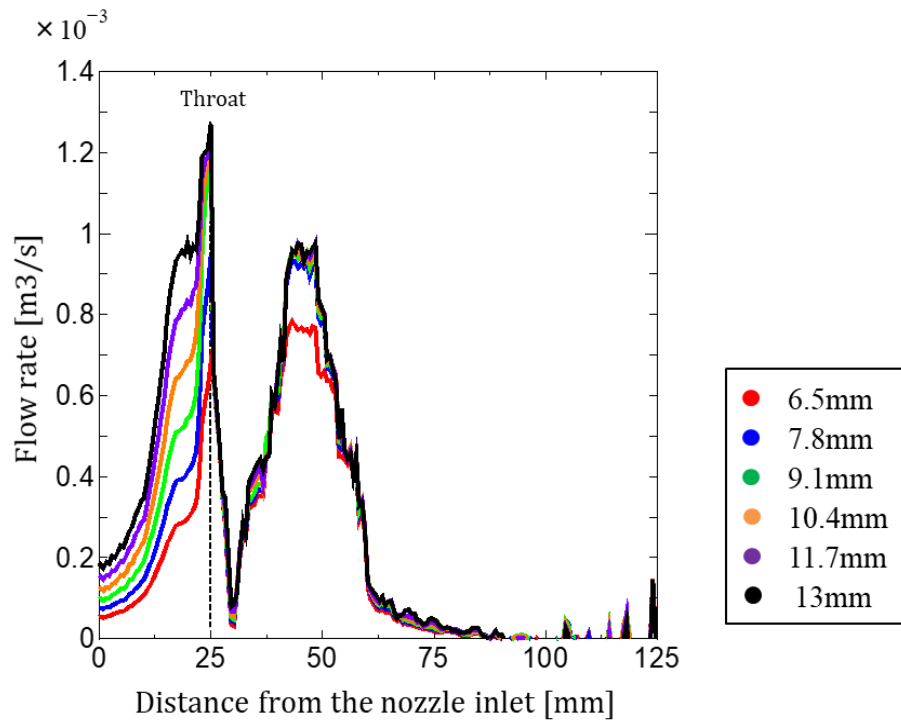


Figure A.31. Flow rate of reattachment flow ($P_L=41$ kPa).

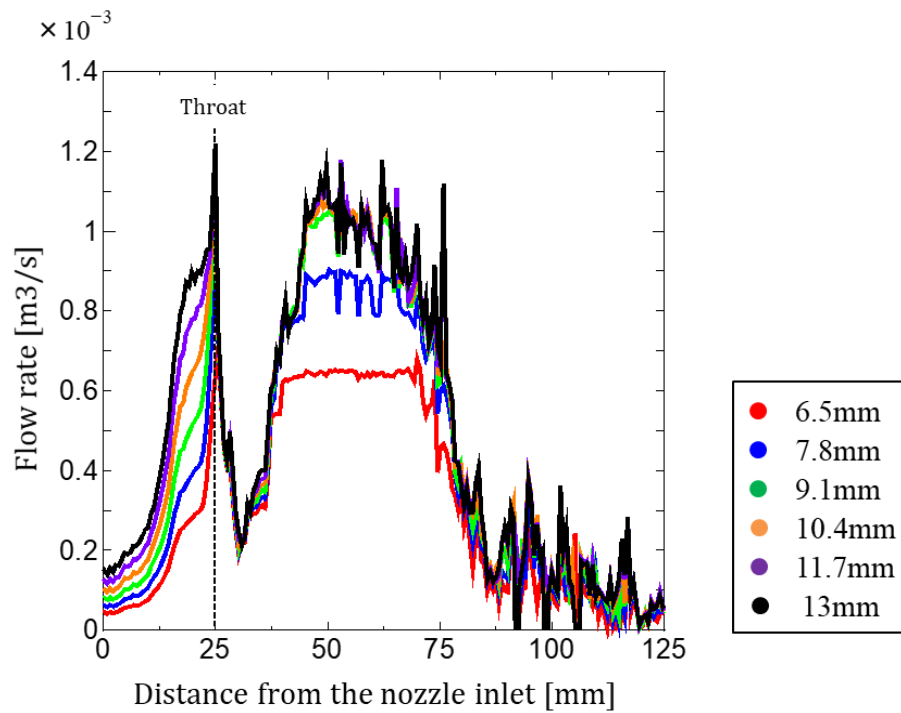


Figure A.32. Flow rate of reattachment flow ($P_L=36$ kPa).

APPENDIX B

PROGRAM FOR EXPERIMENTAL PRESSURE CALCULATION

```
Sub TO_PRESSURE(UPA As Double, UPB As Double, DNA As Double, DNB As  
Double, NZA As Double, NZB As Double)
```

```
    Dim MaxRow As Long
```

```
    Dim MaxCol As Long
```

```
    Dim GAIN As Double
```

```
    Dim AWBN As String
```

```
'
```

```
    Range("A:A").Find(What:="#BeginMark").Select
```

```
    Range(ActiveCell.Address(True, True, xlA1), Cells(Rows.Count, 1).End(xlUp)).EntireRow.Delete
```

```
    Range("A:A").Find(What:="#EndHeader").Select
```

```
    Range("A1", ActiveCell.Address(True, True, xlA1)).EntireRow.Delete
```

```
    MaxRow = Cells(Rows.Count, 1).End(xlUp).Row
```

```
    MaxCol = Cells(1, Columns.Count).End(xlToLeft).Column
```

```
'
```

```
' Select F1
```

```
    Range("F1").Select
```

```
' Time(s) = Time(us)/1000000
```

```
    ActiveCell.FormulaR1C1 = "=(ROW()-2) * 0.0005"
```

```
' End PMS-5M-2 500K
```

```
    Range("F1").Select
```

```
    Selection.AutoFill Destination:=Range(Cells(1, 6), Cells(MaxRow, 6))
```

```
' Select G1
```

```
    Range("G1").Select
```

```

' KEYENCE AP43: Upper Tank
  ActiveCell.FormulaR1C1 = "=" & (RC[-4] & "-" & UPB & " & " & UPA
' End AP43
  Range("G1").Select
  Selection.AutoFill Destination:=Range(Cells(1, 7), Cells(MaxRow, 7))
' Select H1
  Range("H1").Select
' KEYENCE AP44: Lower Tank
  ActiveCell.FormulaR1C1 = "=" & (RC[-4] & "-" & DNB & " & " & DNA
' End AP44
  Range("H1").Select
  Selection.AutoFill Destination:=Range(Cells(1, 8), Cells(MaxRow, 8))
' Select I1
  Range("I1").Select
' JTEKT PMS-5M-2 500K: Nozzle
  ActiveCell.FormulaR1C1 = "=" & (RC[-4] & "-" & NZB & " & " & NZA
' End PMS-5M-2 500K
  Range("I1").Select
  Selection.AutoFill Destination:=Range(Cells(1, 9), Cells(MaxRow, 9))
' Insert Row Title
  Range("A1").Select
  Selection.EntireRow.Insert
  Range("A1").Value = "DATE"
  Range("B1").Value = "TIME(_S)"
  Range("C1").Value = "U (V)"

```

```
Range("D1").Value = "B (V)"
```

```
Range("E1").Value = "N (V)"
```

```
Range("F1").Value = "Time(S)"
```

```
Range("G1").Value = "Upper tank (kPa)"
```

```
Range("H1").Value = "Lower tank(kPa)"
```

```
Range("I1").Value = "Nozzle (kPa)"
```

```
AWBN = Left(ActiveWorkbook.Name, InStrRev(ActiveWorkbook.Name, ".") -
```

```
1)
```

```
fileToClose = AWBN + "-P.csv"
```

```
ActiveWorkbook.SaveAs fileToClose
```

```
ActiveWorkbook.Close SaveChanges:=False
```

```
End Sub
```

```
Sub Average(AveC As Double, AveD As Double, AveE As Double)
```

```
Dim lngLine As Long
```

```
Range("A:A").Find(What:="#BeginMark").Select
```

```
Range(ActiveCell.Address(True, True, xlA1), Cells(Rows.Count, 1).End(xlUp)).EntireRow.Delete
```

```
Range("A:A").Find(What:="#EndHeader").Select
```

```
Range("A1", ActiveCell.Address(True, True, xlA1)).EntireRow.Delete
```

```
lngAve = 0
```

```
lngLine = Range("C1").End(xlDown).Row
```

```
AveC = WorksheetFunction.Average( _ Range("C1:C" & lngLine) _)
```

```

AveD = WorksheetFunction.Average( _
    Range("D1:D" & lngLine) _
)

AveE = WorksheetFunction.Average( _
    Range("E1:E" & lngLine) _
)

MsgBox "Up average = " & AveC & " (V)" & vbCrLf & "Dn average = " &
AveD & " (V)" & vbCrLf & "Nz average = " & AveE & " (V)" & vbCrLf & " " &
vbCrLf & "Total Line Number =" & lngLine

End Sub

Sub CONVERT()

    Dim AveC0 As Double, AveC90 As Double
    Dim AveD0 As Double, AveD90 As Double
    Dim AveE0 As Double, AveE90 As Double
    Dim AC As Double, BC As Double
    Dim AD As Double, BD As Double
    Dim AE As Double, BE As Double
    Dim UPA As Double, UPB As Double
    Dim DNA As Double, DNB As Double
    Dim NZA As Double, NZB As Double
    Dim vntFileName As String
    Dim FileName As String

```

MsgBox "Choose Data File at 0 kPa."

vntFileName = Application.GetOpenFilename()

Workbooks.Open vntFileName

Call Average(AveC0, AveD0, AveE0)

Application.DisplayAlerts = False

Workbooks(2).Close

Application.DisplayAlerts = True

MsgBox "Choose Data File at 90 kPa."

vntFileName = Application.GetOpenFilename()

Workbooks.Open vntFileName

Call Average(AveC90, AveD90, AveE90)

Application.DisplayAlerts = False

Workbooks(2).Close

Application.DisplayAlerts = True

UPA = 90# / (AveC90 - AveC0)

UPB = AveC0

DNA = 90# / (AveD90 - AveD0)

DNB = AveD0

NZA = 90# / (AveE90 - AveE0)

NZB = AveE0

MsgBox " A_Up = " & UPA & vbCrLf & " B_Up = " & UPB & vbCrLf & _


```
        " A_Dn = " & DNA & vbCrLf & " B_Dn = " & DNB &  
vbCrLf & _
```

```
        " A_Nz = " & NZA & vbCrLf & " B_Nz = " & NZB
```

```
,
```

```
    MsgBox "Choose Target Data File."
```

```
        vntFileName = Application.GetOpenFilename()
```

```
        Workbooks.Open vntFileName
```

```
    Call TO_PRESSURE(UPA, UPB, DNA, DNB, NZA, NZB)
```

```
,
```

```
End Sub
```

```
Sub CONVERTWITHTYPICALCOEFF()
```

```
    Dim UPA As Double, UPB As Double
```

```
    Dim DNA As Double, DNB As Double
```

```
    Dim NZA As Double, NZB As Double
```

```
,
```

```
    UPA = 250#
```

```
    UPB = 1#
```

```
    DNA = 50.65
```

```
    DNB = 3#
```

```
    NZA = 34.9143
```

```
    NZB = 0#
```

```
,
```

```
    Call TO_PRESSURE(UPA, UPB, DNA, DNB, NZA, NZB)
```

```
End Sub
```

APPENDIX C
EXPERIMENTAL EQUIPMENT DESIGN DOCUMENT

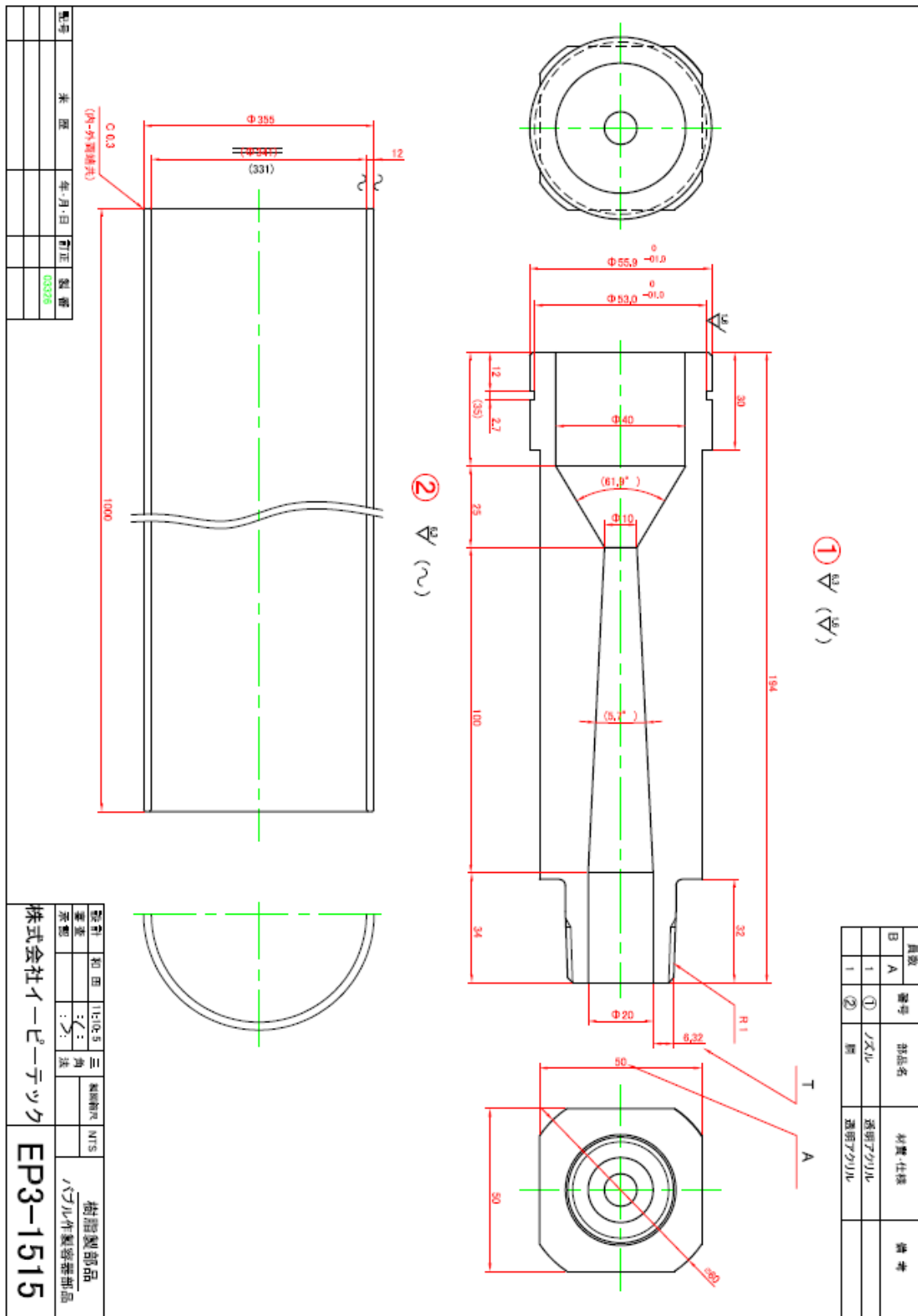


Figure C.1. Acrylic main nozzle.

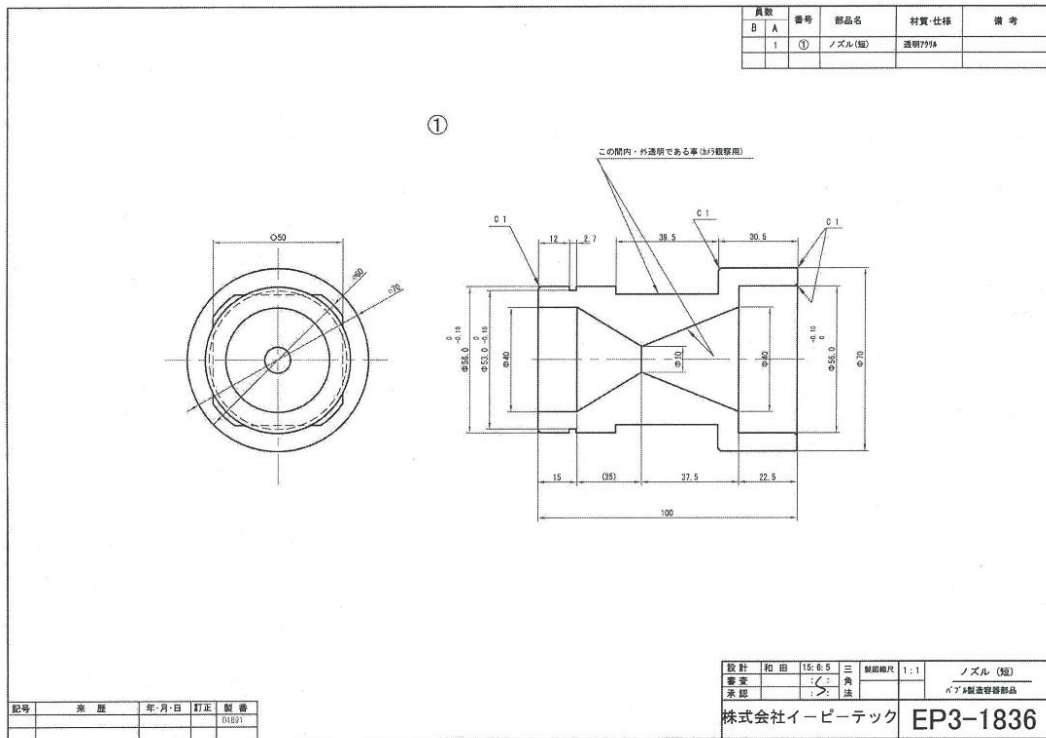


Figure C.3. Acrylic front nozzle.

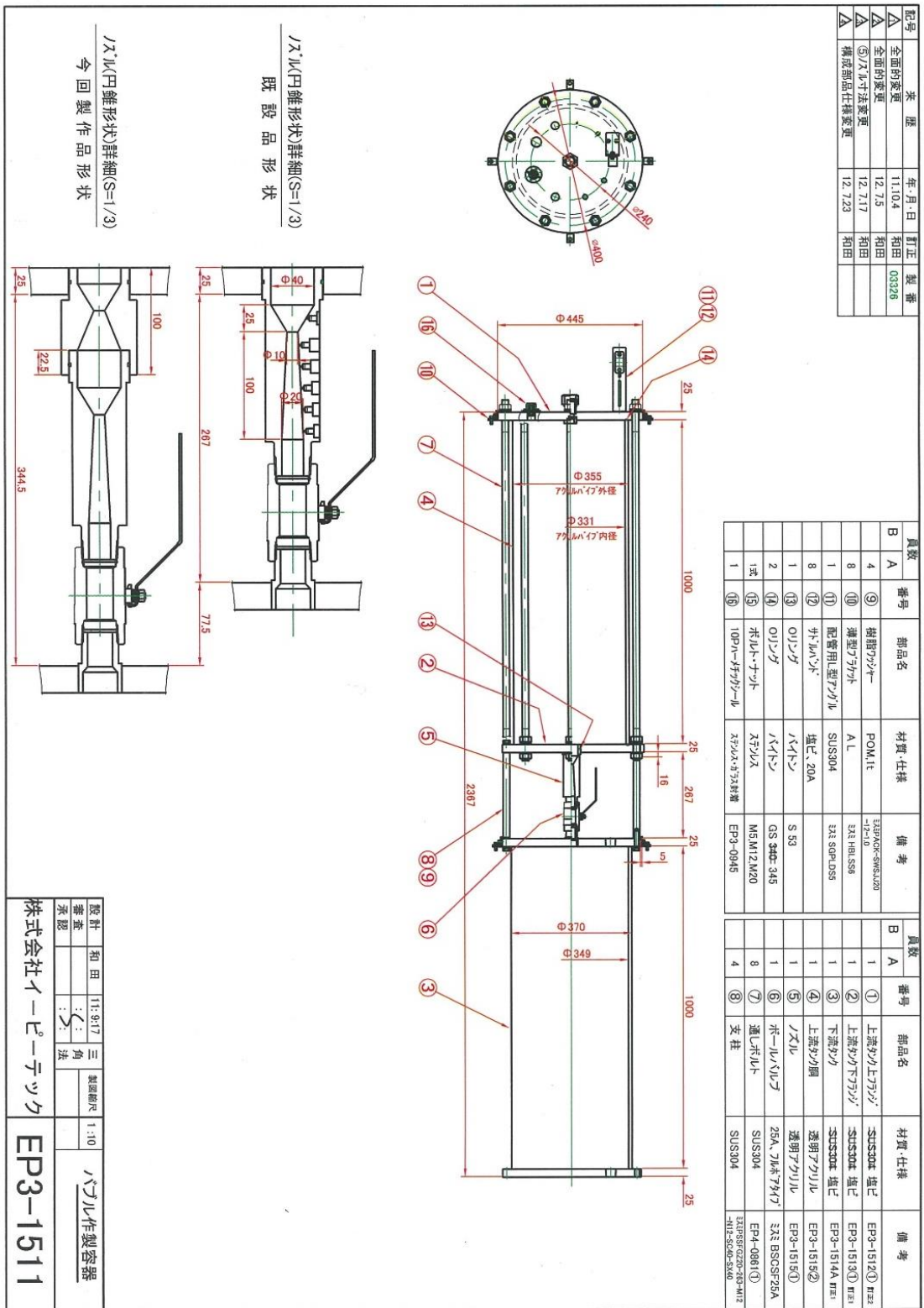


Figure C.4. Connecting two nozzle.

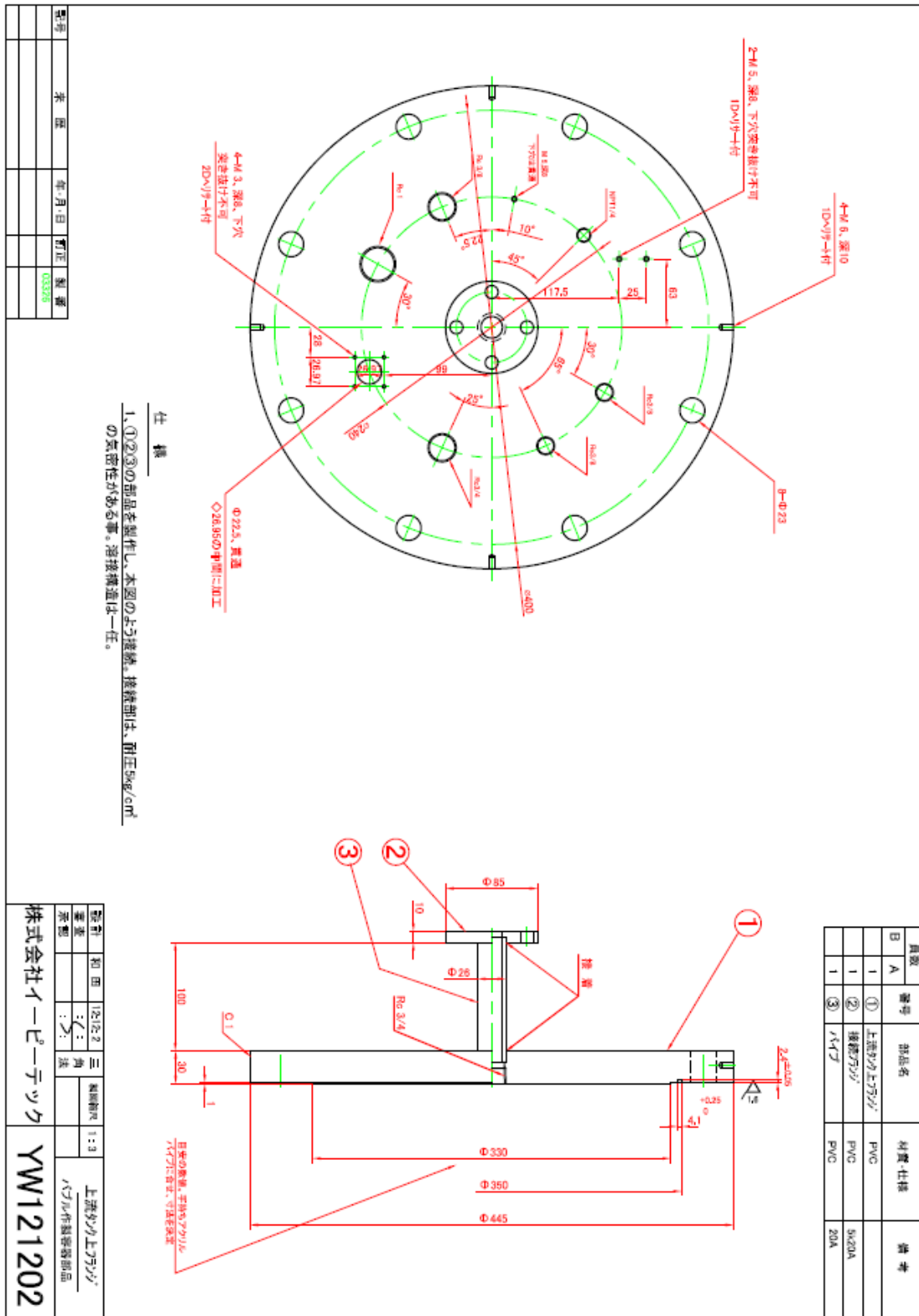


Figure C.5. The cover of the upper tank.

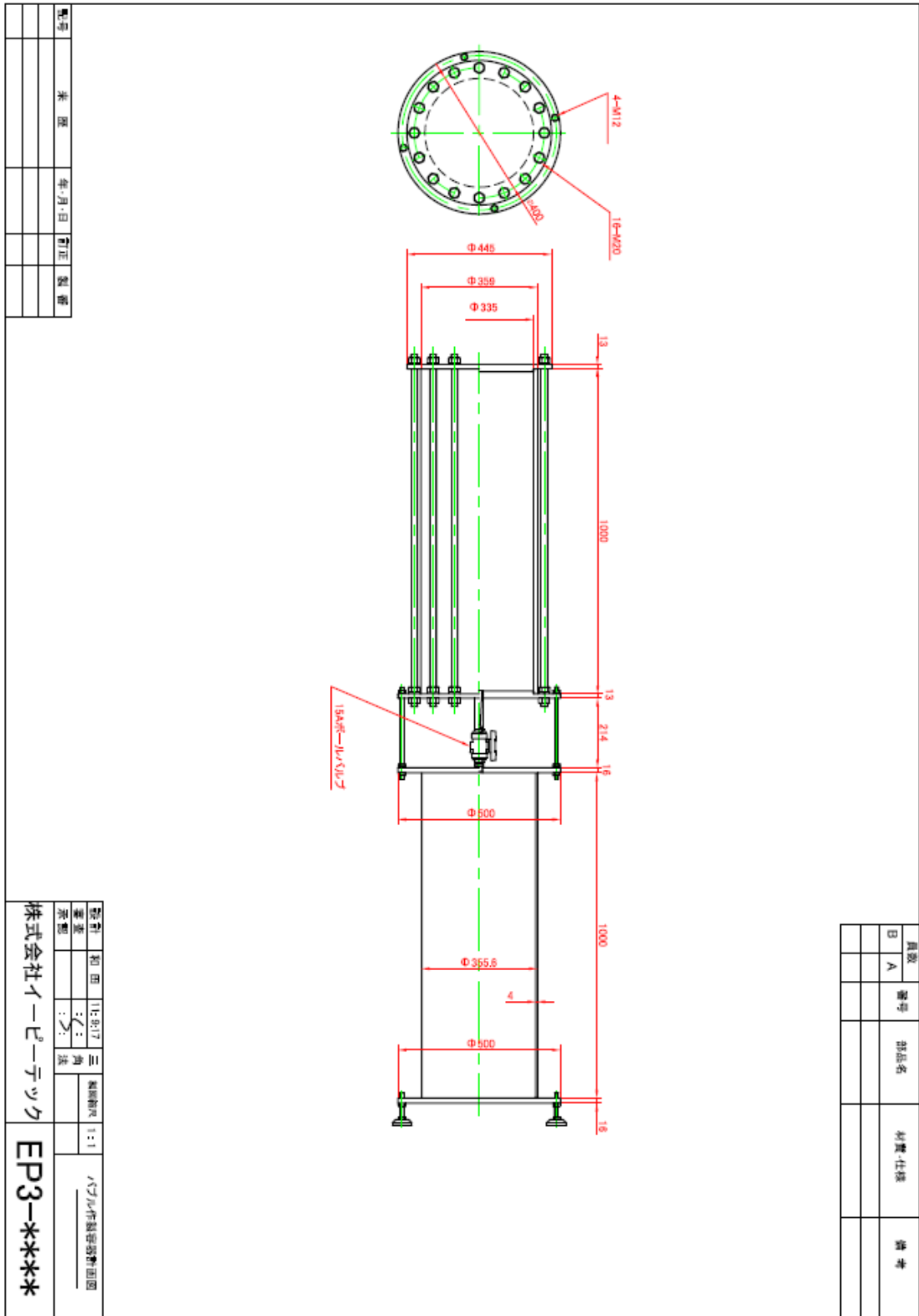


Figure C.6. Upper and lower tank.

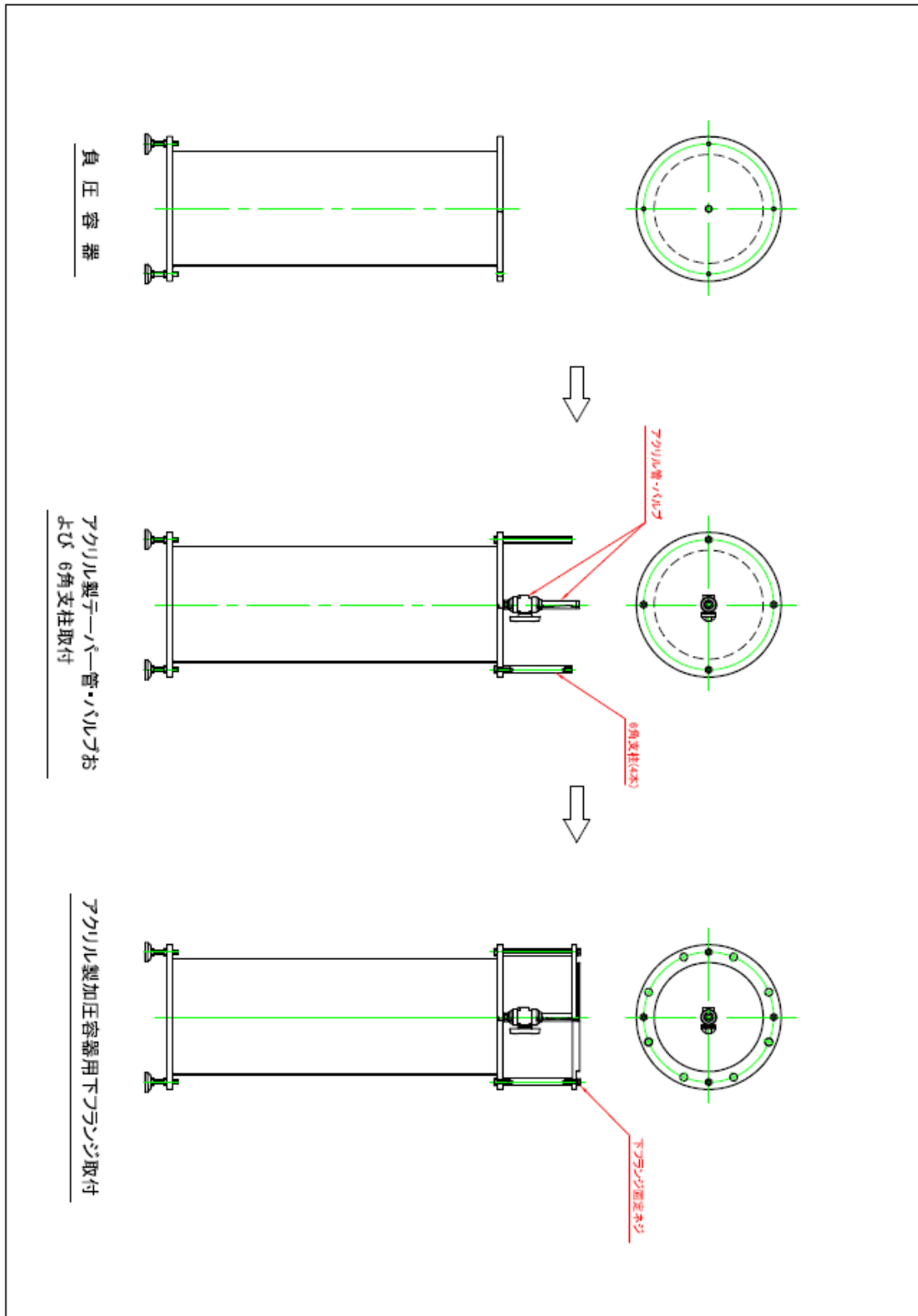


Figure C.7. Assembly Procedure.